



University of  
Stavanger

Faculty of Science and Technology

## MASTER'S THESIS

Study program/ Specialization: Offshore Technology/ Marine and Subsea Technology	Spring semester, 2015.  Open / <del>Restricted</del> access
Writer: <b>Gilang Muhammad Gemilang</b>	..... (Writer's signature)
Faculty supervisor: <b>Dr. Daniel Karunakaran, Ph.D.</b> (University of Stavanger, Subsea 7 Norway) External supervisor(s): <b>Dr. Daniel Karunakaran, Ph.D.</b>	
Thesis title: <b>Feasibility Study of Selected Riser Concepts in Deep Water and Harsh Environment</b>	
Credits (ECTS): 30	
Key words: SCR, Weight Distributed, Lazy Wave, Extreme response Analysis, Downward Velocity, Deep Water, Harsh Environment	Pages: 155  + enclosure: 33 + 1 CD  Stavanger, June 11 2015. Date/year

## Abstract

Today, oil and gas sources are explored in deep water and harsh environment. A riser system is one of the major sub-facilities to transfer oil and gas from the seabed to the host platform. One of the well-known riser systems, the Steel Catenary Riser (SCR), has been an attractive choice for the riser system in deep water. However, the main challenge of the SCR is large motions from the host platforms due to the harsh environment. The large motion of host platforms may induce excessive buckling and fatigue at the touchdown point. The key component of the large motion of the host platform is the downward velocity at the hang-off point where the top-end of the riser is attached to the host platform.

By screening the downward velocities at the hang-off point in the time history graph, the time at which the critical responses (i.e. buckling utilization, bending moment and compression) peak is identified. This study investigates the feasibility of the SCR configuration in terms of the capability to cope with the vessel motion. Several types of the SCR configurations are proposed in this study. The selected configurations of SCR in this study are conventional SCR, Weight Distributed SCR (WDSCR), and Steel Lazy Wave Riser (SLWR). The feasibility of the three riser configurations was analyzed in terms of strength and fatigue performance to understand the limitation of one over the other. The strength assessment of the risers was performed by using load cases, the screening approach was based on different extreme downward velocities at the hang-off point. The checks were according to DNV.

The fatigue performance of the risers was checked considering both wave-induced fatigue and fatigue due to vortex induced vibration. Overall, from the extreme response analysis study, results showed that a feasible conventional SCR configuration can be obtained if the downward velocity at the hang-off point is restricted below 2.6 m/s. It is also found that the downward velocity at the sag-bend of the conventional SCR is restricted below 3.03 m/s. On the other hand, a feasible WDSCR configuration can be obtained, if the downward velocity at the hang-off point is restricted below 3.2 m/s. It is also found that the downward velocity at the sag-bend of the WDSCR is restricted below 3.43 m/s.

The heavy cross section of WDSCR reduces the critical responses (i.e. bending moment, compression and utilization) at the TDP and extends the feasibility of the SCR. The results showed that the SLWR configuration can cope even with a downward velocity of 6 m/s at the hang-off point. The “lazy wave” configuration efficiently absorbs the vessel heave motions. Thereby the SLWR configuration is proven to be the most robust configuration to cope with large motion of the host platform. This study proves that although the SCR feasibility is limited due to vessel heave motion, innovative solutions can be established to extend its feasibility in order to cope with the vessel heave motion in harsh environment.

**Keywords:** Deep Water, SCR, Weight Distributed, Lazy Wave, Extreme response analysis

## Acknowledgement

All glory to the most precious and the most merciful, Allah, who has guided my life to this point.

This thesis is one of the requirements to complete my Master of Science degree in Marine and Subsea Technology, Faculty of Science and Technology, University of Stavanger. I would like to express my deep gratitude to my supervisor, Dr. Daniel Karunakaran, Ph.D for giving me an opportunity to write my thesis in Subsea 7 and for all of the comments, guidance, inputs and patience to evaluate my thesis.

I would also like to express my gratitude to Ove Tobias Gudmestad, Sverre Haver, Airindy Felisita, Sankar Subramanian, Ahmad Makintha Brany, Iqbal Ruswandi, Tomy Nurwanto and Adekunle Peter Orimolade for the discussions and essential assistance during the writing process of this thesis. I also would like to thank my former manager, Bamdad Mehrdad for the hospitality and guidance that has led me to a broad engineering knowledge, and all my colleagues in PT. Saipem Indonesia.

I dedicate my thesis for my beloved parent in Pekanbaru, Ir. Irianto Rab and Solvadiana. A million words cannot express my gratitude and my love for my parents. I also want to thank my sister, Chairunnisa, and my brother, M. Imam Muttaqien. A special thank is also addressed to my beloved wife, Herian Stiyani who has assisted me with a never-ending support. Last but not least, my best wishes go to all of my friends, 'SSSS 2013', 'Mosvangen Friends', 'geng masjid makki', and 'geng AGASTA' for all the memories we had together, it is truly priceless.

Stavanger, 11 June 2015

Gilang Muhammad Gemilang

# Table of Contents

Abstract.....	i
Acknowledgement.....	ii
Table of Contents.....	1
List of Figures.....	7
List of Tables.....	10
Abbreviation.....	12
Chapter 1. Introduction.....	13
1.1 Background.....	13
1.2 Scope and Purpose.....	15
Chapter 2. Deep Water Riser System.....	17
2.1 Introduction.....	17
2.2 Functional Riser System.....	18
2.3 Riser Technology.....	18
2.3.1 Top Tensioned Risers (TTRs).....	18
2.3.2 Compliant Riser.....	20
2.3.3 Hybrid Riser.....	21
2.4 Riser Material.....	23
2.4.1 Flexible Riser.....	23
2.4.2 Rigid Riser.....	24
2.5 Riser Component.....	25
2.5.1 Flex joint.....	25
2.5.2 Tapered stress joint.....	26
2.5.3 Strakes and Fairings.....	26
2.5.4 Buoyancy Module.....	27
2.5.5 Ballast modules.....	27

2.6	Risers Challenges .....	28
2.6.1	Deep Water Challenges .....	28
2.6.2	Harsh Environment Challenges.....	29
2.7	Selected Riser for Thesis Work .....	30
2.7.1	Conventional SCR.....	30
2.7.2	Weight Distributed SCR.....	32
2.7.3	Steel Lazy Wave Riser .....	32
Chapter 3.	Design Code for Riser .....	34
3.1	Introduction .....	34
3.2	Design Principle .....	35
3.3	WSD Code – API RP 2RD .....	36
3.3.1	Allowable Stresses .....	36
3.3.2	Allowable Deflection .....	37
3.3.3	Hydrostatic Collapse .....	37
3.3.4	Overall Column Buckling .....	38
3.3.5	Fatigue/Service Life .....	38
3.4	LRFD Code – DNV-OS-F201 .....	39
3.4.1	Design Loads.....	40
3.4.2	Resistances .....	42
3.4.3	Material Strength.....	44
3.4.4	Ultimate Limit States .....	44
3.4.5	Accidental Limit State.....	49
3.4.6	Serviceability Limit State.....	50
3.4.7	Fatigue Limit State .....	51
3.5	Conclusion.....	52

Chapter 4. Theoretical Background .....	53
4.1 Introduction .....	53
4.2 Waves .....	53
4.2.1 Wave Parameters .....	53
4.2.2 Regular Wave .....	54
4.2.3 Irregular Wave .....	54
4.2.4 Wave Energy Spectrum .....	55
4.3 Currents .....	60
4.4 Floater Responses .....	61
4.5 Hydrodynamic Effects on Slender Cylinder .....	63
4.6 Soil-Riser Interaction .....	66
Chapter 5. Design Basis .....	67
5.1 Introduction .....	67
5.2 Global Analysis .....	67
5.2.1 Static Analysis .....	68
5.2.2 Dynamic Analysis .....	69
5.3 Environmental Data .....	72
5.3.1 Water Depth .....	72
5.3.2 Waves .....	72
5.3.3 Current .....	73
5.3.4 Hydrodynamic Coefficient and Marine Growth .....	74
5.3.5 Soil-riser Interaction .....	74
5.4 Vessel Motion Characteristic .....	75
5.4.1 Coupled and De-coupled analysis .....	75
5.4.2 Host Platform Selection .....	75
5.4.3 Wave Frequency (WF) Floater Motion .....	77

5.4.4	Low Frequency (LF) Floater Motion .....	77
5.5	Riser Data .....	78
5.5.1	Riser Wall thickness .....	78
5.5.2	External Coating .....	79
5.5.3	Buoyancy Modules .....	79
5.5.4	Upper End Termination .....	80
5.5.5	Riser Properties .....	80
5.5.6	Riser Configuration .....	80
5.6	Analysis Concept .....	83
5.6.1	Design Cases .....	83
5.6.2	LRFD calculation .....	84
5.6.3	Extreme Response Methodology .....	85
5.6.4	Analysis Procedure .....	86
5.6.5	Acceptance Criteria .....	87
Chapter 6.	Extreme Response Analysis .....	89
6.1	Introduction .....	89
6.2	Selection of seed components .....	89
6.3	Static Analysis .....	90
6.3.1	Static Analysis of Conventional SCR .....	90
6.3.2	Static Analysis of WDSCR .....	94
6.3.3	Static Analysis of SLWR .....	97
6.3.4	Comparison - Static Results .....	100
6.4	Dynamic Analysis .....	101
6.4.1	Dynamic Analysis of Conventional SCR .....	101
6.4.2	Dynamic Analysis of WDSCR .....	107

6.4.3	Dynamic Analysis of SLWR.....	113
6.5	Summary.....	117
6.6	SLWR for Northern North Sea Condition.....	119
6.6.1	Introduction .....	119
6.6.2	Environmental Data.....	120
6.6.3	Results and Discussion.....	120
6.6.4	Comparison of Critical Sections .....	122
Chapter 7.	Fatigue Analysis.....	124
7.1	Introduction .....	124
7.2	Wave Induced Fatigue .....	125
7.2.1	Design Data .....	125
7.2.2	Assumptions .....	129
7.2.3	Fatigue analysis Procedure.....	129
7.2.4	Fatigue Analysis Results .....	130
7.2.5	Discussion of Wave Induced Fatigue Performance .....	133
7.3	Vortex Induced Vibration (VIV) .....	134
7.3.1	Fatigue Analysis Procedure.....	134
7.3.2	Fatigue Analysis Results .....	135
7.3.3	Discussion of Fatigue Analysis due to VIV .....	136
Chapter 8.	Riser Fabrication and Installation .....	138
8.1	Introduction .....	138
8.2	Fabrication.....	138
8.3	Installation .....	140
8.3.1	Pipe-lay Methods.....	141
8.3.2	Riser Hook-up .....	144



---

8.3.3	Installation of Modules.....	144
Chapter 9.	Conclusion and Recommendation.....	146
9.1	Conclusion.....	146
9.2	Recommendation.....	148
References.....		149
Appendix A - Wall Thickness Calculation .....		153
Appendix B - Sensitivity Analysis Results .....		154
Appendix C - Description of Software Used .....		161
Appendix D - Fatigue Results .....		182

## List of Figures

Figure 1-1 Deep water Development (Ogj, 2010).....	13
Figure 2-1 Essential Functional Elements of a Riser System (API, 2006) .....	17
Figure 2-2 Top Tensioned Risers (TTRs) used on Spar and TLP (Bai and Bai, 2010b) .....	19
Figure 2-3 SCR Standard Compliant Riser Configurations (API, 2006).....	20
Figure 2-4 Global Arrangement of Free Standing Hybrid Riser (FSHR) (Burgess and Lim, 2006).....	22
Figure 2-5 COBRA Riser Configurations (Karunakaran and Baarholm, 2013) .....	22
Figure 2-6 Flexible Riser Layers (API, 2006).....	23
Figure 2-7 Flex Joint (DNV, 2010a) .....	25
Figure 2-8 Tapered Joint (API, 2006) .....	26
Figure 2-9 Strakes and Fairings (API, 2006) (Vivsolutions, 2015) .....	26
Figure 2-10 Buoyancy Modules (Balmoral, 2014) .....	27
Figure 2-11 Typical Ballast Module (Balmoral, 2014).....	27
Figure 2-12 Rigid SCR Hanging-Free Configuration (API, 2006).....	31
Figure 2-13 Weight Distributed SCR (Karunakaran and Legras, 2013).....	32
Figure 2-14 Typical SLWR Configuration in Conjunction with FPSO (Chen and Cao, 2013) .....	33
Figure 3-1 Safety Hierarchy (DNV, 2010a).....	35
Figure 3-2 Propagation Buckling on the Pipe (Tawekal, 2010).....	38
Figure 3-3 De-rating value (DNV, 2010a) .....	44
Figure 4-1 Wave Characteristic (Dean and Dalrymple, 1984).....	54
Figure 4-2 Superposition of Sinusoidal wave components (Journée and Massie, 2001).....	55
Figure 4-3 Divided period of wave into some intervals (Journée and Massie, 2001).....	56
Figure 4-4 Spectral Wave Density (Journée and Massie, 2001) .....	57
Figure 4-5 Wave Record Analysis (Journée and Massie, 2001) .....	58
Figure 4-6 Six Degree of Freedom of the vessel (Calqlata, 2015).....	61
Figure 4-7 Schematic System of Motions and Waves (Journée and Massie, 2001) .....	62
Figure 4-8 Principle of Transfer of Waves into Vessel Response (Journée and Massie, 2001) .....	63
Figure 4-9 Definition of normal force, tangential force and lift force (DNV, 2010b).....	64
Figure 5-1 Effective weight and effective tension (Baltrop, 1998).....	69
Figure 5-2 Line Model in ORCAFLEX (Orcina, 2010).....	70

Figure 5-3 Floating Production System (DNV, 2010a) .....	76
Figure 5-4 Floater Motion Comparison .....	77
Figure 5-5 Riser Configuration .....	81
Figure 5-6 Riser Orientation .....	81
Figure 5-7 SLWR Geomerty .....	82
Figure 5-8 Work Diagram .....	84
Figure 6-1 SCR Intact-Static Configuration for near, mean and far position .....	91
Figure 6-2 Static Effective Tension of SCR with Coating.....	92
Figure 6-3 Static Bending Moment of SCR with Coating .....	92
Figure 6-4 Static Utilization of SCR with Coating .....	93
Figure 6-5 Intact-Static WDSCR Configuration near, mean and far position .....	95
Figure 6-6 Effective Tension Comparison .....	96
Figure 6-7 Static Configuration - Conventional SCR and WDSCR .....	96
Figure 6-8 Static Bending Moment - Conventional SCR and WDSCR .....	97
Figure 6-9 Intact-Static SLWR configuration near, mean and far position .....	98
Figure 6-10 Comparison of Effective Tension – Mean Position – Static .....	100
Figure 6-11 Comparison of Bending Moment – Mean Position- Static .....	100
Figure 6-12 Time History: Effective Tension and Bending Moment -SCR-Coating-LC5- Near-ULS Design.....	104
Figure 6-13 Time History: Bending Moment and Effective Tension - SCR-No Coating-LC6- Near-ULS .....	105
Figure 6-14 Minimum Dynamic Effective Tension SCR-LC5 .....	106
Figure 6-15 Maximum Dynamic Utilization of SCR and WDSCR with Coating.....	108
Figure 6-16 Maximum Dynamic Bending Moment Comparison of SCR and WDSCR with Coating .....	109
Figure 6-17 Maximum Downward Velocity Range for WDSCR and Conventional SCR – Load Case 5.....	109
Figure 6-18 Vertical Velocity VS Bending Moment, WDSCR, LC8, coating .....	112
Figure 6-19 Vertical Velocity VS Bending Moment, WDSCR, LC8, No Coating .....	112
Figure 6-20 Vertical Velocity VS Effective Tension, WDSCR, LC8, Coating.....	113
Figure 6-21 Vertical Velocity VS Effective Tension, WDSCR, LC8, No Coating.....	113
Figure 6-22 Maximum Dynamic Utilization of WDSCR and SLWR with Coating .....	115
Figure 6-23 Maximum Downward Velocity Range for SLWR and WDSCR – Load Case 8116	
Figure 6-24 Utilization VS Max. Downward Velocity at the Hang-off Point .....	118

Figure 6-25 Utilization VS Max. Downward Velocity at Point B .....	119
Figure 6-26 Variation of Top Angle in Time History .....	121
Figure 6-27 Maximum Effective Tension over entire riser length, far and near offset-ULS	122
Figure 6-28 Maximum Bending Moment over entire riser length, far and near offset-ULS .	123
Figure 6-29 Maximum Utilization over entire riser length, far and near offset-ULS .....	123
Figure 7-1 S-N curves in seawater with cathodic protection (DNV, 2010c) .....	126
Figure 7-2 Stress cycling where further fatigue assessment can be omitted (DNV, 2010c)..	126
Figure 7-3 Subdivision of the sea-state scatter diagram into representative blocks .....	128
Figure 7-4 Total Fatigue Damage of SCR .....	131
Figure 7-5 Total Fatigue Damage of WDSCR.....	132
Figure 7-6 Total Fatigue Damage of SLWR.....	133
Figure 7-7 Total Fatigue Damage due to VIV over Entire Riser Length.....	136
Figure 7-8 Vortex Shedding .....	136
Figure 8-1 Mechanized PGTAW Equipment in Operation and Weld Cap Macro Section (Karunakaran et al., 2013).....	139
Figure 8-2 Mechanized PGMAW in operation and typical girth weld showing CMT weld roots (Karunakaran et al., 2013).....	140
Figure 8-3 The Seven Oceans and Seven Borealis Pipe-lay Vessel, Figure from Subsea 7..	141
Figure 8-4 Sketch of S-Lay Method.....	141
Figure 8-5 Sketch of J-lay Method (Chacko et al., 2005) .....	142
Figure 8-6 Spool Base Vigna of Subsea 7, Figure from Subsea 7 .....	143
Figure 8-7 Typical RIT and Flexjoint (Maneschy, 2014) .....	144
Figure 8-8 the Installation of buoyancy Module onto the Riser (Beattie et al., 2013).....	145

## List of Tables

Table 3-1 Classification of Safety Class (DNV, 2010a) .....	36
Table 3-2 Design Matrix for Rigid Risers (API, 2006).....	37
Table 3-3 Examples of Categorization of loads <sup>1)</sup> (DNV, 2010a).....	41
Table 3-4 Load Effect Factor (DNV, 2010a) .....	42
Table 3-5 Safety Class Resistance Factor .....	43
Table 3-6 Material Resistance Factor.....	43
Table 3-7 Simplified Design Check for Accidental Limit States.....	43
Table 3-8 Material strength factor (DNV, 2010a).....	44
Table 3-9 Fabrication Factor (DNV, 2010a) .....	47
Table 3-10 Design Fatigue Factor .....	51
Table 5-1 Wave Data.....	73
Table 5-2 Current Profile .....	73
Table 5-3 Hydrodynamic Coefficient .....	74
Table 5-4 Soil Parameters .....	74
Table 5-5 Minimum Wall Thickness .....	79
Table 5-6 Buoyancy Module Properties.....	79
Table 5-7 Riser Properties.....	80
Table 5-8 SLWR Parameters.....	82
Table 5-9 Environmental Load Case Matrix .....	83
Table 5-10 Design Case Matrix for Each Environmental Load Case .....	84
Table 5-11 Partial Safety Factor for ULS and ALS .....	85
Table 6-1 Load Cases with Corresponding Seed Component.....	89
Table 6-2 SCR Static Results- Functional Loads.....	91
Table 6-3 WDSCR Static Results- Functional Loads .....	95
Table 6-4 Selected Parameters for SLWR configuration.....	98
Table 6-5 SLWR Static Results- Functional Loads .....	99
Table 6-6 SCR-Strength Response Summary for Load Case 3 .....	102
Table 6-7 SCR-Strength Response Summary for Load Case 4 .....	102
Table 6-8 SCR-Strength Response Summary for Load Case 5 .....	103
Table 6-9 SCR without Coating-Strength Response Summary for Load Case 6.....	105
Table 6-10 WDSCR-Strength Response Summary for Load Case 5.....	107
Table 6-11 WDSCR-Strength Response Summary for Load Case 6.....	110

Table 6-12 WDSCR-Strength Response Summary for Load Case 7.....	110
Table 6-13 WDSCR-Strength Response Summary for Load Case 8.....	111
Table 6-14 Summary result of SLWR against LC8 .....	114
Table 6-15 SLWR- Dynamic analysis Summary .....	116
Table 6-16 Summary of Downward Velocity Threshold.....	118
Table 6-17 Strength Analysis Summary .....	120
Table 7-1 Fatigue limit (DNV, 2010c).....	127
Table 7-2 Representative sea-state and lumped probability of occurrence.....	128
Table 7-3 Directional Probabilities .....	129
Table 7-4 Fatigue Life Summary of SCR .....	130
Table 7-5 Fatigue Life Summary of WDSCR.....	131
Table 7-6 Fatigue Life Summary of SLWR.....	132
Table 7-7 Lumped Probability of Occurrence.....	135
Table 7-8 Minimum VIV Fatigue Life.....	135
Table 8-1 Prerequisite for Fabrication of SCR Weld (Karunakaran et al., 2013).....	139

## Abbreviation

ALS	Accidental Limit State
API	American Petroleum Institute
ASME	American Society of Mechanical Engineers
COBRA	Catenary Offset Buoyant Riser Assembly
DFF	Design Fatigue Factor
DNV	Det Norske Veritas
DOF	Degree of Freedom
DSAW	Double Submerged Arc Welded
ERW	Electric Resistance Welded
FE	Finite Element
FLS	Fatigue Limit State
FPS	Floating Production System
FPSO	Floating Production Storage and Offloading
FSHR	Free Standing Hybrid
GOM	Gulf of Mexico
HRT	Hybrid Riser Tower
JONSWAP	Joint Operation North Sea Wave Project
LC	Load Case
LF	Low Frequency
LRFD	Load and Resistance Factor Design
PET	Pipeline Engineering Tool
RAO	Response Amplitude Operator
RIT	Riser Installation Tool
SCF	Stress Concentration Factor
SCR	Steel Catenary Riser
SLOR	Single Line Offset Riser
SLS	Serviceability Limit State
SLWR	Steel Lazy Wave Riser
SMYS	Specified Minimum Yield Stress
SS	Semi-submersible
TDA	Touchdown Area
TDP	Touchdown Point
TLP	Tension Leg Platform
TRB	Three Roll Bending
TTR	Top Tension Riser
ULS	Ultimate Limit State
UOE	Pipe fabrication process for welded pipes
VIV	Vortex Induced Vibration
WF	Wave Frequency
WSD	Working Stress Design
WDSCR	Weight Distributed Steel Catenary Riser

# Chapter 1. Introduction

## 1.1 Background

The Oil and Gas industry has become one of the largest energy sources in the world. The demand for energy continues to increase along with the growth of industries and the population. The International Energy Agency (IEA) in 2004 estimated that the increase in the energy consumption will continue to grow with an average increase of up to 1.6% each year. Due to the increase in energy consumption, governments need to encourage the industry to do more exploration of oil and gas sector.

Today, oil and gas resources on land are limited and dwindling. Therefore, the exploration starts to move to offshore. Oil and gas exploration for offshore is different and more difficult than exploration on land. The main reason is the sea behavior which gives numerous challenges to the oil and gas exploration. In the recent decades, a lot of oil companies started to extend their exploration in the deep sea areas.

Thus, the offshore technologies to explore oil and gas resources in deep water are pursued. As the subsea technology was introduced, exploration and production activities have increased dramatically in deep water. Oil and gas exploration areas such as Santo Basin, Gulf of Mexico, West Africa, and the Norwegian Continental Shelf (NCS) are continually moving into deeper water depths by applying the subsea technology. Figure 1-1 shows the development of hydrocarbon exploration which continues to move to greater water depth over the years.

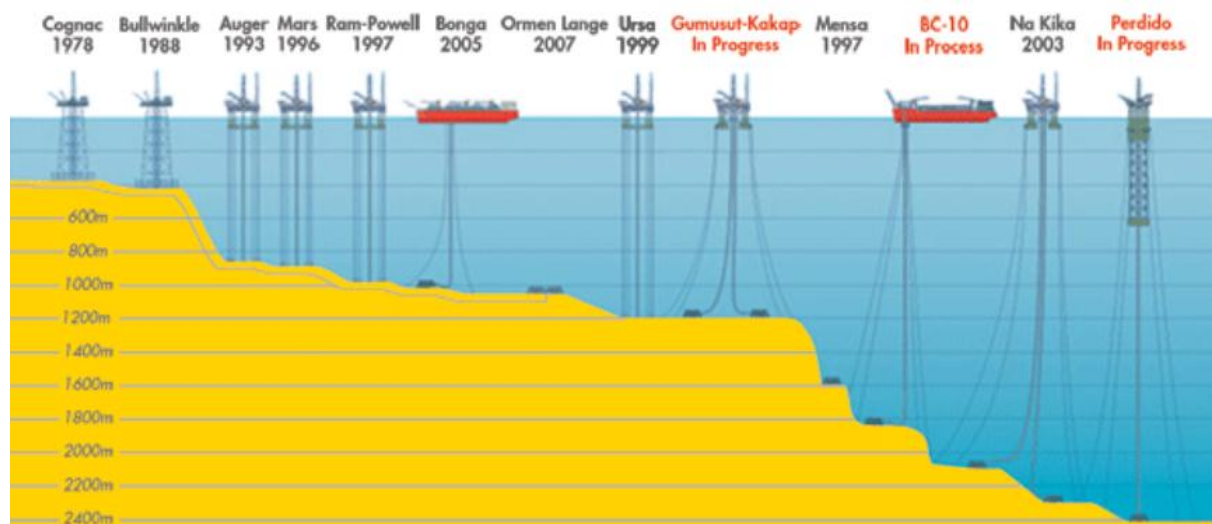


Figure 1-1 Deep water Development (Ogj, 2010)

These water depths vary from 500 to 2400 meters. Each exploration area has its own water depth and its own environmental characteristics which lead to different challenges. Deep water and harsh environment are the most challenging combination of exploration facility. Many developments have been established to tackle these problems that are associated with deep water and harsh environment.



In shallow water, the application of fixed offshore structures is still considered effective and economical, since fixed offshore structures are the most conservative type in the exploration activity. In deep water, the application of fixed offshore structures is no longer economical. This condition encourages industry to establish a new method to accommodate deep water exploration.

The riser system which transports the production fluids from the seabed to the host platform is one of the important facilities in deep water field development. The Floating Production System (FPS) is a proven technology that is developed as a host platform located at the water surface. There are many types of floating production such as Semi-submersible (SS), Floating Production, Storage and Offloading (FPSO), SPAR floater, Floating Production Unit (FPU), Tension Leg Platform (TLP) and their derivatives.

Each floating production system responds dynamically to environmental conditions. The riser concepts in harsh environment experience a great challenge due to large motions of the floating production system. A robust, safe and economical riser concept should be designed to cope with the large motion of the floating production system in deep water and harsh environment. There are many types of riser configuration that have been installed in oil and gas exploration; Steel Catenary Risers (SCR), flexible riser, and hybrid riser.

The selection of riser configuration in deep water depends on unique performance, risk, cost and applicability of each riser concept (Petruzka et al., 2002). The steel catenary riser (SCR) has emerged to be one of attractive choices for recent deep water environments (Phifer et al., 1994). The steel catenary riser consists of simple rigid steel pipe hanging freely from the floating production system to the seabed. The SCR can be used with a large diameter and adequate wall thickness which is able to withstand higher hydrostatic pressure and higher temperature in deep water. The capability to provide large diameters may also allow higher rates of production stream, thus contributing to better use of riser (Hatton and Howells, 1997).

The material of simple rigid riser can be fabricated cheaply, thereby reducing production costs of field development. The SCR configuration forms catenary due to its own weight. The SCR also offers benefit over the top tensioned riser because the SCR requires no heave compensation at the hang-off point (Phifer et al., 1994). On the seabed, the SCR needs no special bottom connection. The problems that might occur in the SCR application include sensitivity to environmental loads and heave motions of the floating production system.

The wave frequency of floater motion might cause excessive bending stress at the touchdown point (TDP), while low frequency of floater motion might cause large offset of the floater, thereby it causes large changes in the curvature of the SCR and changes in the TDP position. For near offset position of the vessel, there may be an induced excessive bending moment at the TDP, while for far offset position, there may be induced high tension at the hang-off point. Moreover, the touchdown point (TDP) and the top region area are subjected to the fatigue (Karunakaran and Baarholm, 2013). Therefore, the strength and fatigue performance of steel catenary riser is still limited. To tackle these challenges, improvement of the SCR configurations have been proposed, and developed such as weight distributed SCR and steel lazy wave riser (SLWR).

The flexible risers have good proficiency to accommodate the high curvature and dynamic motions of the floaters resulted from environmental load (Burgess and Lim, 2006). The flexible risers have been a successful solution for shallow water to the mid water depth riser. In addition, the flexible riser is, in practice, easy to install. However, when it comes to deep water, the flexible riser presents a limitation of practical and economic reasons. In deep water, the cost of flexible pipe is significantly high with increasing depth and it has technical limitations to the maximum diameter, operating pressure and temperature (Hatton and Howells, 1996). Furthermore, the availability of flexible riser is limited to a minimum number of competent vendors.

Another type of riser configuration is hybrid riser. The hybrid riser is the combination of flexible jumper, vertical bundle of rigid riser and sub-surface buoyancy module attached in between (Masturi, 2014). The sub-surface buoyancy module is attached at the top of vertical bundle of rigid riser in deeper water depth away from wave region so as to minimize the hydrodynamic loadings from the sea surface. The flexible jumpers connecting the top end of the riser and the floater are utilized to make the riser system uncoupled to the floater motion. Thus, the hybrid riser is categorized as uncoupled riser. The uncoupled riser is very effective to de-couple large motions of the floater and hence the riser becomes insensitive to fatigue damage (Karunakaran and Baarholm, 2013). Nevertheless, the hybrid riser is an expensive solution since it consists of a number of complex components. The hybrid riser is also hard to install since it has a complex bottom assembly and connection.

## 1.2 Scope and Purpose

Design of Steel Catenary Risers (SCR) has seen increasing challenges in deep water applications due to large motion of the host platform (Yue et al., 2011). The motions of hang-off point, where the riser is attached at the host platform, result from combination of weather conditions. The global strength design of the SCR is measured by dynamic response in the touchdown area, which is mainly driven by the vessel motions (Chen et al., 2009). This thesis focuses mainly on the assessment of the SCR configuration for evaluation in terms of capability to cope with the vessel motion.

The purpose of this study is to investigate the feasibility of the SCR configuration in terms of the capability to cope with the vessel motion. The riser design will be analyzed quantitatively with respect to the strength and the fatigue performances. Several types of SCR configurations are proposed in this study. Each configuration has characteristics which make it better suited for particular applications. The selected configurations of SCR in this study are conventional SCR, Weight Distributed SCR (WDSCR), and Steel Lazy Wave Riser (SLWR).

It is typically challenging to achieve feasibility for a conventional SCR application in conjunction with the Semi-submersible in harsh environment. Thus, the WDSCR and SLWR are proposed to overcome the limitation of the conventional SCR. The three riser configurations will be discussed and analyzed to see the limitation of one over the other based on the capability to cope with the vessel motion. The vertical velocity at the hang-off point is the main design driver for buckling at the TDP (Karunakaran et al., 2013).

The downward velocity at the hang-off point dominates the riser's critical responses (stress/buckling) at the TDP very well (Chen et al., 2009). The downward velocity at the hang-off point is therefore considered in order to capture the limitation of riser integrity in this study. The heave motion of the vessel is the main driver of the downward velocity at the hang-off point since it directly correlates to the vertical motion at the hang-off point. In addition, pitch and roll motion of the vessel can also contribute to downward velocity if the hang-off point position is not located at the vessel center of gravity (COG). The concern is also on the velocity of the riser in the touchdown area since a feasible configuration can be addressed by controlling the dynamic stresses at the TDP.

The study involves a rigorous evaluation to verify both strength and fatigue performance. The strength analyses of all three riser configurations are performed by using comprehensive non-linear time domain analysis. The wave induced fatigue analyses are performed by using a comprehensive irregular wave time domain analysis procedure. The ORCAFLEX software is mainly applied in this study to carry out simulations. In addition, RIFLEX and VIVANA software are also applied for VIV fatigue analysis. A brief description of relevant guidelines for the design of such riser systems will also be discussed.

The scope of thesis is as follows:

- Chapter 2 presents a general description of deep water riser systems. Development of riser system is discussed with the main focus on selected riser configuration.
- Chapter 3 discusses the code check and standard for riser system design.
- Chapter 4 provides the relevant theoretical background for this study.
- Chapter 5 provides basis design of this study. This chapter includes analysis methodology, design data, and the design acceptance criteria.
- Chapter 6 provides extreme response analysis for riser configuration in order to verify the requirement from ultimate limit state and accidental limit state.
- Chapter 7 provides fatigue analyses check for selected riser configuration in order to verify the requirement from the fatigue limit state.
- Chapter 8 provides a general description of fabrication and installation for riser.
- Chapter 9 provides the conclusions and recommendations from the study.

## Chapter 2. Deep Water Riser System

### 2.1 Introduction

Riser systems are the main conduit to transfer fluid between the subsea equipment to the host platforms during the drilling, injection, completion, production and exporting phases. Based on API-RP-2RD, risers may perform the following specific functions (API, 2006):

- Transport fluids between the subsea wells and the floater (i.e. production, injection, circulated fluids).
- Import, export, or circulate fluids between the floater and remote equipment or pipeline systems.
- Guide, monitor and control tubular of intervention or drilling tools into the wells.
- Support auxiliary lines (i.e. flow line, umbilical).
- Incorporate with mooring system for station keeping.

Application of riser system has been extensively used for oil and gas exploration. The application of riser depends on the water depth and environmental condition. The riser system should be configured as optimum as possible to satisfy its functional requirement. The environmental condition depends on the location of exploration. The Gulf of Mexico, Indonesia and West of Africa are still categorized as mild to moderate. When it comes to North Sea Continental (NCS), or Barent Sea, the environmental condition starts to move to harsh environment and promises more challenges to the riser system.

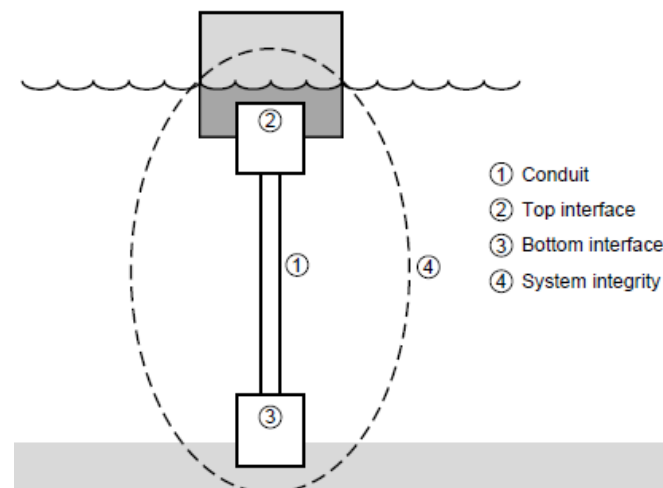


Figure 2-1 Essential Functional Elements of a Riser System (API, 2006)

Riser system consists of essential functional elements, i.e. system integrity, conduit, top interface and bottom interface as shown in Figure 2-1 (API, 2006). From Figure 2-1, it is shown that riser system is the interface between a static structure of the seabed and the dynamic structure of the host platform on the sea surface. From this reason, risers are commonly referred to as dynamic risers (Lien, 2010). Thereby riser should be able to accommodate the dynamic motion from the floater to the relatively static seabed.

## 2.2 Functional Riser System

A host platform needs a conduit to connect with the subsea equipment on the seabed. The riser systems, as the key element for that purpose, provide various functions which call for different type of riser design. Generally, based on the function, risers are divided into 4 functions as follows.

### • Drilling riser

This type of riser applies the concept of Top Tension Risers (TTRs) which is supported by top tension force on FPS in order to maintain vertical motion of riser from a floater to the seabed. The surge motions of floater will act as a prescribed dynamic boundary condition in the riser configuration, while heave relative to vertical motions of the upper riser end is subjected to active control by top tension force. This type of riser is commonly used when drilling mud to and from well or major intervention/work over of the subsea well. This is also employed to serve as a running and retrieving string for the BOP and guide tools/auxiliary lines (DNV, 2010a).

### • Production riser

This type of riser is used for transporting the hydrocarbon fluid between a subsea well and a floater. Mainly, the concept of this riser is according to compliant riser which is configured such that it could absorb floater motion without a heave compensation system.

### • Injection riser

This type of riser is used for injecting or circulating some fluids into the subsea well to enhance production or to serve the maintenance (API, 2006).

### • Export/import riser

This type of riser is used for transporting processed oil or gas between the platform and pipeline system or tanker (API, 2006).

## 2.3 Riser Technology

The dynamic behavior of floater is the main challenge for riser system design. The global riser should be able to cope with the floater motion so that the riser is able to work as per requirement. The suspended sections of riser will absorb this dynamic motion of the floater. Based on the ability of riser to cope with floater motion, riser system is divided into 3 types as follows.

### 2.3.1 Top Tensioned Risers (TTRs)

The Top Tensioned Risers (TTRs) concept is a vertical riser supported by a tensioner located at the floater. The tensioner pulls upward risers on the top part of the riser in order to limit bending and maintain the constant effective tension with an adequate stroke capacity (DNV, 2010a). The top boundary allows the riser and floater to move vertically relative to each other (Bai and Bai, 2010b). The tensioner must maintain a constant target value of tension to prevent excessive bending on the bottom of the riser. Such risers consist of slender metal pipe

cross sections which may be thought of as a continuance of the wellbore to the sea surface (API, 2006). The typical TTRs figure can be seen from Figure 2-2.

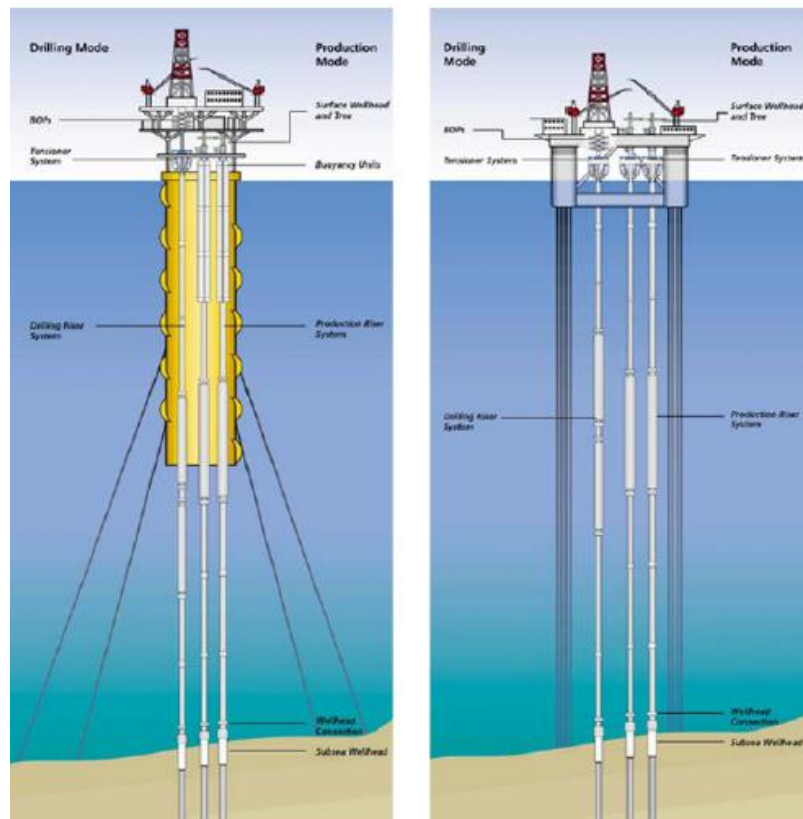


Figure 2-2 Top Tensioned Risers (TTRs) used on Spar and TLP (Bai and Bai, 2010b)

The vertical riser is constrained to follow the horizontal motion of the floater. The relative vertical motion between riser and floater motion is generally denoted stroke (DNV, 2010a). The top tension and stroke capacity are important design parameters governing the behavior of vertical riser. A tapered joint, ball-joint or flex-joint is applied to reduce the bending stress at the termination to the seabed (DNV, 2010a). Generally, the TTRs are used for drilling. Nevertheless, the TTRs can also be used for production, injection and export riser. For deep water application, the riser top tension requirements become significant to support riser weight and avoid bottom compression.

Moreover, harsh environments will cause significant motion of the floater and TTRs. Therefore, at a field with condition of deep water and harsh environment, TTRs becomes technically neither feasible nor economical. The top tensioned risers are applicable for floater with relatively small heave motion, e.g. TLP, Spar, Deep Draft Floater (DDF). Those floaters have a relatively small requirement for stroke capacity with relatively small offsets (Bai and Bai, 2010b).

For other floaters like FPSOs and Semi-Submersibles (SS), the demand for stroke capacity will be much higher for the TTRs, which means that other riser solutions like steel catenary risers (SCRs) or flexible risers are more preferable. For TLP, the top boundary condition is equipped with a heave compensation system to allow vertical motion of the riser. For Spar platforms, the top boundary condition is maintained by buoyancy modules attached along the upper part of the riser inside the moon pool (DNV, 2010a).

### 2.3.2 Compliant Riser

Compliant riser provides flexibility to tolerate floater motion. The name “compliant” comes from the type of riser configuration system with the flexibility to move horizontally. Compliant risers have configuration such that it may absorb floater motions by the change of its geometry without the use of heave compensation systems (DNV, 2010a). This flexibility provides dynamic resistance, allowing riser to operate in deep water and harsh environment.

The material of compliant riser is normally either flexible pipe or rigid pipe. The compliant riser with rigid pipe is commonly addressed as SCR. Thus, the SCR and flexible pipe can be installed with various compliant configurations depend on a number of key factors, e.g. global behavior, structural integrity, materials, costs, environment, host platform motion, field layout and water depth. Some examples of compliant configuration of riser are Steep S, Lazy S, Steep Wave, Lazy Wave, Steep S, or Free Hanging as shown in Figure 2-3.

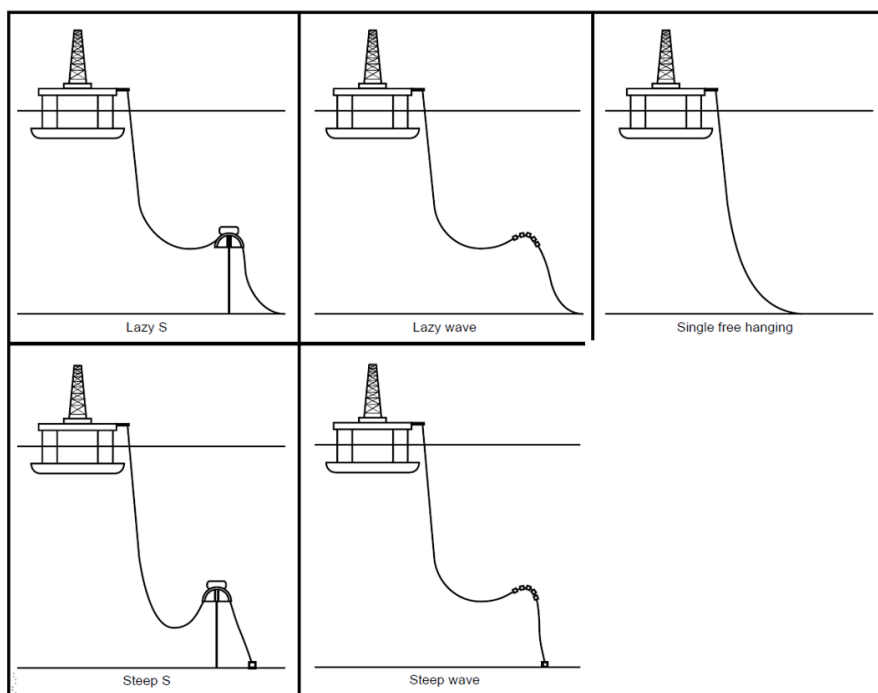


Figure 2-3 SCR Standard Compliant Riser Configurations (API, 2006)

The selection of riser configuration is according to the production requirement and environmental conditions. With such compliant configuration, the riser can cope with larger static and dynamic excursions of the floater compared to the top tensioned risers. The vessel motion characteristics will dedicate the dynamic tension and bending moment variation along the entire riser length in any situations. The connection between the riser and the floater is an essential design issue for compliant riser configurations. Thereby, tapered joint, flex joint and other components are installed in the hang-off area to limit bending curvature and pipe stresses at riser connection (DNV, 2010a).

Free hanging catenary is the simplest configuration of compliant riser and is cost effective for deep water development, particularly under high pressure and high temperature. It is simple, since the requirement for subsea infrastructure is minimum and easy to install. On the contrary, a free hanging catenary configuration is subjected to high bending moment and

buckling due to either wave frequency or low frequency of vessel motions especially at the hang-off point and touchdown point.

Due to high vessel motions, the compression at the riser touchdown point are susceptible to failure. Moreover, SCRs are exposed to large fatigue loads in the touchdown point area, and hang-off area (Bell et al., 2005). In order to overcome such limitations, many compliant configurations have been developed and established as shown in Figure 2-3. In this thesis, the free hanging riser (conventional SCR) is selected as preliminary riser configuration. Afterwards, the SCR configuration will be modified to weight distributed SCR and steel lazy wave riser (SLWR) to improve its performance in terms of strength and fatigue design.

### 2.3.3 Hybrid Riser

The hybrid riser adopts both concepts of top tensioned risers (TTRs) and compliant (flexible) riser by applying a vertical pipe tensioned by subsurface buoyancy can and flexible riser (jumper). There are many types of hybrid riser; Free Standing Hybrid Riser (FSHR), hybrid riser tower, grouped Single Line Offset Riser (SLOR). The top of the vertical riser is positioned at a distance below the water surface with some offset to the floater such that a horizontal length of flexible jumper can be fitted to accommodate large motion from the floater. The flexibility is then provided by the horizontal length of jumper, which has high curvature capability (Hatton and Howells, 1996).

As the jumper is flexible pipe, this configuration allows the floater motion to be absorbed by the jumpers and subsurface buoyancy can, thereby it reduces the dynamic motions over the rest of the riser (Bell et al., 2005). The floater motions are effectively absorbed by the flexible jumper, hence the steel pipe becomes less susceptible to fatigue issue. This riser configuration is characterized as uncoupled risers as it effectively isolates the dynamic motion of the floater from the vertical riser. With such a configuration, the hybrid riser can therefore be used with a wide range of floater in deep water or even ultra-deep water application and harsh environment.

Free Standing Hybrid Riser (FSHR), one of the hybrid risers, has a typical vertical riser section which is tensioned by buoyancy cans positioned at a distance below the water surface (Burgess and Lim, 2006). The top end of the riser has offset from the host vessel such that a suitable length of flexible pipe (jumper) connects the top end of the riser to the vessel. Such arrangement can accommodate the vessel motions. The Free Standing Hybrid Riser can be seen in Figure 2-4. However, hybrid riser is an expensive solution due to its complex and numerous components, e.g. sub-surface buoy can, flex joint, riser bundle, bottom connection assembly, etc. Moreover, hybrid riser is hard to install.

As development is being progressed, the vertical tensioned riser can be substituted with steel catenary riser with hanging free configuration. This hybrid riser is commonly referred to as Catenary Offset Buoyant Riser Assembly (COBRA). The COBRA concept is a modification of the hybrid riser concept, in which the aim is to combine flexibility features of hybrid concept with simplicity and economical features of the SCR. The result is the combination of steel catenary riser section, sub-surface buoy which is tethered down to the seabed, and flexible jumper. (Karunakaran and Baarholm, 2013).



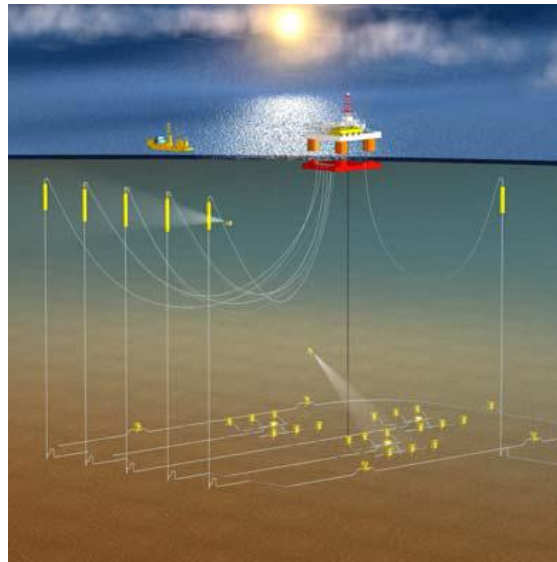


Figure 2-4 Global Arrangement of Free Standing Hybrid Riser (FSHR) (Burgess and Lim, 2006)

The top of the catenary riser section is connected to the host platform by a flexible jumper. According to Karunakaran and Baarholm (2013), this concept removes the main problems of fatigue and buckling issues at the touchdown point of steel catenary riser and also avoids the use of complicated bottom assembly and spools of hybrid riser tower. The sample arrangement of the COBRA concept for 1500 m water depth is shown in Figure 2-5. The hybrid riser provides flexibility, excellent dynamic behavior, low fatigue damage and pressure resistance.

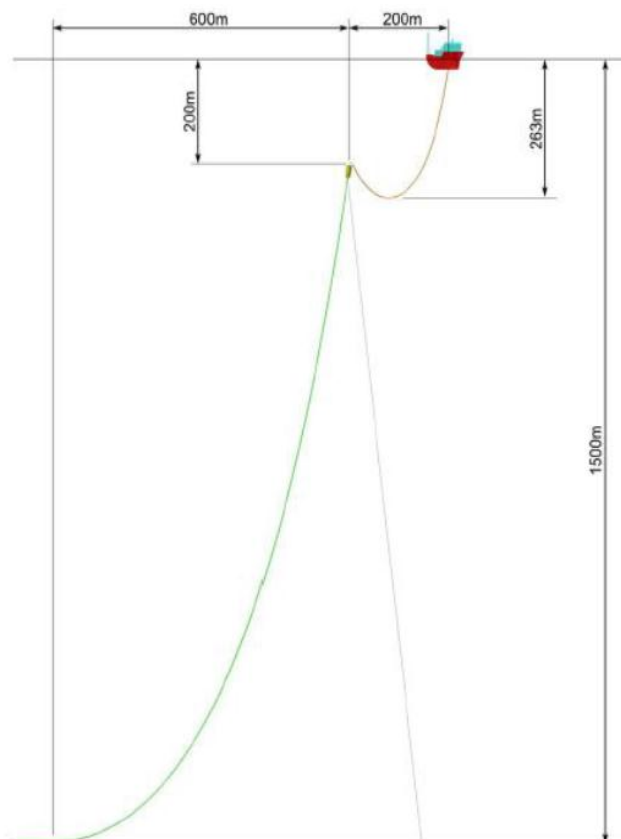


Figure 2-5 COBRA Riser Configurations (Karunakaran and Baarholm, 2013)

## 2.4 Riser Material

Material for riser systems is selected to accommodate the riser requirement. The selection of material is driven by internal fluid, external environment, loads, temperature, service life, fatigue resistance, and corrosion resistance (DNV, 2010a). In addition, the selection of materials depends on chemical composition of the transported fluid since various transported fluids may cause corrosion or erosion. According to material selection, risers can be divided into the flexible riser and rigid riser.

### 2.4.1 Flexible Riser

Flexible riser is a pipe with low bending stiffness and high axial tensile stiffness, which consists of several numbers of independent layers. Basically, there are two types of flexible pipe; bonded and non-bonded types (API, 2006). Bonded pipes comprise individual and different layers of elastomer, fabric and steel wrapped together with a process of vulcanization. Generally, bonded pipe is only used for short sections e.g. jumper. In contrast, unbonded pipe is used for long sections for dynamic application.

A non-bonded pipe comprises several individual and different layers having no adhesion between them (API, 2006). The layers are a carbon-steel circumferential layer for internal pressure loads, a stainless steel internal carcass for collapse resistance, tensile armor layers for axial strength, and an extruded watertight external sheath. The flexible riser has been a successfully applied for shallow water. It also can be used for flow line systems. Flexible riser has high flexibility, allowing riser to bend with high curvature. The typical flexible riser layers can be seen in Figure 2-6. Flexible riser has numerous advantages, e.g. easy to install, reusable, etc.

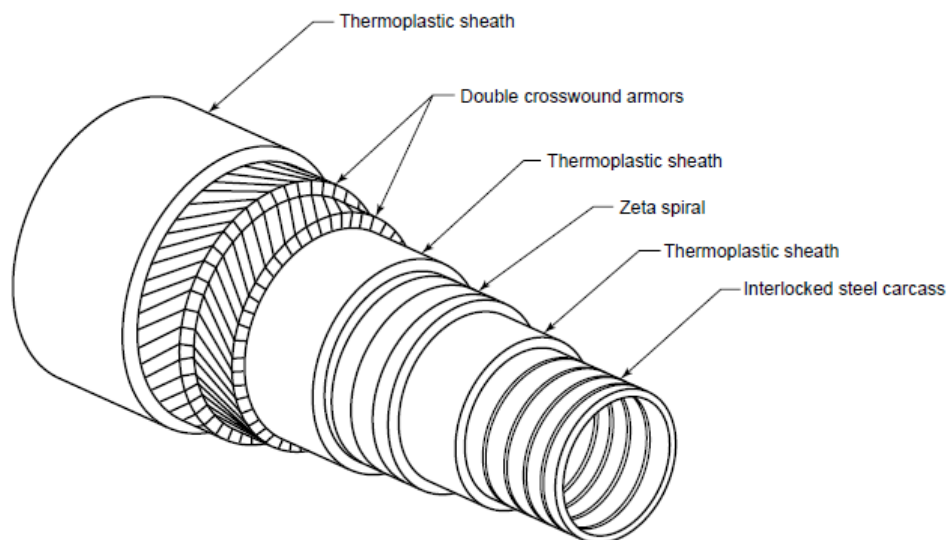


Figure 2-6 Flexible Riser Layers (API, 2006)

The flexible riser has been extensively used for providing flexibility and resistance to corrosion. The flexible riser applies pipe-in-pipe method to fit the entire layer in one section. The layers are arranged such that it can improve flow assurance, resistance to corrosion, and capability to resist external and internal pressure. The capability of flexible riser becomes a proven technology, especially in mid water and shallow water.

However, as the exploration of oil and gas moves to deeper water, the flexible riser has technical and economical limitation mainly caused by development cost. As the water becomes deeper, the length of the riser becomes longer and might cause expensive cost. Furthermore, in the future, the need for higher number of risers and larger diameter is predicted (Howells and Hatton, 1997). This limitation of flexible riser has become the main reason to develop alternative technology to overcome that challenge. Consequently, alternative types of riser have been eagerly pursued. Thus, when it comes to deep water, rigid riser emerges as an alternative.

## **2.4.2 Rigid Riser**

### **2.4.2.1 Carbon Steel Pipe**

The selection of materials using a carbon steel pipe was applied since the 1950s based on the standard API 5L Code of pipe material selection. The requirements on carbon steel quality differ from the characteristics of the material (e.g. yield/tensile strength, modulus of elasticity). Based on API 5L code, there are several types of pipe material, namely X46, X52, X56, X60, X64, X70 and X80. The number indicates the yield stress strength of the material.

Each type of material has the characteristics of the composite and each constituent material. The specifications of steel material depend on the chemical composition, strength of materials, and tolerance in the pipeline industry. However, the carbon steel materials tend to corrode due to:

- Sweet corrosion = combination of CO<sub>2</sub> and water
- Sour corrosion = H<sub>2</sub>S

Thereby, riser materials selection and internal corrosion mitigation strategies should consider the fluids that are expected to be in contact with the riser both internally and externally during service life (API, 2006). Thereby the selection of material should be determined to get the appropriate material according to the needs of riser systems. The following criteria can be used in the selection of materials for pipes.

- Mechanical properties, including yield strength, resistance to withstand a static load, dynamic load, and elasticity in the manufacturing process.
- Weld ability, ease and strength of the pipe material in the welding process.
- Corrosion resistance, the ability of a material to resist corrosion.
- Cost, related to the costs per unit of measure of the material.
- Availability, related to the availability and supply of materials on the market

### **2.4.2.2 Titanium pipe**

The titanium material offers several benefits over the carbon steel material due to a significantly low modulus of elasticity implying a higher degree of flexibility. Furthermore, the yield stress of titanium is much higher and the specific weight is much lower than carbon steel material (DNV, 2010a). The titanium also offers high fatigue resistance and generally high chemical resistance. This fact leads titanium to become preferable than the carbon steel material since the titanium material provides predominance with respect to strength, flexibility and weight.

However, titanium is much more expensive than steel, such that the carbon steel material is considered to be applied rather than titanium material in deep water. Therefore, the “Titanium Catenary Risers” (TCR) is only a candidate material of riser for following conditions (Bell et al., 2005):

- When in considerably shallow water depth location where the fatigue problems and extreme response are greater than in deeper water.
- When sour service requires a material that has higher fatigue resistance than carbon steel.

## 2.5 Riser Component

This section describes main riser connectors and components commonly used in riser design. DNV-OS-F201 and API-RP-2RD are mainly used for reference. In order to hold riser stable and fulfill design criteria, critical locations of riser are equipped with several components that have the ability to provide sufficient leakage tightness, fatigue resistance and structural resistance for all related conditions (DNV, 2010a).

### 2.5.1 Flex joint

The flex joints are often used as the interface between the riser and the upper termination point. The flex joint provides flexibility to accommodate motion between host platform and the riser. The flex joints are also used to allow rotational deflections in risers without yielding large torsional moments near the top-end termination of the riser (API, 2006). Flex joint can be modeled as a linear spring with appropriate rotational stiffness properties.

This spring is important for fatigue performances in the hang-off area since the flex joint rotational stiffness contributes to riser fatigue response. For deep water application, the design of the flex joint will consider the effect of top tension ranges of the riser for fatigue purpose (Bai and Bai, 2010a). Thus, the range of top tension should be ascertained during the motion analysis statically and dynamically that the design limits of the flex joints are not exceeded.

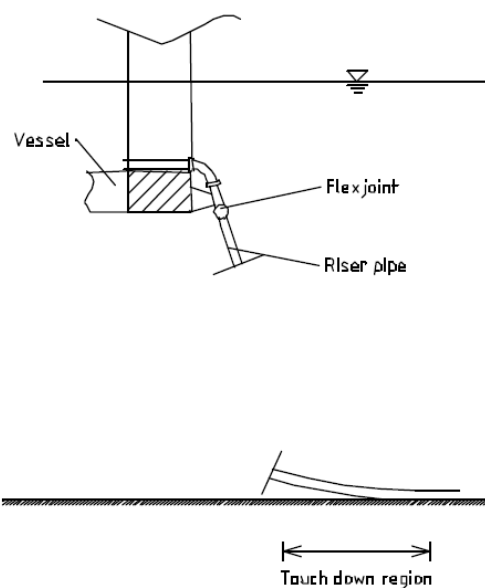


Figure 2-7 Flex Joint (DNV, 2010a)

## 2.5.2 Tapered stress joint

The tapered stress joint is used to accommodate a transition member to avoid excessive bending and fatigue issue between stiffer sections and less stiff sections of a riser. It contributes to reduce local bending stress and provide a means of distributing riser curvature arising from bending at either end (API, 2006). The main idea of tapered stress joint is through the use of a transition member with linearly different of stiffness where the bending stiffness at one end has a higher stiffness while the opposite end has lower stiffness (API, 2006). The idea can be accomplished by varying the wall thickness of the transition member linearly while maintaining a constant internal diameter of the riser, see Figure 2-8.

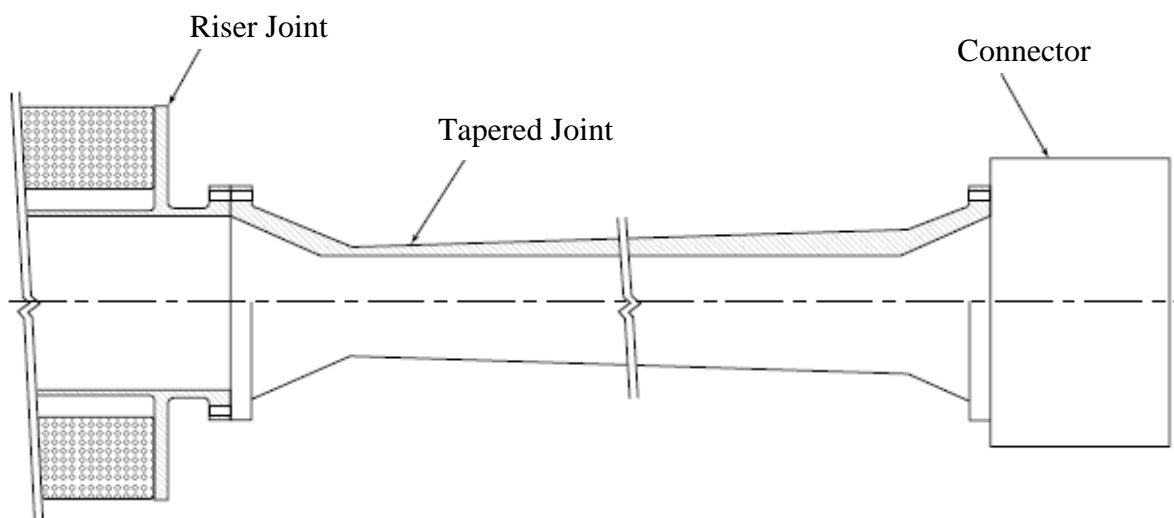


Figure 2-8 Tapered Joint (API, 2006)

## 2.5.3 Strakes and Fairings

The strong current creates regular shedding of vortices in the wake region of the downstream side of the flow. The shedding vortices induce vortex-induced vibrations (VIV) effect on the riser that might cause fatigue damage. The helical strakes and fairings are devices that are added along the suspended riser to suppress VIV effect. They can be installed to riser in critical segment length of the riser. The design of helical strakes and fairings are such that they act to decrease the vibration by controlling the flow pattern around the riser. Figure 2-9 shows the pictorial representation showing helical strakes and fairings.

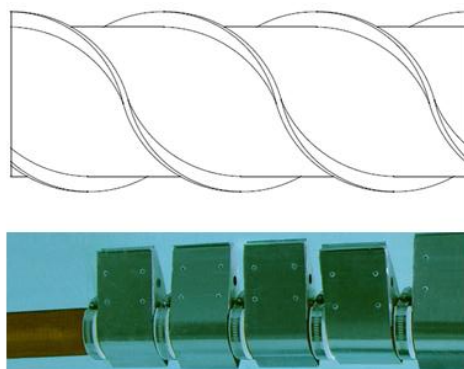


Figure 2-9 Strakes and Fairings (API, 2006) (Vivsolutions, 2015)

## 2.5.4 Buoyancy Module

The buoyancy modules are used to shape lazy wave configuration. These buoyancy modules are added along to some length of the riser to decouple the dynamic motion from floater and to decrease the top payload. The density of buoyancy module material is less than water density; thereby it provides a net upward force onto the riser. Balmoral offshore is one of the qualified suppliers which provide high quality of buoyancy modules. The densities and composition of the buoyancy modules should be based on operational requirements such as hydrostatic pressure, water ingress, riser diameter, etc.

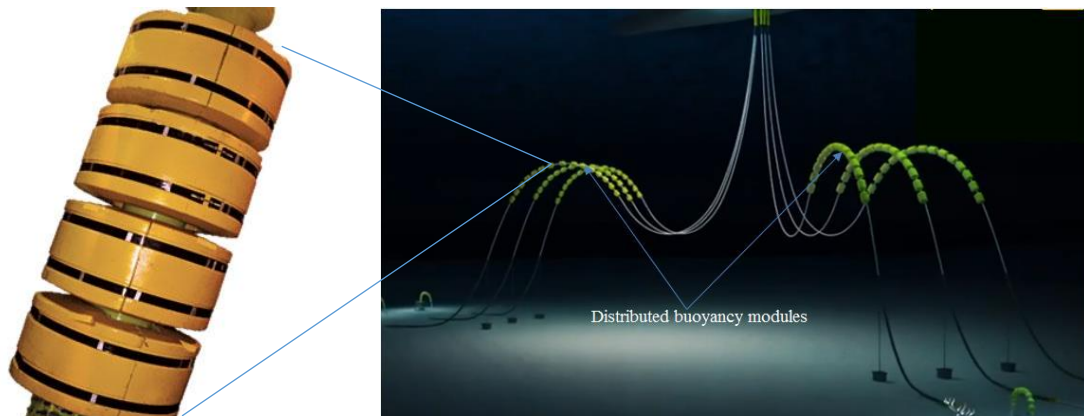


Figure 2-10 Buoyancy Modules (Balmoral, 2014)

## 2.5.5 Ballast modules

One of methods to add weight in the riser is by using the practiced ballast modules. These modules are obtainable in various dimensions and can be attached over riser per joint with 2000 kg weight at each specific interval of 12 m (Karunakaran et al, 2013). The installation of these modules is exactly like the installation of buoyancy modules. A typical ballast module is illustrated in Figure 2-11.



Figure 2-11 Typical Ballast Module (Balmoral, 2014)

The ballast modules consist of following component:

- Internal clamp;
- Split ballast element;
- Tensioning assembly and
- Fastening system.

## 2.6 Risers Challenges

The designing riser system includes a number of considerations, e.g. water depth, pressure, temperature, floater motions, thermal management, hydraulic issues, etc. In this study, the riser systems are encountered with deep water and harsh environment as challenges. Harsh environments might increase the complexity of riser design (Karunakaran et al., 2005). Both challenges are considered to be the most challenging combination for riser system design. Therefore, Section 2.6 will discuss those challenges with respect to riser design.

### 2.6.1 Deep Water Challenges

#### 2.6.1.1 Riser Weight

The suspended length of the riser is getting longer proportionally with deep water, hence risers weight increases proportionally with water depth as well. This leads to higher top tension force at the host platform (floater), which is usually referred to as top payload. The top payload is one of the important keys in the host platform type selection. The host platform capacity has to be able to accommodate the maximum top payload from a large number of riser systems and mooring systems.

#### 2.6.1.2 Riser Sizing

The internal diameter and wall thickness are the main parameters of riser size. The consideration of internal diameter selection is related to hydraulic purposes. Meanwhile, the wall thickness selection is related to capacity to withstand external and internal pressure of the riser. The external pressure is mainly driven from hydrostatic pressure of sea water whilst the internal pressure is mainly driven from internal fluid.

The wall thickness of the riser should be selected to accommodate external pressure and internal pressure to avoid collapse and bursting, respectively. The concern is also given in installation stage. During the installation stage, the riser is commonly in empty condition. The empty riser should have adequate resistance against the collapse failure due to external hydrostatic pressure.

#### 2.6.1.3 Spreading Area

The riser systems require large radial spreading area in deep water. As the water depth increases, the risers need to be laid down in a larger area to achieve the proper configurations. For steel catenary riser (SCR) configuration, typical radial spread is 1.0 to 1.5 times the water depth. Consequently, if the water depth is 1000 m, there should be spreading area of 1500 m for riser configuration. This spreading issue should be considered when selecting the riser configuration and positioning (Howells & Hatton, 1997).

#### 2.6.1.4 Current

In deep water, the current effects become significant, as the suspended riser becomes long and vulnerable to vortex induced vibration (VIV), especially for large current speed in deep water. The VIV effect may give a significant contribution to fatigue damage on the risers. This leads to the requirement for VIV suppression such as helical strakes or fairings along the critical area of the riser.

### **2.6.1.5 Installation**

During the installation period, the empty risers should have an adequate wall thickness to provide collapse and local buckling resistance against external hydrostatic pressure. Different technologies have been developed to install offshore risers in deep water. The risers can be installed when the environmental condition allows relatively small motions of installation vessel. Generally, several installation methods are J-Lay, S-Lay and reel-lay. These three installation methods require adequate capacity of the installation vessels.

The installation vessel should be chosen accordingly with the requirement of such high tensioning system of risers. Up to date, the maximum tension limit is around 1000 Te for tensioning systems of installation vessels. Most installation vessels have capacities of over 500 Te (Burgess and Lim, 2006).

The installation window in deep water is also another aspect that needs to be considered for riser installation. A greater water depth requires the longer riser length to be installed, and consequently long installation period is needed. Installation challenges in deep water can be summarized as follows:

- Limited number of installation vessels;
- Limited installation windows;
- High installation costs;
- Complex installation methods.

## **2.6.2 Harsh Environment Challenges**

### **2.6.2.1 Dynamic motion of FPS**

The large motions of the FPS due to combination of waves, currents, and winds become great challenges in designing riser system in harsh environmental conditions. The dynamic motions of the FPS contribute to buckling and fatigue issues in the touchdown area (Karunakaran et al., 2005). In addition, fatigue performance in the hang-off area is also influenced by dynamic motion of FPS.

The selection of Floating Production System (FPS) concept is highly dependent on the riser design. The riser arrangements should have the capability to accommodate the low frequency (LF) and wave frequency (WF) motion of FPS responses. Moreover, in the harsh environment, the FPS motion may have larger offsets. The SCR configuration should then be arranged such that it can cope with FPS motion.

### **2.6.2.2 Fatigue performance**

The main challenge for the design of the SCR in harsh environments is fatigue in the hang-off area and touchdown area (Karunakaran et al., 2013). Moreover, the strong current may generate vortex shedding in the downstream side of the riser; hence, it contributes to fatigue damage onto the riser.

### **2.6.2.3 Installation**

In mild environments, riser installation can be performed in almost all months of a year thus suitable weather windows are very large. However, in harsh environments, riser installation



can only be performed in a relatively calm day. This fact leads to more challenge of riser installation as suitable weather windows are very small in harsh environment. The harsh environment limits the installation window; hence, the installation window has to deal with more uncertainty. The installation window is usually limited to summer time and some days in spring time when the air pressures and temperatures are constant.

## 2.7 Selected Riser for Thesis Work

The selected riser for thesis work is the Steel Catenary Riser (SCR) with following configuration:

- Conventional SCR,
- Weight Distributed SCR (WDSCR) and
- Steel Lazy Wave Riser (SLWR)

This section will present the description of each selected riser configuration of SCR.

### 2.7.1 Conventional SCR

The conventional SCR is a simple hanging-free configuration. The name “catenary” simply originates from the catenary shape of the riser that is due to its self-weight. This is a simple drape starting at the floater and curving through nearly 90 degrees to a horizontal orientation on the seabed. The SCR is self-compensated for the heave movement without heave compensation. The SCR is installed using an offshore pipe-lay vessel. The steel catenary risers (SCRs) concept is a promising solution for future deep water applications. SCR is known to be economical in terms of both installation and construction. Compared to the flexible risers, the SCR has emerged to be easier and cheaper to produce.

The SCR also has high resistance to the internal and external pressure to operate in even deep water due to the material. The material of steel may also be modified to different alloys for higher strength capacity. The SCR can be mounted in a size that is long enough from the floater to the seabed. A flex joint is installed at the top-end of the riser at the host platform to accommodate rotation and deflection.

On the seabed, the riser system does not require a special connection bottom system. Some length of the pipe is required on the seabed before any seabed termination/connection. This length allows for any movement caused by vessel offset. Alternatively, the riser can extend to become part of the subsea pipeline. This reduces the complexity and cost, so that the SCR can be regarded as a simple riser system.

The description of the SCR is presented in Figure 2-12. The design, fabrication, welding, and installation challenges of the SCR are mainly related to the high top tensions, high pressure, high temperature and sour service. The first SCR was initially implemented on Auger development in the GoM in 1994. Since then, a number of SCR has been installed in some oil and gas development fields such as gum, and Brazil. In 2004, SCR is firstly installed in West Africa in which conjunction to an FPSO on the Bonga field offshore Nigeria (Alliot et al., 2005). At the late of 2008, more than 100 SCRs have been installed in deep water worldwide with the majority installed in the Gulf Of Mexico (Bai and Bai, 2010b).

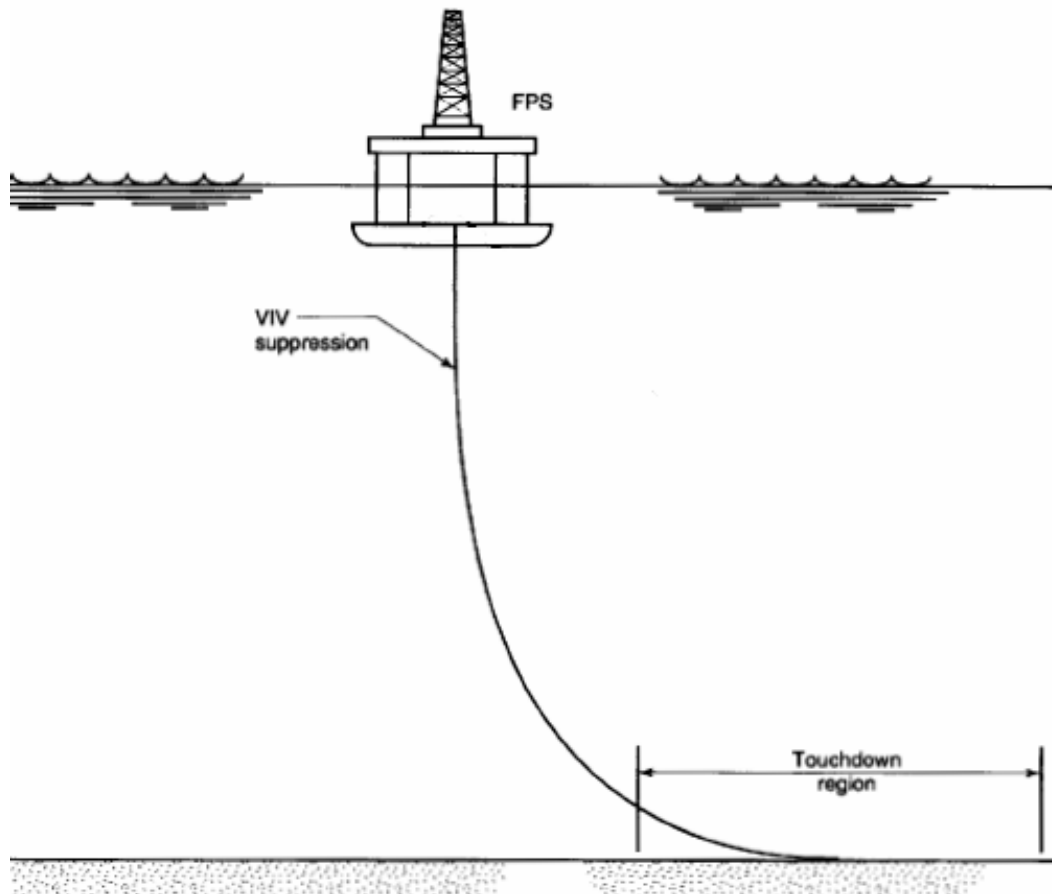


Figure 2-12 Rigid SCR Hanging-Free Configuration (API, 2006)

However, for deep water applications and harsh environments where vessel motions are severe, it is difficult for conventional catenary riser configuration to meet both strength and fatigue design criteria, especially in the touchdown area. The problems that might occur on the SCR include sensitivity to the waves, current and dynamic motion of the floater. The large vessel offset due to harsh environment results in the change of suspended length of riser and thereby changes the TDP position as well. Together with heave motion of the floater, the riser is therefore lifted off and laid down onto the seabed continuously (Bai and Bai, 2010b).

Hence, the touchdown area becomes critical to fatigue and buckling issue for steel catenary risers. Soil-riser interaction and heave motion of floater are the main contribution to fatigue damage on the riser. In addition, the current might also contribute to fatigue damage along the suspended length of the riser. The vortex was introduced around the riser as current is obstructed by riser body. This can be anticipated by using VIV suppression in the suspended length of riser as described in Figure 2-12.

As the development is being progressed, the conventional SCR concepts have been developed with some modifications such that the SCR can be used in harsh environment and deep water. The optimization studies of SCR configuration are discussed in this thesis to present the feasibility study of SCR configuration and its derivatives to cope with the large vessel motion. The next section will discuss the further development of the conventional SCR.

## 2.7.2 Weight Distributed SCR

One of the developments of conventional SCR is weight distributed SCR. Both strength and fatigue requirement criteria of SCR design can be successfully solved by varying the weight along the suspended risers with the heavy modules. One study, from Karunakaran et al. (2013), shows that by varying heavy and light coating along the suspended risers, SCR strength and fatigue performance can be upgraded expressively. The concept involves varying weight along the suspended riser, with the lightest possible cross-section in the touchdown area (TDA) and heaviest possible cross-section at the bottom of the straight section of the riser. By using a heavy cross-section at the straight part of the riser, the stresses around the TDP is significantly reduced. However, this may also increase the vessel payload and the dynamic axial stress.

The SCR with weighted sections, which improve SCR response at critical area, is a potential alternative solution for the application of SCRs in deep water and harsh environment (Foyt et al., 2007). According to Karunakaran et al. (2013), the distribution weight can be achieved by using well qualified ballast modules that are attached at certain sections of SCR. The ballast module is shown in Figure 2-11. This weight distributed SCR concept can be fabricated and installed in the same way as traditional SCRs. Figure 2-13 shows the schematic of weight distributed SCR.

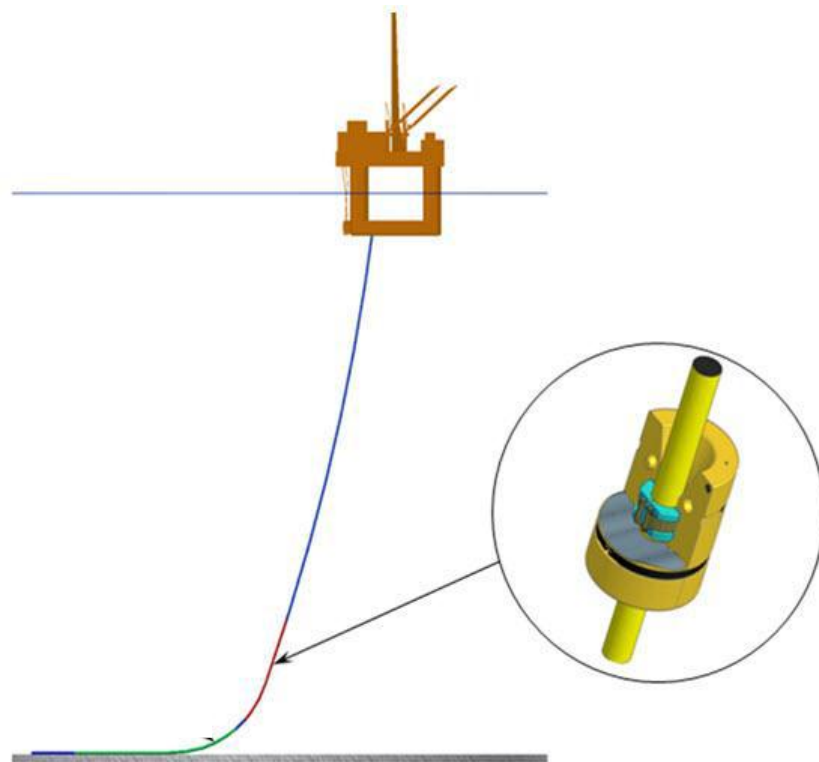


Figure 2-13 Weight Distributed SCR (Karunakaran and Legras, 2013)

## 2.7.3 Steel Lazy Wave Riser

The SLWR is the SCR with buoyancy modules added to the middle section of the riser to decouple the vessel motions from the TDP region, and to reduce the vessel payload. This configuration is more compliant than the conventional SCR. The compliant configuration

allows significantly large horizontal offset of floater compared to conventional SCR without significant change in TDP position. The less the TDP moves, the more efficiency of de-coupled system is achieved.

The SLWR has therefore significantly less TDP movement than the SCR, and thereby improve the riser strength and fatigue performance (Senra et al, 2011). The SLWR approaches smoothly to the seabed in a horizontal manner. However, the extra buoyancy introduces additional bending stress at the sag-bend and the hog-bend region. High static bending moment at the sag-bend and the hog-bend are design issues for lazy wave configurations (Karunakaran et al., 1996). Therefore, it is important to ensure low curvatures at the sag-bend and hog-bend.

Moreover, the buoyancy modules are expensive and difficult to install. Consequently, SLWR configuration has to be optimized in tradeoff to minimize buoyancy modules while maximize riser performance as well. This fact attracts continuous development of SLWR to optimize such efficient configuration of “lazy wave” that meets the riser performance target and saves development costs. The illustration of SLWR configuration in conjunction with FPSO is shown in Figure 2-14.

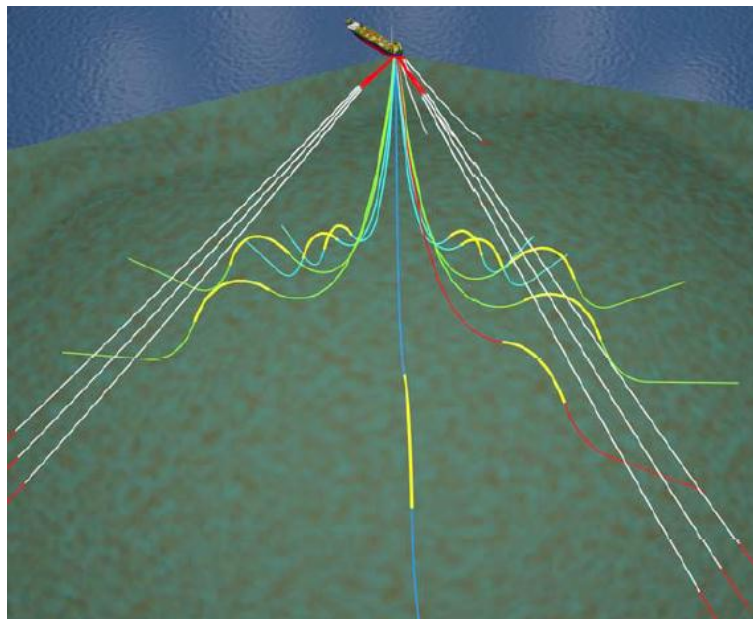


Figure 2-14 Typical SLWR Configuration in Conjunction with FPSO (Chen and Cao, 2013)

## Chapter 3. Design Code for Riser

### 3.1 Introduction

Risers are subjected to numerous loads that vary from the normal to accidental event. The risers should be designed based on accepted standards and regulations to withstand load effects during its service life. This can be achieved by taking into consideration the various design conditions that may involve throughout its expected lifetime. The minimum requirements for risers have to be established to meet criteria for construction, installation, commissioning, operation, maintenance, requalification, and abandonment.

The design is safe when the resistance is more than the specific minimum requirement for the given conditions. Selection of wall thickness sizing should be carried out using a design code taking into account for burst, collapse and buckling criteria. The riser should be designed in order to meet those criteria. The safety factor is applied to cover uncertainty and inaccuracy in the analysis of each stage of riser application. Thus, the safety factor is incorporated in design check. Design codes are distinguishable according to two fundamental design approaches as listed below.

- Working Stress Design (WSD) and
- Load and Resistance Factor Design (LRFD)

The WSD utilizes only one uniform safety factor to cover uncertainty and inaccuracy from expected responses and resistance for each limit state. Meanwhile, the LRFD uses various safety factors to cover uncertainty and inaccuracy from each specific response and resistance for each limit state. Design codes such as API, ISO, HSE, NPD, DNV and ABS are all examples of guidelines used when designing riser systems. The following are most commonly applicable codes for design of deep water risers (Kavanagh et al., 2003)

- API RP 2RD, “Design of Risers for Floating Production Systems (FPSs) and Tension-Leg Platforms (TLPs)”, 1998;
- API RP 1111, “Design, Construction, Operation, and Maintenance of Offshore Hydrocarbon Pipelines (Limit State Design)”, 3rd Edition 1999;
- ASME B31.4, “Pipeline Transportation Systems for Liquid Hydrocarbons and Other Liquids, Chapter IX – ‘Offshore Liquid Pipeline Systems’”, 1998 Edition;
- ASME B31.8, “Gas Transmission and Distribution Piping Systems”, Chapter VIII - "Offshore Gas Transmission", 1999 Edition;
- Offshore Standard DNV-OS-F201, Dynamic Risers 2010.

This chapter describes the LRFD and WSD method for good understanding of riser basis evaluation. The selection of the method will be concluded at the end of this chapter. The WSD method presented in this study is according to API-RP-2RD, while the LRFD method is according to DNV-OS-F201.

## 3.2 Design Principle

According to the functional requirement of the risers stated by API, the objective of riser system is to ensure the transportation of fluid safe, continuous and concurrent between seabed and host platform (floater). From that objective, riser systems are a part of a flow assurance chain. In order to accomplish the flow assurance purposes, the riser should be designed, fabricated, constructed, operated and maintained based on standardized design codes. This standard should consider safety philosophy related to human life, financial issues, public safety and protection of the environment. According to DNV, the integrity of a riser system is ensured to safety philosophy for various aspects as illustrated in Figure 3-1.

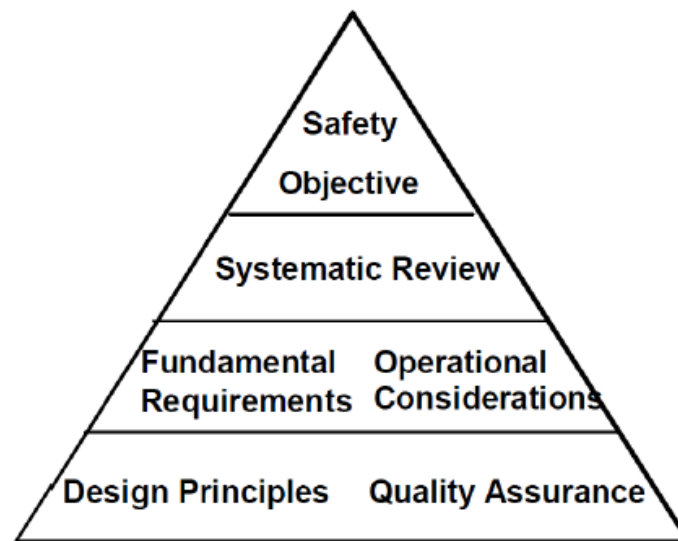


Figure 3-1 Safety Hierarchy (DNV, 2010a)

In order to attain that objective, any hazardous impact is subjected to be minimized or eliminated to be as low as reasonably practicable (ALARP Principle). A systematic assessment by using Quantitative Risk Analysis (QRA) may offer adequate design parameter to select a suitable safety class with respect to structural failure probability. Thus, the riser can be designed with different safety requirements based on the given conditions of the riser system.

DNV provides different safety requirements in respect to riser design, depending on the safety class to which the riser fits. The safety classes of riser system will be classified into one or more safety classes. According to DNV (2010a), the safety class of a riser depends on the following factors (DNV, 2010a).

- The hazard potential of the fluid in the riser, e.g. fluid category.
- The location of the part of the riser that is being designed.
- Whether the riser is in operation or temporary state.

DNV provides a classification of safety classes for the riser design based on the potential failure consequences. Table 3-1 presents the classification of safety classes which is discussed in DNV-OS-F201 section C204 (DNV, 2010a).

Table 3-1 Classification of Safety Class (DNV, 2010a)

Safety Class	Definition
Low	Where failure implies low risk of human injury and minor environmental and economic consequences.
Normal	For conditions where failure implies risk of human injury, significant environmental pollution or very high economic or political consequences.
High	For operating conditions where failure implies high risk of human injury, significant environmental pollution or very high economic or political consequences

### 3.3 WSD Code – API RP 2RD

This section addresses design guidelines with Working Stress Design (WSD) method for typical riser design in conjunction with the Floating Production Systems (FPS). The WSD method, as reflected in the previous section, is generally based on the principles of limiting stresses of riser under normal, extreme and accidental conditions. The WSD method accounts for uncertainty and inaccuracy with only a single safety factor. The criteria of riser failure mechanisms are discussed in this section including allowable stresses, allowable deflection, hydrostatic collapse, overall column buckling, fatigue/service life (API, 2006).

#### 3.3.1 Allowable Stresses

Based on API-RP-2RD section 3.4, structural design is based on an allowable stress approach that defines acceptability on the basis that the calculated stresses in the riser are below allowable stresses for all applicable loading conditions. With such an approach, the riser design should be arranged to resist external and internal loads. Guidelines consider three principal stresses to be established in extreme condition.

The riser is considered to be a plain pipe with axisymmetric geometry. The three principal stresses for plain pipe are in the axial, hoop and radial directions (API, 2006). Meanwhile, torsion and transverse shear are insignificant for plain round pipe. The three principal stresses are calculated at all critical locations in the riser to form a combined stress using the von Mises yield criterion defined by the following equation:

$$\sigma_e = \frac{1}{\sqrt{2}} \sqrt{(\sigma_1 - \sigma_2)^2 + (\sigma_2 - \sigma_3)^2 + (\sigma_3 - \sigma_1)^2} \quad (3.1)$$

Where

$\sigma_e$  = Von Mises Equivalent Stress

$\sigma_1, \sigma_2, \sigma_3$  = Principal Stresses

According to API (2006) section 5.2.3, the equivalent von Mises stresses should be less than allowable stresses as shown in following inequalities:

$$(\sigma_p)_e < C_f \sigma_a \quad (3.2)$$

Where

$(\sigma_p)_e$  = Equivalent von Mises stress where the principal stresses consist of primary membrane stresses.

$\sigma_a = C_a \sigma_y$  = basic allowable combined stress.

$C_a$  = allowable stress factor,  $C_a = 2/3$

$\sigma_y$  = material minimum yield strength

$C_f$  = design case factor, refer to Table 3-2; this factor is calculated by considering load category, environmental condition, and pressure (API, 2006).

Table 3-2 Design Matrix for Rigid Risers (API, 2006)

Design Case	Load Category	Environmental Condition	Pressure	Reduced Tensioner Capacity or One Mooring Line Broken	Cf
1	Operating	Maximum Operating	Design	No	1
2	Extreme	Extreme	Design	No	1.2
3	Extreme	Maximum Operating	Extreme	No	1.2
4	Extreme	Maximum Operating	Design	Yes	1.2
5	Temporary	Temporary	Associated	No	1.2
6	Test	Maximum Operating	Test	No	1.35
7	Survival	Survival	Associated	No	1.5
8	Survival	Extreme	Associated	Yes	1.5

### 3.3.2 Allowable Deflection

The deflections of the riser should be limited to avoid excessive bending stresses. Even though riser stress and bending radius are within the allowable limit, large riser curvatures may overstress tubing or other parts constrained to move with the riser body (API, 2006). In addition, riser deflections should also be controlled to prevent multiple risers from obstructing other equipment or components.

### 3.3.3 Hydrostatic Collapse

#### 3.3.3.1 Collapse Pressure

In deep water application, external pressure from hydrostatic pressure is high. Excessive external pressure may result in collapse failure. Consequently, the riser should be able to withstand external pressures experienced at any period during installation or operation. The maximum allowable external design pressure ( $P_a$ ) should be less than the predicted collapse pressure ( $P_c$ ) times the design factor ( $D_f$ ). The calculation can be expressed in following equation.

$$P_a \leq D_f P_c \quad (3.3)$$

Where

$P_a$  = External Design Pressure

$P_c$  = Predicted Design Collapse Pressure

$D_f$  = 0.75 for seamless or Electric Resistance Welded (ERW) API pipe.



= 0.60 for (DSAW) internally cold expanded API pipe.

### 3.3.3.2 Collapse Propagation

Propagation buckling is a deformation of the cross section of pipe that extends and propagates along the pipe. Propagation buckling is normally caused by difference of external and internal hydrostatic pressure. The principle of propagation of buckling is the pressure that may cause the propagation buckle (buckle initiation pressure) whose value is greater than the resistance to prevent the propagation of the buckle (collapse pressure). This commonly applies to pipes that have uniform properties along the pipeline. However, propagation buckling will not happen if there is no local buckling happens.

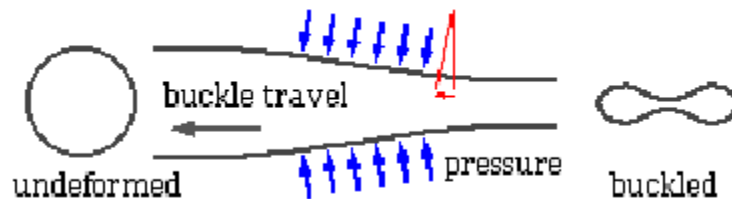


Figure 3-2 Propagation Buckling on the Pipe (Tawekal, 2010)

In order to mitigate collapse propagation, features such as buckle arrestors can be incorporated into the design to limit the propagation of a propagating failure at critical region. In order to avoid propagation buckling, the design pressure differential ( $P_d$ ) from external and internal pressure should be less than the predicted propagation pressure differential ( $P_p$ ) times the design factor ( $D_p$ ). The design criterion to prevent collapse propagation is provided in the following equation.

$$P_d < D_p P_p \quad (3.4)$$

Where

$P_d$  = design pressure differential

$P_p$  = predicted propagation pressure differential

$D_p$  = design factor = 0.72

These criteria are applicable for riser with metal tubular that used in deep water application.

### 3.3.4 Overall Column Buckling

The overall column buckling is induced by excessive negative effective tension along the entire riser lengths. The negative effective tension is usually referred to as compression. The consequences of excessive compression are excessive bending moment and excessive curvature at critical locations. Compression may cause buckling on the riser. The overall column buckling can be prevented by providing tension at the top end termination of the riser.

### 3.3.5 Fatigue/Service Life

The design fatigue life of riser is defined as the life predicted by cumulative fatigue damage ratio calculations throughout its design life. The cumulative fatigue damage is calculated with

associated safety factor. The selected value of the safety factor is dependent on the pollution, risk and the difficulty of inspection. At the location, where the risk and difficulty of inspection are high, the safety factor of 10 is considered. At the location, where the risk and difficulty of inspection are low, the safety factor of 3 is considered. In order to satisfy fatigue criteria, the following equation should be satisfied:

$$\sum_i SF_i D_i < 1.0 \quad (3.5)$$

Where

$D_i$  = fatigue damage ratio

$SF_i$  = associated safety factor

### 3.4 LRFD Code – DNV-OS-F201

This section will discuss the fundamental principle of Load and Resistance Factored Design (LRFD) method according to DNV-OS-F201. The LRFD method is also referred to as partial safety factor method. DNV-OS-F201 states that the fundamental principle of LRFD method considers some limit states to ensure the riser design is safe throughout its service life. The limit states are associated with some of the failure modes including bursting, collapse and propagation buckling. Based on DNV-OS-F201, the general descriptions of limit states are grouped into following four categories:

- **Ultimate Limit State (ULS)**  
This limit state requires that the riser must be able to remain intact and avoid rupture over the service period. For operating condition, this limit state corresponds to the maximum resistance to applied loads with  $10^{-2}$  annual exceedence probability;
- **Accidental Limit State (ALS)**  
This limit state requires that the riser must be able to remain intact and avoid rupture due to accidental loads (e.g. infrequent loads);
- **Serviceability Limit State (SLS)**  
This limit state requires that the riser must be able to remain in service and operate properly. This limit state corresponds to criteria limiting or governing the normal operation (functional use) of the riser;
- **Fatigue Limit State (FLS)**  
This limit state requires that the riser must be able to remain fit to operate during service life from accumulated excessive fatigue crack growth or damage under cyclic loading.

The acceptance criteria are calibrated using a reliability-based methodology for each particular safety class. The sum of applicable load factor effects incorporated with various load effect factors is compared to the resistance factor. Based on DNV-OS-F201, the general LRFD safety format can be expressed as follows.

$$S_d (S_p; \gamma_F S_F; \gamma_E S_E; \gamma_A S_A) \leq \frac{R_K}{\gamma_{SC} \cdot \gamma_m \cdot \gamma_c} \quad (3.6)$$

Where

$S_d$  = Sum of design load factor

$S_p$  = Pressure loads

$S_F$  = Load effect from functional loads (vector or scalar)

$S_E$  = Load effect from environmental loads (vector or scalar)

$S_A$  = Load effect from accidental loads (vector or scalar)

$\gamma_F$  = Load effect factor for functional loads (vector or scalar)

$\gamma_E$  = Load effect factor for environmental loads

$\gamma_A$  = Load effect factor for accidental loads

$\gamma_{SC}$  = Resistance factor to take into account the safety class

$\gamma_m$  = Resistance factor to take into account for material and resistance uncertainties

$\gamma_c$  = Resistance factor to take into account for special conditions

$R_K$  = Generalized resistance (vector or scalar)

### 3.4.1 Design Loads

In the LRFD method, the classification of loads is distinguished in order to cope with specific uncertainties of a particular source in a rational way. The classification loads used in LRFD are as follows:

- Pressure load effect (P);
- Functional load effects (F);
- Environmental load effects (E) and
- Accidental load effects (A).

The examples of the each load group are presented in the following table (DNV, 2010a).

Table 3-3 Examples of Categorization of loads<sup>1)</sup> (DNV, 2010a)

<i>F</i> -loads	<i>E</i> -loads	<i>P</i> -loads <sup>7)</sup>
Weight and buoyancy <sup>6)</sup> of riser, tubing, coatings <sup>6)</sup> , marine growth <sup>2)</sup> , anodes, buoyancy modules, contents and attachments Weight of internal fluid Applied tension for top-tension risers Installation induced residual loads or pre-stressing Pre-load of connectors Applied displacements and guidance loads, including active positioning of support floater Thermal loads Soil pressure on buried risers Differential settlements Loads from drilling operations Construction loads and loads caused by tools	Waves Internal waves and other effects due to differences in water density. Current Earthquake <sup>4)</sup> Ice <sup>3)</sup> Floater motions induced by wind, waves and current, i.e.: — Mean offset including steady wave drift, wind and current forces — Wave frequency motions — Low frequency motions	External hydrostatic pressure Internal fluid pressure: hydrostatic, static and dynamic <sup>5)</sup> contributions, as relevant Water Levels
<b>NOTES</b> 1) Accidental loads, both size and frequency, for a specific riser and floater may be defined by a risk analysis. 2) For temporary risers, marine growth can often be neglected due to the limited duration of planned operations. 3) Ice effects shall be taken into account in areas where ice may develop or drift. 4) Earthquake load effects shall be considered in the riser design for regions considered being seismically active. 5) Slugs and pressure surges may introduce global load effects for compliant configurations. 6) Includes also absorbed water. 7) Possible dynamic load effects from P-loads and F-loads shall be treated as E-loads, e.g. slug flow.		

The summations of the load effects for each category are established by multiplying the corresponding load effect safety factor. Specific calculation is presented below for bending moment and effective tension.

$$M_d = \gamma_F M_F + \gamma_E M_E + \gamma_A M_A \quad (3.7)$$

Where

$M_d$  = Bending moment design

$M_F$  = Bending moment from functional loads

$M_d$  = Bending moment from environmental loads

$M_d$  = Bending moment from accidental loads

Design effective tension for functional, accidental and environmental induced load effects

$$T_{ed} = \gamma_F T_{eF} + \gamma_E T_{eE} + \gamma_A T_{eA} \quad (3.8)$$

Where

$T_{ed}$  = Effective tension design

$T_{eF}$  = Effective tension from functional loads

$T_{eE}$  = Effective tension from environmental loads

$T_{eA}$  = Effective tension from accidental loads

Where the effective tension ( $T_e$ ) is given as follows:

$$T_e = T_w - P_i A_i + P_e A_e \quad (3.9)$$

Where

$T_e$  = Effective tension

$T_w$  = True wall tension (i.e. axial stress resultant found by integrating axial stress over the cross-sectional area)

$P_i$  = Internal local pressure

$A_i$  = External local pressure

$P_e$  = Internal cross-sectional area

$A_e$  = Internal cross-sectional area

As shown in the above formulas, each particular load is multiplied by corresponding load effect safety factor. DNV suggests load effect factors for all limit states design. The applicable load effect factors are given in Table 3-4 for all limit states and safety class.

Table 3-4 Load Effect Factor (DNV, 2010a)

Limit State	Functional load effect	Environmental load effect	Accidental load effect
	$\gamma_F$	$\gamma_E$	$\gamma_A$
<b>ULS</b>	1.1	1.3	NA
<b>FLS</b>	1	1	NA
<b>SLS</b>	1	1	1
<b>ALS</b>	1	1	1

DNV suggests the value of reduced functional load ( $\gamma_{RF}$ ) of 0.91 and the value of reduced environmental load ( $\gamma_{RE}$ ) of 0.77 for ultimate limit states.

### 3.4.2 Resistances

The resistance factors are also applied to design strength check. DNV suggests applying resistance factors as follows:

- Safety class factor ( $\gamma_{SC}$ ) is composed of resistance depending on safety class for failure consequences (refer to Table 3-5).
- Material resistance factor ( $\gamma_m$ ) is incorporated for material and resistance uncertainties with relevant limit states (refer to Table 3-6).
- Condition factor ( $\gamma_C$ ) is accounted for special conditions. The particular condition is specified explicitly at all corresponding limit states (refer to Table 3-7)

Table 3-5 Safety Class Resistance Factor

Safety Class resistance factor ( $\gamma_{sc}$ )		
Low	Normal	High
1.04	1.14	1.26

Table 3-6 Material Resistance Factor

Material resistance factor ( $\gamma_m$ )	
ULS & ALS	SLS & FLS
1.15	1

Table 3-7 Simplified Design Check for Accidental Limit States

Condition factor ( $\gamma_C$ )			
Prob. of occurrence	Safety class low	Safety class normal	Safety class high
$>10^{-2}$	Accidental loads may be regarded similar to environmental loads and may be evaluated similar to ULS design check		
$10^{-2}-10^{-3}$	To be evaluated on a case by case basis		
$10^{-3}-10^{-4}$	$\gamma_C=1.0$	$\gamma_C=1.0$	$\gamma_C=1.0$
$10^{-4}-10^{-5}$	Accidental loads or events may be disregarded	$\gamma_C=0.9$	$\gamma_C=0.9$
$10^{-5}-10^{-6}$		$\gamma_C=0.8$	
$<10^{-6}$			

The calculation of the wall thickness of the riser should consider the possibilities that the nominal wall thickness may be reduced. From this consideration, the fabrication allowance and corrosion allowance are added in final wall thickness of the riser. The DNV suggests using a minimum wall thickness so-called  $t_1$  for bursting and collapse failure modes.

On the other hand, for the failure likely to occur due to external loading, DNV suggests using minimum wall thickness so-called  $t_2$  to be calculated by only considering the corrosion allowance. The wall thickness calculations for the riser design are given in equations (3.10) and (3.11).

$$t_1 = t_{nom} - t_{fab} - t_{corr} \quad (3.10)$$

$$t_2 = t_{nom} - t_{corr} \quad (3.11)$$

Where

$t_{nom}$  = Specified (nominal) pipe wall thickness

$t_{fab}$  = Fabrication allowance

$t_{corr}$  = Corrosion allowance

### 3.4.3 Material Strength

The material strength can be changed over time, temperature and some practical consideration. Consequently, the material strength, yield and tensile strength, will be given in following formula.

$$f_y = (SMYS - f_{y,temp}) \cdot \alpha_u$$

$$f_u = (SMTS - f_{u,temp}) \cdot \alpha_u$$

Where

SMYS = specified minimum yield stress at room temperature

SMTS = specified minimum tensile stress at room temperature

$F_{y,temp}$  = temperature de-rating factor for yield stress, DNV recommends de-rating temperature effects of the yield strength for C-Mn steel, refer to Figure 3-3.

$F_{u,temp}$  = temperature de-rating factor for tensile stress

$\alpha_u$  = material strength factor, refer to Table 3-8

Table 3-8 Material strength factor (DNV, 2010a)

Normal	Supplementary requirement U
0.96	1

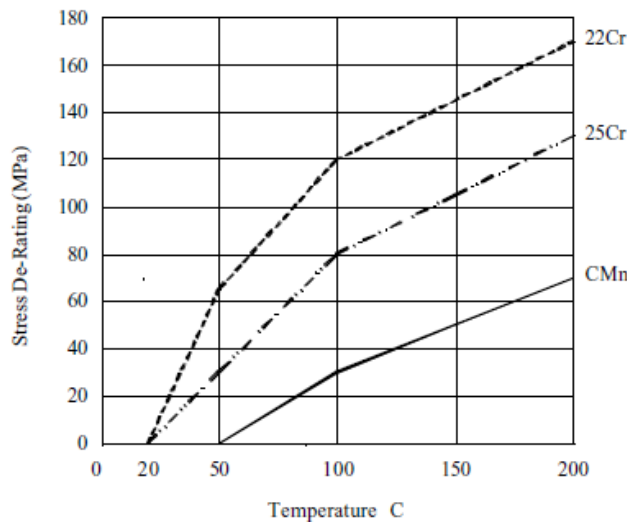


Figure 3-3 De-rating value (DNV, 2010a)

### 3.4.4 Ultimate Limit States

The ultimate limit state (ULS) design requires that the risers be able to withstand the loads from the maximum load combinations for an annual exceedence probability of  $10^{-2}$ . The consequence of failure of meeting this limit states are the collapse of the riser structurally. DNV suggests typical failure modes for this limit states that need to be considered in the design. The typical failure modes are as follows:

- Bursting
- Hoop Buckling (collapse)
- Propagating Buckling
- Gross plastic deformation, local buckling and hoop buckling
- Unstable fracture and gross plastic deformation
- Liquid tightness
- Global buckling

#### 3.4.4.1 Bursting

A riser should be designed to transport fluid without bursting. Each riser must undergo checks on burst pressure from the bottom-end connection to top-end connection. The burst resistance should be designed to cope with the local differential pressure of internal pressure and external pressure, which also known as hoop stress. The maximum internal pressure and minimum external pressure might be located at the top-end, since at that location the external pressure is minimal and there is internal pressure. Pipe members subjected to internal overpressure will be designed to meet the following expression at all cross sections.

$$(p_{li} - p_e) \leq \frac{p_b(t)}{\gamma_m \cdot \gamma_{SC}} \quad (3.12)$$

Where

- $t$  = Pipe wall thickness  
 $\gamma_{SC}$  = Safety class factor, refer to Table 3-5  
 $\gamma_m$  = Material resistance factor, refer to Table 3-6  
 $p_{li}$  = Local incidental pressure  
 $p_e$  = External pressure  
 $f_y$  = Yield strength  
 $f_u$  = Tensile strength  
 $p_b$  = Burst resistance

$P_b$  is the minimum burst resistance required to prevent riser from bursting. The actual burst resistance is dependent on the riser material such as yielding limit and tensile limit of the riser. The actual  $P_b$  resistance value of pipe is determined from the minimum value of the following two equations.

$$p_{b\_yield}(t) = \frac{2}{\sqrt{3}} \frac{2t_1}{D-t} \cdot f_y \quad (3.13)$$

$$p_{b\_tensile}(t) = \frac{2}{\sqrt{3}} \frac{2t_1}{D-t} \cdot \frac{f_u}{1.15} \quad (3.14)$$

Where



$D$  = Outer diameter of pipe

$t_1$  = Minimum wall thickness, refer to equation (3.10)

The local incidental pressure ( $p_{li}$ ) is the maximum expected internal pressure with a low annual exceedence probability. Normally, the incidental surface pressure is taken 10% greater than the design pressure ( $p_d$ ).

$$p_{li} = p_{ld} + 0.1 \cdot p_d \quad (3.15)$$

$$p_{ld} = p_d + \rho_i \cdot g \cdot h \quad (3.16)$$

Where

$p_{ld}$  = Local internal design pressure

$p_d$  = Design pressure, the maximum surface pressure during normal operations

$\rho_i$  = Internal fluid density

$g$  = Gravity acceleration

$h$  = Height difference between the actual location and the internal pressure reference point

The minimum required wall thickness for riser without allowance of fabrication and corrosion is given below.

$$t_1 = \frac{D}{\frac{4}{\sqrt{3}} \cdot \frac{\min(f_y; \frac{f_u}{1.15})}{\gamma_m \cdot \gamma_{SC}} \cdot (p_{li} - p_e)} + 1 \quad (3.17)$$

Hence the final wall thickness is defined by adding fabrication allowance and corrosion allowance into the wall thickness.

$$t_{nom} = t_1 + t_{fab} + t_{corr} \quad (3.18)$$

Where

$t_{nom}$  = Final (nominal) pipe wall thickness

$t_{fab}$  = Fabrication allowance

$t_{corr}$  = Corrosion allowance

#### 3.4.4.2 System Hoop Buckling (Collapse)

If the external pressure is dominant compared to internal pressure, the wall thickness selection of the pipe will be governed by external pressure. The pipe should be designed to withstand collapse from the external pressure. The maximum external force is located at the bottom section of the riser. DNV suggests selecting the wall thickness of collapse criteria with respect to the local differential pressure of external pressure and internal pressure. Pipe member therefore will be designed to meet the following conditions.

$$(p_{li} - p_e) \leq \frac{P_c(t)}{\gamma_m \cdot \gamma_{SC}} \quad (3.19)$$

Where

$p_e$  = External pressure

$p_{min}$  = Minimum internal pressure

$p_c$  = Hoop buckling resistance, which is given by

$$(P_c(t) - P_{el}(t)) \cdot (P_c^2(t) - P_p^2(t)) = P_c(t) \cdot P_{el}(t) \cdot P_p(t) \cdot f_o \cdot \frac{D}{t} \quad (3.20)$$

Where

$$f_o = \frac{D_{max} - D_{min}}{D} \quad (3.21)$$

$f_o$  = The initial ovality

$p_{el}$  = Elastic collapse pressure (instability) of pipe, which is given by:

$$P_{el}(t) = \frac{2E \left( \frac{t}{D} \right)^3}{1 - \nu^2} \quad (3.22)$$

$p_p$  = Plastic collapse pressure

$$P_p = 2 \cdot \frac{t}{D} \cdot f_y \cdot \alpha_{fab} \quad (3.23)$$

$\alpha_{fab}$  = Fabrication factor, see Table 3-9

Table 3-9 Fabrication Factor (DNV, 2010a)

Tensile strength or seamless pipe	Compressive strength for welded pipe	
	UOE	UO/TRB
1	0.85	0.925

### 3.4.4.3 Propagating Buckling

A riser should be designed to be able to prevent from propagation of buckling. This failure mode is initiated by local buckle. The local buckle will propagate until external pressure drops due to change in pipe properties. This criterion is to ensure that a possible local buckle remains local and does not yield to the collapse of adjoining pipe sections. Therefore, the propagating buckling check is required as follows:

$$(P_e - P_{min}) \leq \frac{P_{pr}}{\gamma_c \gamma_m \gamma_{SC}} \quad (3.24)$$

$$P_{pr} = 35 \cdot f_y \cdot \alpha_{fab} \left( \frac{t_2}{D} \right)^{2.5} \quad (3.25)$$

Where

$t_2$  = Minimum wall thickness, refer to equation (3.11)

$\gamma_C$  = Special condition factor for buckle propagation. The value is equal to 1.0 if no propagation factor is allowed or 0.9 if buckle is allowed in a short distance.

$p_{pr}$  = Propagation buckling resistance

By solving the equation, Hence the final wall thickness is obtained by adding and corrosion allowance into the wall thickness

$$t_{nom} = t_2 + t_{corr} \quad (3.26)$$

Where

$t_{nom}$  = Final (nominal) pipe wall thickness

$t_{corr}$  = Corrosion allowance

As seen in the equation, the propagation buckle resistance is only dependent on the yield strength of the material, fabrication factor and  $t/D$  ratio. Once a local buckle has been initiated, the pipe buckle will develop longitudinally through the neighboring pipe section as long as the buckling propagation resistance is less than the hydrostatic pressure.

Normally, propagating buckling criterion results in significantly thicker wall thickness compared to other criteria. Consequently, the design will be too conservative if this criterion has to be met. In practice, the designer would withstand the propagation buckling by installing buckle arrestor at the critical region rather than using thicker wall thickness uniformly. This solution would save a significant amount of riser weight and cost.

#### 3.4.4.4 Combined load Criteria

After checking riser against internal pressure and external pressure, riser is then checked to withstand combination load, including effective tension, bending moment, and net internal and external overpressure. DNV suggests the riser design to satisfy the following equation with correspondence of the loading type. The pipe member subjected to bending moment, effective tension and net internal over pressure will be designed to satisfy the equation (3.27). Meanwhile, the pipe member subjected to bending moment, effective tension and net external overpressure will be designed to satisfy the equation (3.28).

$$\{\gamma_{SC} \cdot \gamma_m\} \left\{ \left( \frac{|M_d|}{M_k} \cdot \sqrt{1 - \left( \frac{P_{id} - P_e}{P_b(t_2)} \right)^2} \right) + \left( \frac{T_{ed}}{T_k} \right)^2 \right\} + \left( \frac{P_{id} - P_o}{P_b(t_2)} \right)^2 \leq 1 \quad (3.27)$$

$$\{\gamma_{SC} \cdot \gamma_m\}^2 \left\{ \left( \frac{|M_d|}{M_k} \right) + \left( \frac{T_{ed}}{T_k} \right)^2 \right\}^2 + \{\gamma_{SC} \cdot \gamma_m\}^2 \left( \frac{P_o - P_{min}}{P_c(t_2)} \right)^2 \leq 1 \quad (3.28)$$

$$M_k = f_y \cdot \alpha_c \cdot (D - t_2)^2 t_2 \quad (3.29)$$

$$T_k = f_y \cdot \alpha_c \cdot \pi (D - t_2)^2 t_2 \quad (3.30)$$

Where

$M_d$  = Design bending moment, refer to equation (3.7)

$T_{ed}$  = Design effective tension, refer to equation (3.8)

$P_{ld}$  = Local internal design pressure, refer to equation (3.16)

$M_k$  = Plastic bending moment resistance

$T_k$  = Plastic axial force resistance

$P_c$  = Hoop buckling capacity

$\alpha_c$  = Strain hardening factor (no greater than 1.2)

$$\alpha_c = (1-\beta) + \beta \cdot \frac{f_u}{f_y} \quad (3.31)$$

$$\beta = \begin{cases} (0.4 + q_h) & \text{for } D/t_2 < 15 \\ (0.4 + q_h) \cdot (60 - \frac{D}{t_2}) & \text{for } 15 < D/t_2 < 60 \\ 0 & \text{for } D/t_2 > 60 \end{cases} \quad (3.32)$$

$$q_h = \begin{cases} \frac{(P_{ld} - P_e)}{P_b(t_2)} \cdot \frac{2}{\sqrt{3}} & \text{for } P_{ld} > P_e \\ 0 & \text{otherwise} \end{cases} \quad (3.33)$$

### 3.4.5 Accidental Limit State

During the operation, the riser can be subjected to irregular conditions which may come from incorrect operations or unexpected loads. From that, the accidental limit state (ALS) is introduced to avoid such disastrous accidents in the risers system due to unexpected loads, so that a given accidental scenario will not lead to a complete loss of the integrity of the structure. Accidental loads on the risers system are typically driven by unplanned occurrences, which may be categorized into (not limited to) the following events (DNV, 2010a).

- Fires and explosions
- Impact or collisions, e.g. riser interference, dropped objects/anchors, floater impacts, etc.
- Hook or snag loads, e.g. dragging anchor
- Failure of support system, e.g. heave compensating system malfunction, loss of buoyancy, loss of mooring line, etc.
- Exceedence of incidental internal overpressure
- Environmental events, e.g. earthquake, tsunamis, iceberg, etc.

Risk analyses and relevant experiences are required in order to assess appropriate accidental loads in terms of occurrence probability and other relevant issues. Furthermore, accidental loads are dependent on influencing factors such as personnel qualifications, operational procedures, arrangement of the installation, quality of equipment, safety systems and control procedures (DNV, 2010a).

The design of accidental loads is then classified based on the annual probability of the occurrences and the effect of an accidental event. The main purpose of this limit state is to ensure that the riser system is able to withstand relevant functional loads in the extreme condition and avoid disastrous failure that may cause a hazard, environmental damage and financial loss.

Before proceeding to perform the ALS design check, the risers should already be checked to satisfy the ultimate limit states design. In order to define the operational limit of the riser, a service limit state (SLS) should also be introduced as well in compliance with riser's functional requirements. DNV suggests a simplified design check for relevant value of load effect factors depending on safety class and annual probability of occurrence. A simplified check with respect to accidental load is shown in Table 3-7.

### 3.4.6 Serviceability Limit State

The service limit states are associated with sustainability of functional riser throughout its service life. The determination of acceptable limit for normal operation is established based on the specific functional requirement of riser system. There are some tools to ensure that the riser can work properly, such as FMEA, HAZOP and design review meetings. These tools will be a useful systematic procedure for SLS identification (DNV, 2010a).

However, not meeting SLS criteria will not lead to failure and such conditions should be evaluated and monitored carefully to make sure that the riser will not exceed the ultimate limit state (ULS) and accidental limit states (ALS). Consequently, ALS and ULS will be defined in accordance with exceedance of SLS. The exceedance of SLS can be monitored by maintenance, inspection and implementation of early warning for unpredicted occurrence.

The limitations of SLS are associated with deflections, vibrations, displacements and rotation of global riser or ovalisation of the riser pipe. DNV outlines some limitations that need to be controlled in the global riser design as follows.

- Ovalisation limit due to bending

The ovalisation is a deviation of the perimeter of a round pipe section. This has the shape of cross section as an elliptic cross section. The cross section of pipe should be prevented from premature local buckling due to bending together with the out-of-roundness tolerance from the fabrication of the pipe. The ovalisation of round pipe section is limited to 3.0% such that the ovalisation fulfills following equation (DNV, 2010a).

$$f_o = \frac{D_{max} - D_{min}}{D} \leq 0.03 \quad (3.34)$$

- Riser stroke

Riser stroke is a term implying the movement of the tensioner at the top-end part of the riser. A tensioner maintains relatively constant tension along the top part of the riser in order to limit bending. A tensioner must continue to pull upward as the riser and floater move relatively to each other. The travel of the tensioner is referred to as a stroke. Riser stroke determines the input parameter for the tensioner, clearance and draw works. Riser strokes

should be designed with sufficient capacity to avoid damage to the riser and its components (DNV, 2010a).

### 3.4.7 Fatigue Limit State

The riser system is subjected to cyclic loading during the entire service life, which might cause fatigue damages. The fatigue damage due to cyclic loads should be calculated and accumulated to predict the fatigue life of the riser. In the operating condition of the risers, there are many fatigue sources contributing to failure damages to riser. Fatigue damage sources include (DNV, 2010a):

- Currents (VIV);
- Waves (daily waves, extreme waves);
- Vessel motions (first and second order);
- Slugging.

Fatigue limit states are then suggested to ensure that the riser systems satisfy a minimum requirement life-service of the riser. DNV suggests two assessments for calculating fatigue damage as follows.

#### 1. Method based on S-N curves

This method is an assessment of short-term distribution of nominal stress range. According to DNV, the criterion of fatigue limit state design by considering S-N curves is written below (DNV, 2010a):

$$D_{fat} \cdot DFF \leq 1.0 \quad (3.35)$$

Where

$D_{fat}$  = Accumulated fatigue damage (Palmgren-Miner rule)

$DFF$  = Design fatigue factor, see Table 3-10

Table 3-10 Design Fatigue Factor

Safety Class (DFF)		
Low	Normal	High
3	6	10

#### 2. Methods based on fatigue crack propagation

Fatigue damage can be observed from crack propagation of riser parts. Consequently, the riser should be designed and inspected so that the maximum expected initial defect size would not grow to a critical size throughout its service life. DNV provides a formula to estimate fatigue crack growth life as follows (DNV, 2010a).

$$\frac{N_{tot}}{N_{cg}} \cdot DFF \leq 1.0 \quad (3.36)$$

Where

$N_{tot}$  = Total number of applied stress cycles during service or to in-service inspection

$N_{cg}$  = Number of stress cycles necessary to increase the defect from the initial to the critical defect size

$DFF$  = Design fatigue factor, refer to Table 3-10

### 3.5 Conclusion

WSD method is simple and easy to use by utilizing only one uniform safety factor under particular condition. It has been used in the most of riser system design. However, this method can lead to too conservative design of riser which is not economical. This fact leads industry to find an alternative method in order to trade-off the total development cost and reliability of riser design. On the other hand, the load and resistance factor design (LRFD) promises more efficient design with various safety factors for each load and resistance. The value of the safety factor is taken from relevant experience and knowledge to make riser design reliable and economical.

For this thesis, the riser systems are designed based on the Load and Resistance Factor Design (LRFD) method of DNV-OS-F201. The design check used in determining the wall thickness is as the same as in DNV-OS-F101. The main reason for selecting this method is because the LRFD method presents a more flexible and optimal design with various safety factors. Thereby LRFD method is considered better than the WSD method. In summary, the design criteria of LRFD method are considered in this study.

## Chapter 4. Theoretical Background

### 4.1 Introduction

The purpose of this chapter is to present fundamental theories and understanding of riser analysis. General summary of theoretical background related to riser analysis will be discussed in order to enhance the understanding of riser design. The theoretical backgrounds are limited to waves, currents, floater responses, hydrodynamic effects of slender structure and soil-riser interaction.

### 4.2 Waves

#### 4.2.1 Wave Parameters

The Wave is a major component in designing the environmental effects of offshore structures. Waves can be generated in many ways, such as friction between the wind and the sea surface, tides or by the earthquake/plate movement on the ocean floor. Wave theories are approximations to actual waves. It is used to describe waves on mathematical expression under given conditions that satisfy the assumptions made in relevant derivation. Waves that occur in the sea surface are generally generated by the wind. When the wave is generated, the force of gravity and surface tension will react to cause wave propagation. An ideal form of small amplitude waves in deep water is sinusoidal. The most important parameters in describing the waves are:

- The wave length  $L$  = the horizontal distance between two peaks or two troughs waves following each other.
- The wave height  $H$  = the vertical distance between the wave crests and troughs. The half of  $H$  is the same as amplitude of wave ( $a$ ).
- The wave period  $T$  = time taken to reach the wave trajectory.
- The water depth  $d$  = the water depth where the wave propagated.

Other parameters, such as velocity and acceleration of water particles and wavelength can be derived from wave theory. Other wave parameters are the angular frequency  $\omega = 2\pi/T$ , the wave number  $k = 2\pi/L$ , the wave celerity  $C = L/T = \omega/k$ , the wave steepness  $\varepsilon = H/L$ , the relative depth  $d/L$ , and the relative wave height  $H/d$ . Wave characteristics can also be defined in terms of dimensionless parameters such as  $H/L$ ,  $H/d$ , and  $d/L$ . Figure 4-1 shows a two dimensional schematic of waves propagating in the  $x$  direction.

As shown in Figure 4-1, the highest point of the wave is the crest and the lowest point is the trough. Although the ideal waveform is sinusoidal, the real wave formation on the water surface is usually random; it is induced by so many waves with various wavelength ( $L$ ), wave height ( $H$ ), wave period ( $T$ ) and wave direction. Consequently, these waves can be seen as a superposition of many regular harmonic wave components, each single wave has an amplitude, length, period, frequency and direction as its own characteristic. For irregular wave, normally significant wave height ( $H_s$ ) and peak period ( $T_p$ ) are the parameters to



represent the sea-state realizations. Wave energy spectra will be discussed to explain those parameters.

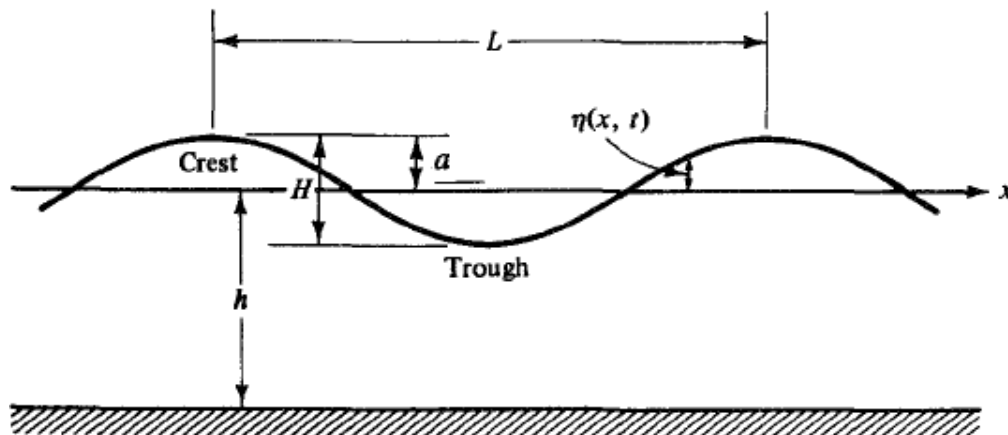


Figure 4-1 Wave Characteristic (Dean and Dalrymple, 1984)

### 4.2.2 Regular Wave

The Regular waves are sinusoidal, small in amplitude, two-dimensional (2-D) and progressively definable by wave height ( $H$ ) and wave period ( $T$ ) in a given water depth (DNV, 2010b). The distance between any two corresponding points on successive sine waves dedicates wave length and periods for measurement. Such points are also called zero-crossings, and are used to detect in a wave record. Regular wave is divided in two categories, which are linear wave and non-linear wave. Linear wave is referred to as the regular wave with relatively small steepness, where the wave steepness is the ratio of wave height ( $H$ ) and wavelength ( $L$ ). Non-linear wave is referred to as a regular wave with bigger steepness. It has more peaked at the crest and flatter in the troughs (Nurwanto, 2012).

### 4.2.3 Irregular Wave

Actual sea surface hardly form an exactly linear (regular) wave or sine wave. Normally, the waves in nature, have nonlinear character which has irregular and random shapes. This wave is referred to as irregular wave. The irregular waves can be obtained by adding together many regular waves of different frequencies, amplitudes and propagation directions. Most of the waves are generated by wind friction, also called wind wave. Wind wave can be classified into 2 categories:

- Wind-induced wave

A sea waves are driven by prevailing local wind field, which is very irregular.

- Swell

A swell is waves which have propagated out of the area of the local wind field. They are no longer generated by the local wind and could even propagate for hundreds of miles even to areas where no wind prevails. Individual swell wave can be regarded as a regular wave with long period and small amplitude (Journée and Massie, 2001).

Random wave can be approached as a superposition of a number of regular waves. This superposition allows one to predict very complex irregular behavior of the sea surface in terms of theory of regular waves. This superposition method was introduced in hydrodynamics by (St. Denis and Pierson, 1953), and is illustrated in Figure 4-2.

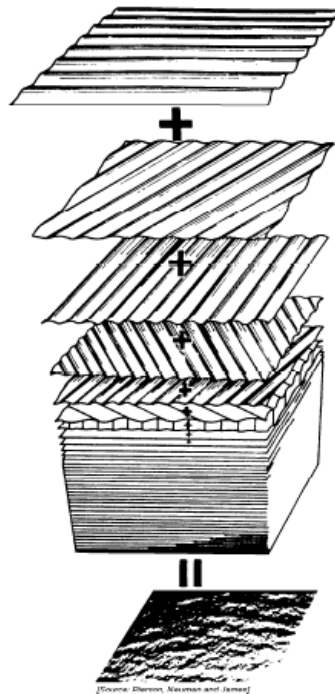


Figure 4-2 Superposition of Sinusoidal wave components (Journée and Massie, 2001)

To measure this randomness of ocean waves, the irregular wave theory applies statistical and probabilistic theories with simplification method. One method is to transform the sea surface into a summation of simple sine waves using Fourier theory to define new wave characteristics in terms of the spectrum. The spectrum of the waves will be discussed in the next section.

#### 4.2.4 Wave Energy Spectrum

Every single wave in the wave train contains an amount of energy which is kinetic energy and potential energy as written in following equation.

$$E = \frac{1}{2} \cdot \rho \cdot g \cdot H^2 \quad \text{Per unit horizontal sea surface area} \quad (4.1)$$

These energies are characterized based on wave lengths, periods and heights. As mentioned previously, ocean wave is a superposition of many regular waves and become irregular wave with different wave height and periods. Consequently, this wave energy is different for every individual wave. In order to quantify the energy of whole waves, the approach of energy spectrum is introduced. In order to capture such energy spectrum, the investigation is carried out based on wave observation.

Wave observation records the time history of every single wave. Hence the time history of the divided wave period in time domain is transformed into a wave energy spectrum in the

frequency domain by using Fourier series analysis to obtain each frequency characteristic of waves as shown in Figure 4-3. Fourier analysis showed that periodic function of  $\zeta(t)$  can be characterized over the interval  $-T/2 < t < T/2$  as the sum of infinite samples measured in the interval periods of sinusoidal functions with harmonic wave frequencies (Journée and Massie, 2001).

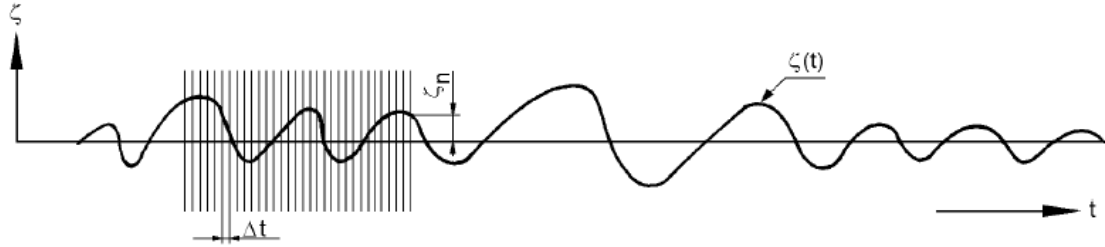


Figure 4-3 Divided period of wave into some intervals (Journée and Massie, 2001)

The total period of the wave sample can be defined as follows:

$$\tau = N \cdot \Delta t \quad (4.2)$$

It can be seen that every time shift has different amplitude  $\zeta(t)$ . The height of the surface at a selected location in the sea can be obtained by using Fourier analysis of the total superposition of incidental regular wave amplitude. The Fourier series is described as follows:

$$\zeta(t) = a_o + \sum_{n=1}^{\infty} [a_n \cos \frac{2n\pi}{T} t + b_n \sin \frac{2n\pi}{T} t] \quad (4.3)$$

Where

$$a_o = \frac{1}{T} \int_{-T/2}^{T/2} \zeta(t) dt \quad (4.4)$$

$$a_n = \frac{2}{T} \int_{-T/2}^{T/2} \zeta(t) \cos \frac{2n\pi}{T} t dt \quad (4.5)$$

$$b_n = \frac{2}{T} \int_{-T/2}^{T/2} \zeta(t) \sin \frac{2n\pi}{T} t dt \quad (4.6)$$

Considering the wave process has averaged at mean sea level, thus  $a_o = 0$

$$\zeta(t) = \sum_{n=1}^{\infty} [a_n \cos \frac{2n\pi}{T} t + b_n \sin \frac{2n\pi}{T} t] \quad (4.7)$$

After some trigonometric manipulations, the amplitude  $\zeta(t)$  can be written as follows:

$$\zeta(t) = \sum_{n=1}^{\infty} \zeta_n \cos(\omega_n t - \theta_n) \quad (4.8)$$

Where

$$\zeta_n = \sqrt{a_n^2 + b_n^2} \quad (4.9)$$

$$\theta_n = \arctan\left(\frac{b_n}{a_n}\right) \quad (4.10)$$

Thus, any wave process can be represented with given amplitudes  $\zeta_n$  and phase  $\theta_n$ . The energy in a harmonic wave is proportional to the amplitude squared; hence a function of wave spectrum energy is obtained. The wave energy is obtained in the frequency domain of wave from time domain by using a fourier transformation. The definition of the wave energy spectrum is expressed in following formula.

$$S_\zeta(\omega_n) = \frac{1}{2} \frac{\zeta_n^2}{\Delta\omega} \quad (4.11)$$

Where,  $\Delta\omega$  represents the distance between two successive frequencies over time history of waves. The wave spectrum energy is represented in Figure 4-4.

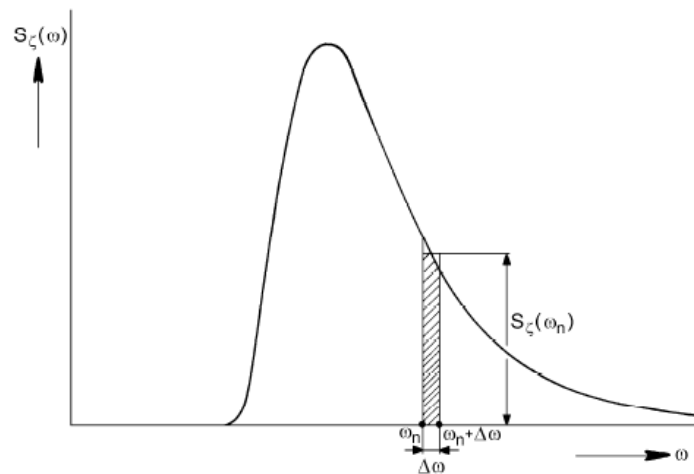


Figure 4-4 Spectral Wave Density (Journee and Massie, 2001)

The area under the spectrum is known as variance  $\sigma_\zeta^2$  or  $m_{0\zeta}$  as written in following equation.

$$\sigma_\zeta^2 = m_{0\zeta} = \int_0^\omega S_\zeta(\omega_n) d\omega \quad (4.12)$$

Figure 4-5 shows a graphical interpretation of how wave spectrum is generated from individual wave. The irregular waves are plotted to wave energy spectrum of corresponding frequency. The irregular wave history in the time domain of the left part of the figure can be expressed with Fourier series analysis as the sum of many regular wave components. Each regular wave is then interpreted in the frequency domain. The phases will be random. The right part of the figure is the accumulation of the summed wave components interpreted as the wave energy spectrum in the frequency domain.

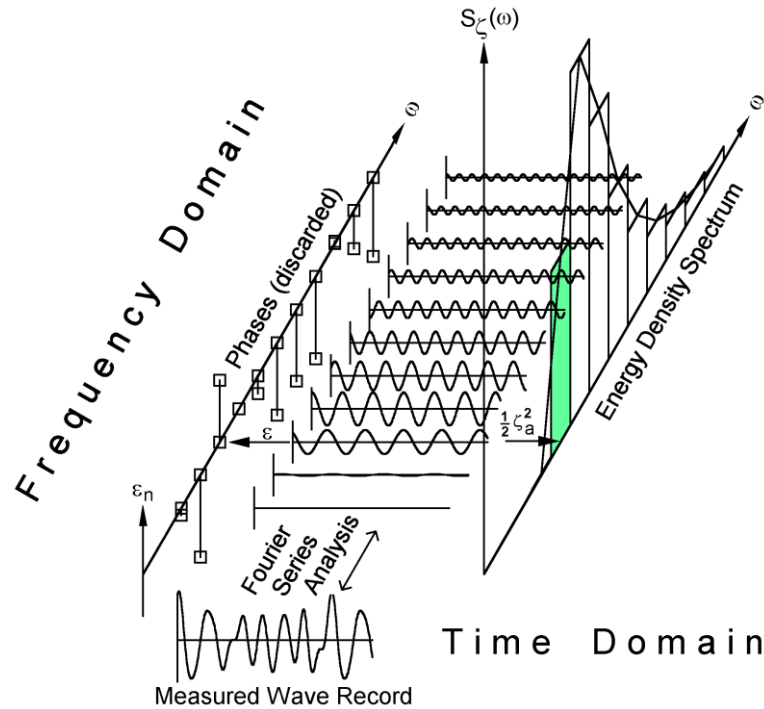


Figure 4-5 Wave Record Analysis (Journée and Massie, 2001)

The value of the wave energy spectrum,  $S_{\zeta}(\omega_n)$ , are then plotted with corresponding frequency. The statistical method is used to determine the irregular wave characteristics by calculating the moments of the area under the spectrum. The order moment is identified with “n” and the general formula for calculating spectrum moment is as follows.

$$m_{n\zeta} = \int_0^{\infty} \omega^n \cdot S_{\zeta}(\omega_n) d\omega \quad (4.13)$$

This formula can be used for computing the area under the spectrum at  $n = 0$ , which is also known as variance as shown in equation 4.12. Thus, some important wave parameters can be obtained from spectral moments. Significant wave height ( $H_s$ ) was introduced as four times the root mean square of the area under the spectrum. Mean zero-crossing wave period is the average time between successive crossings of the mean water level in an upward direction or downward direction.

$$H_{1/3} = 4 \cdot \sqrt{m_{0\zeta}} \quad = \text{significant wave amplitude (Hs)} \quad (4.14)$$

$$T_Z = 2\pi \cdot \sqrt{\frac{m_{0\zeta}}{m_{2\zeta}}} \quad = \text{mean zero- crossing wave period} \quad (4.15)$$

Wave spectrum represents the actual sea-state condition of a particular site. JONSWAP Spectrum and the Pierson-Moskowitz Spectrum are types of wave spectrum. Both spectra describe wind sea conditions that often occur in the most severe sea-states (DNV, 2010b). The type of the spectrum is selected based on the characteristic of the sea-state condition at given location. Pierson Moskowitz spectrum assumed that if the wind is steady over a long time and

a large area, it is originally proposed for fully-developed sea, which is most typically happened in “large water area” such as Gulf of Mexico, North Atlantic and Offshore Brazil. Based on DNV, The Pierson Moskowitz spectrum  $S_{pm}(\omega)$  can be expressed mathematically in following equation.

$$S_{pm}(\omega) = \frac{5}{16} \cdot Hs^2 \cdot \omega_p^4 \cdot \omega^{-5} \cdot \left( -\frac{5}{4} \left( \frac{\omega}{\omega_p} \right)^{-4} \right) \quad (4.16)$$

Where  $\omega_p = \frac{2\pi}{T_p}$  = the angular spectral frequency (4.17)

Meanwhile, the JONSWAP spectrum is applied for relatively “small water area” or “fetch limited area” such as North Sea. This was resulted from an extensive wave measurement known as Joint Operation North Sea Wave Project. JONSWAP is the modification of Pierson Moskowitz (PM) spectrum with typically high non-dimensional peak shape parameter in some frequency where most the frequency of the wave occurs. For peak shape parameter ( $\gamma$ ) = 1, the JONSWAP spectrum is equal to Pierson Moskowitz (PM) spectrum. Based on DNV, JONSWAP spectrum  $S_j(\omega)$  can be expressed mathematically in following equation.

$$S_j(\omega) = A_\omega \cdot S_{pm}(\omega) \cdot \gamma^{\exp\left(-0.5 \cdot \left(\frac{\omega - \omega_p}{\sigma \omega_p}\right)^2\right)} \quad (4.18)$$

Where

$$A_\omega = 1 - 0.287 \ln(\gamma) \text{ (a normalizing factor)}$$

$S_{pm}(\omega)$  = Pierson Moskowitz Spectrum

$\gamma$  = Non-dimensional peak shape parameter, according to DNV-RP-C205, if no particular peak shape parameter is given, the relation between the significant wave height and peak period should be applied to define peak shape parameter.

$$\gamma = 5 \quad \text{for } \frac{Tp}{\sqrt{Hs}} \leq 3.6$$

$$\gamma = \exp(5.75 - 1.15 \frac{Tp}{\sqrt{Hs}}) \quad \text{for } 3.6 < \frac{Tp}{\sqrt{Hs}} < 5$$

$$\gamma = 1 \quad \text{for } 5 < \frac{Tp}{\sqrt{Hs}}$$

$\sigma$  = Spectral width parameters

$$\sigma = 0.07 \quad \text{for } \omega \leq \omega_p$$

$$\sigma = 0.09 \quad \text{for } \omega > \omega_p$$

## 4.3 Currents

The current has a profile over the water depth. Generally, profile and direction of the current will be selected using the best statistics available. Based on DNV, Currents generally occur from contribution of current components as follows (DNV, 2010b).

- Tidal current  $V_{c,tide}$ ,  
Tidal Current is generated by astronomical motions of other gravitational objects.
- Wind drift current  $V_{c,wind}$ ,  
Wind drift current is generated by wind stress and atmospheric pressure over sea surface.
- Density induced/ Soliton current  $V_{c,sol}$ ,  
This current is generated by different density.
- Global ocean/ circulation current  $V_{c,glob}$ ,  
This current is generated by the global ocean circulation in large scale, e.g. Gulfs stream.
- Loop and eddies current  $V_{c,eddy}$ .  
This current is swirling water that can penetrate deeply in the sea column.

Current flow in the horizontal direction is assumed to vary with depth. The magnitude and direction of tidal currents on the surface are usually determined based on measurements at the site. For the design purpose, the total incidental current velocity  $V_{c,tot}$  should be taken as the vector sum of each current component as expressed in equation (4.19). If the current data of particular site is not available, DNV suggests following equation (DNV, 2010b).

$$V_{c,tot}(z) = V_{c,tide}(z) + V_{c,wind}(z) + \dots \quad (4.19)$$

$$V_{c,tide}(z) = V_{c,tide}(0) \left( \frac{d_o + z}{d_o} \right)^\alpha \quad (4.20)$$

$$V_{c,wind}(z) = V_{c,wind}(0) \left( \frac{d + z}{d} \right)^\alpha \quad (4.21)$$

Where

- $V_{c,tot}(z)$  = Total current velocity at level z  
 $z$  = Distance from still water level, positive upwards, negative downwards  
 $V_{c,tide}(0)$  = Tidal current velocity at still water level  
 $V_{c,wind}(0)$  = Wind drift current velocity at still water level  
 $d$  = Water depth at given location  
 $d_o$  = Reference depth, taken as 50 m above still water level  
 $\alpha$  = Exponent, typically 1/7

## 4.4 Floater Responses

The motion of the floating structure is a response to external loading depending on its characteristic shape. The motion of the free-floating structure comprises 6 degrees of freedom with reference to the center of gravity point (COG). The six degrees of freedom comprises 2 orientations; translational motion and rotational motion. Figure 4-6 shows the direction of six (6) degrees of freedom.

### 1. Translational motion

- Surge, transverse movement direction of the x-axis
- Sway, transverse movement direction of the z-axis
- Heave, transverse movement direction of the y-axis

### 2. Rotational motion

- Roll, rotational movement of the x-axis
- Pitch, rotational movement of the y-axis
- Yaw, rotational movement of the z-axis

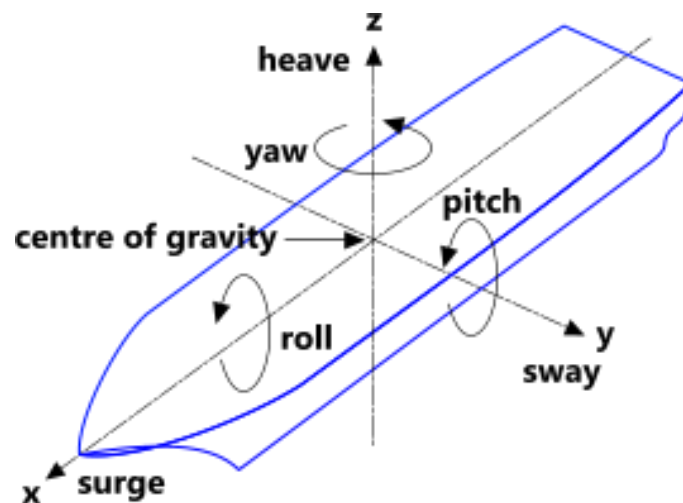


Figure 4-6 Six Degree of Freedom of the vessel (Calqlata, 2015)

Irregular waves contain the energy distribution over the wave frequencies which can be interpreted as a wave energy spectrum. The wave energy spectrum is an input to a system that possess linear characteristics of waves. As the wave passes through the floater, the output of the system is the motion of the floater as a response to wave. The responses of the floating structure can also be interpreted as a response spectrum. The schematic diagram of this system is shown in Figure 4-7.



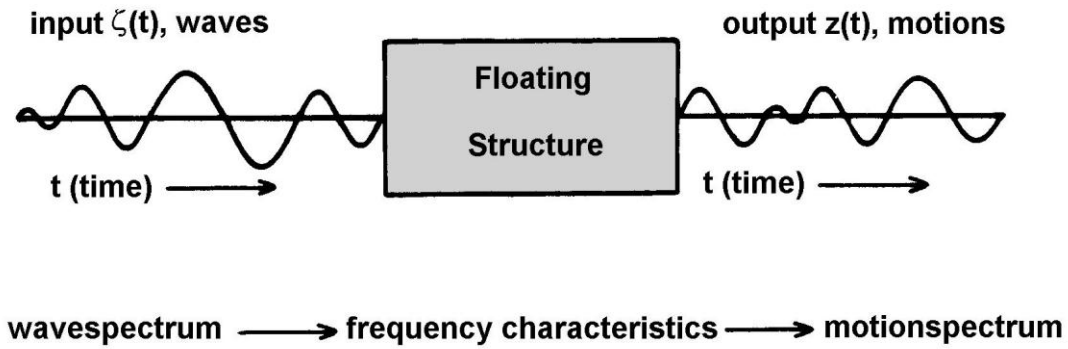


Figure 4-7 Schematic System of Motions and Waves (Journée and Massie, 2001)

This floater motion has an irregular behavior just as the irregular wave that causes the motion. According to Journée and Massie (2001), by knowing the wave energy spectrum and characteristic response of floater motion, the response spectrum of floater can be obtained. The motion of the floater is categorized into two types of motion; first order and second order motion. The first order of the motion components of a floating structure is referred to as wave frequency, while the second order of the motion components of floating structure is referred to as slow drift motion or low frequency.

### 1. Wave Frequency (WF)

These are the response of floater moving at short period as a result of direct consequence of first order wave actions. Response Amplitude Operator (RAO) is a transfer function that can convert the function of wave forces into motion of a floating structure. The RAO data are dimensionless parameter to determine harmonic motions of floater in six degrees of freedom, both translational and rotational. The RAO origin is at the center of gravity of the floater. RAO is a transfer function for transforming wave energy spectrum to response spectrum. The transformation of the spectrum can be explained in following equation.

$$S_z(\omega) = \left| \frac{z_a}{\zeta_a}(\omega) \right|^2 \cdot S_\zeta(\omega) \quad (4.22)$$

Where

$S_z(\omega)$  = Motion energy spectrum

$S_\zeta(\omega)$  = Wave energy spectrum

$z_a$  = Heave amplitude

$\zeta_a$  = Wave amplitude

The principle of the transformation of wave energy spectrum to response spectrum can be described in the following figure.

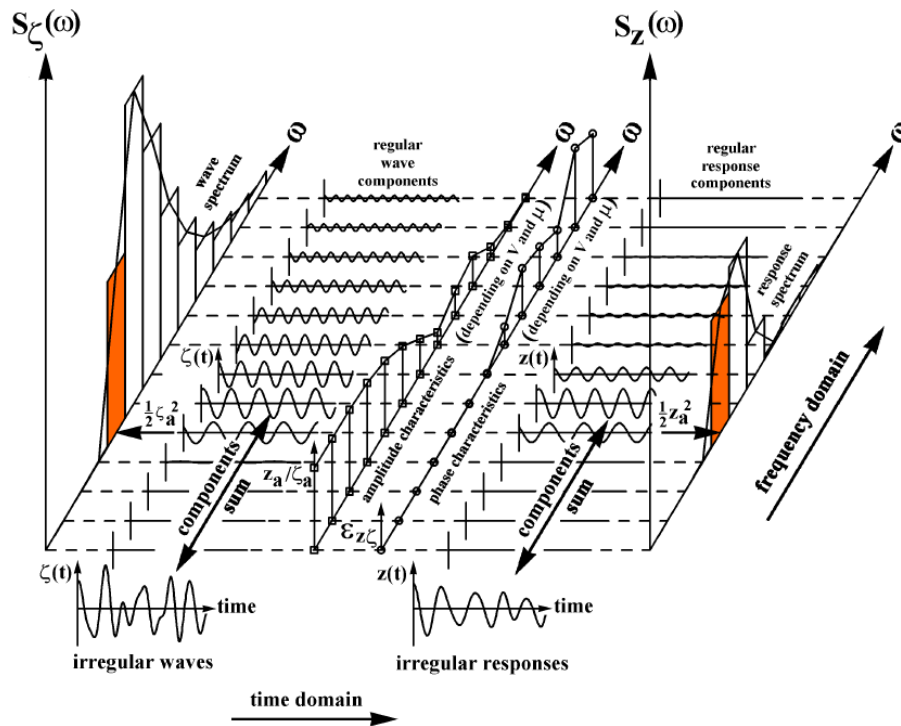


Figure 4-8 Principle of Transfer of Waves into Vessel Response (Journée and Massie, 2001)

## 2. Low Frequency (LF)

These are floater motions as a result of second order wave effects and wind gust loading. This motion is also called slow drift motion, since it takes longer periods ranging from 30 to 300 seconds (DNV, 2010a). The second order determines the offset of the floater during its service life. The following are types of floater offset position (Nurwanto, 2012).

- Mean offset: Mean offset is the initial position of the floaters.
- Near offset: the floater is displaced along the plane of the riser towards the touchdown point.
- Far offset: the floater is displaced along the plane of the riser away from the touchdown point.
- Cross offset: the floater is displaced perpendicular to the plane of the riser.

## 4.5 Hydrodynamic Effects on Slender Cylinder

Riser is considered as slender members with cross-sectional dimensions. The diameter of the riser is sufficiently small to allow the gradients of velocity and acceleration of water to be neglected (DNV, 2010b). Consequently, the hydrodynamic force on the riser can be calculated with the Morison equation. The Morison equation is an empirical formula of the fluctuating force of fluid flow. The following are some condition for the Morison equation.

1. The outer diameter of the riser ( $D$ ) should be smaller than the wavelength ( $L$ ). The criteria that are described in following formula,  $\frac{D}{L} \leq 0.2$ , where  $D$  is the diameter of the slender structure and  $L$  is the wavelength. If the diameter is larger than the

wavelength; then the diffraction effect has to be used instead in order to find total wave force imposing the slender structure.

2. The wave will not break at the pile with following criteria  $\frac{H}{L} \leq \frac{1}{7}$ , where H is wave height and L is wave length. If a wave breaks at the slender structure, then we must use the slamming coefficient instead.
3. The riser should not move significantly, when the wave hit the riser. The riser is assumed to be not significantly moved if it satisfies the following criteria  $\frac{a}{D} \leq 0.2$ , where “a” is the displacement of the riser and D is the outer diameter of the riser.

In conclusion the Morison equation can be applied, if the wave is not affected by the presence of the riser body. Morison equation consists of two components; drag force and inertia force. The drag force is induced by friction between the fluid and cylinder and the difference of pressure between upstream and downstream side.

The inertia force is related to newton’s second law where forces result from accelerations. The total hydrodynamic force acting in the same direction is the sum of the drag force and inertia forces. In addition to hydrodynamic forces, the lift force is also involved in terms of loading to the riser. The lift force is perpendicular to the oncoming flow direction. The lift force is induced by the difference of pressure around the riser. According to the direction of the hydrodynamic force acting on the riser, hydrodynamic loading can be divided into two components; the tangential force ( $F_t$ ) and the normal force ( $F_n$ ). The description of tangential, normal and lift force of hydrodynamic forces is shown in Figure 4-9.

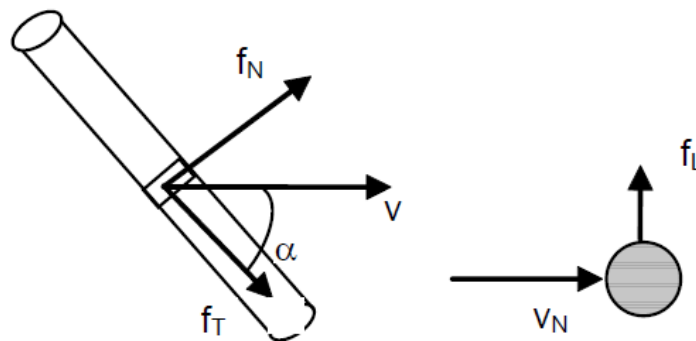


Figure 4-9 Definition of normal force, tangential force and lift force (DNV, 2010b)

DNV suggests suitable Morison equations for the slender cylinder in normal direction and tangential direction (DNV, 2010a).

$$F_n = \frac{1}{2} \rho C_D^n D_h |v_n - \dot{r}_n| + \rho \frac{\pi D_b^2}{4} C_M^n \dot{v}_n - \rho \frac{\pi D_b^2}{4} (C_M^n - 1) \ddot{r}_n \quad (4.23)$$

$$F_t = \frac{1}{2} \rho C_D^t D_h |v_t - \dot{r}_t| + \rho \frac{\pi D_b^2}{4} C_M^t \dot{v}_t - \rho \frac{\pi D_b^2}{4} (C_M^t - 1) \ddot{r}_t \quad (4.24)$$

Where

$F_n$  = Force per unit length in normal direction (N/m)

$F_t$  = Force per unit length in tangential direction (N/m)

- $\rho$  = Water density (Kg/m<sup>3</sup>)
- $C_D^n$  = Drag coefficients in normal direction
- $C_D^t$  = Drag coefficients in tangential direction
- $C_M^n$  = Inertia coefficients in normal direction
- $C_M^t$  = Inertia coefficients in tangential direction
- $D_h$  = Hydrodynamic diameter (m)
- $D_b$  = Buoyancy diameter (m)
- $v_n$  = Flow velocity in normal direction (m/s)
- $v_t$  = Flow velocity in tangential direction (m/s)
- $\dot{v}_n$  = Flow acceleration in normal direction (m/s<sup>2</sup>)
- $\dot{v}_t$  = Flow acceleration in tangential direction (m/s<sup>2</sup>)
- $\dot{r}_n$  = Structural velocity in normal direction (m/s)
- $\dot{r}_t$  = Structural velocity in tangential direction (m/s)
- $\ddot{r}_n$  = Structural acceleration in normal direction (m/s<sup>2</sup>)
- $\ddot{r}_t$  = Structural acceleration in tangential direction (m/s<sup>2</sup>)

The value of  $C_D$ ,  $C_L$  and  $C_M$  is practically taken from the experiment for appropriate value, since the coefficients are determined from several parameters that are listed below.

1. Riser body shape

The value of Inertia and Drag coefficients of three dimensional objects depends on the shape of the structure. In this case, the shape of riser is a cylinder. DNV suggests such coefficients for steady flow in DNV-RP-C205 at Appendix D and Appendix E, (DNV, 2010b);

2. Reynold Number (Re)

$$Re = \frac{UD}{\nu}$$

Where U is the flow velocity, D is the outer diameter and  $\nu$  is the kinematic viscosity;

3. Keulegan Carpenter number (KC)

$$KC = \frac{U_M T}{D}$$

Where  $U_M$  the free stream velocity amplitude of the oscillatory flow, T is the period of oscillatory flow and T is the period of oscillation;

4. Roughness ratio ( $\epsilon$ )

$$\epsilon = \frac{k}{D}$$

Where  $k$  is the dimension of roughness on riser body and  $D$  is the outer diameter of the riser. The number of  $k$  may change over some periods of time due to marine growth;

5. Reduced velocity ( $V_R$ )

$$V_R = \frac{U}{f_n D}$$

Where  $U$  is the velocity of the flow,  $f_n$  is the natural frequency of the riser and  $D$  is the outer diameter of the riser.

## 4.6 Soil-Riser Interaction

The soil riser interaction can influence the extreme response and fatigue performance of the riser at the touchdown point (TDP) since the TDP is a critical part of the design of the riser. The TDP moves over time, reflecting movements of the vessel and riser configuration. The heave motion of the floater may induce in-plane loads; while lateral loads from current and waves may induce out-of-plane loads. The oscillatory of those loads might become a complex interaction between riser movement and the seabed at the touchdown point (TDP).

The oscillatory of those loads might make riser penetrate into the soil and thereby increasing the soil resistance (Karunakaran et al., 2005). Thus, it is important to model soil properties as accurately as possible to represent the actual condition of the soils in order to obtain correct predictions of soil-riser interaction. In practice, the soil-riser interaction is commonly quantified as a linear spring (Bai and Bai, 2010a). In this study, the soil will be modeled by using the friction coefficient assigned in the axial and lateral directions relative to the longitudinal axis of the riser.

## Chapter 5. Design Basis

### 5.1 Introduction

The design data and methodology that is applicable for the analysis of selected riser concepts are provided in this chapter. It has been decided that three types of selected riser concepts be analyzed in respect of riser performances during operating conditions. The objective of this study has therefore been to investigate the three riser concepts in terms of the capability to cope with vessel motion. The reader will refer to Chapter 4 for theoretical backgrounds that are related to this thesis work (e.g. waves, current and floater responses).

The design data is the basis for modeling, analyses and verification of the riser behavior in deep water field. The riser configuration will be designed and optimized in order to satisfy both strength and fatigue requirement. The analysis utilizes the finite element method in the computer modeling with non-linear time domain analysis. The analysis model will be performed by using the ORCAFLEX Software (Version 9.7a), a proven offshore marine systems program developed by Orcina which has the capability to perform static and dynamic analysis of risers (Orcina, 2010). Detail description of ORCAFLEX program is provided in Appendix C.

### 5.2 Global Analysis

Global analysis of the riser is performed to verify the strength design of riser against the global load effects. The global analysis will be based on accepted principles of model discretization, environmental loading, soil properties and material properties to determine reliable global load effects on the riser system (DNV, 2010a). The riser model comprises accurate modeling of mass, stiffness, damping and hydrodynamic load effects along the entire riser length and boundary conditions of top and bottom connection (DNV, 2010a). The riser model will be discretized with sufficient number of segments and nodes to represent actual riser. The global analysis consists of static analysis and dynamic analysis.

The static analysis determines the equilibrium configuration of the system under functional load such as self-weight, buoyancy, hydrostatic effect, etc. The result of static analysis is used as an initial configuration for dynamic simulation. The dynamic analysis run motions of the model over specified periods, starting from the position derived by the static analysis (Orcina, 2010). The period of dynamic simulation is defined as a number of consecutive stages. According to DNV, the scope of global analysis will include a global cross section description in relationship of resulting force-displacement. The output of global response analysis is categorized as follows (DNV, 2010a):

- Resulting cross-sectional forces, e.g. effective tension, bending moments, torsional moment;
- Global riser deflections, e.g. curvature, elongation, angular orientation;
- Global riser position, e.g. co-ordinates, translations, distance to other structures, position of touchdown point on the seafloor, and
- Support forces at termination to rigid structures, e.g. resulting force and moments.

## 5.2.1 Static Analysis

As explained earlier, the static analysis is performed to establish static equilibrium configuration of the riser as the initial point for dynamic simulation. The static analysis establishes the static equilibrium configuration under functional loadings such as weight, buoyancy, hydrostatic effect and top tension. The riser configuration will be evaluated to remain intact with both riser terminations at top and bottom. Based on ORCAFLEX manual, static equilibrium is established in a series of iterative stages (Orcina, 2010):

1. At the start of the calculation, the initial positions and connection of the vessels, lines and buoys are defined by the data.
2. The equilibrium configuration for each line is calculated based on the type of line ends.
3. The out of balance load acting on each free body is calculated. Thereby a new position of each free body is estimated. The free body includes node, buoy, etc. The process is repeated until the out of balance load on each free body is zero.

In most cases, the static analysis process is very fast and reliable. Sometimes, for very complex systems with numerous free bodies and many interconnections, convergence may take long time. The static analysis can also be considered as a steady state analysis. Static riser analyses will be performed by using a nonlinear finite element method. Based on DNV, basic loading of finite element method is distinguished into following components (DNV, 2010a):

1. Volume forces

The static equilibrium configuration of riser in water is influenced by the weights of the riser, the hydrostatic loadings (e.g. hydrostatic pressure and buoyancy) and fluid contents. Based on Baltrop, the static equilibrium configuration can be calculated by using the simplified method of effective tension and the effective weight (Baltrop, 1998). Figure 5-1 displays the equilibrium conditions of a curved segment of riser under the volume forces. The weight and tension of the riser are then altered to effective weight and effective tension respectively. The equation for effective weight and tension are shown below:

$$W_{eff} = \gamma_s A_s + \gamma_i A_i - \gamma_o A_o$$

$$T_{eff} = \gamma_s A_s + \gamma_i A_i - \gamma_o A_o - \rho_i U_i^2 A_i$$

Where

- $\gamma$  = Weight density
- A = Cross sectional area
- P = Pressure
- T = Tension
- $\rho$  = Density
- W = Weight
- i = Internal
- o = External

s = Structural  
t = True

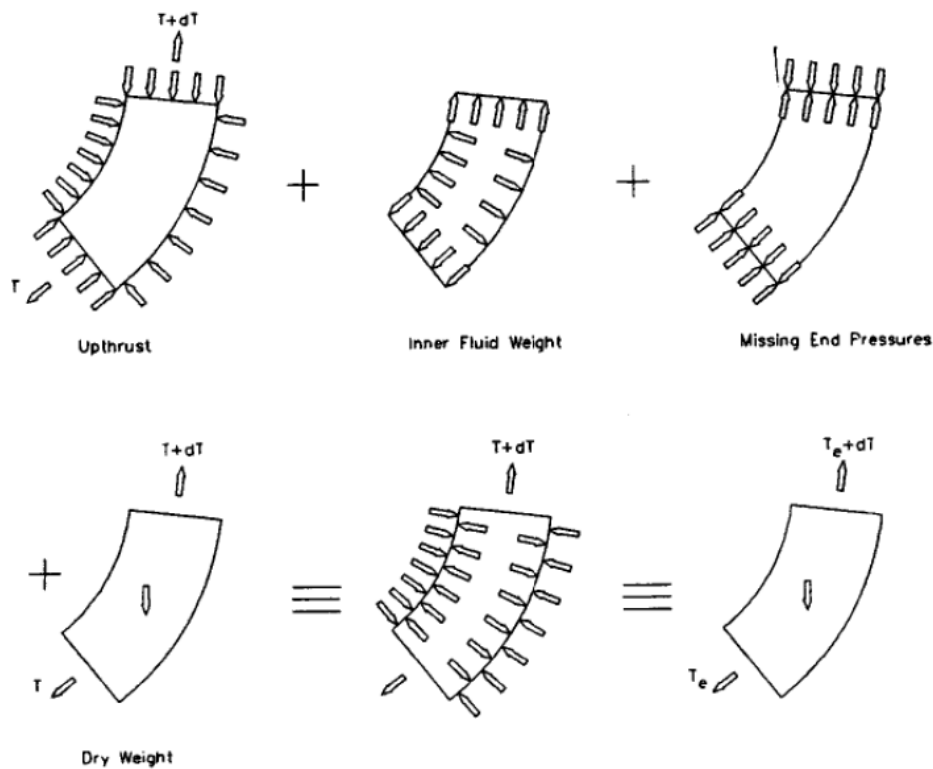


Figure 5-1 Effective weight and effective tension (Baltrop, 1998)

## 2. Specified forces

Specified forces are used for the system where additional forces are applied to the riser. An example of specified force is applied top tension. Normally, the applied top tension is used for top tension risers (TTRs) system which provides tension at the top of riser to keep the riser under particular tension state, and to avoid compression force which might lead to excessive buckling. For selected riser in this study, the top tension force of riser is only provided from the self-weight of the riser without applying tension at the top. The applied tension force may only exist on installation stage. Therefore, in this study, specified forces are not considered.

## 3. Prescribed displacement

Prescribed displacement is identified as displacement at the supports from a stress free location into the specified positions. The prescribed displacement is then applied to establish the displacement at the boundary conditions of riser by iterative approach.

## 4. Displacement dependent forces

Displacement dependent forces are the current load. The steady current is applied to the riser to obtain the final position of static equilibrium which includes the current load effect.

### 5.2.2 Dynamic Analysis

Dynamic analyses of the riser are performed considering excitation force due to current, direct wave, low frequency (LF) and wave frequency (WF) floater motions. The WF floater motions



are calculated by using corresponding RAO data. The LF floater is the effect of average environmental forces to the floater as described in section 4.4. Combined WF and LF should be considered in dynamic analysis. LF floater motions are represented as fixed offset positions of the floater to account for average environmental forces (DNV, 2010a).

The combination of interactions between floater motions, riser configuration and environmental loadings produces nonlinearities in the riser system. To solve these problems, the dynamic finite element method is commonly used to describe the nonlinearities. The nonlinear effects which are considered in dynamic analysis are as follows (DNV, 2010a):

- Inertia forces
- Geometric stiffness
- Nonlinear material properties
- Damping forces
- External forces (time-dependent) (e.g. hydrodynamic loading)
- Contact issues (e.g. bottom contact, riser collision, vessel contact, etc.)

The finite element method will be performed by using ORCAFLEX software. ORCAFLEX uses a finite element model as the basic concept of modeling. A single length of pipe comprises the model of several nodes and segments with boundary of end A and B. Figure 5-2 shows the general ORCAFLEX line model. Each node is connected with two straight segments. Each segment has the properties of mass, weight, buoyancy, drag, stiffness and other properties to represent riser sections.

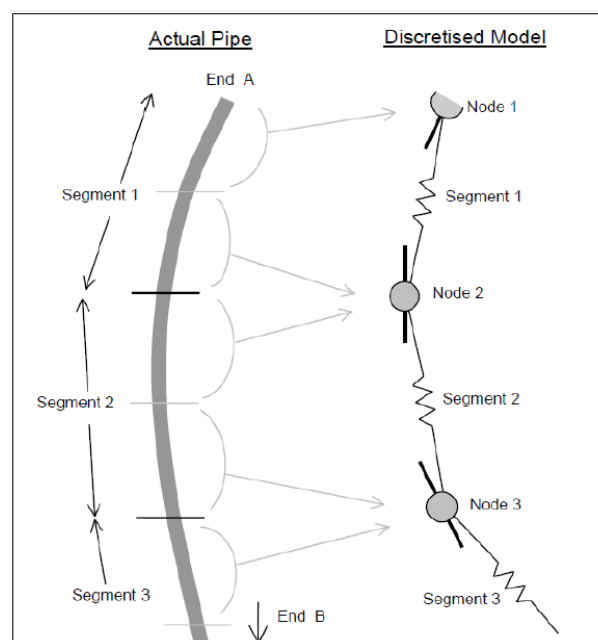


Figure 5-2 Line Model in ORCAFLEX (Orcina, 2010)

Forces and moments are applied at the nodes. Each segment is represented as two co-axial telescoping rods that are connected by axial and torsional spring and dampers. The bending properties of the line are represented by rotational spring and dampers at each end of the segment (Orcina, 2010). According to d'Alembert's principle, the equilibrium of inertia forces,

damping forces and forced oscillations to each node of structural riser can be described by the equation of dynamic equilibrium:

$$M\ddot{x} + C\dot{x} + Kx = F(t)$$

Where

$x$  = Matrix of nodal displacement vectors

$\dot{x}$  = Matrix of nodal velocity vectors

$\ddot{x}$  = Matrix of nodal acceleration vectors

$M$  = System mass matrix

$C$  = System damping matrix

$K$  = System stiffness matrix

$F(t)$  = System external forces (time-dependent)

The dynamic analysis is performed over specified periods, starting from the position derived from the static analysis. The period of simulation is defined as a number of consecutive stages. Before the main simulation stage, there is a build-up stage, during which the wave and vessel motions are smoothly ramped up from zero to fully develop.

This provides a gentle start and reduces the transients that are generated from a static position to full dynamic motion. This build-up stage is numbered as 0 and its length should normally be set to at least one wave period. The build-up stage is followed by stage 1 until the end of simulation time (Orcina, 2010). The period of simulation is determined by user considering the time origin of environmental loads. Normally, the time origin of environmental loads is set to be zero, so all of the time frames coincide with global time.

In addition, nonlinearities are important for the statistical response characteristics of the riser system exposed to irregular loading (DNV, 2010a). Time domain analysis is the method of analysis to capture the prediction of extreme response of irregular loading. The appropriate treatment of nonlinearities components is then important to design criteria. DNV suggests some available features to solve nonlinearities for dynamic analysis as follows.

- Nonlinear time domain analysis

Nonlinear time domain analysis utilizes Newton-Raphson method for step by step numerical integration of the incremental dynamic equilibrium equations. The non-linearities of stiffness, damping, inertia and external force are then evaluated at each step to dynamic solution. The nonlinear approach will give a sufficient description of all nonlinear effects. Hence the nonlinear approach gives a good representation of a possible non-Gaussian response. Nonlinear time domain analysis is then appropriate for irregular analyses to estimate extreme responses with adequate statistical confidence (DNV, 2010a).

- Linearized time domain analysis

Linearized time domain analysis utilizes linearization of the dynamic equilibrium equations including stiffness, damping and inertia forces at the static equilibrium position. Consequently, the system stiffness, damping and mass matrices are set to be constant throughout the analysis. The linearized time domain provides a good representation for the system where hydrodynamic loading is the major nonlinear contribution (DNV, 2010a).

- Frequency domain analysis

Frequency domain analysis linearizes stiffness, damping, inertia and external forces at the static equilibrium position. The irregular analysis is performed by using stochastic linearization for combined loading (i.e. wave, current). Frequency domain analysis provides a Gaussian distribution in the response spectrum. In general, it is not recommended for extreme response prediction (DNV, 2010a).

From all features given above, for riser strength analysis in deep water field and harsh environmental condition where irregular analyses are required to estimate extreme responses with adequate statistical confidence, nonlinear time domain analysis is then selected for this study. The time for this method can be managed by varying the length of each segment along different region of the riser. A critical area of the riser will be discretized with shorter segments to provide detail result analysis.

## 5.3 Environmental Data

### 5.3.1 Water Depth

In this study, the water depth of 1500 m is selected with a constant sea water density of  $1025 \text{ kg/m}^3$  and temperature of  $10^\circ\text{C}$ . The term of deep water refers to water depths of more than 500 m, and ultra-deep water refers to water depths of more than 2000 m (Bai and Bai, 2010b). The water depth of 1500 m is then classified as deep water.

### 5.3.2 Waves

As the purpose of this study is to investigate the limitation of selected riser concepts in terms of capability to cope with vessel motion, thus the different load cases are applied in order to generate different vessel motions. The load cases comprise wave data and current data. The various wave data have been selected for case study. The extreme sea-state is modelled by irregular waves, using modified JONSWAP spectrum, which characterizes the North Sea condition in this study. The sea water area in this study is then considered as fetch limited area.

The JONSWAP spectrum requires information about the significant wave height ( $H_s$ ) and spectral peak period ( $T_p$ ) to complete the simulation of irregular wave, while the peak shape parameter ( $\gamma$ ) is determined by relationship formula of wave height ( $H_s$ ) and peak period ( $T_p$ ) as described in section 4.2.4 and in equation 4.18. The significant wave height ( $H_s$ ) is ranging from 4 m to 18 m with a uniform peak period ( $T_p$ ) of 16 seconds.

Table 5-1 presents the selected Hs and Tp values with corresponding peak shape parameters for this study.

Table 5-1 Wave Data

Wave Characteristics	Hs (m)	Tp (s)	Y
Load Case 1	4	16	1
Load Case 2	5	16	1
Load Case 3	6	16	1
Load Case 4	7	16	1
Load Case 5	8	16	1
Load Case 6	9	16	1
Load Case 7	10	16	1
Load Case 8	11	16	1.224
Load Case 9	12	16	1.550
Load Case 10	13	16	1.909
Load Case 11	14	16	2.298
Load Case 12	15	16	2.715
Load Case 13	16	16	3.158
Load Case 14	17	16	3.623
Load Case 15	18	16	4.108

### 5.3.3 Current

The current data in this study follow a typical current profile in the North Sea. The current profile is a function of current velocities over water depth which is maximum at the sea-surface and minimum at the bottom. For extreme response analysis, current profiles for 10-year return period in North Sea is considered as shown in Table 5-2.

Table 5-2 Current Profile

Water depth	10-year current
m	m/s
0	1.65
-50	1.26
-100	1.25
-200	1.09
-300	0.83
-400	0.74
-500	0.43
-600	0.6
-800	0.6
-1000	0.55
-1200	0.55
3 m above the seabed	0.46

### 5.3.4 Hydrodynamic Coefficient and Marine Growth

The Morison equation is applied to calculate the hydrodynamic load from the waves and current to the riser body. As discussed in chapter 4, the hydrodynamic coefficient is required to complete the calculation of hydrodynamic loads. Both appropriate drag and inertia coefficients should be chosen to obtain the accurate hydrodynamic load effects on the riser body. The drag and inertia coefficient is then defined based on several parameters that are listed in section 4.5 (i.e. Reynolds number, Keulegan-Carpenter number, reduced velocity, body shape and the surface roughness of a structure).

Constant value of drag coefficient can be conservatively used over the entire depth. According to DNV, for cylindrical plain pipes, drag coefficient between 0.7 and 1.0 and an inertia coefficient of 2.0 can be used. The conservative approach is adopted for safe design, and therefore the value is kept constant over the entire depth. During service life, the effect of marine growth may appear and result in an increase in hydrodynamic load. In this study, the effect of marine growth is considered to be covered by the selected hydrodynamic coefficient conservatively. The drag, added mass and inertia coefficient are denoted  $C_D$ ,  $C_A$  and  $C_M$  respectively. The selected hydrodynamic coefficients in this thesis work are presented in Table 5-3. The added mass coefficient is taken as inertia coefficient minus one as described in the following expression.

$$C_A = C_M - 1$$

Table 5-3 Hydrodynamic Coefficient

Coefficient Types	Value
Drag Coefficient, $C_D$	1.1
Inertia Coefficient, $C_M$	2.0
Added Mass Coefficient, $C_A$	1.0

### 5.3.5 Soil-riser Interaction

As discussed in the section 4.6, the soil-riser interactions are modeled by linear soil stiffness and friction. The appropriate friction coefficient and soil stiffness are then selected to accurately model the interaction between the riser and the seabed. The selected soil parameters are shown in Table 5-4.

Table 5-4 Soil Parameters

Parameter	Value
Normal friction parameter	0.5
Axial friction coefficient	0.3
Horizontal lateral/axial soil stiffness	200 kN/m <sup>2</sup>
Vertical soil stiffness	50 kN/m <sup>2</sup>

## 5.4 Vessel Motion Characteristic

### 5.4.1 Coupled and De-coupled analysis

Riser's dynamic responses are highly dependent on vessel motion as a response to environmental loading. The top end of the riser is attached to the vessel at the hang-off point so that the motion of the top end of the riser will follow the vessel motion. Slender structures such as mooring lines, tether and riser system are tied back to the vessel. Thus, the vessel will respond to environmental loads and also be influenced by the damping of these structures. Thereby combinations of dynamic behavior between floater, mooring and riser system consist of an integrated dynamic system in a complex way (DNV, 2010a).

The effect of mooring lines, tethers and risers may significantly influence the vessel motion. This is usually referred to as coupling effect. The coupled analysis considers the interaction between the hydrodynamic behavior of the vessel, mooring lines, tethers and risers in response to environmental loads (Rodrigues et al., 2008). Coupled analysis is expected to give less vessel motion if compared to vessel motion obtained from de-coupled analysis. Therefore, the coupled analysis is considered to be a more accurate analysis, optimum and less conservative method (Rodrigues et al., 2008). However, coupled analysis requires comprehensive computational effort. Meanwhile, in de-coupled analysis, vessel motion is not influenced by the dynamic behavior of the mooring lines and risers.

The de-coupled analysis considers the WF floater motion as dynamic excitation of the wave and the LF floater motion as vessel offset quasi-statically. The specific vessel offsets are considered as a representation of the LF effect. In summary, the WF floater motions will be defined by Response Amplitude Operations (RAOs) data of floater, while the LF floater motions will be defined by specific vessel offsets in de-coupled analysis. As the objective of this study is to investigate the limitation of the selected riser concept in terms of capability to cope with vertical velocity at the hang-off point, then de-coupled methodology is then sufficient for achieving the objective. Therefore, de-coupled methodology will be considered in this study.

### 5.4.2 Host Platform Selection

The WF floater motion and LF floater motion are based on the type of the floater. There are many types of floater used in deep water application such as FPSO, TLP, Semi-submersible, SPAR as shown in Figure 5-3. Floater motion is the main driver for riser's selection and design. In this section, the type of floater will be discussed and selected for this study.

#### FPSOs

FPSOs have been successfully installed in shallow waters in harsh environments, and in deep and ultra-deep waters in benign environments (Olufsen et al., 2003). FPSOs geometry is like a big vessel. In conjunction with turret mooring, FPSOs have the ability to weather-vane with environmental load passively or actively. FPSOs are sensitive to wave since it has a natural period of heave in the range of the period of the wave in typical sea energy as the consequences of having large area crossing with water area. FPSOs have very large horizontal offset and is very sensitive to surge and sway excitations as the consequences of its low

viscous hull damping (DNV, 2010d). In summary, FPSO is hardly suitable for SCR in deep water and harsh environment, and therefore the FPSO is not considered for this study.

### **TLP**

TLPs have been successfully installed in water depth up to 1500 m in Magnolia field in benign environments, and in water depths up to 350 m in harsh environments (Odland, 2013). The tendon, or also called as tension leg, is the vertical tether with certain tensioning capacity, which is connecting TLP to seabed. The tendon is designed such that TLP has a smaller natural period of heave (less than 4 seconds) than typical wave periods to avoid resonance with sea energy.

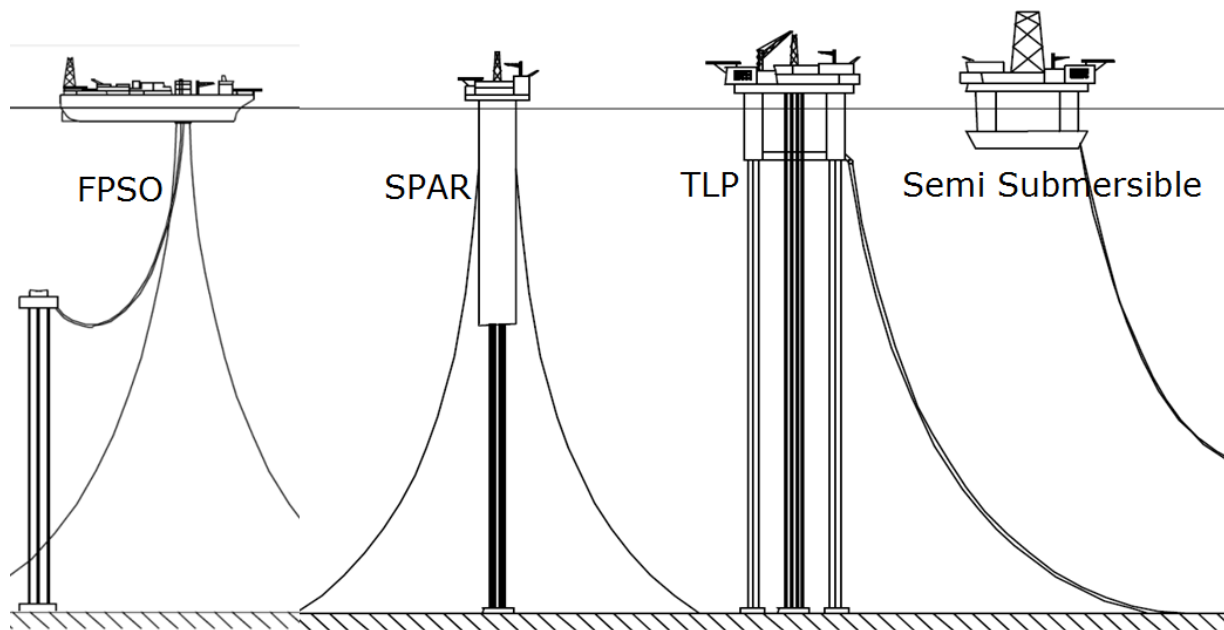


Figure 5-3 Floating Production System (DNV, 2010a)

### **SPARs**

SPARs have been successfully deployed in deep and ultra-deep water, with a current record of up to 2500 m water depth in the Perdido field (Odland, 2013). SPARs have cylindrical hull as deep draft supporting the deck, which is encircled by helical strokes to avoid VIV effects on structures. SPAR is typically installed in very deep waters and is permanently moored to the seabed with the spread mooring system. The deep draft design of spars makes SPAR less affected by wind, wave and currents and allows for both dry tree and wet tree of the subsea production. The center of gravity of SPAR is lower than the center of buoyancy of SPAR, giving it a good stability (Orimolade, 2014). SPARs typically have a long natural period of heave thus avoiding resonance with sea energy.

### **Semi-submersible**

Semi-Submersibles have been installed in water depths of more than 2000 m in benign environments, and in water depths of up to 300 m in harsh environments. Semi-submersibles have good motion characteristics and are used for both drilling and production (Odland, 2013). Semi-submersibles have natural periods of heave above the typical natural wave

periods range to avoid resonance with sea energy, making them an attractive choice for deep water development.

Semi-submersibles comprise a number of semi-submerged circular columns and horizontally extending pontoons being immersed as the drafts. In order to improve the stability, Semi-submersible's circular columns have to be designed with a large diameter, however, increasing the diameter size may result in reducing heave natural period. Thus, it is important to trade-off the diameter size of circular columns to improve stability and also ensure that heave natural period of Semi-submersible above the typical natural wave periods range.

By considering the trend of floater type for SCR application, the selected host platform for this study is semi-submersible. In summary, Figure 5-4 is presented to see the differences of each floater's heave natural period against typical natural wave periods range.

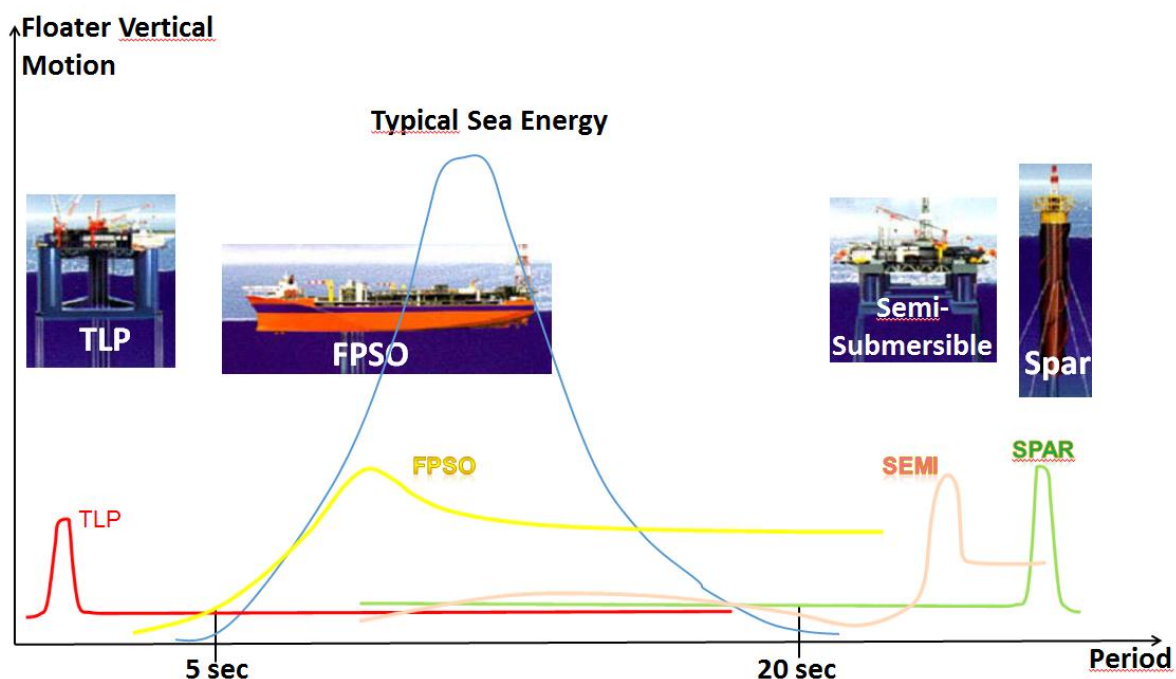


Figure 5-4 Floater Motion Comparison

### 5.4.3 Wave Frequency (WF) Floater Motion

The wave frequency floater motions are a direct consequence of first order wave forces acting on the floater which can be interpreted as vessel motion in 6 degrees of freedom, both translational and rotational. Basically, the wave frequency floater motion can be simply converted from wave characteristics to floater motion by using Response Amplification Operator (RAO) as discussed in section 4.4. The RAO origin is located at the center of gravity of the floater. The RAO data of the Semi-submersible for this study is confidential and is therefore not given in this thesis report, however.

### 5.4.4 Low Frequency (LF) Floater Motion

The LF floaters motions, or also called as slow drift motion, are related to horizontal motions as the floater moves from the initial position to specific offset position. In this study, together with the mooring system, the offset of Semi-submersible is set to be 8% of water depth for



intact condition (ULS design) and 10% of water depth in the case of one mooring line failure (ALS design). The term “damage” refers to ALS design, while the term “intact” refers to ULS design. The following vessel offsets are used in the strength analysis.

- Operation Condition – Intact mooring : 120 m
- Accidental Condition – One mooring line broken : 150 m

## 5.5 Riser Data

### 5.5.1 Riser Wall thickness

The wall thickness of the riser is calculated in the design stage. The DNV-OS-F201 will be used as reference for calculating minimum required wall thickness. The minimum required wall thickness is determined in accordance with ultimate limit state (ULS) design. All pipe cross sections are designed to adequately withstand internal pressure and external pressure to meet burst criteria and collapse criteria respectively. The pipes may also be designed to satisfy minimum wall thickness requirements to withstand buckling propagation. Normally, the wall thickness requirement from criteria of buckling propagation is relatively too thick than the criteria of burst and collapse.

It is therefore not economical to design riser that has the ability to avoid propagating buckling over entire riser length. Thus, the minimum wall thickness requirement of propagating buckling can be taken care by keeping local buckle remains local and does not lead to successive propagating buckle to the neighboring pipe sections. In practice, the method to do that is by using buckle arrestor at some critical regions of the riser. In addition to the final wall thickness, the corrosion allowance of 3 mm and the fabrication allowance of 2.5 mm will be included in the wall thickness calculation.

The appropriate parameters will be chosen according to DNV-OS-F201, such as safety class resistance, load effect factors, de-rating factor and material resistance factor which are listed in chapter 3. Based on the design basis requirement, an internal pipe diameter of 10 inches is required to provide a means of transportation of hydrocarbon fluids from the subsea equipment to the surface facility. In this study, the carbon steel material of grade X65 is used for steel riser. The fabrication factor is set to be one since the riser pipe is seamless. Safety class is set to be high. The system pressure test is performed as well. The purpose of the system pressure test is to prove the pressure containment integrity of the pipe.

The riser is flooded with oil in this study. The density of oil is  $800 \text{ kg/m}^3$ . The design pressure of 500 bars in operating condition and 575 bars in test condition are considered in this analysis. A water depth of 1500 m is used to calculate the maximum hydrostatic pressure on the riser. The unity check is determined by using Pipeline Engineering Tool (PET) software. The software is based on DNV-OS-F101 which is the same as in DNV-OS-F201 as mentioned in chapter 3. Based on an initial assessment, the wall thickness of 25 mm is selected and will be checked based on criteria of burst in operation and test condition, collapse and propagating buckling. Table 5-5 provides the minimum wall thickness results for steel pipe with an internal diameter of 10 inches.

Table 5-5 Minimum Wall Thickness

<b>Burst (Operating Condition)</b>	<b>Burst (Test Condition)</b>	<b>Collapse</b>	<b>Propagating Buckling</b>
21.42 mm	18.53 mm	17.07 mm	24.88 mm

It is shown in Table 5-5 that the selected wall thickness is able to fulfill the criteria of burst, collapse and propagating buckling. This result indicates that the wall thickness of 25 mm is adequate to resist the internal and external net overpressures. The highest requirement for wall thickness is given by criteria of propagating buckling and almost the same as the selected wall thickness. In order to improve the safety level and to avoid propagating buckling, the buckle arrestor can be installed at some critical regions. In summary, the minimum wall thickness requirement is then satisfied with the selected wall thickness of 25 mm.

Detail calculations of the wall thickness design are presented in Appendix A.

### 5.5.2 External Coating

The external coating is applied uniformly along the entire riser length. The purposes of coating are to give corrosion protection, mechanical protection or thermal insulation for riser (Karunakaran et al., 2005). In sensitivity analysis, riser configuration with coating and riser configuration without coating are included in case study to see how coating influence the capability of riser to cope with vertical velocity at the hang-off point. The property of external coating is described as follows.

- External coating wall thickness : 50.8 mm
- External coating density : 700 kg/m<sup>3</sup>

### 5.5.3 Buoyancy Modules

The buoyancy modules are required at certain lengths of riser to achieve the lazy wave configuration. The buoyancy module is modeled to give net buoyancy force. Individual buoyancy modules are installed at specified uniform intervals recognized as pitch, along a certain length of the riser. The pitch of 12 m is considered in this study. The distributed buoyancy modules are modeled with appropriate net buoyancy force per unit length. Table 5-6 presents the main properties of the buoyancy modules used in this study.

Table 5-6 Buoyancy Module Properties

<b>Parameter</b>	<b>Value</b>	<b>Unit</b>
<b>Material Density</b>	395	kg/m <sup>3</sup>
<b>Outer diameter</b>	746	mm
<b>Inner diameter</b>	254	mm
<b>Pitch</b>	12	m
<b>Normal drag coefficient</b>	1.54	-
<b>Axial drag coefficient</b>	0.084	-
<b>Normal added mass coefficient</b>	1.0	-
<b>Axial added mass coefficient</b>	0.37	-
<b>Weight in water</b>	-706	N/m

## 5.5.4 Upper End Termination

In this study, the top end of the riser is equipped with flex joint to relieve stress at the interface of dynamic riser and the host platform. In the extreme loading conditions, the top end is modeled as pinned. The top end is modeled as pinned since the flex-joint stiffness will not influence the riser response in extreme loading conditions (Karunakaran et al., 2005). However, in the fatigue analysis, rotational stiffness at the top end will influence the fatigue response of the riser cross-section in the hang-off area. The rotational stiffness are presented in Table 5-7 for the fatigue analysis.

## 5.5.5 Riser Properties

The wall thickness of the riser is in accordance with previous calculations. Together with all discussed parameters and calculation, the riser has following properties as shown in Table 5-7.

Table 5-7 Riser Properties

No.	Parameter	Symbol	Value	Unit
1	Outer Diameter	OD	304	mm
2	Internal Diameter	ID	254	mm
3	Wall thickness	t	25	mm
4	Type of Material of pipeline	Grade X65		
	Specified Minimum Yield Stress	SMYS	448.2	MPa
	Specified Minimum Tensile Strength	SMTS	530.9	MPa
5	Corrosion allowance	$t_{corr}$	3	mm
6	Fabrication allowance	$t_{fab}$	2.5	mm
7	Yield derating factor	$F_{y,temp}$	0	MPa
8	Tensile derating factor	$F_{u,temp}$	0	MPa
9	Steel Density	$\rho_s$	7850	kg/m <sup>3</sup>
10	Modulus Elasticity	E	207	GPa
11	Poisson Ratio	V	0,3	
12	Content density	$\rho_c$	800	kg/m <sup>3</sup>
13	Ovality	$f_o$	2	%
14	Fabrication factor	$\alpha_{fab}$	1	
15	Hardening Factor	$\alpha_c$	0.92	
16	Material Strength Factor	$\alpha_u$	1	
17	Wellhead Design Pressure	$P_d$	500	Bars
18	System Test Pressure	$P_t$	575	Bars
19	Flex joint rotational stiffness	K	50	kN.m/deg

## 5.5.6 Riser Configuration

In this study, the three configurations are being investigated; the conventional SCR (SCR), the weight distributed SCR (WDSCR) and the steel lazy wave riser (SLWR). The typical riser configuration of weight distributed SCR and conventional SCR is quite similar. The hang-off

point is equipped with flex joint in Semi-Submersible (SS). The TDP area is also referred to as touchdown area (TDA) where the riser approaches the seabed. The typical configurations of them are shown in Figure 5-5.

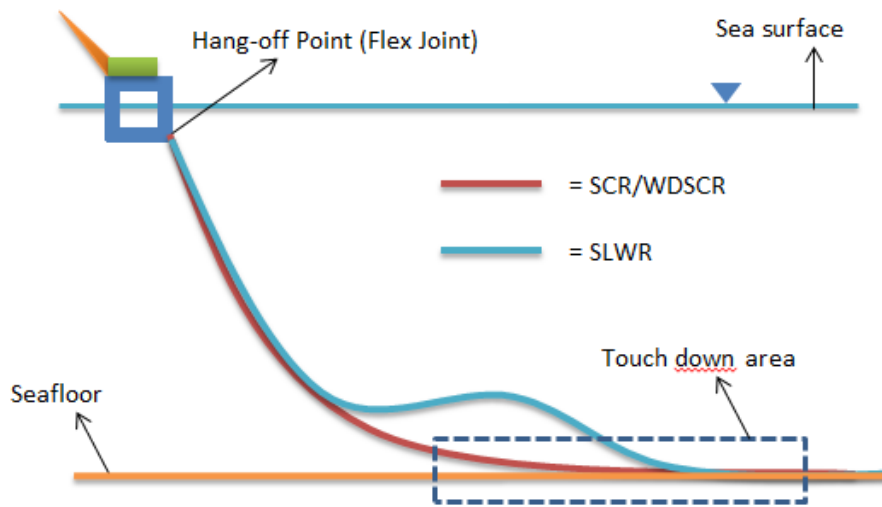


Figure 5-5 Riser Configuration

The direction of environmental loading, which consists of wave and current loading, is set to be parallel to lay direction of riser in order to capture the worst scenario in strength analysis. The floater position is set to be far and near offset position in order to capture the effect of slow drift motion of the floater. The near offset position refers to the environmental load direction and floater displacement towards the lay direction of the riser, while the far offset position refers to environmental load direction and floater displacement away from the lay direction of riser, see Figure 5-6.

The hang-off point, where the riser is attached, is located at 15 m from the center of the vessel and 21 m below the sea surface.

Figure 5-6 shows the orientation of riser’s lay direction and environmental direction from top view.

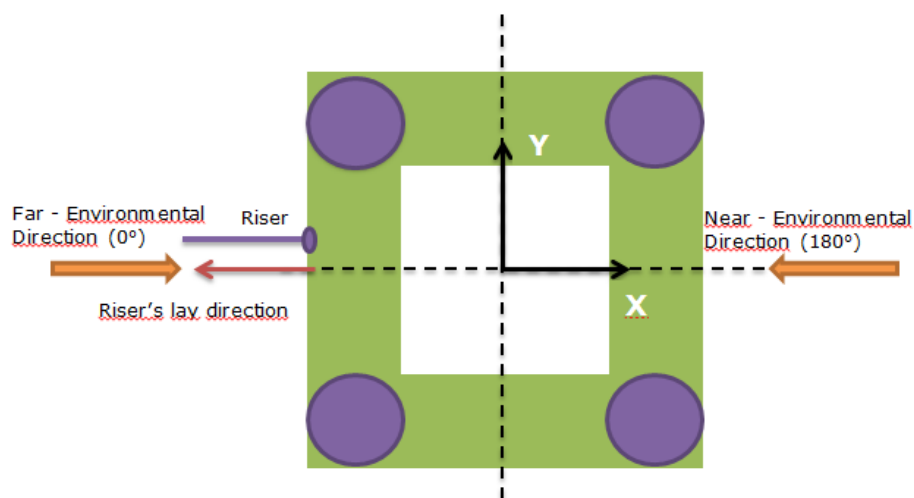


Figure 5-6 Riser Orientation

As the configuration and additional design parameters of the SLWR are complex, the SLWR design has been developed with continuous work from both academic and industries to optimize its configuration (Chen and Cao, 2013). Due to its complex geometry, the parameters and variables are introduced to define the SLWR geometry in this study. A typical configuration and parameters of SLWR geometry is described in Figure 5-7 and Table 5-8.

Table 5-8 SLWR Parameters

Symbols	Parameters
$S_1$	Upper catenary section length
$S_2$	Buoyant section length
$S_3$	Lower catenary section length
$D$	Water depth
$H_1$	Horizontal distances between hang-off and TDP
$H_2$	Horizontal distances between hang-off and seabed connection point
$V_1$	Vertical distances between lowest sag-bend and highest hog-bend
$V_2$	Vertical distances between lowest sag-bend seabed

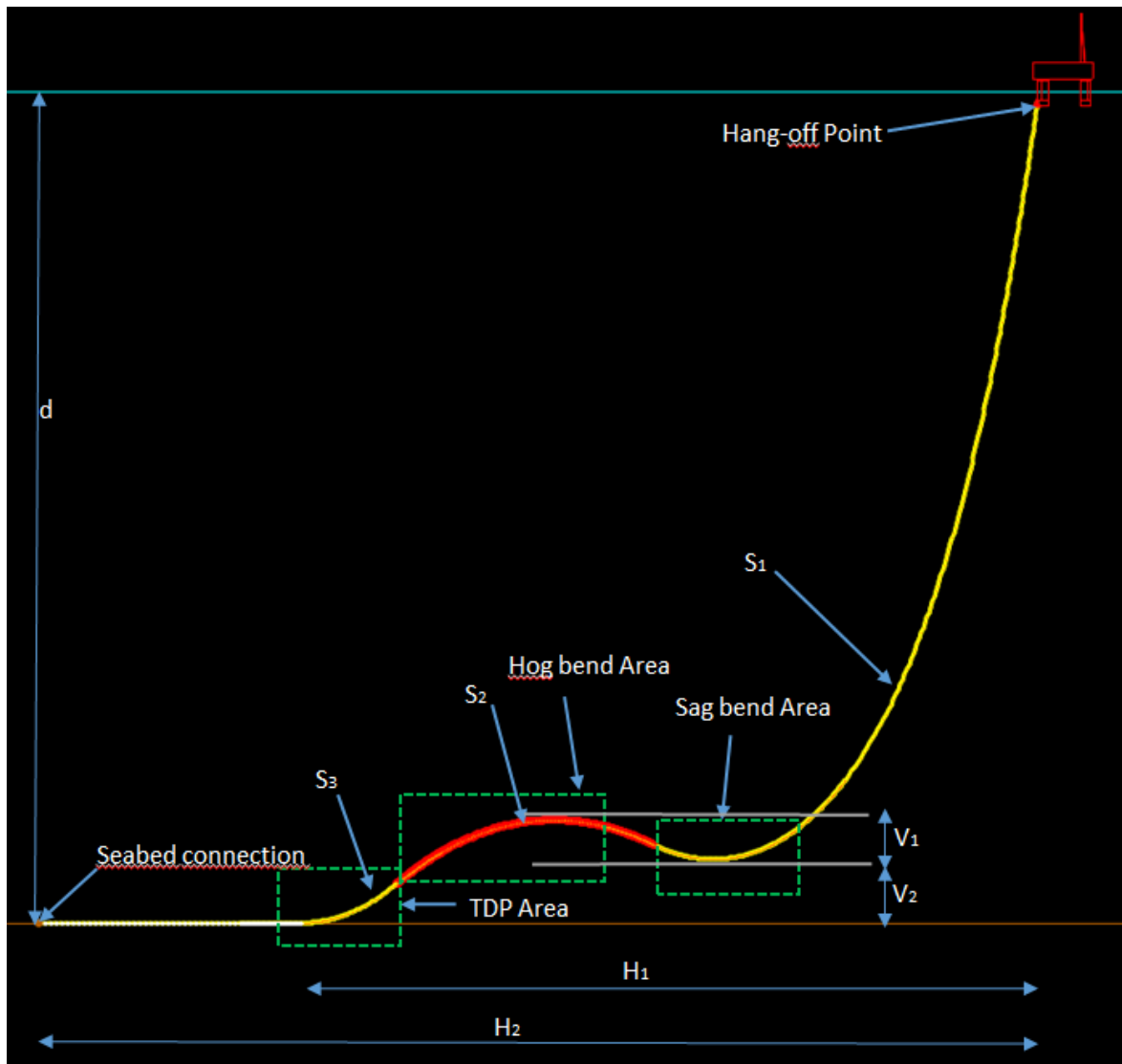


Figure 5-7 SLWR Geometry

## 5.6 Analysis Concept

### 5.6.1 Design Cases

Load cases are the set of the environmental loads which comprise wave and current load. As discussed earlier, each riser model will be analyzed with various load cases in this study for extreme response analysis.

According to DNV (2010a), an adequate set of load cases should be selected in order to:

- Present extreme combined load effects;
- Represent all related limit states;
- Represent both permanent and temporary conditions;
- Represent the range of operating conditions and functional applications;
- Study variation of critical parameters at different locations along the entire riser.

Considering that, load cases are applied in  $0^\circ$  and  $180^\circ$  direction (in-plane with the riser's lay direction) for far and near offset position, respectively in order to capture the worst scenario in strength analysis (Karunakaran and Baarholm, 2013). Thus, the current flow and wave direction is the same direction as the vessel offsets. This scenario is described in Figure 5-6.

The lateral load cases are not considered in this study since they are not critical for riser dimensioning. Lateral load cases can be critical for interference between risers (Karunakaran et al., 2005). In extreme response analysis, the 10-year current profile and various wave data are selected as various load cases for giving a number of different extreme vertical velocities at the hang-off point. The various load cases considered in extreme response analysis are presented in Table 5-9.

Table 5-9 Environmental Load Case Matrix

Load Case	Wave			Current Profile
	Hs (m)	Tp (s)	$\Upsilon$	
1	4	16	1	10-year
2	5	16	1	10-year
3	6	16	1	10-year
4	7	16	1	10-year
5	8	16	1	10-year
6	9	16	1	10-year
7	10	16	1	10-year
8	11	16	1.224	10-year
9	12	16	1.550	10-year
10	13	16	1.909	10-year
11	14	16	2.298	10-year
12	15	16	2.715	10-year
13	16	16	3.158	10-year
14	17	16	3.623	10-year
15	18	16	4.108	10-year

Thus, the load cases will be applied in 0° and 180° direction with corresponding vessel offset position as presented in the design cases matrix, see Table 5-10.

Table 5-10 Design Case Matrix for Each Environmental Load Case

No.	Stage/Limit State	Load type	Environmental Load Direction	Offset	Excursion distance (x)
1	Static	Functional	-	Mean	0 m
2	Dynamic - ULS	Functional + Environment	0°	Far	120 m
3	Dynamic - ULS	Functional + Environment	180°	Near	-120 m
4	Dynamic - ALS	Functional + Environment	0°	Far	150 m
5	Dynamic - ALS	Functional + Environment	180°	Near	-150 m

The design cases matrix are applied for each load case which is the environmental load. In summary, the work diagram for each load case is presented in Figure 5-8.

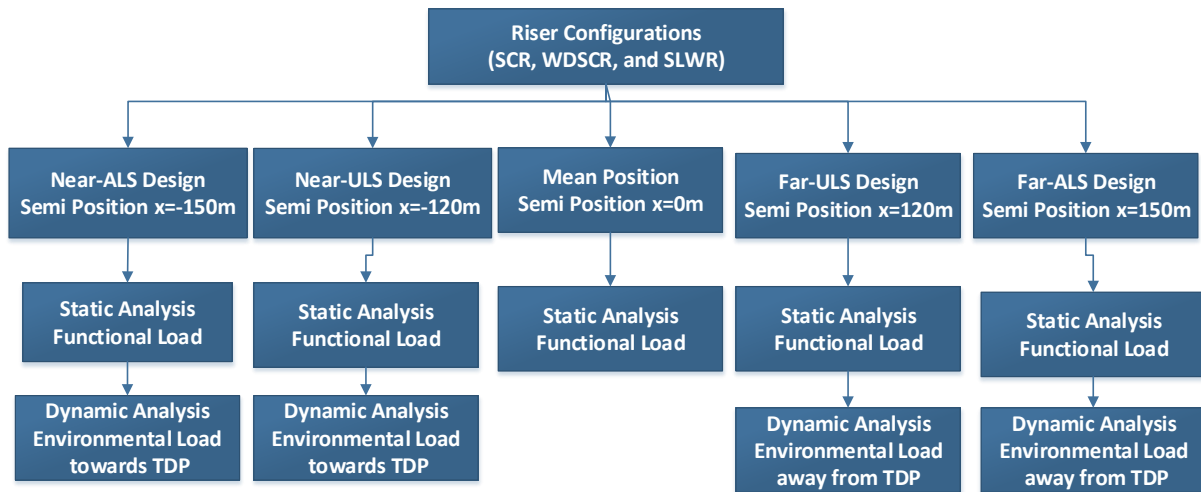


Figure 5-8 Work Diagram

### 5.6.2 LRFD calculation

According to DNV-OS-F201, the environmental (e) and functional (f) loads are calculated separately to determine the LRFD result. Functional loads are established in static analysis, while the environmental loads are established in dynamic analysis as presented in Figure 5-8. The combination load from the model is treated as linear superposition of functional load and environmental load as described in following formula (DNV, 2010a).

$$\vec{M}_E(t) = \vec{M}(t) - \vec{M}_F(t)$$

$$T_E(t) = T(t) - T_F(t)$$

The design values of each corresponding response are then established with given partial safety factor in following formula.

$$M_d(t) = \|\gamma_F \vec{M}_F - \gamma_E \vec{M}_E(t)\|$$

$$T_{ed}(t) = \gamma_F T_{eF} - \gamma_E T_{eE}(t)$$

Afterwards, the utilization over time history is established as follows:

$$g(t) = g(M_d(t), T_{ed}(t), \Delta p, R_k, \Lambda)$$

Where

$g(t)$  = utilization or the generalized load effect at a specific location on the riser

$M_d, M_e, M_f$  = bending moment for design values, environmental load, and functional load

$T_{ed}, T_e, T_f$  = effective tension for design values, environmental load, and functional load

$\Delta p$  = local differential pressure

$R_k$  = vector of cross-sectional capacities

$\Lambda$  = vector of safety factors (i.e. material, safety class and condition factors).

The combinations of partial safety factors used in checking ULS and ALS conditions are selected as shown in Table 5-11.

Table 5-11 Partial Safety Factor for ULS and ALS

	ULS	ALS
<b>Functional, <math>\gamma_F</math></b>	1.1	1.0
<b>Environmental load, <math>\gamma_E</math></b>	1.3	1.0
<b>Reduced Functional, <math>\gamma_{RF}</math></b>	0.91	-
<b>Reduced Environmental, <math>\gamma_{RE}</math></b>	0.77	-

### 5.6.3 Extreme Response Methodology

At an early stage in the design process, reasonable estimates on the percentile response, simulation duration, and number of simulation should be established for extreme response analysis. According to Norsok N-003, calculation of characteristic action effects may be based on selected short term sea-states for systems significantly influenced by nonlinear behavior (Norsok, 2007). The design storm approach is applicable in connection with a nonlinear action effect (Norsok, 2007).

The extreme response calculation is based on nonlinear time domain analysis for nonlinear action effect. The irregular wave of the JONSWAP spectrum described in section 5.3.2 is used to model the sea-state realization. The main objective of choosing a number of wave data is to generate different vertical velocities at the hang-off point for cases study. Random wave trains are characterized in terms of user-defined seed number of wave component, significant wave height ( $H_s$ ), peak period ( $T_p$ ), giving a sea-state realization.

The phases, which are associated with each wave component, are pseudo-random (Orcina, 2010). ORCAFLEX uses a random number generator and the user-defined seed to assign phases of wave components (Orcina, 2010). The same user-defined seed component will give the same phases and vice-versa. Therefore, each wave train from the randomly selected seed component will generate different sea-state realization and also the different response of the structure. To ascertain that the extreme value distribution for each load case is properly accounted for, a number of 3-hour simulations with different random seeds are considered to obtain adequate statistical confidence of short term sea-states.



The number of 3-hour simulations should be sufficient that the upper tail of the distribution function for the 3-hour maximum sea-state is well modeled (DNV, 2013). A sufficient approximation for the q-probability response/load is then estimated by solving (Haver, 2010):

$$F_{X_{3h}|H_s T_p}(x|h_q^*, t_q^*) = \alpha$$

Where  $h_q^*$  and  $t_q^*$  are the parameter which gives the worst sea-state for the problem under consideration.  $\alpha$  is the percentile response (Haver, 2010). One may instead select the median response, rather than selecting a higher percentile response ( $\alpha$ ) as the short term characteristic. The percentile response level will depend on the nature of the response problem, but a default choice of 90% percentile response has been recommended in Haver et al. (1998). This is also adopted by Norsok standard N-003 (Norsok, 2007). Thus, for this study, 90% percentile response ( $\alpha$ ) is considered for each load case.

Based on DNV-OS-E301 section 2.2.10, an alternative to one long simulation, to which an extreme value distribution will be fitted, could be to simulate several (10-20) realizations of duration 3-hours (DNV, 2013). Thus, 20 random seed simulations will be considered for each load case to obtain the extreme value distribution. For one seed simulation, one can find a sea-state realization and 3-hour maximum response denoted  $X$ . By repeating the time domain simulation 20 times with different random seeds, 20 independent “observations” of the 3-hour maximum responses are then obtained,  $\{X_1, X_2, X_3, \dots, X_{20}\}$ .

The 90% percentile response for each load case is then obtained from those 3-hour maximum responses  $\{X_1, X_2, X_3, \dots, X_{20}\}$  by using extreme value distribution, for instance, Gumbel distribution. (Haver, 2010). This is important since each set of wave train, from the randomly selected seed components, generates different sea-state realization and different response. The 90% percentile response of downward velocity at the hang-off point is considered to capture the capability of riser to cope with the vessel motion. This is because the downward velocity at the hang-off point dominates the riser’s critical responses (stress/buckling) in the global strength design (Chen et al., 2009). In order to cover possible higher order wave effects, the selected seed component is slightly rounded upwards from 90% percentile response. The purpose of 3-hour simulation, 90% percentile response and consideration of 20 seed components in this study is to ensure the extreme response analysis is performed in accordance with DNV-OS-F201, for adequate statistical confidence.

#### 5.6.4 Analysis Procedure

The riser strength analysis is performed by following procedures as provided below:

1. Semi-submersible is modeled with appropriate RAO data at mean position;
2. 20 random seed components are selected for each load case;
3. The 3-hour maximum responses of downward velocities at the hang-off point are obtained from 20 random seed components. This step is repeated for 15 load cases. Thus the total simulation is 15 x 20;

4. The seed component satisfying 90% percentile response is obtained from extreme value distribution. This step is repeated for 15 load cases. The selected seed components for each load case are thereafter established;
5. The conventional SCR, WDSCR and SLWR are modeled with discrete beam segments consisting of the shorter segment in the critical region (i.e. hang-off point and touchdown area);
6. Static riser configuration is established for SCR, WDSCR and SLWR;
7. Static analysis is performed and checked for every offset position;
8. The load cases with the selected seed component are applied in 0 degree and 180 degree direction for far and near offset position respectively;
9. Dynamic analysis is performed for near-ULS, far-ULS, near-ALS and far-ALS design cases by considering non-linear time domain analysis and irregular wave theory of JONSWAP within 3-hour dynamic simulation. The strength assessment is performed by applying the load cases based on the extreme downward velocity at the hang-off point;
10. The following riser response characteristics are observed and discussed:
  - Maximum Effective Tension
  - Maximum Compression
  - Maximum Bending Moment
  - Maximum Utilization (LRFD)

### 5.6.5 Acceptance Criteria

To ensure the riser design criteria has been satisfied, the following acceptance criteria are adhered to in this analysis:

#### **Buckling Utilization Factor**

Based on DNV-OS-F201, the consistent treatment moment-tension relationship is a important issue for the acceptance criteria of all combined load in LRFD format. To ensure the riser design satisfies the design criteria, it is convenient to consider utilization or generalized loading expressed by the following generic equation (DNV, 2010a):

$$g(t) = g(M_d(t), T_{ed}(t), \Delta p, R_k, \Lambda)$$

Where

$g(t)$  = utilization or the generalized load effect functions at a specific location on the riser

$M_d$  = design values for bending moment

$T_{ed}$  = design values for effective tension

$\Delta P$  = local differential pressure

$R_k$  = vector of cross-sectional capacities

$\Lambda$  = vector of safety factors (i.e. material, safety class and condition factors).

As  $g(t)$  is varied over time, the maximum  $g(t)$  is obtained from the maximum value of each component function and is considered for conservative load effect. The acceptance criteria

require the generalized load effect (utilization) to be less than unity for both static and dynamic response. This criterion is given by:

$$g_{\max} < 1$$

Thus, the maximum buckling utilization factor should be less than 1.0 for all limit state design (ULS and ALS). The calculation of LRFD is performed by ORCAFLEX.

### **Compression**

Excessive compression (negative minimum tension) is unwanted. Therefore, the compression is avoided or be minimal.

### **Fatigue Life for Wave Induced Fatigue Analysis**

The minimum acceptable fatigue life is 250 years for wave induced fatigue analysis.

### **Fatigue Life for Fatigue Analysis due to VIV**

The minimum acceptable fatigue life is 500 years for VIV fatigue analysis.

## Chapter 6. Extreme Response Analysis

### 6.1 Introduction

This chapter presents the extreme response analysis of the selected riser concepts. The brief methodology of the extreme response analysis is presented in the previous chapter. The main software program for modeling and analysis in this study is the ORCAFLEX. A general description of the main features of this software program is provided in the Appendix C. The general procedure adopted in this study is summarized as follows:

- Selection of seed component for each load case;
- Static analysis, this section gives the determination of an optimum static configuration for the conventional SCR, WDSCR and SLWR. The strength assessment is performed to optimize the riser arrangement in order to attain proper model;
- Dynamic analysis, the strength analysis is performed in the extreme sea-states under the combined actions of waves and currents for each load case;
- Conclusion, this section present discussion of the results.

### 6.2 Selection of seed components

This section contains the selection of seed components. The brief description of the methodology is discussed in section 5.6.3. 20 simulations of 3-hour duration are performed with 20 different randomly seed components to generate different sea-state realizations for each load case. Thus, there are 20 x 15 simulations were performed. The 20 random seed components are ordered from 1 to 20. The order of seed is denoted “m”. The different sea-state realizations generate different velocities at the hang-off point. Consequently, 20 maximum responses of downward velocities at the hang-off point are obtained. The 20 maximum responses of downward velocities at the hang-off point from each seed are sorted from smallest to largest such that they can fit into an extreme value distribution.

The downward velocity and corresponding seed component, giving 90% percentile response, from the extreme value distribution are then obtained and selected. The results of the selection of seed components (m) are summarized for all load cases in Table 6-1. The downward velocity at the hang-off in the Table 6-1 is the 90% percentile response from the extreme value distribution. The increase in downward velocity is observed as increase number of load case; therefore, this load case will then be used for the next analysis.

Table 6-1 Load Cases with Corresponding Seed Component

Load Case	Wave			Current Profile	Downward Velocity at the hang-off (m/s)	Seed Order (m)
	Hs (m)	Tp (s)	Y			
1	4	16	1	10-year	1.34	11
2	5	16	1	10-year	1.68	11
3	6	16	1	10-year	1.75	11
4	7	16	1	10-year	2.04	11

5	8	16	1	10-year	2.33	11
6	9	16	1	10-year	2.62	11
7	10	16	1	10-year	2.91	11
8	11	16	1.224	10-year	3.27	2
9	12	16	1.550	10-year	3.71	18
10	13	16	1.909	10-year	3.84	8
11	14	16	2.298	10-year	4.09	9
12	15	16	2.715	10-year	4.10	18
13	16	16	3.158	10-year	5.10	16
14	17	16	3.623	10-year	5.67	5
15	18	16	4.108	10-year	6.00	9

## 6.3 Static Analysis

This section presents the optimum static configuration and static analyses for the conventional SCR, WDSCR and SLWR at mean, near and far offset position. In general, the riser properties are presented in Table 5-7. As discussed earlier, the riser is attached 21 meter below sea level at Semi-submersible. To understand how the coating influences the riser configuration, the configuration will be modeled twice, one is with coating and other one is without coating.

To understand how the different offsets of the semi-submersible give different static responses, 120 meter offset of intact mooring will be investigated in static analysis. The near offset position refers to the Semi-submersible's displacement in-plane towards the touchdown point, while the far offset position refers to Semi-submersible's displacement in-plane away from the touchdown point.

In static analysis, the consideration is given to functional loads and no environmental load is applied. The interest results from static analyses for strength design are static effective tension force and static bending moment. The maximum DNV utilizations, determined using only functional load partial factor of safety, are also presented to ensure that the static configuration is within the acceptable criteria.

### 6.3.1 Static Analysis of Conventional SCR

The conventional SCR is hung from the Semi-Submersible as shown in Figure 6-1. For simplicity purpose, the term "conventional SCR" is referred to as "SCR". In order to model an optimum SCR configuration, the riser is set to have a top angle of 15° relative to vertical in mean position.

The total riser length is 2831 m. An illustration of these offset positions and the resulting SCR configuration in intact mooring is shown in Figure 6-1. The static equilibrium of SCR configuration gives the static results. Although, the analysis was performed for the entire riser length, the summary static results of the SCR are presented in Table 6-2.

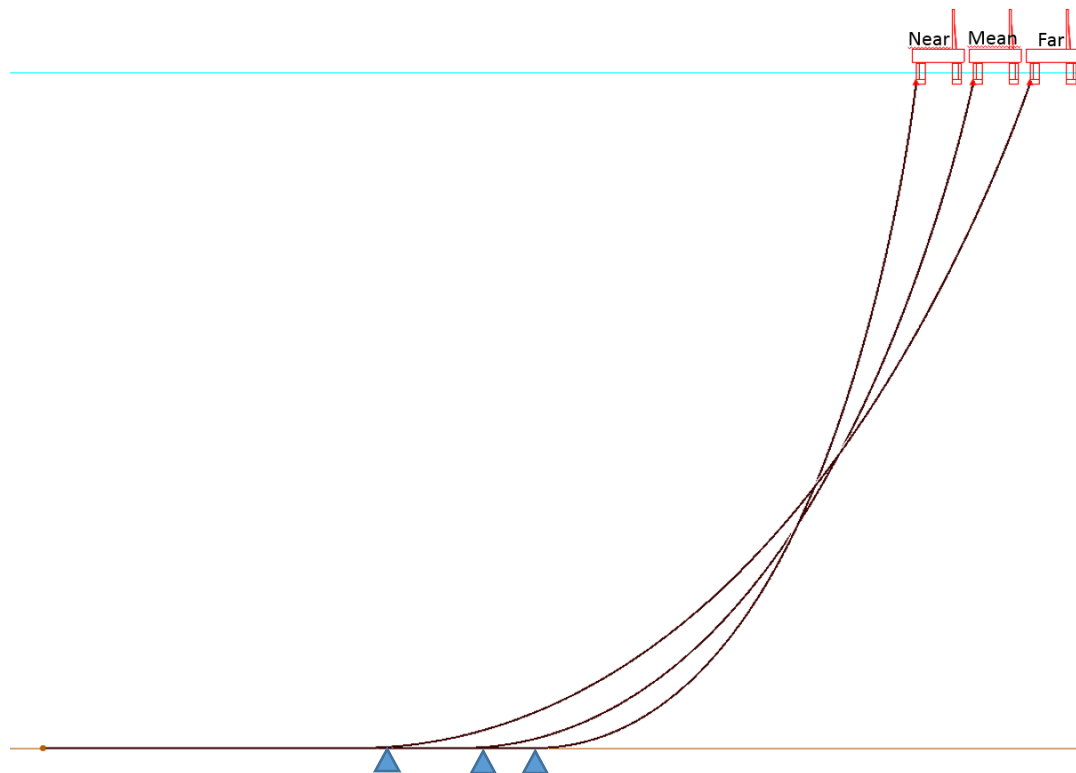


Figure 6-1 SCR Intact-Static Configuration for near, mean and far position

Table 6-2 SCR Static Results- Functional Loads

SCR Intact – Static	Coating			No Coating		
	Far	Mean	Near	Far	Mean	Near
Hang-off angle (°)	21	15	10	21	15	10
Effective top tension (kN)	2699	2341	2108	3114	2700	2432
Max. Bending Moment (kN.m)	54	85	137	54	85	137
Max. DNV Utilization (LRFD)	0.28	0.27	0.34	0.31	0.27	0.35

### **Discussion of SCR Static Analysis Results:**

The following is a general discussion of the SCR response under functional loadings at far, mean and near vessel position:

- It can be seen that the different offset positions give significant impact on the configuration. The TDP location changes significantly, which causes the different static and dynamic behavior for the different offset positions.
- The SCR with coating is having less effective top tension than the SCR without coating. This is the consequence of having the coating density of  $700 \text{ kg/m}^3$  and thickness of 2 inches, giving upward buoyancy to the riser. Therefore, the riser with coating is lighter than the riser without coating.
- Equal maximum bending moment and hang-off angle are observed for the SCR with coating and for the SCR without coating. The maximum bending moment occurred in the TDA.
- The SCR without coating has more utilization factor than the SCR with coating for static equilibrium. The maximum utilization value is 0.35 and is located in the TDA.

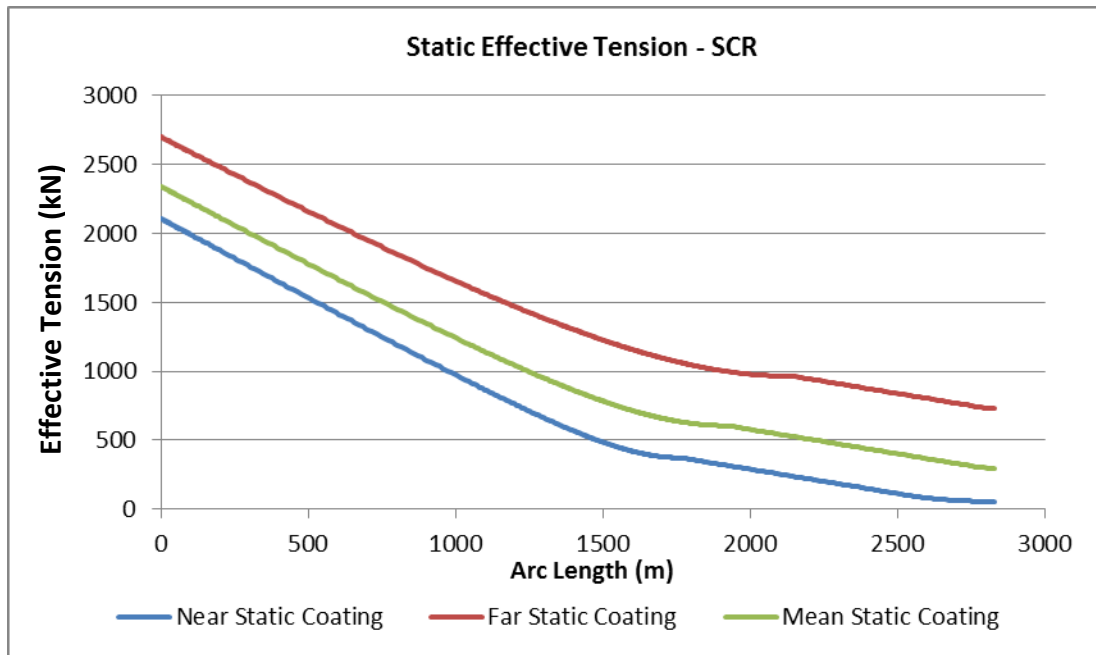


Figure 6-2 Static Effective Tension of SCR with Coating

- From the Figure 6-2, it can be seen that the static effective tension is a function of riser length. The maximum effective tension occurred at the hang-off point since the whole submerged weight of the riser is supported at the hang-off point. The far offset position gives the highest effective top tension due to its longest suspended length. On the other hand, the near offset position gives the lowest effective top tension due to its shortest suspended length.

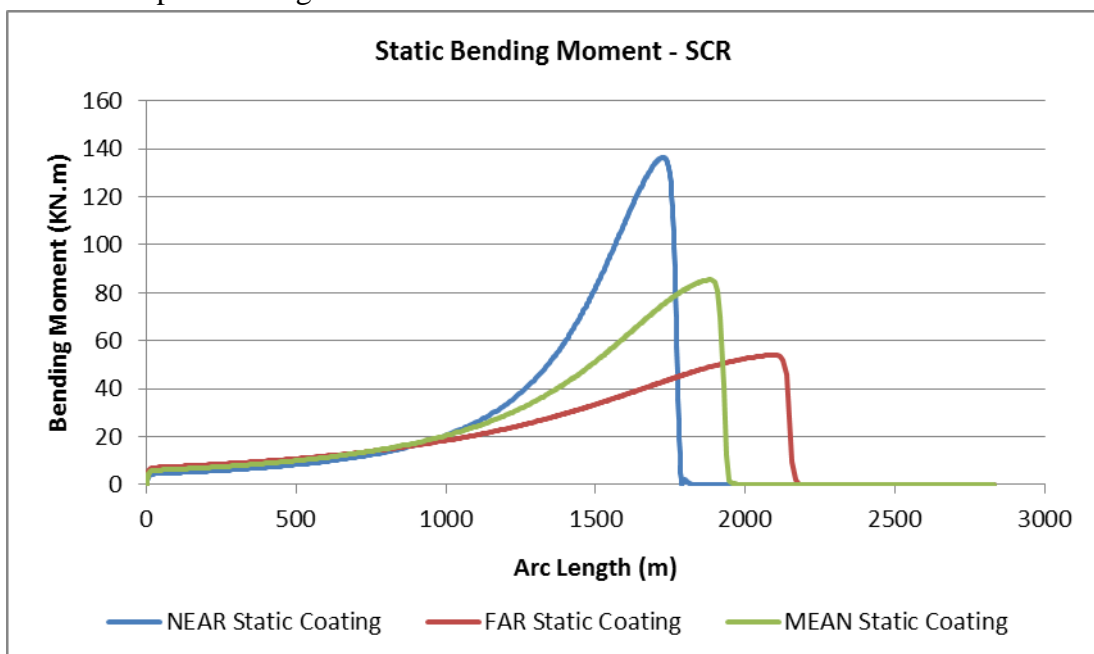


Figure 6-3 Static Bending Moment of SCR with Coating

- From the Figure 6-3, the maximum bending moment occurred in the TDA since the TDA is where the riser starts bending to lay horizontally on the seabed. The bending

moments in the top region are significantly small, since the rotational stiffness of flex joint is modeled as pinned, permitting the riser to rotate freely at the hang-off point.

- The near offset position gives the highest bending moment compared to the mean and the far offset position. This is the consequence of the small sag-bend curvature which results in the high static bending moment when the floater is in near offset position, see Figure 6-3. On the other hand, for the far offset position, the large sag-bend curvature is observed in the TDA which results in significantly low static bending moment.
- It is also important to keep in mind that the bending moment is dependent on how the the riser approaches the seabed. In the far offset position, the bending moment is approaching the seabed in smoother way than the near offset position, see Figure 6-1. Therefore, the far offset position gives significantly low static bending moment. Thus, the smoother approach of the riser to the seabed, the less bending moment of the riser in the TDA.
- From the results, the significant change in location of the TDP between far case and near case is an important design consideration with respect to bending moment.

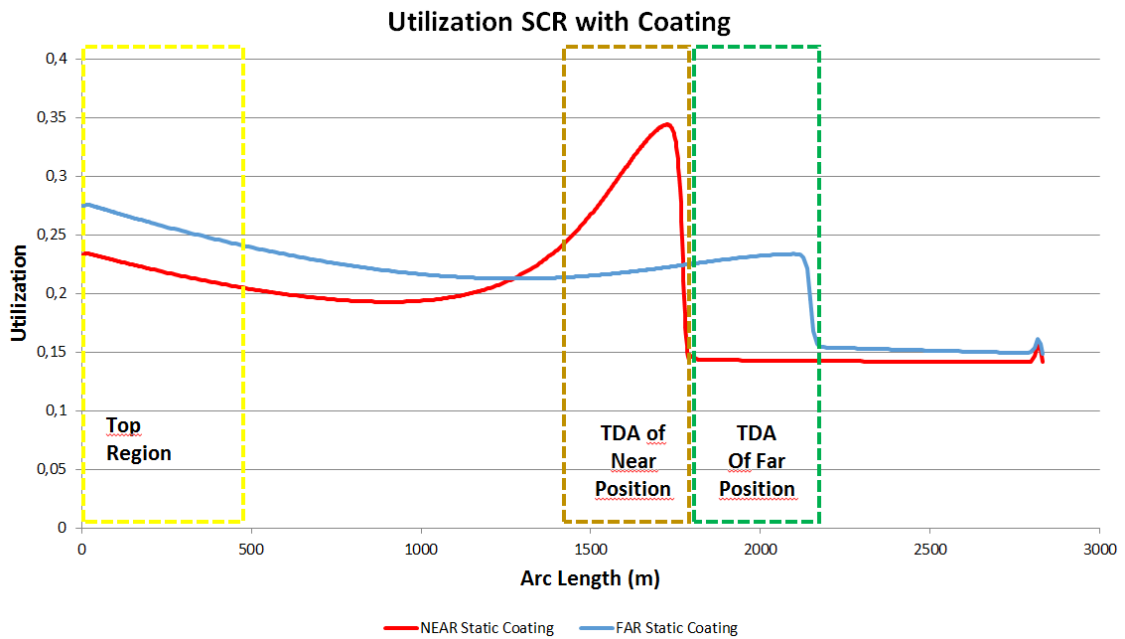


Figure 6-4 Static Utilization of SCR with Coating

- For the near offset position, the maximum utilization occurred in the TDA. For the far offset position, the maximum utilization occurred in the top region, see Figure 6-4. This is an indication that the maximum utilization is driven by the effective tension for the far offset position, while the maximum utilization is driven by the bending moment for the near offset position.
- The maximum utilization in the near offset position is more than the maximum utilization in the far offset position. This is an indication that the near offset position is more critical to the extreme response in the design.
- From the results above, it can be concluded that the bending moment is of greater importance than the effective tension, and will be the driving design parameter for the



riser. This is because the riser has structurally greater capacity to endure axial loads than lateral loads.

### 6.3.2 Static Analysis of WDSCR

The Weight Distributed SCR (WDSCR) is originally the modification of the conventional SCR. The modification is achieved by adding heavy riser cross-section at the bottom of the straight section of the SCR. According to Karunakaran et al. (2013), adding heavy riser cross-section at the bottom of straight section of the SCR will reduce dynamics of the straight section, thus decreasing the dynamic stresses in the TDA (Karunakaran et al., 2013). For deep water applications, this modification will increase the top tension and the dynamic axial stress in the top region.

The length of the heavy cross section is 300 m. The heavy cross-section comprises ballast modules which are attached per riser joint with 2000 kg weight at each interval length of 12 m. Consequently, there are 26 ballast modules along 300 m. In optimization study, it has been observed that if heavy cross sections touch the seabed, there will be excessive bending moment in the TDA. This is the consequence of the sudden drop of riser's sag-bend when the heavy cross section touches the seabed. Therefore, it is necessary to prevent the heavy cross section from touching seabed under any circumstances.

However, the heavy cross section should be placed at the bottom of the riser's straight section to effectively reduce the dynamic behavior in the TDA. Therefore, the following factors are considered to optimize the location where the heavy cross section is installed onto the riser.

1. An attachment type of the ballast module with 2000 kg weight is modeled.
2. To locate the ballast modules correctly, nodes are set with intervals of 12 m where the ballast module is added since the ballast module is added to each node.
3. Sufficient clearance height between the end of heavy cross section and the seabed in static equilibrium, to prevent the end of heavy cross section from touching the seabed in dynamic analysis.
4. The end of heavy cross section is located at 80 m above the seabed in the mean position in the static equilibrium.

Together with the consideration above, an ideal static configuration of the WDSCR is established as the base case configuration for further analyses. An illustration of the different offset positions and the resulting WDSCR configuration in intact mooring is shown in Figure 6-5. The red point is the ballast modules that are installed on each node along 300 m riser length. Although, the analysis was performed for the entire riser length, the summary static results of the WDSCR are presented in Table 6-3.

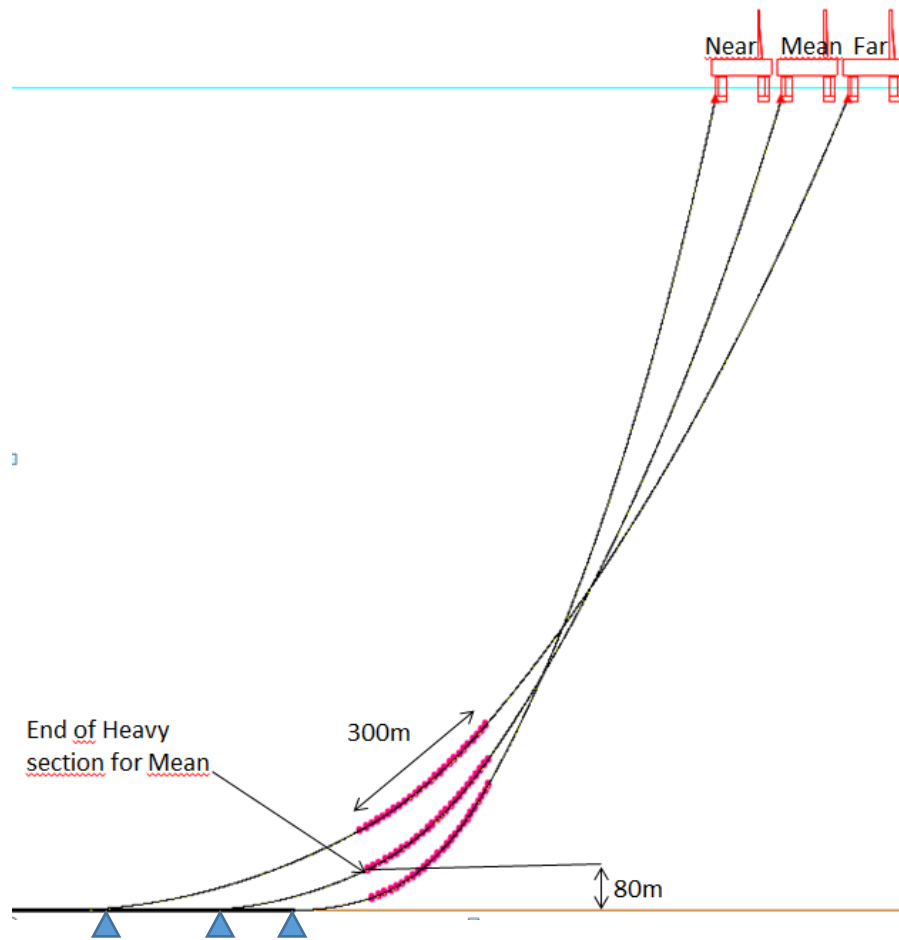


Figure 6-5 Intact-Static WDCR Configuration near, mean and far position

Table 6-3 WDCR Static Results- Functional Loads

WDCR Intact – Static	Coating			No Coating		
	Far	Mean	Near	Far	Mean	Near
Hang-off angle (°)	21	15	12	20	15	12
Effective top tension (kN)	3273	2859	2576	3688	3221	2906
Max. Bending Moment (kN.m)	73	112	183	69	106	173
Max. DNV Utilization (LRFD)	0.32	0.32	0.42	0.36	0.32	0.40

### **Discussion of WDCR Static Analysis Results:**

Most of the characteristics of the WDCR are similar to the conventional SCR, for instances, the maximum utilization and bending moment occurred in the near offset position, while the maximum effective top tension occurred in the far offset position. The following will discuss the WDCR response under functional loadings in the far, mean and near vessel position specifically in comparison with the conventional SCR:

- It can be seen that the different offset positions give significant impact on the configuration of the WDCR. The TDP location changes significantly, which causes the different static and dynamic behavior for the different offset positions.
- The WDCR without coating has more top tension, but less bending moment than the WDCR with coating, since the WDCR without coating is heavier than the WDCR with coating.

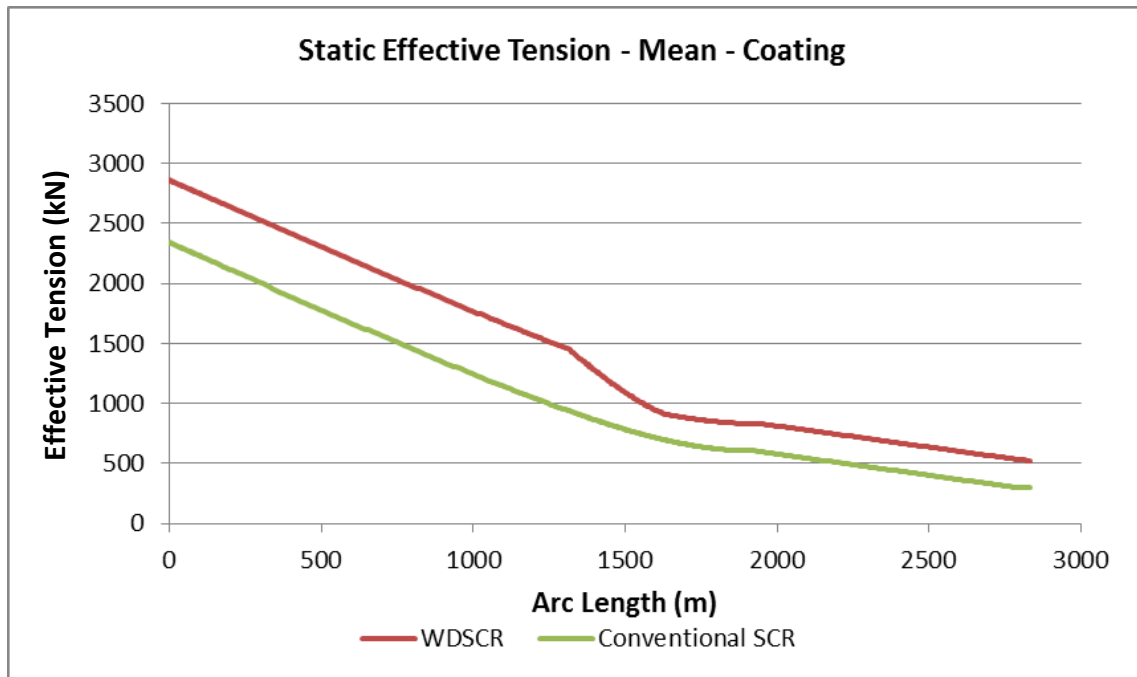


Figure 6-6 Effective Tension Comparison

- Figure 6-6 shows the comparison of WDSR and SCR in the mean position with coating. The WDSR has more effective top tension than the SCR in all corresponding positions. This is the consequences of installing heavy cross section at the bottom of straight section.

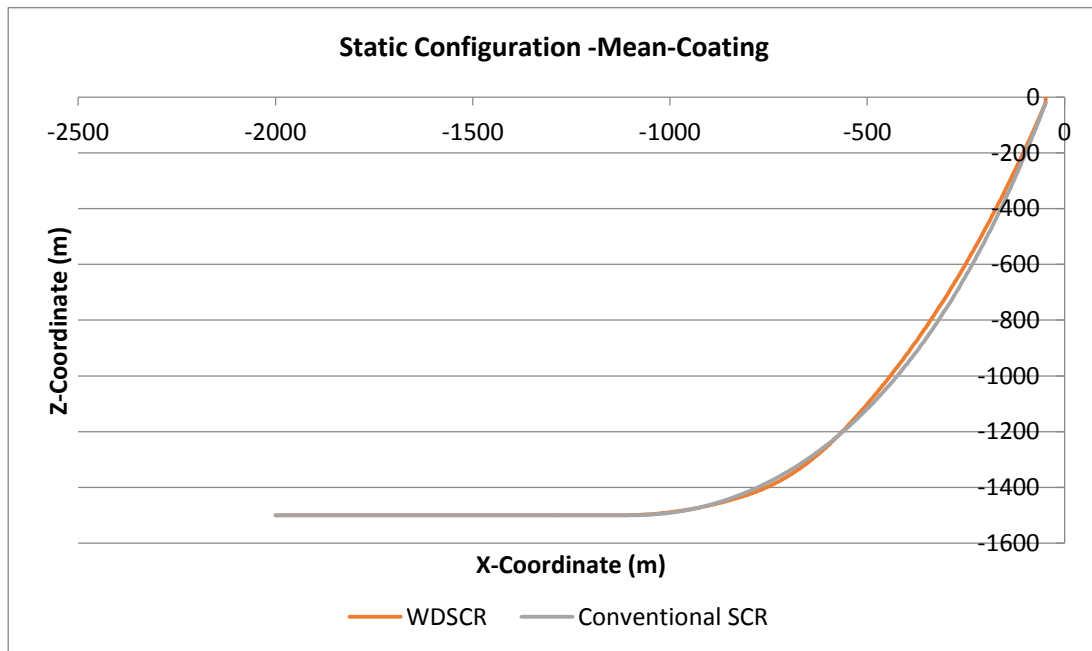


Figure 6-7 Static Configuration - Conventional SCR and WDSR

- The approach of the SCR to the seabed is smoother than the approach of the WDSR to the seabed, see Figure 6-7. This is the consequence of installing the heavy cross sections at the bottom of straight section. Thereby the static bending moment of the

WDSCR is more than the static bending moment of the conventional SCR as seen in Figure 6-8.

- Although, the static bending moment of the WDSCR is higher than the static bending moment of the conventional SCR, the heavy cross sections will reduce the dynamic response of the WDSCR in the TDA. Thereby the WDSCR is more insensitive to vessel heave motion than the SCR in dynamic response. This will be discussed in dynamic analysis section.
- It can be seen from Figure 6-8, the WDSCR has 2 peaks of bending moment which are located at the end of heavy cross section and at the TDP.

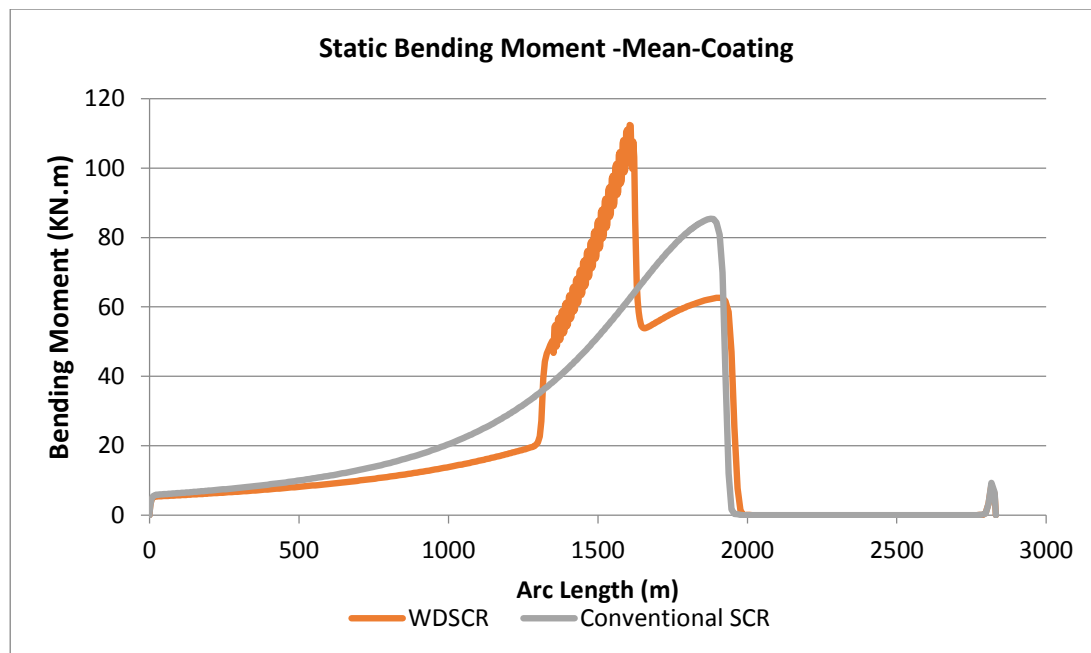


Figure 6-8 Static Bending Moment - Conventional SCR and WDSCR

### 6.3.3 Static Analysis of SLWR

The SLWR is originally a modification of the SCR as well. It has several buoyancy modules at the midsection of the riser, thus the configuration of riser is changed into lazy wave. These buoyancy modules can de-couple the dynamic motion of floater from the TDP and reduce the top payload. The properties of buoyancy module are presented in Table 5-6.

Since the buoyancy modules introduce additional stress in the sag-bend and hog-bend, high bending stresses at the sag-bend and the hog-bend become design issues for lazy wave configurations (Karunakaran et al., 1996). Therefore, it is important to ensure low bending stresses at the sag-bend and hog-bend. In order to achieve an ideal configuration, the following factors are considered.

- Optimized number of buoyancy elements and the position of buoyancy elements, to ensure that the SLWR design has “low lazy configuration”.
- Sufficient vertical distances between the lowest sag-bend and the highest hog-bend for all vessel positions, especially in the far offset position, since far offset position gives the minimum vertical distances between the lowest sag-bend and the highest hog-

bend. This is important to isolate the TDP motion from the sag-bend motion. This is also important to maintain the same position of TDP in the different vessel offsets.

- Sufficient clearance between the lowest sag-bend and the seabed, to prevent the sag-bend from touching the seabed under any circumstances, especially when the vessel is in the near offset position, since the near offset position gives the minimum clearance between the lowest sag-bend and the seabed.

Together with the considerations above, an ideal static configuration of the SLWR is established. The selected parameters are presented in Table 6-4 as the base case of the SLWR configuration. An illustration of offset positions and the resulting SLWR configuration in intact mooring is shown in Figure 6-9.

Table 6-4 Selected Parameters for SLWR configuration

Parameter	Value	Unit
Total riser length, $L$	2842	m
Upper section length, $S_1$	1680	m
Buoyant section length, $S_2$	500	m
lower section length, $S_3$	662	m
Horizontal distances between hang-off and touchdown point, $H_1$ (at mean position)	1330	m
Horizontal distances between hang-off and seabed connection, $H_2$	1802	m
Vertical distances between lowest sag-bend & highest hog-bend, $V_1$ (at mean position)	72	m
Vertical distances between lowest sag-bend and seabed, $V_2$ (at mean position)	115	m
Vertical distances between lowest sag-bend and highest hog-bend, $V_1$ (at far position)	29	m
Vertical distances between lowest sag-bend and seabed, $V_2$ (at near position)	80	m

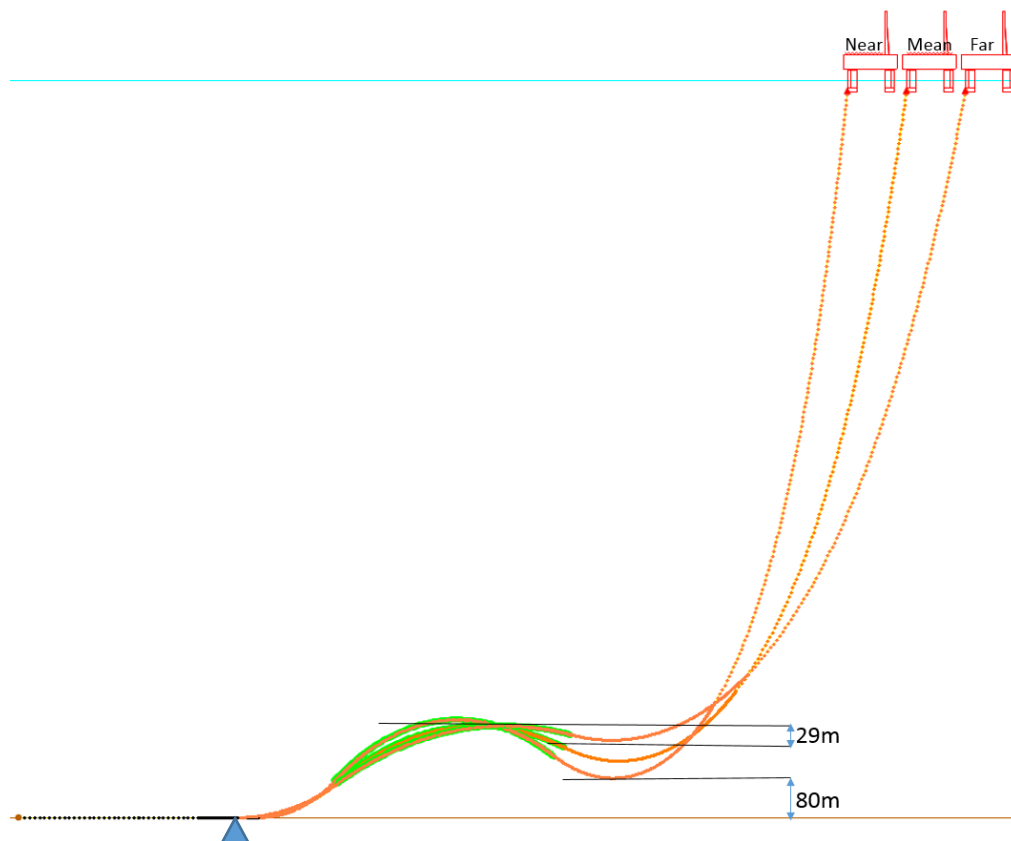


Figure 6-9 Intact-Static SLWR configuration near, mean and far position

The static results of the SLWR are summarized in Table 6-5 .

Table 6-5 SLWR Static Results- Functional Loads

	Critical Location	Coating			No Coating		
		Far	Mean	Near	Far	Mean	Near
Hang-off angle (°)	Top	11	8	6	11	8	6
Effective Top Tension	Top	1910	1859	1832	2225	2165	2133
Effective tension (kN)	Sag-bend	443	343	281	492	369	291
	Hog-bend	440	339	276	493	370	292
	TDP	439	338	275	492	369	291
Max. Bending Moment (kN.m)	Sag-bend	145	201	272	144	202	277
	Hog-bend	88	122	165	75	106	146
	TDP	141	191	250	141	193	256
Max. DNV Utilization (LRFD)	Sag-bend	0.36	0.44	0.54	0.36	0.44	0.55
	Hog-bend	0.28	0.32	0.39	0.26	0.30	0.36
	TDP	0.35	0.42	0.51	0.35	0.43	0.52

### **Discussion of SLWR Static Analysis Results:**

The following is a general discussion of the SLWR response under functional loadings in the far, mean and near vessel position:

- It can be seen that the different offset positions do not change the TDP location. The only change is identified in the configuration of the sag-bend and hog-bend. Thereby it is important to establish sufficient vertical distances between lowest sag-bend and highest hog-bend to maintain the same TDP position.
- The effective tensions at the sag-bend, hog-bend, and TDP are fairly equal. This indicates that the forces acting at the sag-bend, hog-bend and TDP are mainly horizontal.
- The SLWR without coating has more effective top tension than the SLWR with coating since the SLWR without coating is heavier than the SLWR with coating.
- The maximum bending moment at the hog-bend is fairly low compared to the maximum bending moment at the sag-bend and the TDP. The maximum bending moment at the hog-bend is lowest at the far offset position and is highest at the near offset position.
- The near offset position gives more bending moment than far offset position. This is because the smaller curvature of lazy wave configuration is achieved at the near offset position compared to the far offset position, see Figure 6-9.
- The utilization at the sag-bend and the TDP are higher than the utilizations at the hog-bend. This indicates that the sag-bend and TDP are more critical to extreme response in the SLWR design.
- The maximum utilization value is 0.55 at the sag-bend of the SLWR without coating.

### 6.3.4 Comparison - Static Results

In this section, the static results of three riser configurations with coating will be compared in terms of effective tension and bending moment for entire riser length. Only mean position is compared. The aim is to show different responses of the three riser configuration in terms of static equilibrium. From the Figure 6-10, it can be analyzed that the WDSCR has the greatest effective tension since it has the heavy cross sections.

On the other hand, the SLWR has the lightest riser configuration since it is equipped with the buoyancy modules, giving net upward buoyancy to the riser. The effective tension at the hang-off point is referred to as the top payload. Consideration should be given to the WDSCR in terms of capacity of the floater to accommodate such top payload. It is also observed that the static effective tension of WDSCR has a sudden drop in the area of the heavy cross sections. This is because the region below heavy cross sections is not affected by the contribution of axial loads from the heavy cross sections.

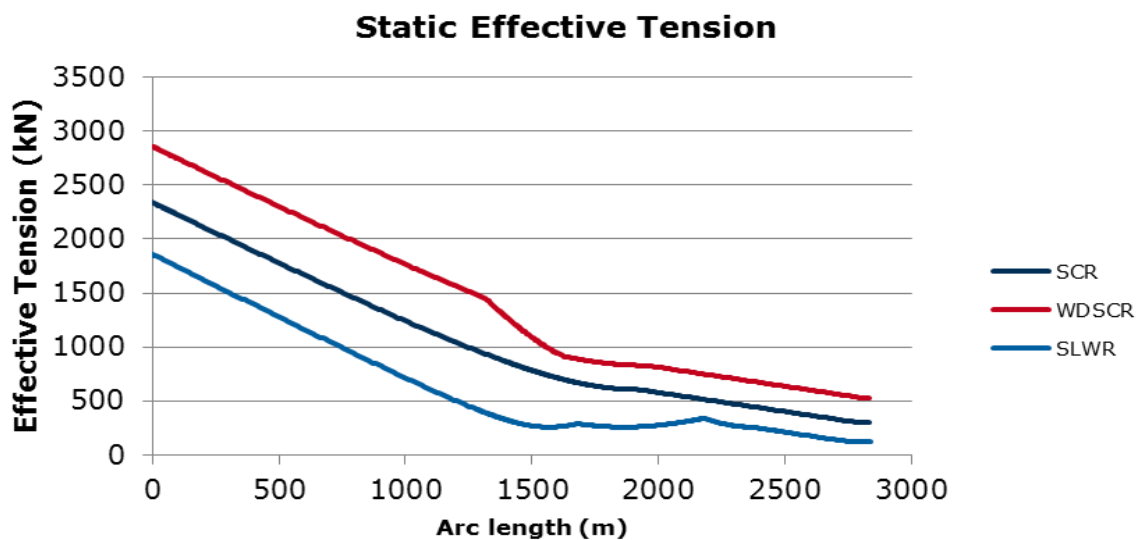


Figure 6-10 Comparison of Effective Tension – Mean Position – Static

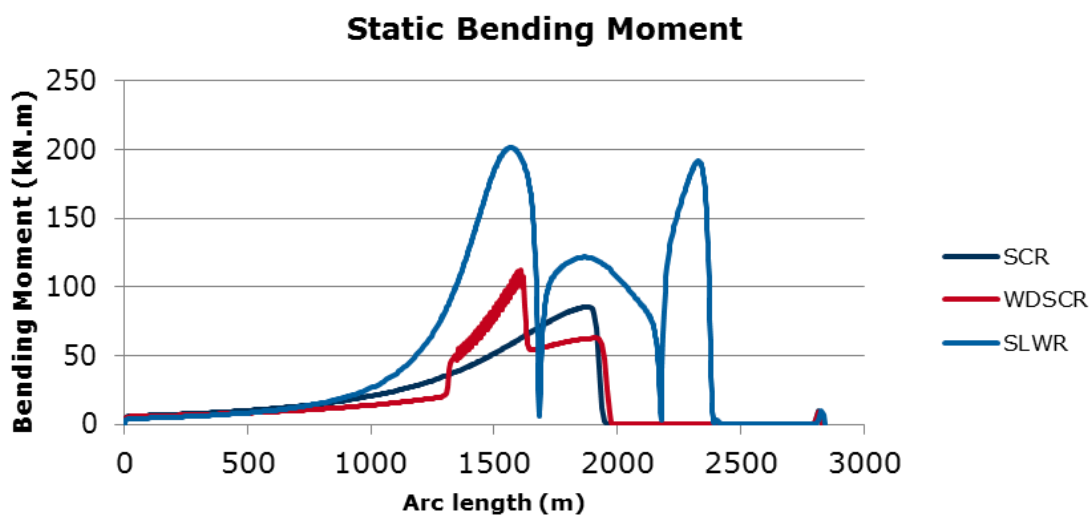


Figure 6-11 Comparison of Bending Moment – Mean Position- Static

From the Figure 6-11, it can be analyzed that the SLWR has the greatest static bending moment compared to the SCR and the WDSCR. These three peaks of bending moment occurred at the sag-bend, hog-bend and TDP. This is the consequences of lazy wave configuration resulting in small curvature at the sag-bend, hog-bend and TDP. The WDSCR has greater static bending moments than the SCR in this case as discussed earlier.

## 6.4 Dynamic Analysis

The dynamic analysis was carried out considering ULS and ALS design to analyze the dynamic response of the SCR, WDSCR and SLWR. The intact condition refers to ULS design for 120 meter offsets and the damage condition refers to ALS design for 150 meter offsets. The extreme response is estimated using time domain analysis based on many 3-hour long random simulations. The riser integrity was then checked against the load cases as presented in Table 6-1. The interest results from the dynamic analyses for the strength design are dynamic effective tension force and dynamic bending moment. Compression is also one of the interest results in the dynamic analysis, since it might result into riser buckle. The compression can be identified as the negative effective tension or minimum effective tension.

The three riser configuration will be checked to see how it can accommodate the floater motion induced from the load cases. The capability of the riser to cope with floater motion is indicated by the utilization of the riser. If the utilization is less than unity, the riser is then considered within the allowable design criteria and vice-versa. For the preliminary design, the conventional SCR is checked against the load case 3. If the conventional SCR configuration is still within the allowable design criteria, then the next load case is performed until the certain load case where the SCR is not able to cope with.

Afterwards, the WDSCR configuration is checked against the load case which the SCR is not able to cope with. Subsequently, the WDSCR configuration is checked against the next load cases until the certain load case which the WDSCR is not able to cope with. Eventually, the SLWR configuration is checked against the load case which WDSCR cannot cope with.

The SLWR will then be checked against all the rest of load cases until the load case 15. This methodology is carried out since the SCR is the most sensitive configuration to the vessel motion. The extreme analysis was carried out as described in section 5.6. The environmental load of waves and current were applied in-plane with the riser's lay direction for both  $0^\circ$  and  $180^\circ$  direction with far and near position, respectively. This scenario is considered to capture the worst scenario. The next section will discuss the dynamic analysis result for both with coating and without coating to see how coating influences the dynamic responses of the riser.

### 6.4.1 Dynamic Analysis of Conventional SCR

#### Load Case 3

The summary of the dynamic analysis responses of the conventional SCR against the load case 3 is presented in Table 6-6 for ULS and ALS design.



Table 6-6 SCR-Strength Response Summary for Load Case 3

Load Case 3	Semi Position				
	Coating	Intact		Damage	
		Far	Near	Far	Near
Max. Effective Tension (kN)	3758	2455	3952	2356	
Max. Compression (kN)	0	0	0	21	
Max. Bending Moment (kN.m)	93	374	84	428	
Max. DNV Utilization (LRFD)	0.43	0.77	0.37	0.71	
<b>No Coating</b>					
Max. Effective Tension (kN)	3922	2721	4121	2629	
Max. Compression (kN)	0	0	0	0	
Max. Bending Moment (kN.m)	77	287	67	333	
Max. DNV Utilization (LRFD)	0.43	0.62	0.38	0.59	

The maximum utilization is observed in near-ULS design. The maximum utilizations of the SCR with coating and the SCR without coating are 0.77 and 0.62, respectively and are observed in the TDA. This is an indication that the near-ULS design is more critical to extreme response to the design. The compression is only identified in the near-ALS design of the SCR with coating. The maximum downward velocity at the hang-off point is 1.75 m/s. This showed that the SCR configuration can cope with downward velocity of 1.75 m/s.

#### Load Case 4

As the results of the SCR are within allowable design criteria for the load case 3, the next analysis is to check the SCR integrity against the load case 4. The summary of the dynamic analysis responses of the SCR against the load case 4 is presented in Table 6-7 for ULS and ALS design.

Table 6-7 SCR-Strength Response Summary for Load Case 4

Load Case 4	Semi Position				
	Coating	Intact		Damage	
		Far	Near	Far	Near
Max. Effective Tension (kN)	4019	2530	4232	2421	
Max. Compression (kN)	0	80	0	107	
Max. Bending Moment (kN.m)	124	466	104	529	
Max. DNV Utilization (LRFD)	0.47	0.91	0.40	0.85	
<b>No Coating</b>					
Max. Effective Tension (kN)	4123	2784	4338	2685	
Max. Compression (kN)	0	0	0	0	
Max. Bending Moment (kN.m)	89	345	77	401	
Max. DNV Utilization (LRFD)	0.46	0.72	0.41	0.68	

The near-ALS design has more compression than the near-ULS design. The maximum utilization is observed in the near-ULS design. Both the SCR with coating and the SCR without coating have maximum utilization of 0.91 and 0.72, respectively which are still

within allowable design criteria. The maximum downward velocity at the hang-off point is 2.04 m/s. This showed that, the SCR configuration can cope with downward velocity of 2.04 m/s.

### **Load Case 5**

As the results of the SCR are within the allowable design criteria for the load case 4, the next analysis is to check the SCR integrity against the load case 5. The summary of the dynamic analysis responses of the SCR against the load case 5 is presented in Table 6-8 for ULS and ALS design.

Table 6-8 SCR-Strength Response Summary for Load Case 5

Coating	Semi Position			
	Intact		Damage	
	Far	Near	Far	Near
<b>Max. Effective Tension (kN)</b>	<b>4305</b>	<b>2604</b>	<b>4537</b>	<b>2485</b>
<b>Max. Compression (kN)</b>	<b>0</b>	<b>181</b>	<b>0</b>	<b>206</b>
<b>Max. Bending Moment (kN.m)</b>	<b>173</b>	<b>586</b>	<b>146</b>	<b>654</b>
<b>Max. DNV Utilization (LRFD)</b>	<b>0.51</b>	<b>1.14</b>	<b>0.44</b>	<b>1.01</b>
<b>No Coating</b>				
<b>Max. Effective Tension (kN)</b>	<b>4345</b>	<b>2847</b>	<b>4576</b>	<b>2741</b>
<b>Max. Compression (kN)</b>	<b>0</b>	<b>14</b>	<b>0</b>	<b>52</b>
<b>Max. Bending Moment (kN.m)</b>	<b>110</b>	<b>422</b>	<b>94</b>	<b>487</b>
<b>Max. DNV Utilization (LRFD)</b>	<b>0.50</b>	<b>0.85</b>	<b>0.43</b>	<b>0.79</b>

The SCR with coating has maximum utilization of 1.14 which is no longer within the allowable design criteria for the near-ULS design. In contrast, the SCR without coating has the maximum utilization of 0.85 which is still within the allowable design criteria for the near-ULS design. This showed that the SCR without coating can cope with higher downward velocity at the hang-off point compared to the SCR with coating. The maximum downward velocity at the hang-off point is 2.33 m/s in this case. The maximum utilization at the TDP and the maximum downward velocity at the hang-off point occurred at the same time.

This is an indication that the maximum downward velocity at the hang-off point induces the maximum utilization at the TDP for the SCR with coating. To see how the responses of the SCR with coating associate with the vertical velocity at the hang-off point, the vertical velocity at the hang-off point and the SCR responses (i.e. bending moment and the effective tension) at the TDP are then plotted over time history for the near-ULS design, see Figure 6-12.

From the upper part of Figure 6-12, it can be seen from the graph that the vertical velocities at the hang-off point and the effective tensions at the TDP synchronize with respect to the “rise” and “fall”, while the maximum downward velocity at the hang-off point associates directly with the minimum effective tension (compression) at the TDP. This is an indication that the maximum downward velocity at the hang-off point induces the maximum compression at the TDP.

From the lower part of Figure 6-12, it can be seen from the graph that the vertical velocities at the hang-off point and bending moments at the TDP synchronize with respect to the “rise” and “fall” in the opposite direction, while the maximum downward velocity at the hang-off point associates directly with the maximum bending moment at the TDP. This is an indication that the maximum downward velocity at the hang-off point induces the maximum bending moment at the TDP.

It can be concluded that the maximum downward velocity at the hang-off point induces both the maximum bending moment (586 kN.m) and the maximum compression (181 kN) at the TDP simultaneously. The combination of the maximum bending moment and the maximum compression results in the excessive buckling utilization to riser. The maximum downward velocity at the hang-off point can be concluded as a key driving parameter of riser integrity. To sum up, the SCR with coating is not able to cope with maximum downward velocity of 2.33 m/s.

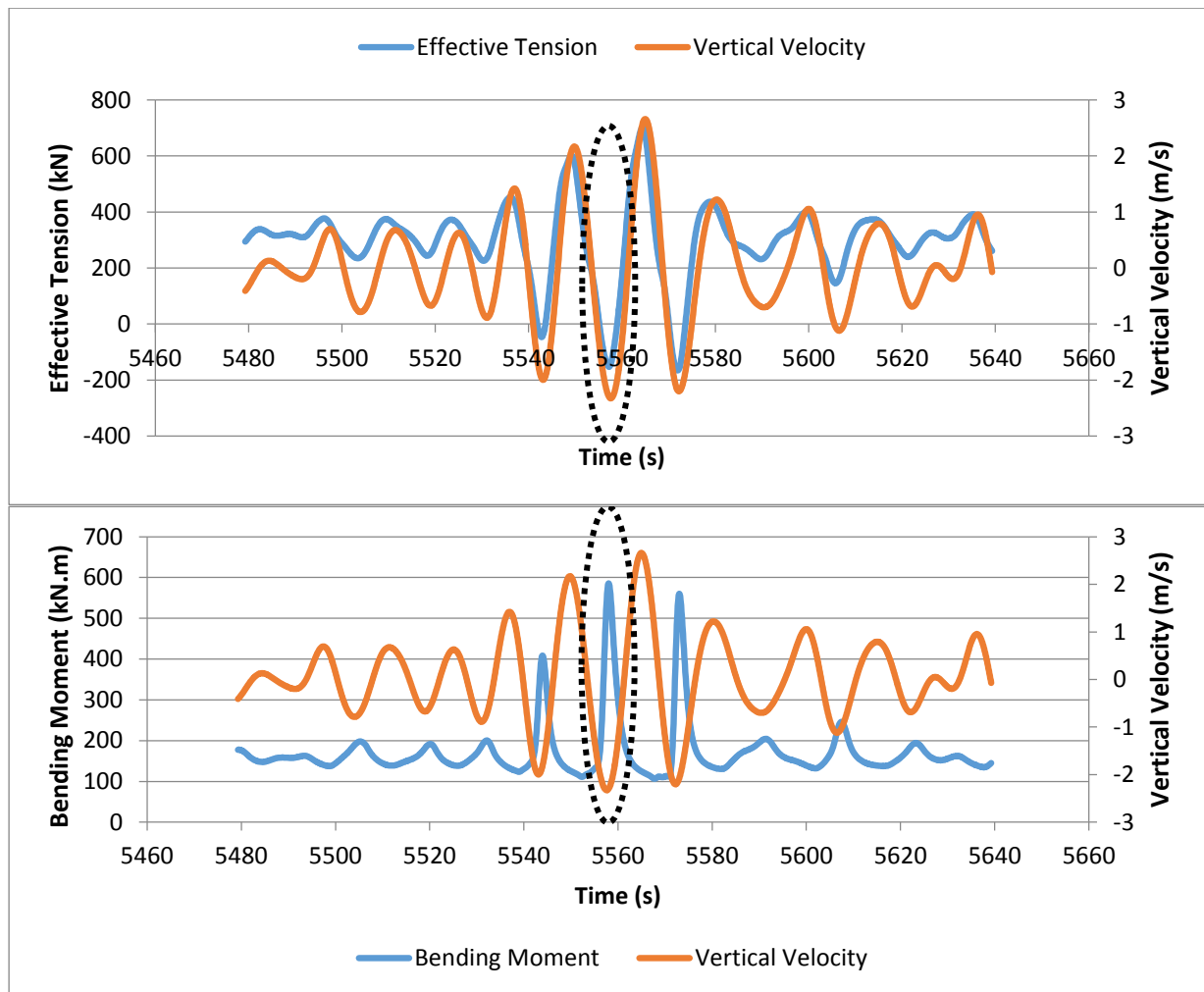


Figure 6-12 Time History: Effective Tension and Bending Moment -SCR-Coating-LC5- Near-ULS Design

### **Load Case 6**

As the results of the SCR without coating is within allowable design criteria for the load case 5, the SCR without coating is then checked against the load case 6. The summary of the

dynamic analysis responses of the conventional SCR against load case 6 is presented in Table 6-9 for ULS and ALS design.

Table 6-9 SCR without Coating-Strength Response Summary for Load Case 6

Load Case 6	Semi Position				
	No Coating	Intact		Damage	
		Far	Near	Far	Near
Max. Effective Tension (kN)	4585	2911	4834	2798	
Max. Compression (kN)	0	103	0	140	
Max. Bending Moment (kN.m)	143	521	120	595	
Max. DNV Utilization (LRFD)	0.54	1.03	0.46	0.94	

Since the maximum utilization is 1.03 for near-ULS design, the SCR without coating is no longer within allowable design criteria for the load case 6. The maximum downwards velocity at the hang-off point in this case is 2.62 m/s. A time-history plot of the vertical velocities at the hang-off point and the effective tensions at the TDP is shown in the upper part of Figure 6-13, while a time-history plot of the vertical velocities at the hang-off point and the bending moments at the TDP is shown in the lower part of Figure 6-13.

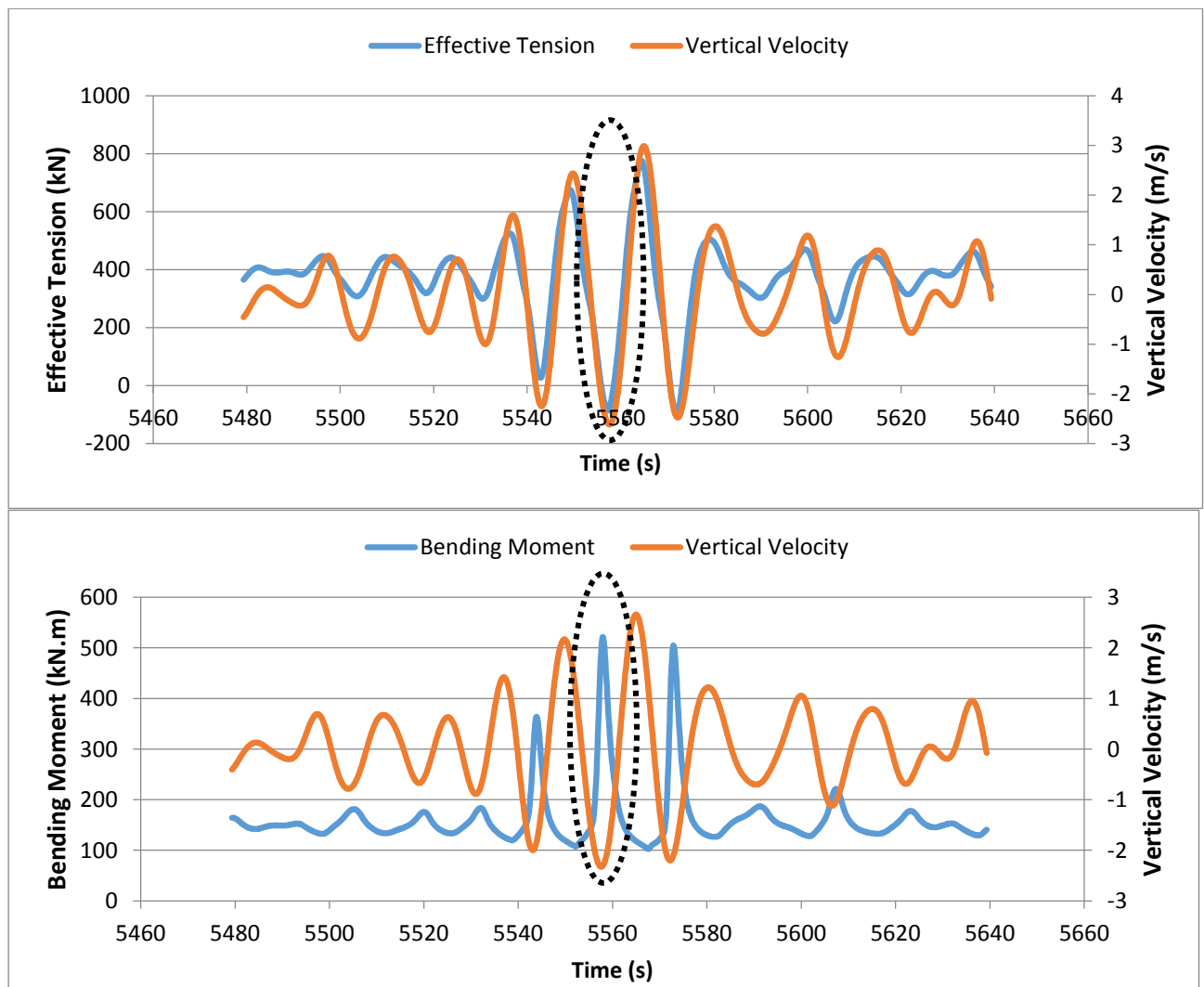


Figure 6-13 Time History: Bending Moment and Effective Tension - SCR-No Coating-LC6-Near-ULS

From the upper part of Figure 6-13, it can be seen from the graph that the vertical velocities at the hang-off point and the effective tensions at the TDP synchronize with respect to the “rise” and “fall”, while the maximum downward velocity at the hang-off point associates directly with the minimum effective tension (compression) at the TDP. From the lower part of Figure 6-13, it can be seen from the graph that the vertical velocities at the hang-off point and the bending moments at the TDP synchronize with respect to the “rise” and “fall” in the opposite direction, while the maximum downward velocity at the hang-off point associates directly with the maximum bending moment at the TDP.

Together with the maximum bending moment and the maximum compression, riser is subjected to buckling, giving excessive buckling utilization to the riser. These responses explain how the maximum downward velocity determines the maximum utilization. This phenomenon is identical with the previous case. In summary, the SCR without coating is not able to cope with maximum downward velocity of 2.62 m/s.

In general, the following are summarized from the conventional SCR response:

- The difference between the static utilization and the dynamic utilization is more than 0.7 for the near-ULS design for the load case 5. This difference can be even higher in harsher environment. This is an indication that the SCR is very sensitive to floater heave motion.
- The SCR with coating has higher utilization than the SCR without coating. This is an indication that coating makes riser lighter and more sensitive to the floater heave motion. Thus, it can be concluded that the heavier the riser, the less sensitive riser to the floater heave motion for SCR configuration.
- For near-ULS design with load case 5, the maximum compression of the SCR with coating is 181 kN and the maximum compression of the SCR without coating is 14 kN, see Figure 6-14. The compression (negative effective tension) is unwanted as compression might result into riser buckle. This is an indication that the lighter SCR has more compression than the heavier SCR. The SCR needs to be heavy enough to avoid compression.

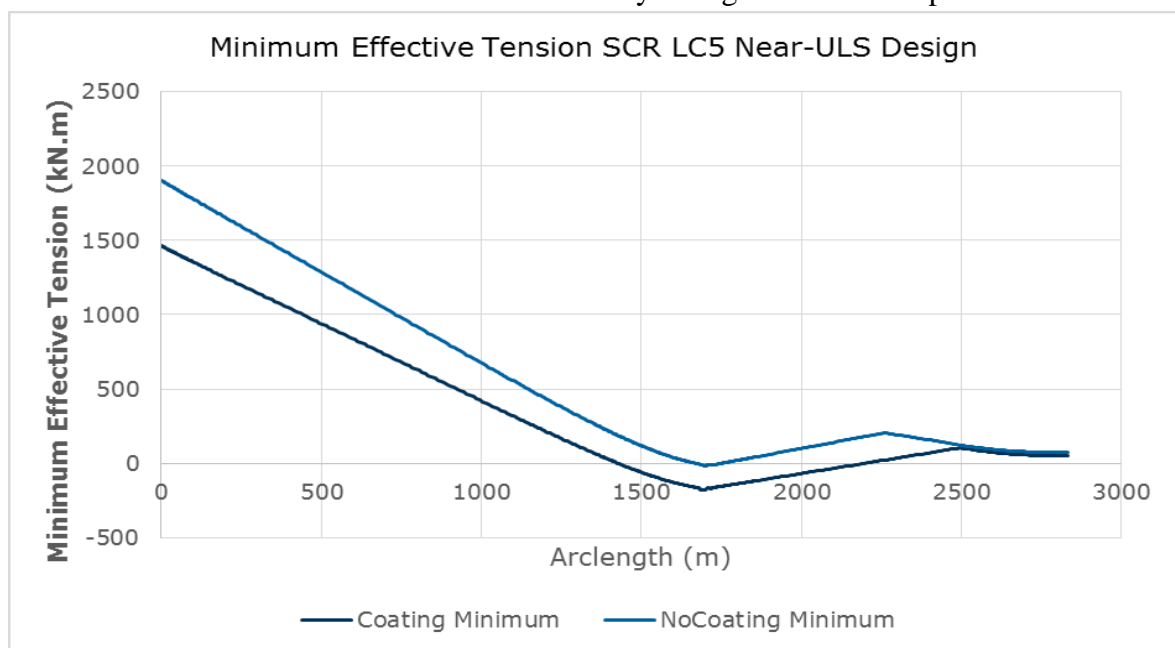


Figure 6-14 Minimum Dynamic Effective Tension SCR-LC5

- The near-ULS design always gives the maximum utilization. This is an indication that the near-ULS design is the critical to the design for SCR configuration.
- From the Figure 6-12 and the Figure 6-13, it can be seen that the upward velocity increases the effective tensions and decreases the bending moments at the TDP. Oppositely, the downward velocity decreases the effective tension and increases the bending moment.
- The maximum downward velocity induces the combination of the maximum compression and the maximum bending moment. The combination of the maximum compression (negative effective tension) and the maximum bending moment induces the maximum utilization.
- The maximum utilization and maximum downward velocity at the hang-off point occurred simultaneously. This is an indication that the maximum downward velocity at the hang-off point can be concluded as a key driving parameter of riser integrity.

## 6.4.2 Dynamic Analysis of WDSCR

### Load Case 5

The WDSCR integrity is checked against the load case 5. The summary of the dynamic analysis responses of the WDSCR against load case 5 is presented in Table 6-10 for ULS and ALS design.

Table 6-10 WDSCR-Strength Response Summary for Load Case 5

Load Case 5	Semi Position			
	Intact		Damage	
	Far	Near	Far	Near
<b>Coating</b>				
<b>Max. Effective Tension (kN)</b>	<b>4902</b>	<b>3097</b>	<b>5163</b>	<b>2963</b>
<b>Max. Compression (kN)</b>	<b>0</b>	<b>0</b>	<b>0</b>	<b>0</b>
<b>Max. Bending Moment (kN.m)</b>	<b>111</b>	<b>297</b>	<b>96</b>	<b>372</b>
<b>Max. DNV Utilization (LRFD)</b>	<b>0.59</b>	<b>0.64</b>	<b>0.50</b>	<b>0.64</b>
<b>No Coating</b>				
<b>Max. Effective Tension (kN)</b>	<b>4976</b>	<b>3365</b>	<b>5231</b>	<b>3240</b>
<b>Max. Compression (kN)</b>	<b>0</b>	<b>0</b>	<b>0</b>	<b>0</b>
<b>Max. Bending Moment (kN.m)</b>	<b>80</b>	<b>244</b>	<b>69</b>	<b>297</b>
<b>Max. DNV Utilization (LRFD)</b>	<b>0.58</b>	<b>0.55</b>	<b>0.50</b>	<b>0.54</b>

In general, the following are summarized from the WDSCR response against load case 5:

- In dynamic analysis, providing heavy cross sections at the bottom of straight section could improve significantly the riser integrity by reducing the maximum utilization from 1.14 to 0.64. The maximum utilization of the SCR and the WDSCR are then plotted over the entire length in Figure 6-15 for near-ULS design. It is seen clearly how WDSCR improve the riser integrity by having much less utilization at the TDP.
- Figure 6-16 presents the comparison of the SCR and the WDSR in terms of maximum dynamic bending moment over entire riser length for near-ULS design. It is seen from Figure 6-16, the heavy cross section reduces the dynamic bending moment at the TDP. The

dynamic bending moment is reduced significantly about 300 kN.m by introducing heavy cross section for the WDSCR.

- It is observed that no compression occurred in the WDSCR for load case 5, while compression occurred in the SCR for load case 5 as described in Table 6-8. This is an indication that the heavy cross section reduces the dynamic behavior of the riser; thereby the negative effective tension can be eliminated or reduced.
- The WDSCR becomes less sensitive to floater heave motion compared to the SCR. This is the consequences of adding the heavy cross section at the bottom of straight section.
- The maximum utilization is 0.64 and 0.55 for coating and no coating respectively, for near-ULS design. This has been identified that the coating makes riser lighter and more sensitive to the floater heave motion, thus the WDSCR with coating has higher utilization than the WDSCR without coating.
- In this case, the maximum downward velocity at the hang-off point is 2.33 m/s. This shows that the WDSCR can cope with downward velocity of 2.33 m/s at the hang-off point.

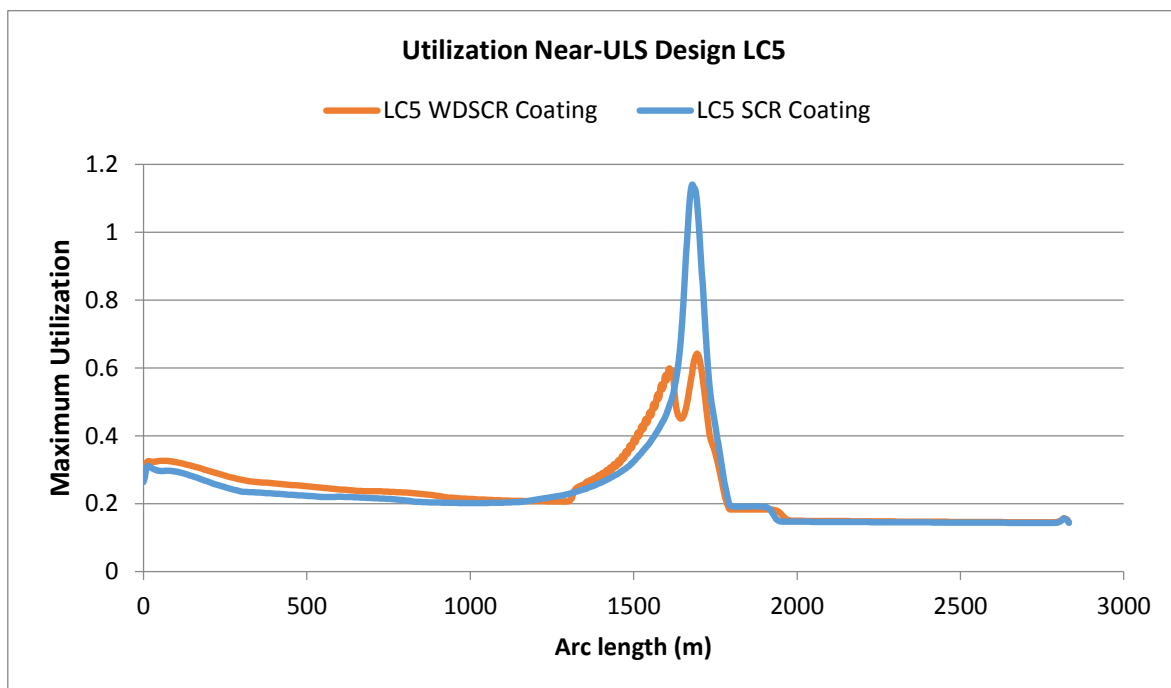


Figure 6-15 Maximum Dynamic Utilization of SCR and WDSCR with Coating

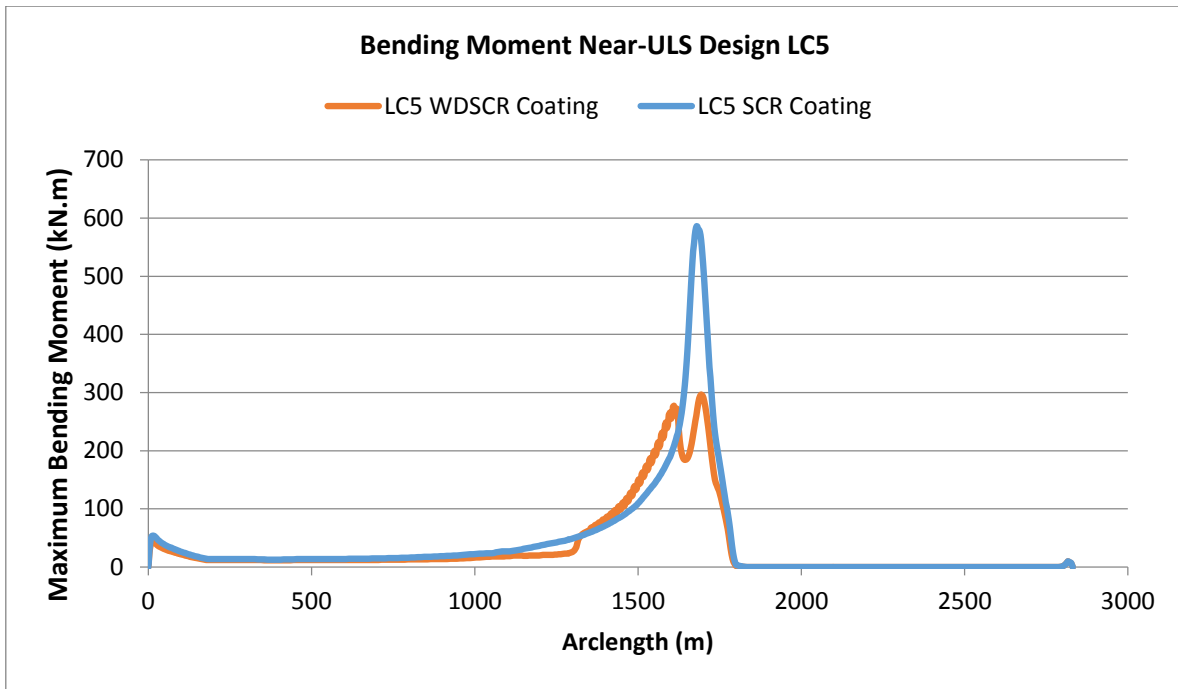


Figure 6-16 Maximum Dynamic Bending Moment Comparison of SCR and WDSCR with Coating

To further investigate the strength improvement of the WDSCR compared to the conventional SCR for load case 5, the range of dynamic motions along the entire riser length is investigated. The best interest from dynamic motions for strength analysis is the maximum downward velocity at the TDP where the maximum utilization occurred. The maximum downward velocity along the entire riser length for the SCR with coating and the WDSCR with coating is presented in Figure 6-17.

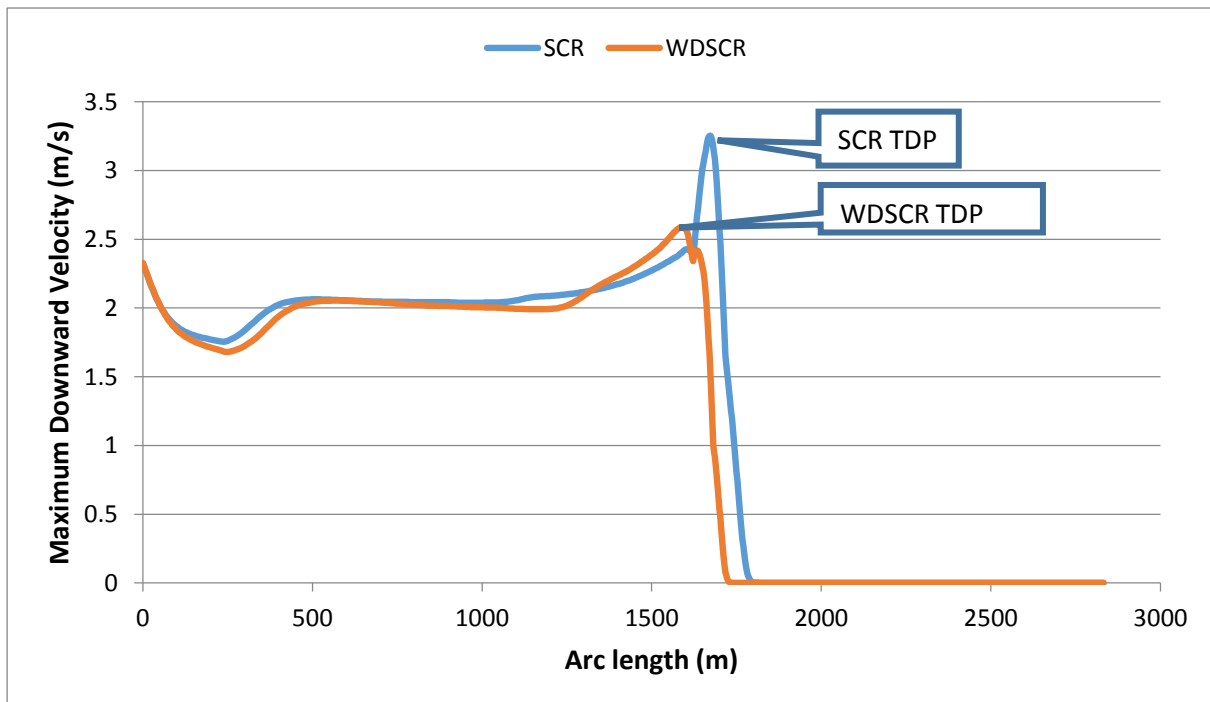


Figure 6-17 Maximum Downward Velocity Range for WDSCR and Conventional SCR – Load Case 5



From the Figure 6-17, it can be analyzed that the ballast modules are effective to reduce the dynamic motion at the TDP, resulting in lower utilization. Even though the WDSCR and SCR have the same downward velocity at the hang-off point, the WDSCR configuration has much lower dynamic motion at the TDP compared to the SCR as seen in Figure 6-17. This lower dynamic motion of the WDSCR is also beneficial from a fatigue point of view. This explains why heavy cross sections can improve the SCR response in the critical area. This gives a good understanding that the WDSCR configuration has more capability to cope with floater heave motion with significantly lower utilization at the TDP compared to the SCR.

### **Load Case 6**

The summary of the dynamic analysis responses of the WDSCR against the load case 6 is presented in Table 6-11 for ULS and ALS design.

Table 6-11 WDSCR-Strength Response Summary for Load Case 6

Load Case 6	Semi Position				
	Coating	Intact		Damage	
		Far	Near	Far	Near
<b>Max. Effective Tension (kN)</b>	<b>5219</b>	<b>3180</b>	<b>5504</b>	<b>3038</b>	
<b>Max. Compression (kN)</b>	<b>0</b>	<b>72</b>	<b>0</b>	<b>83</b>	
<b>Max. Bending Moment (kN.m)</b>	<b>159</b>	<b>372</b>	<b>137</b>	<b>414</b>	
<b>Max. DNV Utilization (LRFD)</b>	<b>0.65</b>	<b>0.77</b>	<b>0.54</b>	<b>0.69</b>	
<b>No Coating</b>					
<b>Max. Effective Tension (kN)</b>	<b>5227</b>	<b>3439</b>	<b>5502</b>	<b>3310</b>	
<b>Max. Compression (kN)</b>	<b>0</b>	<b>0</b>	<b>0</b>	<b>0</b>	
<b>Max. Bending Moment (kN.m)</b>	<b>101</b>	<b>299</b>	<b>86</b>	<b>317</b>	
<b>Max. DNV Utilization (LRFD)</b>	<b>0.63</b>	<b>0.65</b>	<b>0.53</b>	<b>0.56</b>	

The maximum utilization is observed in near-ULS design. The maximum utilizations are 0.77 and 0.65 for the WDSCR with coating and the WDSCR without coating, respectively. In this case, the maximum downward velocity at the hang-off point is 2.62 m/s. This shows that WDSCR can cope with downward velocity of 2.62 m/s at the hang-off point.

### **Load Case 7**

The summary of the dynamic analysis responses of the WDSCR against the load case 7 is presented in Table 6-12 for ULS and ALS design.

Table 6-12 WDSCR-Strength Response Summary for Load Case 7

Load Case 7	Semi Position				
	Coating	Intact		Damage	
		Far	Near	Far	Near
<b>Max. Effective Tension (kN)</b>	<b>5560</b>	<b>3270</b>	<b>5869</b>	<b>3120</b>	
<b>Max. Compression (kN)</b>	<b>23</b>	<b>179</b>	<b>0</b>	<b>195</b>	
<b>Max. Bending Moment (kN.m)</b>	<b>235</b>	<b>468</b>	<b>204</b>	<b>463</b>	
<b>Max. DNV Utilization (LRFD)</b>	<b>0.71</b>	<b>0.94</b>	<b>0.59</b>	<b>0.76</b>	

<b>No Coating</b>				
<b>Max. Effective Tension (kN)</b>	<b>5500</b>	<b>3522</b>	<b>5795</b>	<b>3386</b>
<b>Max. Compression (kN)</b>	<b>0</b>	<b>18</b>	<b>0</b>	<b>52</b>
<b>Max. Bending Moment (kN.m)</b>	<b>133</b>	<b>369</b>	<b>113</b>	<b>387</b>
<b>Max. DNV Utilization (LRFD)</b>	<b>0.68</b>	<b>0.77</b>	<b>0.57</b>	<b>0.66</b>

The maximum utilization is observed in near-ULS design. The maximum utilizations are 0.94 and 0.77 for the WDSCR with coating and the WDSCR without coating respectively. In this case, the maximum downward velocity at the hang-off point is 2.91 m/s. This shows that the WDSCR can cope with downward velocity of 2.91 m/s at the hang-off point.

### **Load Case 8**

The summary of the dynamic analysis responses of the WDSCR against the load case 8 is presented in Table 6-13 for ULS and ALS design.

Table 6-13 WDSCR-Strength Response Summary for Load Case 8

<b>Load Case 8</b>	<b>Semi Position</b>				
	<b>Coating</b>	<b>Intact</b>		<b>Damage</b>	
		<b>Far</b>	<b>Near</b>	<b>Far</b>	<b>Near</b>
<b>Max. Effective Tension (kN)</b>	<b>5546</b>	<b>3309</b>	<b>5757</b>	<b>3137</b>	
<b>Max. Compression (kN)</b>	<b>335</b>	<b>373</b>	<b>465</b>	<b>433</b>	
<b>Max. Bending Moment (kN.m)</b>	<b>298</b>	<b>661</b>	<b>311</b>	<b>591</b>	
<b>Max. DNV Utilization (LRFD)</b>	<b>0.71</b>	<b>1.28</b>	<b>0.57</b>	<b>0.93</b>	
<b>No Coating</b>					
<b>Max. Effective Tension (kN)</b>	<b>5499</b>	<b>3557</b>	<b>5718</b>	<b>3400</b>	
<b>Max. Compression (kN)</b>	<b>0</b>	<b>196</b>	<b>0</b>	<b>247</b>	
<b>Max. Bending Moment (kN.m)</b>	<b>180</b>	<b>531</b>	<b>187</b>	<b>556</b>	
<b>Max. DNV Utilization (LRFD)</b>	<b>0.68</b>	<b>1.05</b>	<b>0.56</b>	<b>0.88</b>	

The maximum utilizations are no longer within allowable design criteria. The maximum utilization of the WDSCR with coating is 1.28, while the maximum utilization of the WDSCR without coating is 1.05. The WDSCR is not feasible for load case 8. In this case, the maximum downward velocity at the hang-off point is 3.27 m/s. The vertical velocities at the hang-off point and the bending moments at the TDP are plotted over time history for the WDSCR with coating and for the WDSCR without coating in Figure 6-18 and Figure 6-19 respectively. It is seen from the graph that the vertical velocities at the hang-off point and the bending moments at the TDP synchronize with respect to the “rise” and “fall” in the opposite direction, while the maximum downward velocity at the hang-off point associates directly with the maximum bending moment at the TDP. This is an indication that the maximum downward velocity at the hang-off point induces the maximum bending moment at the TDP.

It can be analyzed, from comparing both Figure 6-18 and Figure 6-19, that the maximum bending moment of the WDSCR with coating is greater than the maximum bending moment of the WDSCR without coating. This is an indication that the WDSCR without coating, which is heavier, is better to avoid excessive bending moment than the WDSCR with coating.

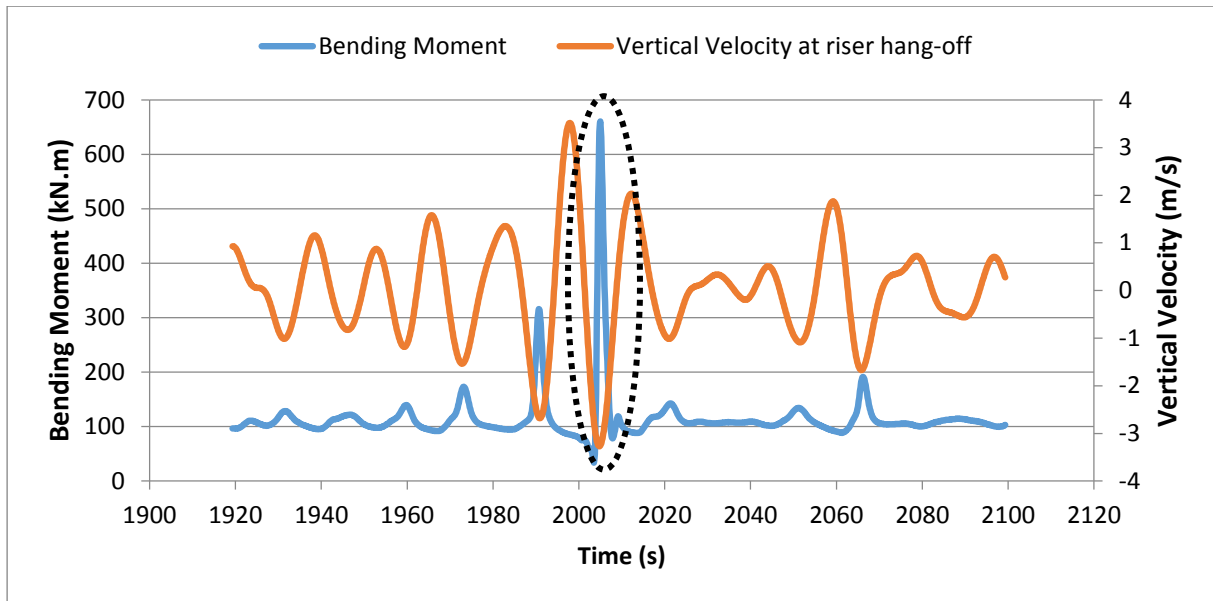


Figure 6-18 Vertical Velocity VS Bending Moment, WDSCR, LC8, coating

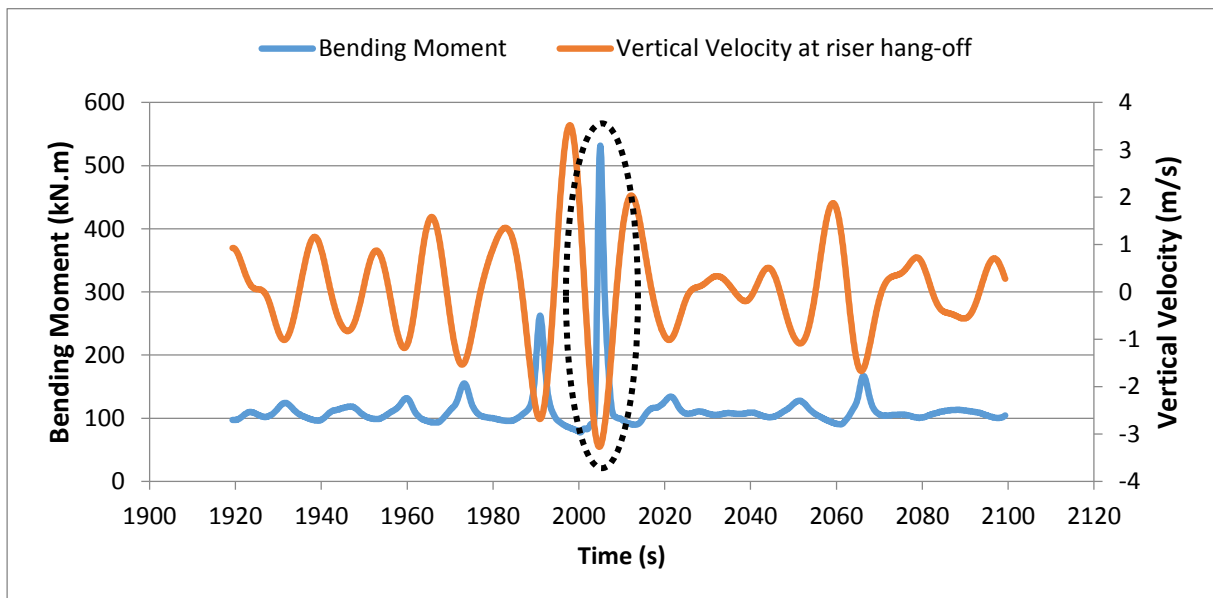


Figure 6-19 Vertical Velocity VS Bending Moment, WDSCR, LC8, No Coating

The vertical velocities at the hang-off point and effective tensions at the TDP are plotted over time history for the WDSCR with coating and the WDSCR without coating in Figure 6-20 and Figure 6-21 respectively. It is seen from the graph that the vertical velocities at the hang-off point and the effective tensions at the TDP synchronize with respect to the “rise” and “fall”, while the maximum downward velocity at the hang-off point associates directly with the minimum effective tension (compression) at the TDP. This is an indication that the maximum downward velocity at the hang-off point induces the maximum compression at the TDP. It can also be analyzed that the maximum compression of the WDSCR with coating is 373 kN, while the maximum compression of the WDSCR without coating is 196 kN. This is an indication that the WDSCR without coating, which is heavier, is better to avoid excessive compression than the WDSCR with coating.

The combination of the maximum compression and maximum bending moment results in excessive utilization. Therefore, the utilization of WDSCR is more than unity which is not within the allowable criteria. This is a good understanding that the downward velocity at the hang-off point dominates the WDSCR's critical responses in the global strength design.

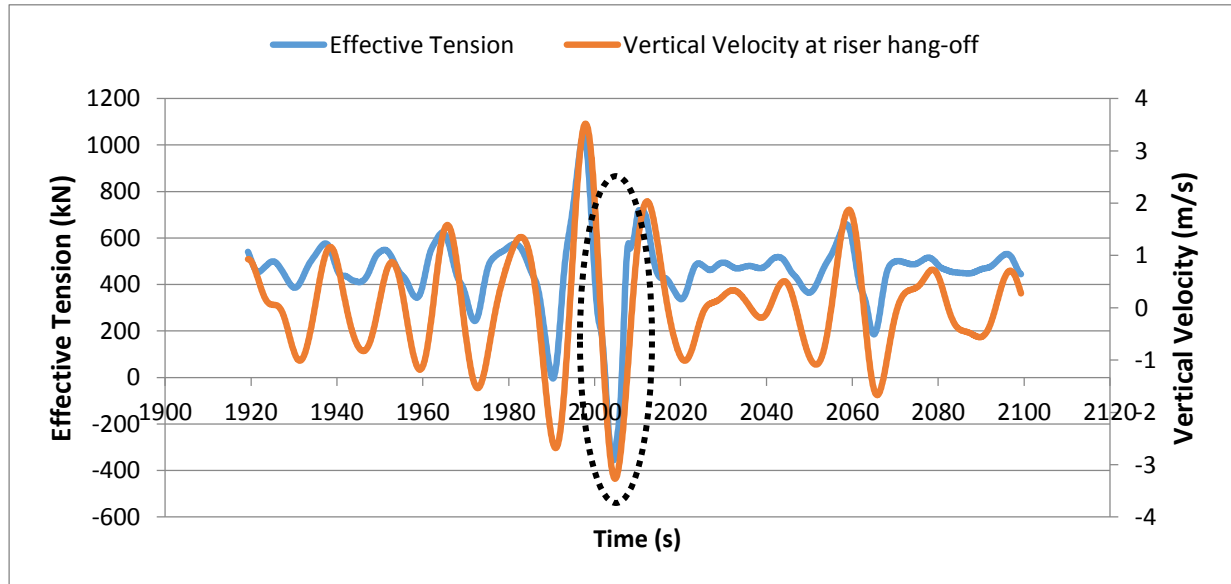


Figure 6-20 Vertical Velocity VS Effective Tension, WDSCR, LC8, Coating

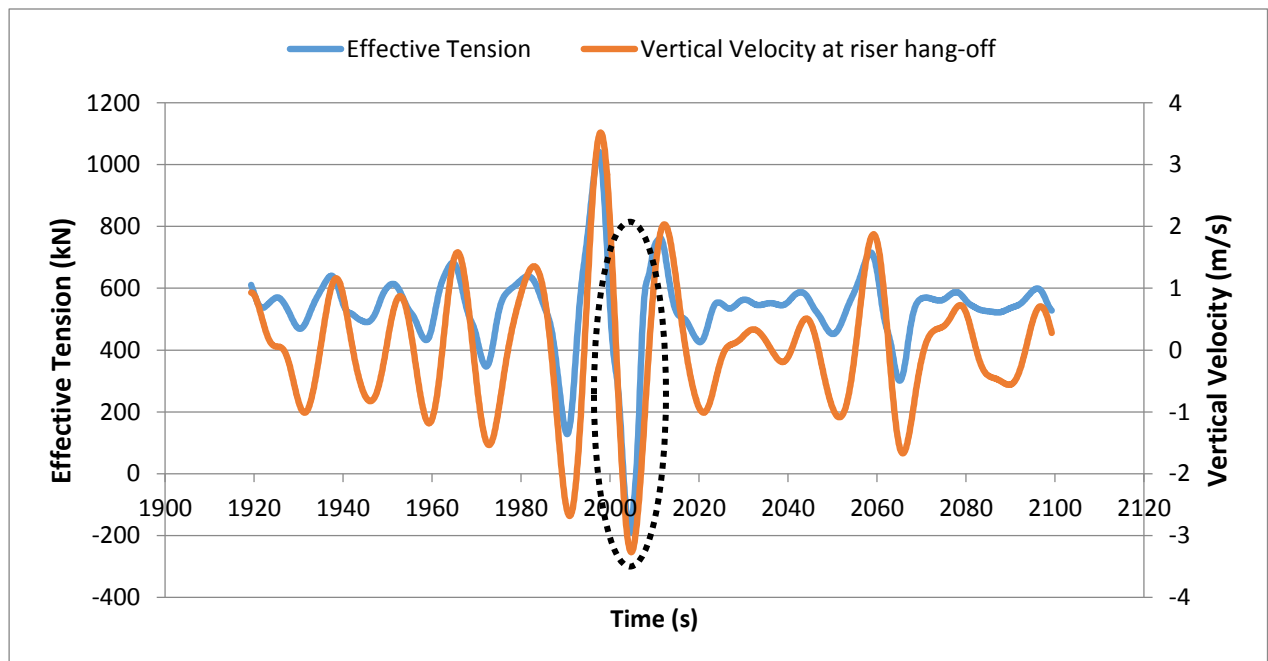


Figure 6-21 Vertical Velocity VS Effective Tension, WDSCR, LC8, No Coating

### 6.4.3 Dynamic Analysis of SLWR

As the results of the WDSCR are not within allowable design criteria for the load case 8, the next analysis is to check SLWR integrity against the load case 8. The summary of the dynamic analysis responses of SLWR against the load case 8 is presented in Table 6-14 for ULS and ALS design.

Table 6-14 Summary result of SLWR against LC8

Load Case 8 Coating	Semi Position			
	Intact		Damage	
	Far	Near	Far	Near
Max. Effective Top Tension (kN)	2547	2296	2552	2307
<b>Sag-bend</b>				
Max. Effective Tension (kN)	775	314	832	292
Max. Bending Moment (kN.m)	166	331	161	353
Max. DNV Utilization (LRFD)	0.40	0.66	0.36	0.61
<b>Hog-bend</b>				
Max. Effective Tension (kN)	763	289	824	273
Max. Bending Moment (kN.m)	139	228	138	245
Max. DNV Utilization (LRFD)	0.36	0.51	0.33	0.47
<b>TDP</b>				
Max. Effective Tension (kN)	763	257	824	246
Max. Bending Moment (kN.m)	166	325	163	345
Max. DNV Utilization (LRFD)	0.41	0.66	0.36	0.60
Load Case 8 No Coating	Semi Position			
	Intact		Damage	
	Far	Near	Far	Near
Max. Effective Top Tension (kN)	2747	2532	2763	2537
<b>Sag-bend</b>				
Max. Effective Tension (kN)	807	355	869	332
Max. Bending Moment (kN.m)	161	329	154	352
Max. DNV Utilization (LRFD)	0.39	0.66	0.35	0.61
<b>Hog-bend</b>				
Max. Effective Tension (kN)	794	308	858	290
Max. Bending Moment (kN.m)	120	202	117	216
Max. DNV Utilization (LRFD)	0.34	0.47	0.30	0.43
<b>TDP</b>				
Max. Effective Tension (kN)	793	275	857	260
Max. Bending Moment (kN.m)	166	323	161	342
Max. DNV Utilization (LRFD)	0.40	0.65	0.36	0.60

In general, the following are observed from the SLWR response against the load Case 8:

- All utilizations are within allowable design criteria. The maximum utilization is 0.66 at the sag-bend area for the near-ULS design.
- It can be concluded that the near-ULS design is more critical to extreme response in the SLWR design.

- The difference between the static utilization and dynamic utilization is only 0.12 for near-ULS design, and 0.05 for far-ULS design. This indicates that the SLWR is not sensitive to floater heave motion, thereby the static equilibrium dominates the global strength design.
- Results of utilization from both SLWR with coating and SLWR without coating are fairly equal. This indicates that the coating does not influence the SLWR integrity significantly.

The comparison of the maximum utilization between the SLWR with coating and the WDSCR with coating is presented in Figure 6-22 for near-ULS design with load case 8. It can be analyzed from Figure 6-22, although the SLWR configuration introduces utilization at the sag-bend, hog-bend and TDP, the maximum utilization of the SLWR is much lower than the maximum utilization of the WDSCR. This is an indication that the lazy wave configuration can distribute the stress over the riser length efficiently with buoyancy modules and result in lower utilizations compared to the WDSCR.

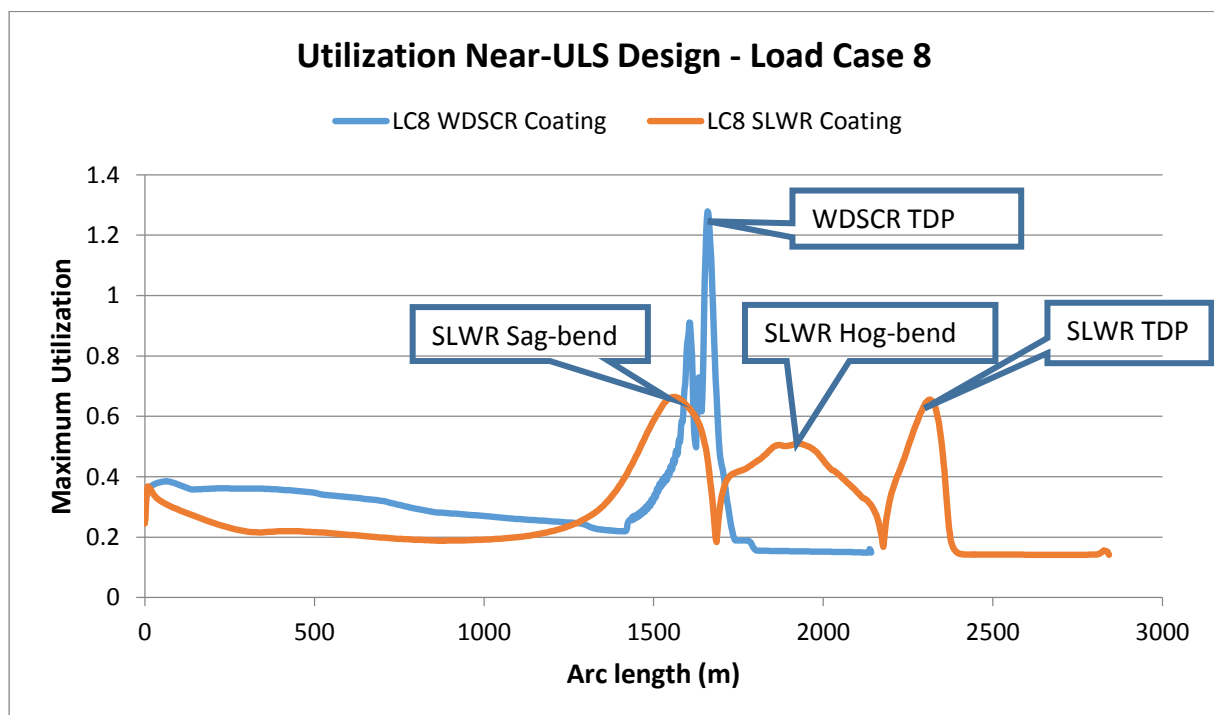


Figure 6-22 Maximum Dynamic Utilization of WDSCR and SLWR with Coating

To further investigate the strength improvement for the SLWR compared to the WDSCR with load case 8, the range of dynamic motions along the entire riser length is investigated. The best interest from the dynamic motions of riser is the maximum downward velocity at the TDP. The maximum downward velocity along the entire riser length for the WDSCR and the SLWR is presented in Figure 6-23.

From the Figure 6-23, it can be analyzed that the buoyancy modules are effective to isolate the dynamic motion of the floater from the TDP motion, resulting in lower utilizations. The “lazy wave” configuration efficiently absorbs the floater heave motion. Even though the WDSCR and the SLWR have the same downward velocity at the hang-off point, the SLWR configuration has much lower dynamic motion at the TDP compared to the WDSCR. This lower dynamic motion of SLWR is also beneficial from a fatigue point of view. This gives a

good understanding that the SLWR configuration has more capability to cope with floater heave motion with significantly lower motion at the TDP compared to the WDSCR.

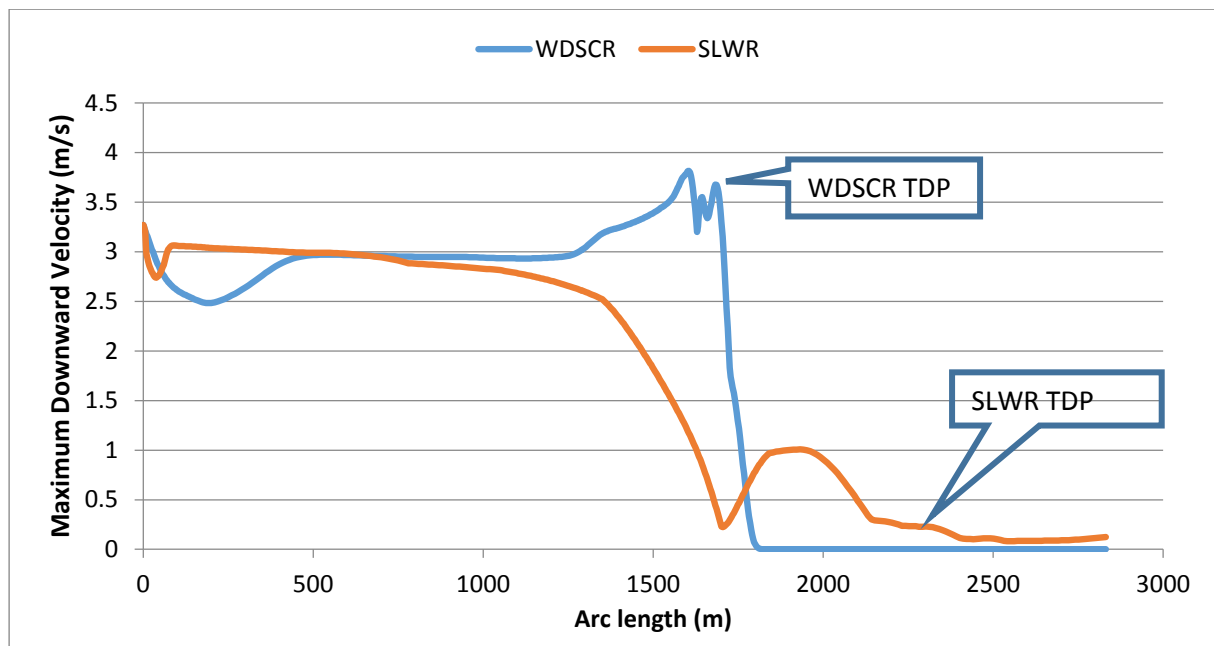


Figure 6-23 Maximum Downward Velocity Range for SLWR and WDSCR – Load Case 8

The next analysis is to check SLWR integrity against the rest of all load cases, the summary of the analysis is presented in Table 6-15. The results showed that the SLWR configuration can cope with the rest of all load cases. The detail analysis results for the SLWR against the rest of all load cases (9, 10, 11, 12, 13, 14, 15) are provided in Appendix B.

Table 6-15 SLWR- Dynamic analysis Summary

Load Case	SLWR Summary Result Max. DNV Utilization (LRFD)	Semi Position			
		Intact		Damage	
		Far	Near	Far	Near
LC9	Coating	0.42	0.67	0.37	0.62
	No Coating	0.41	0.66	0.36	0.61
LC10	Coating	0.44	0.68	0.38	0.62
	No Coating	0.41	0.67	0.37	0.62
LC11	Coating	0.47	0.68	0.41	0.62
	No Coating	0.45	0.68	0.4	0.62
LC12	Coating	0.46	0.69	0.41	0.63
	No Coating	0.44	0.69	0.39	0.63
LC13	Coating	0.52	0.72	0.48	0.64
	No Coating	0.47	0.72	0.43	0.64
LC14	Coating	0.64	0.73	0.59	0.66
	No Coating	0.52	0.73	0.48	0.65
LC15	Coating	0.76	0.75	0.73	0.67
	No Coating	0.6	0.75	0.58	0.67

The SLWR integrity is still within allowable criteria for load case 15. The maximum downward velocity at the hang-off point is 6 m/s in load case 15, which means that the SLWR can cope with a maximum downward velocity of 6 m/s at the hang-off point.

## 6.5 Summary

The conventional SCR, WDSCR and SLWR responses have been screened with different maximum downward velocity at the hang-off point. The capability of riser to cope with floater motion is assessed with LRFD utilization. The maximum bending moment and the maximum compression at the TDP have been identified when the maximum downward velocity at the hang-off point occurred at the same time. The combination of the maximum bending moment and the maximum compression may result into riser buckle. Therefore, it can be concluded that the downward velocity at the hang-off point is the main driving factor for riser integrity.

However, for SLWR configuration, the floater motion can be isolated from the TDP motion very well by introducing buoyancy modules at the hog-bend area. The SLWR configuration can cope with the downward velocity of 6 m/s at the hang-off point. Figure 6-24 presents the result of the utilization as y-axis and the downward velocity at the hang-off point as the x-axis for each riser configuration. Figure 6-24 is obtained from the results of the resulting maximum utilization and the maximum downward velocity from each load case.

By considering the allowable design criteria, the threshold of the maximum downward velocity at the hang-off point is identified for each riser configuration. The feasible SCR with coating can be obtained if the downward velocity at the hang-off point is restricted below 2.15 m/s as the line crossing the value of unity in y-axis. On the other hand, the feasible SCR without coating can be obtained if the downward velocity at hang-off point is restricted below 2.6 m/s.

The feasible WDSCR with coating can be obtained if the downward velocity at the hang-off point is restricted below 3 m/s. On the other hand, the feasible WDSCR without coating can be obtained if the downward velocity at the hang-off point is restricted below 3.2 m/s. The SLWR has shown superior performance over the SCR and the WDSCR as the SLWR can cope with the downward velocity of 6 m/s at the hang-off point.

From the results, it can also be analyzed that the SCR without coating can cope with greater downward velocity at the hang-off point than the SCR with coating. It also can be seen that the WDSCR without coating can cope with greater downward velocity at the hang-off point than the WDSCR with coating. However, the SLWR configuration with coating and the SLWR without coating give fairly equal results. It can be concluded that the uniform external coating influence the riser integrity for the SCR/WDSCR. The heavier the SCR/WDSCR, the better riser integrity is achieved to cope with the large motion of the host platform. On the other hand, the effect of uniform external coating is not significant for the SLWR.

The next analysis is to analyze the threshold of downward velocity in the touchdown area for the SCR and the WDSCR. The interest location is at 50 meters above seabed when vessel is in mean position, which is referred to as point B. Figure 6-25 presents the result of the



maximum utilization as the y-axis and the downward velocity at point B as x-axis for the SCR and the WDSCR. It is found from a separate study that the feasible SCR can be obtained, if the downward velocity at point B is restricted below 2.54 m/s for the SCR with coating and 3.03 m/s for the SCR without coating. Furthermore, the downward velocity at point B is restricted below 3.07 m/s for the WDSCR with coating and 3.43 m/s for the WDSCR without coating. These thresholds of downward velocity are summarized in Table 6-16.

Table 6-16 Summary of Downward Velocity Threshold

Threshold of downward velocity (m/s)		
Riser Configuration	Hang off point	Point B
SCR with coating	2.15	2.54
SCR without coating	2.60	3.03
WDSCR with coating	3.00	3.07
WDSCR without coating	3.20	3.43

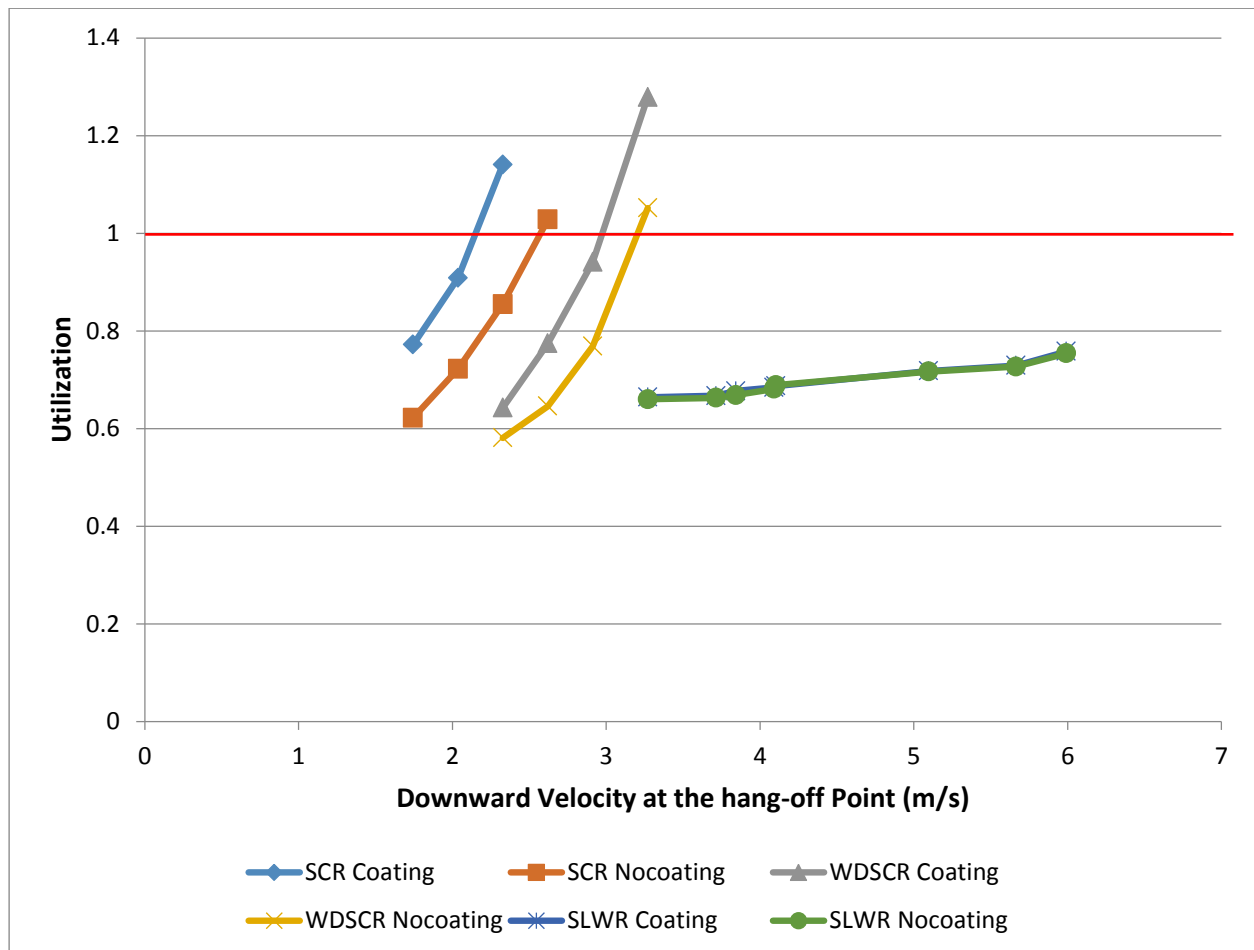


Figure 6-24 Utilization VS Max. Downward Velocity at the Hang-off Point

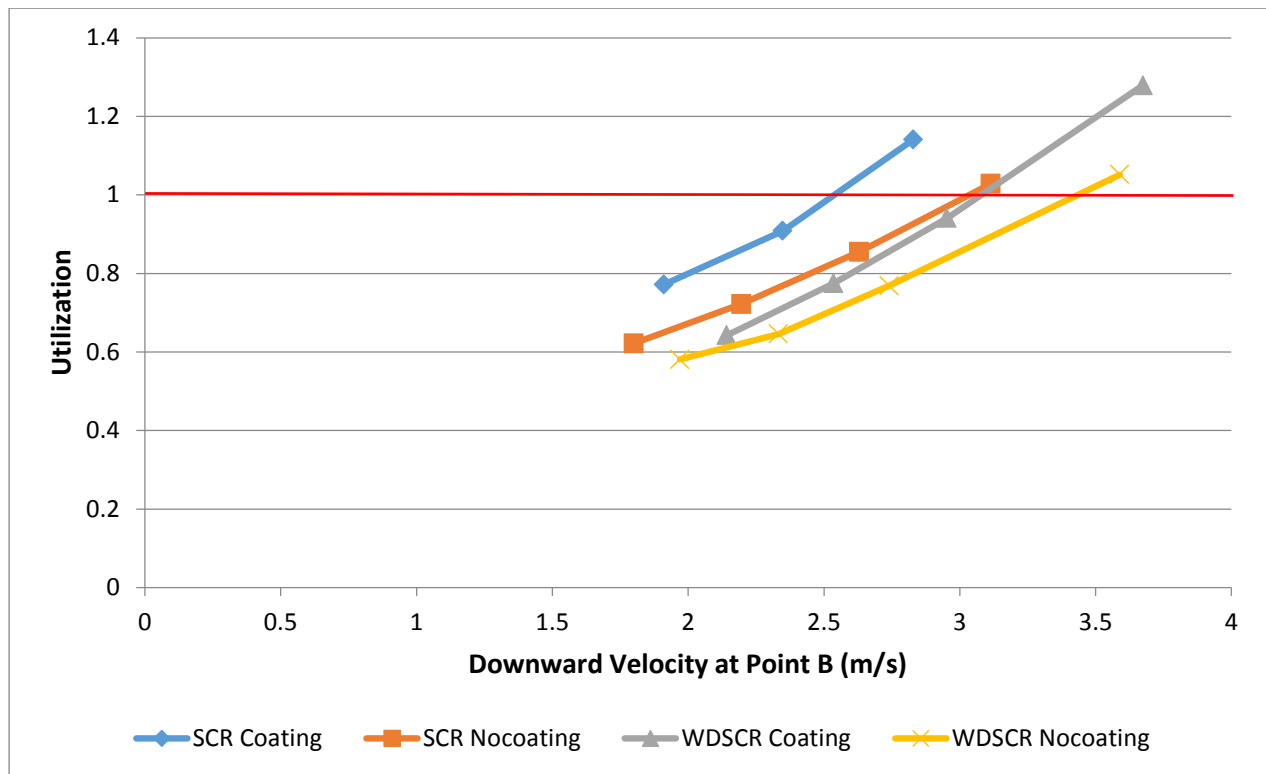


Figure 6-25 Utilization VS Max. Downward Velocity at Point B

## 6.6 SLWR for Northern North Sea Condition

### 6.6.1 Introduction

Since only the SLWR configuration can cope with severe dynamic motions of the floater, the extreme response analysis is carried out for the SLWR in the North Sea environment. The aim is to confirm that the SLWR application in extreme sea-states of North Sea satisfies the strength requirement. The SLWR without coating is selected for this analysis. The extreme response calculation is carried out using non-linear time domain analysis. The design storm approach of single wave data is considered in this analysis since it is relevant in connection with nonlinear action effects (Norsok, 2007). As the study location is in the North Sea, the JONSWAP spectrum is applied to model irregular wave as described in section 4.2.4.

To make sure that the extreme value distribution of the storm condition is appropriately accounted for, the 90% percentile response from the 20 realizations of '3-hour storm' period is considered as the extreme response value for the extreme response analysis. The objective of the long simulation time and consideration of 20 realizations in this study is to ensure the extreme response analysis is performed in accordance with DNV-OS-F201 for satisfactory statistical confidence. The interest responses of the SLWR are bending moment, effective tension, compression and utilization in critical locations, i.e. the sag-bend, hog-bend and TDP.

The static results of the SLWR were established in section 6.3.3. For dynamic analysis, environmental load of waves and current were applied in-plane with the riser's lay direction in both  $0^\circ$  and  $180^\circ$  direction for far and near offset position, respectively.

## 6.6.2 Environmental Data

The strength analyses were performed with 100-year waves and 10-year currents for intact condition and damage condition. The 10-year current profile is presented in Table 5-2. The significant wave height of 17 m and corresponding peak period of 18.8 seconds are the wave parameters for the design storm combination in the North Sea. Peak shape parameter ( $\Upsilon$ ) is determined based on the relationship of significant wave and peak period as described in section 4.2.4.

In summary, the extreme sea-state is modeled by irregular waves of JONSWAP with 100-year sea-state as follows:

- Significant wave height ( $H_s$ ) : 17.0 m
- Corresponding wave peak period ( $T_p$ ) : 18.8 s
- Peak shape parameter ( $\Upsilon$ ) : 1.66

## 6.6.3 Results and Discussion

The SLWR satisfies the strength requirement both for ULS and ALS design. The summary of the strength analysis is presented in Table 6-17.

Table 6-17 Strength Analysis Summary

North Sea	Semi Position			
	Intact		Damage	
No Coating	Far	Near	Far	Near
Max. Top Angle	15.83	17.83	16.85	18.19
Min. Top Angle	0.22	3.76	0.83	3.78
Effective Top Tension (kN)	3086	2777	3177	2793
<b>Sag-bend</b>				
Max. Effective Tension (kN)	1132	415	1278	392
Max. Compression (kN)	0	6	0	4
Max. Bending Moment (kN.m)	237	351	238	370
DNV Utilization (LRFD)	0.51	0.70	0.46	0.64
<b>Hog-bend</b>				
Max. Effective Tension (kN)	1153.675	364	1311	343
Max. Compression (kN)	0	0	0	0
Max. Bending Moment (kN.m)	224	224	231	232
DNV Utilization (LRFD)	0.51	0.51	0.45	0.45
<b>TDP</b>				
Max. Effective Tension (kN)	1153	299	1311	278
Max. Compression (kN)	0	0	0	0
Max. Bending Moment (kN.m)	240	380	242	395
DNV Utilization (LRFD)	0.51	0.75	0.46	0.67

Overall, the following are observed from the SLWR response when exposed to extreme sea-state condition:

- The SLWR top angle varies as the responses to extreme sea-state conditions. The static top angle is  $8^\circ$  relative to vertical. The range of the top angle's variations in dynamic analysis is between  $-7.8^\circ$  to  $+10.2^\circ$ . The variation of the top angle of SLWR is plotted over time history in Figure 6-26.
- The maximum effective top tension is 3177 kN and is observed at the top end of the riser for the far-ALS design.
- There are no significant residual compression loads in the riser for all limit states.
- The maximum bending moment is 395 kN.m and is observed at the TDP for the near-ALS design.
- Maximum utilizations for all limit states are kept below allowable limits. The most critical buckling utilization is 0.75 and is observed at the TDP for near-ULS design.
- The difference between the static utilization and the dynamic utilization is around 0.2 for corresponding offset position. This indicates that the SLWR is insensitive to the floater heave motions; hence the static equilibrium dominates the global strength design.
- In summary, the extreme response has been performed with extensive study for the SLWR without coating. The result of extreme response analysis is within the allowable design criteria and the SLWR is feasible to be applied in typical Northern North Sea condition.

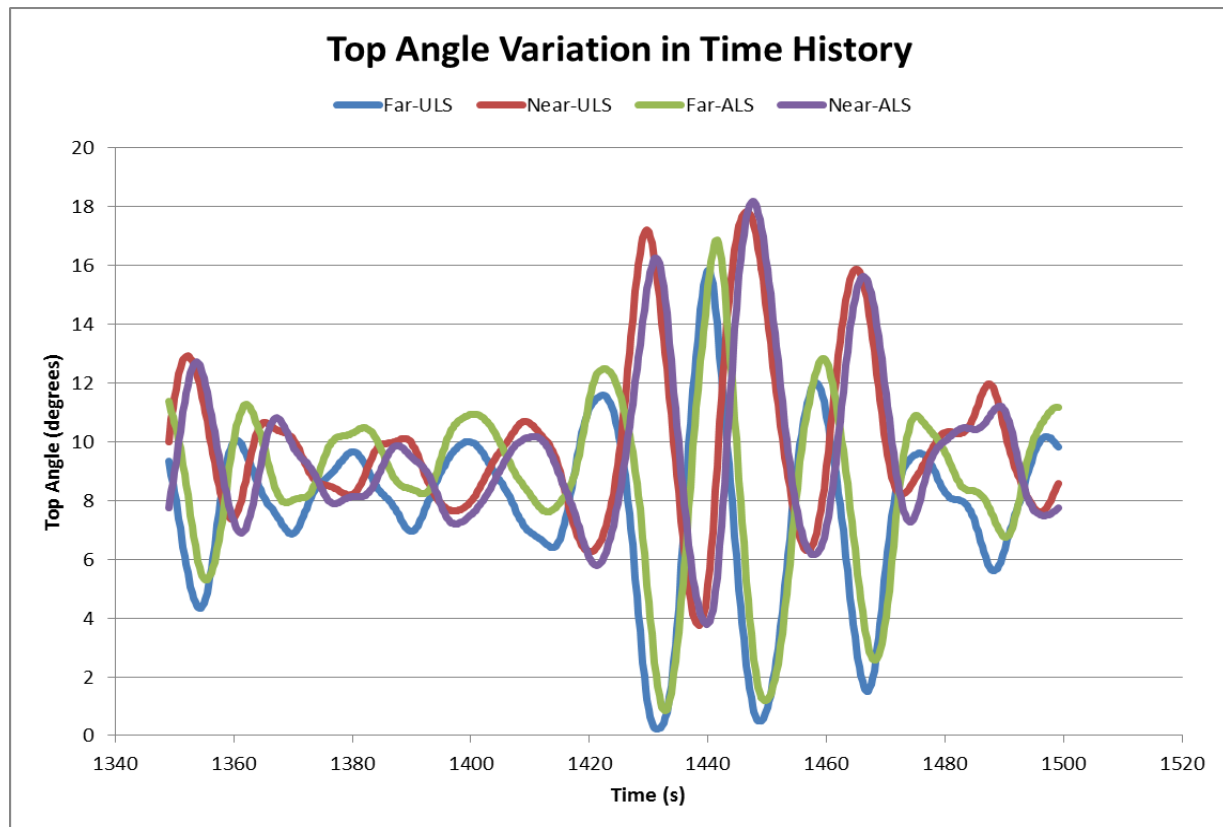


Figure 6-26 Variation of Top Angle in Time History

### 6.6.4 Comparison of Critical Sections

It can be analyzed from Table 6-17 that the SLWR responses at the sag-bend, hog-bend and TDP are different. To see the differences between those sections, the maximum dynamic response of SLWR is plotted over the entire length for far-ULS design and near-ULS design. The compared responses are the maximum dynamic effective tension, the maximum dynamic bending moment and maximum dynamic utilization.

It can be analyzed from the Figure 6-27, the effective tension at the sag-bend, hog-bend and TDP is fairly equal in far offset position. This is an indication, that the effective tension is horizontally distributed along sag-bend, hog-bend and TDP. On the other hand, the effective tension is gradually reduced from the sag-bend to the TDP in near offset position.

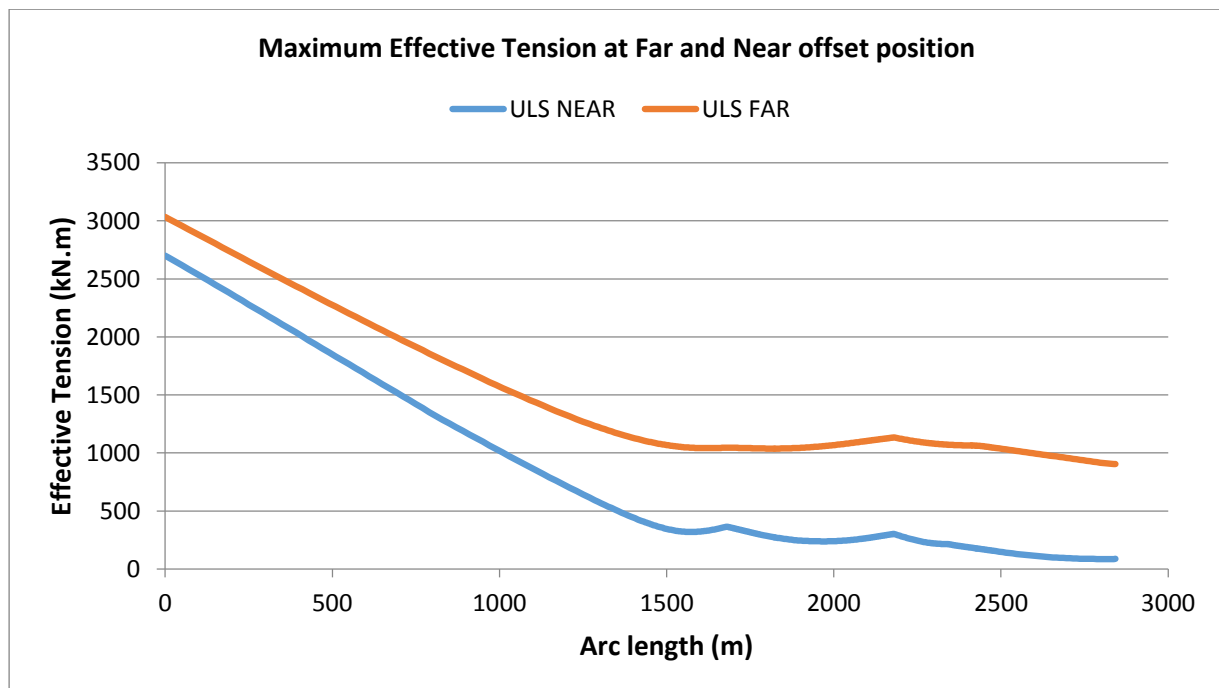


Figure 6-27 Maximum Effective Tension over entire riser length, far and near offset-ULS

From Figure 6-28, it can be analyzed that the bending moments at the sag-bend and the TDP are greater than the bending moment at the hog-bend in the near offset position. This indicates that the sag-bend and the TDP are more critical to extreme response in design. However, the bending moment at the hog-bend is at its peak when the vessel is in the far offset position. The maximum bending moment at the hog-bend is almost identical with the maximum bending moment at the sag-bend and the TDP in the far offset position.

Figure 6-29 shows the maximum utilization over entire riser length. It can be seen that, the maximum utilization envelope is identical to the maximum bending moment envelope. This is because the riser has structurally less capacity to withstand lateral load than axial load. It is analyzed from Figure 6-29, the maximum utilization occurs in the near offset position. This indicates that the near offset position is more critical to extreme response in the design. The maximum utilization in the top region also occurred in the far offset position, since the maximum effective tension occurred in the far offset position.

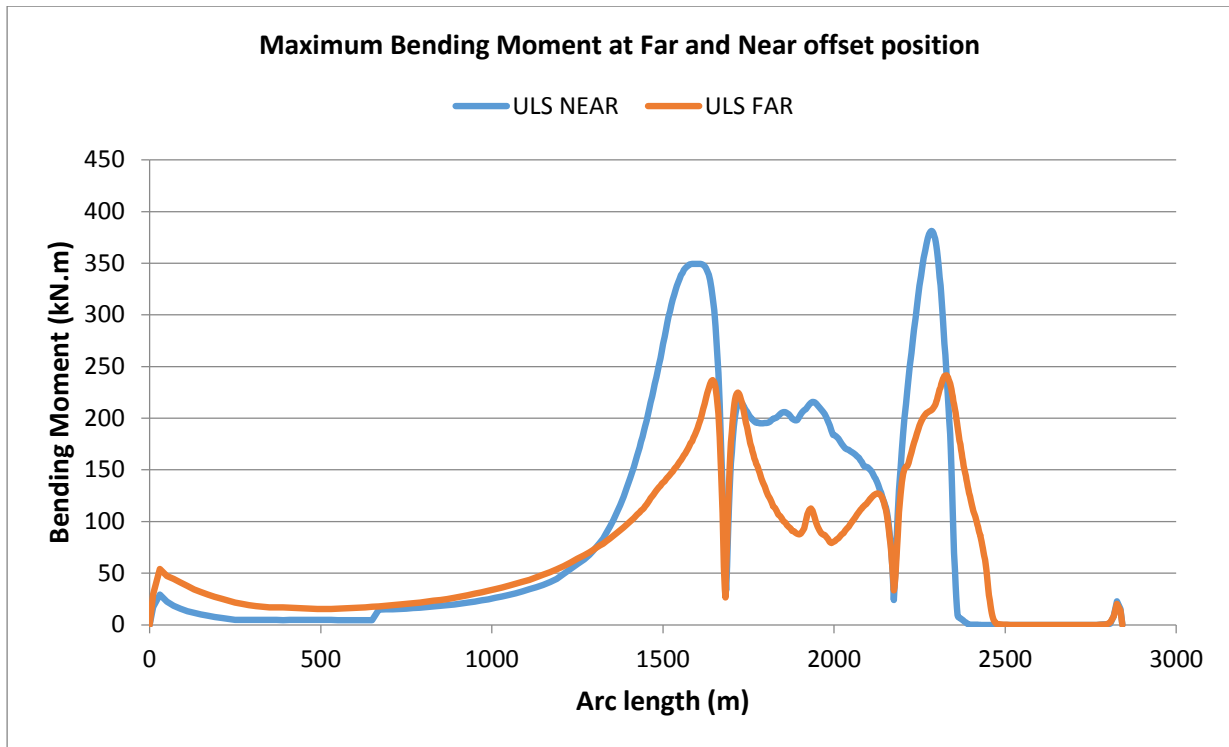


Figure 6-28 Maximum Bending Moment over entire riser length, far and near offset-ULS

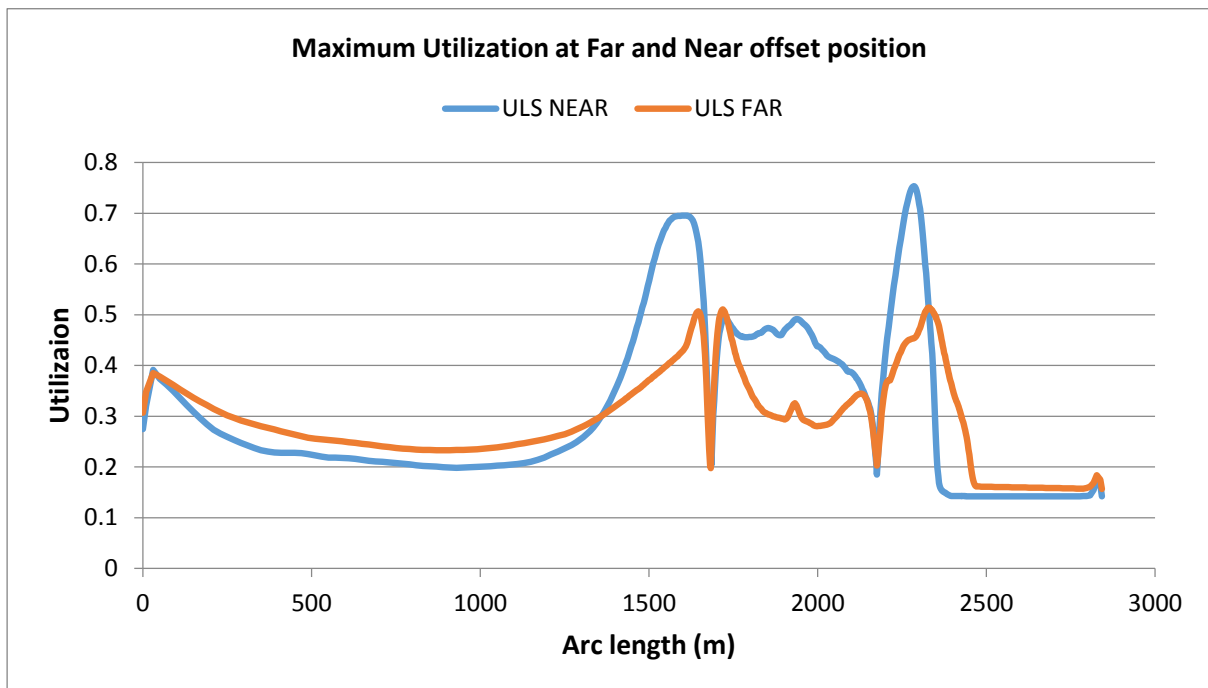


Figure 6-29 Maximum Utilization over entire riser length, far and near offset-ULS

From all results of the extreme response analysis, the SLWR is feasible for deployment in deep water and harsh environment, in typical Northern North Sea condition. The fatigue analysis will be performed to assess the fatigue performance of the SCR, the WDSCR and the SLWR against the FLS design criteria in the next section.

## Chapter 7. Fatigue Analysis

### 7.1 Introduction

A slender structure is subjected to dynamic environmental actions in deep water and harsh environment. Random waves and current generate oscillatory motions to the riser and the host platform. The riser is being lifted up and laid down repeatedly upon the seabed as responses to the floater heave motion. These environmental loads and vessel motions induce continuously cyclic stresses on the riser system. In addition, Vortex Induced Vibrations (VIV) contributes to fatigue damage due to the current. The current creates unsteady and turbulent vortex flow patterns around the cylinder section.

This is referred to as vortex shedding. If the vortex shedding frequency and the eigen frequency of the riser are matched, the structure would start to vibrate in either cross-flow or in-flow direction. According to DNV (2010a), the main sources causing fatigue damage to riser are addressed as follows:

- Wave-induced stress cycles;
- Low-frequency stress cycles;
- Vortex-induced vibrations (VIV) stress cycles;

The fatigue life at a point of riser pipe is defined as the time to grow a crack over the wall thickness. The critical region of riser for fatigue damage is located at the welded joint connection near the touchdown point since there is a complex interaction between the dynamic motion of the riser and the seabed on that region (Karunakaran et al., 2005). Thereby the welded joint connection at the TDP is the most susceptible to crack initiation due to fatigue damage. An inadequate fatigue life might cause fatigue failure of the riser system during service life. Therefore, it is important to ensure that the riser system has an adequate fatigue life during service life.

The calculations of fatigue life are carried out by using the ORCAFLEX software for wave induced fatigue analysis, while the calculations of fatigue life are carried out using VIVANA software for fatigue VIV analysis. The objective of this study is to analyze the fatigue performance of the conventional SCR, the WDSCR and the SLWR. The conventional SCR, the WDSCR and the SLWR without coating are selected in this fatigue analysis. Thereby wave induced fatigue analysis is performed for the three riser configurations to understand the different fatigue behavior of them and check against the FLS design criteria.

Afterwards, the fatigue VIV analysis is performed. The analysis methodology for wave induced fatigue analysis is a nonlinear time domain applying irregular wave models. The analysis methodology for fatigue VIV analysis is a combination of nonlinear time domain and frequency domain procedure. The fatigue response is very critical for SCR in harsh environment (Karunakaran and Baarholm, 2013). Thereby a very comprehensive fatigue analysis is performed with reliable data from typical Northern North Sea location.

## 7.2 Wave Induced Fatigue

### 7.2.1 Design Data

#### Riser data

In wave induced fatigue analysis, the mean vessel position is considered. The conventional SCR, the WDSCR and the SLWR without coating are selected in this fatigue analysis. The properties of riser are presented in Table 5-7.

#### S-N Curve

The S-N curve methodology is used in performing fatigue analysis in this study. The S-N curve is generally the stress range versus number of cycles to failure (DNV, 2010a). The S-N curves determine the fatigue capacity of riser in seawater with cathodic protection. The S-N curves determine the number of stress cycles to failure (N) for a given constant stress range (S). The S-N curve is given in following formula (DNV, 2010a):

$$\log N = \log \bar{a} - m \log S$$

$$S = S_o \cdot SCF \left( \frac{t}{t_{ref}} \right)^k$$

Where:

N = number of stress cycle to failure

S = stress range

$\bar{a}$ , m = empirical constant

S<sub>o</sub> = nominal stress range

SCF = stress concentration factor

t<sub>ref</sub> = reference wall thickness equal 25mm for welded connection

t = thickness through which a crack will most likely grow.

=t<sub>ref</sub> is used for thickness less than t<sub>ref</sub>.

k = thickness exponent on fatigue strength

= 0.10 for tubular butt welds made from one side

= 0.25 for threaded bolts subjected to stress variation in the axial direction

The S-N curve data are based on fatigue testing of small specimens subjected to dynamic loading in test laboratories (DNV, 2010c). Based on DNV (2010c), different S-N curves for seawater environments with cathodic protection are given in Figure 7-1. The selection of S-N curves is determined from the weld detail and quality. This study will consider C2-curve and D-curve for fatigue analysis, the basis for this is demonstrated in previous work by



Karunakaran et al. (2006). The C2-curve is expected to give more fatigue life compared to the D-curve for the riser sections.

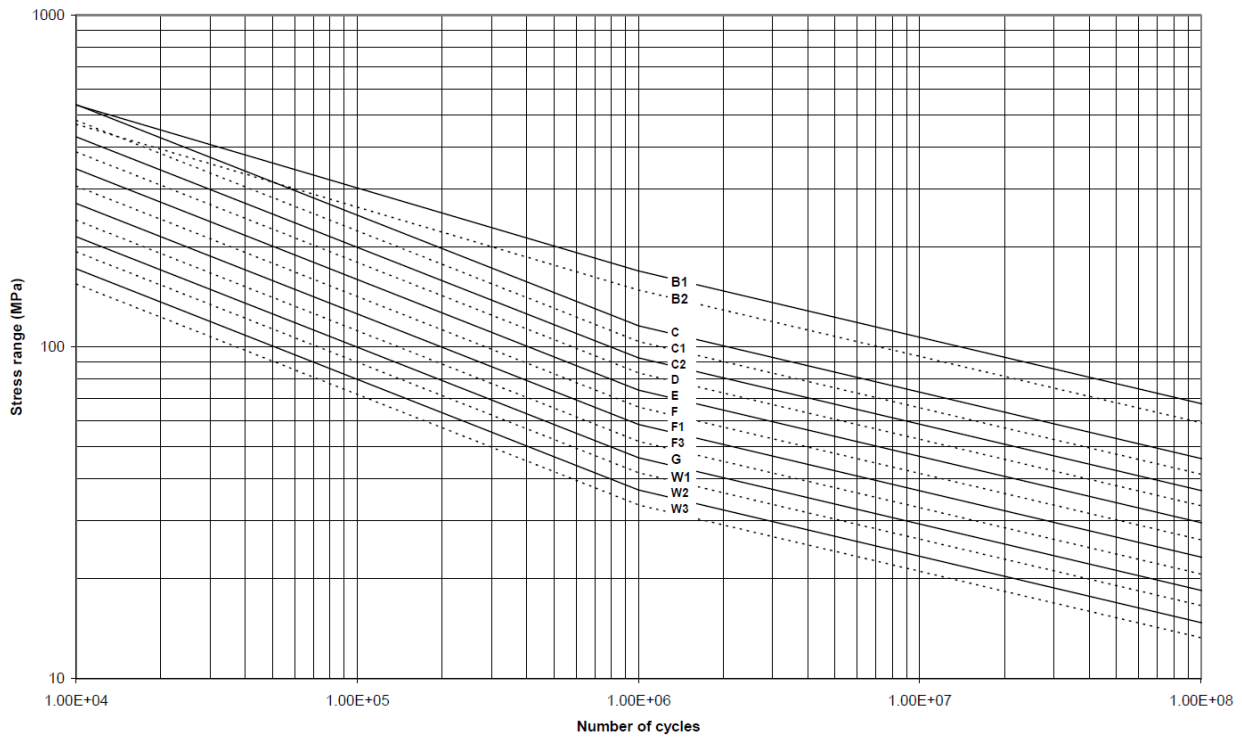


Figure 7-1 S-N curves in seawater with cathodic protection (DNV, 2010c)

### Fatigue Limit

The fatigue limit, so-called endurance limit, is established for calculating fatigue damage. Fatigue limit is determined as a cutoff stress range, which the stress ranges below this limit can be omitted from fatigue assessment. Based on DNV (2010c), the application of the fatigue limit is illustrated in Figure 7-2. From the figure, a detailed fatigue analysis can be omitted if the largest stress cycle is below the fatigue limit. However, if the stress cycle is above the fatigue limit, the stress cycle is included in the fatigue assessment.

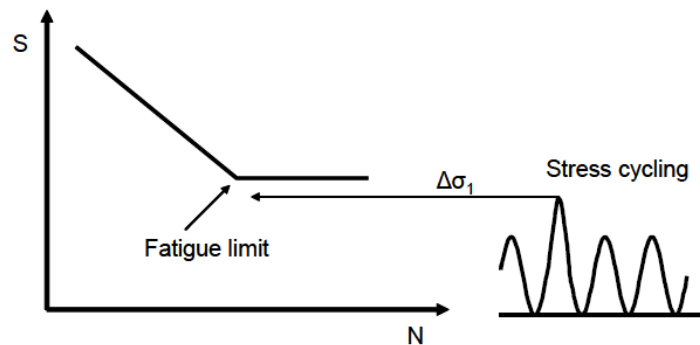


Figure 7-2 Stress cycling where further fatigue assessment can be omitted (DNV, 2010c)

The fatigue limit is set at  $10^7$  cycles from S-N curve. Consequently, each curve has different fatigue limit. The fatigue limit for D-curve and C2-curve are presented in table 7-1 as per DNV-RP-C203.

Table 7-1 Fatigue limit (DNV, 2010c)

S-N Curve	Fatigue Limit at 10 <sup>7</sup> cycles
Curve C2	58.48 Mpa
Curve D	52.63 Mpa

### **Selection of Stress Concentration Factor (SCF)**

The SCF is used to account for the concentrated stress at connection points due to a local increase in the intensity of a stress area. The SCF is obtained by application of finite element analyses over the cross section of the pipe. This factor is used to account for a possible local increase in the stress field due to the geometric stress amplifier of two adjacent joints, which occur in the riser component (DNV, 2010a). SCF may be defined as the ratio of hot spot stress range to local nominal range (DNV, 2010c). According to DNV (2010c), SCF value can be assessed based on the following analytical expression:

$$SCF = 1 + \frac{3\delta_m}{t} e^{-\sqrt{t/D}}$$

Where:

t = wall thickness of pipe

D = outer diameter of pipe

$\delta_m$  = representative eccentricity due to imperfections in geometry

Based on that expression, an estimated SCF value of 1.2 is considered to calculate fatigue damage for C2-curve and D-curve.

### **Sea-state Data**

The assessment of fatigue performance requires procedure of a long-term model to account for the variability in sea-states (Norsok, 2007). A typical wave scatter diagram from the Northern North Sea environment is used for fatigue analysis. The sea-state will be subdivided into 18 representative blocks to account for possible sea-state condition at the site as shown in Figure 7-3. The “star” in the Figure 7-3 denotes the selected representative sea-state blocks at which the non-linear dynamic response is simulated.

18 representative sea-states blocks in 12 directions are selected to calculate total fatigue damage. 18 representative sea-states in 12 directions are performed in 1-hour time simulation. Each representative sea-state block has the highest occurrence rate within that block. The lumped probability of occurrence is presented in Table 7-2. The lumped probability of occurrence is a percentage of occurrences of each block over all occurrences.

Table 7-2 Representative sea-state and lumped probability of occurrence

No.	Hs (m)	Tp (s)	$\Upsilon$	Lumped Probability (%)
1	1.5	5.5	1.80	9.21
2	1.5	9.5	1.00	29.35
3	1.5	16.5	1.00	0.92
4	2.5	6.5	2.78	5.47
5	2.5	10.5	1.00	21.71
6	2.5	16.5	1.00	1.19
7	3.5	6.5	5.00	3.33
8	3.5	12.5	1.00	12.05
9	3.5	17.5	1.00	0.46
10	4.5	9.5	1.82	5.20
11	4.5	14.5	1.00	2.79
12	5.5	9.5	2.98	2.93
13	5.5	15.5	1.00	1.18
14	6.5	12.5	1.12	2.16
15	7.5	12.5	1.65	1.09
16	8.5	13.5	1.53	0.53
17	10.5	14.5	1.83	0.41
18	13.5	16.5	1.80	0.03
Total				100.00

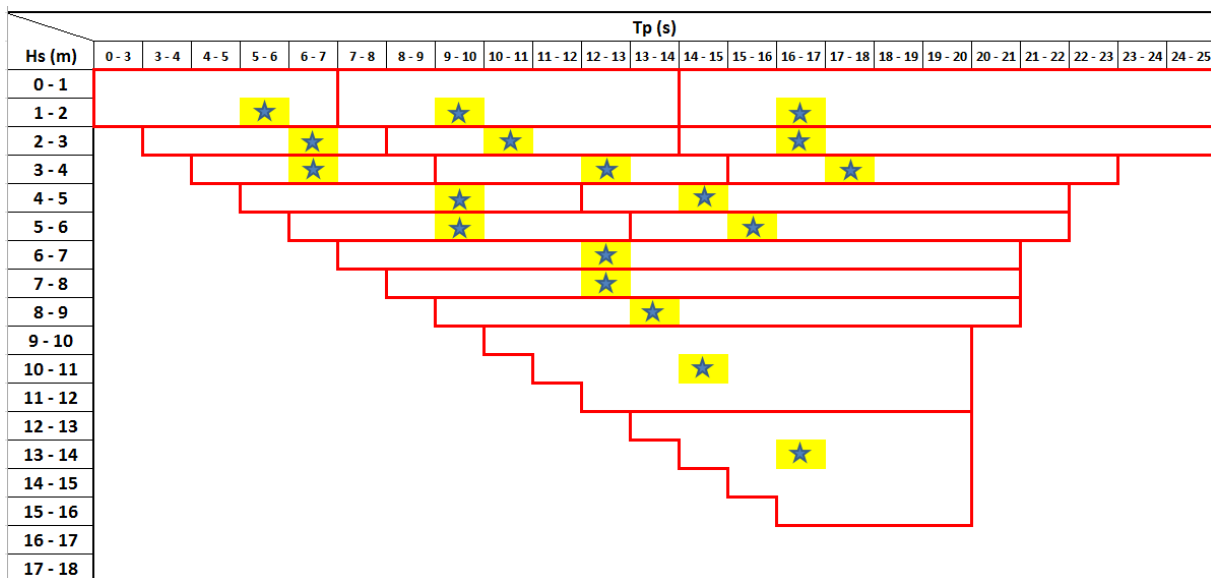


Figure 7-3 Subdivision of the sea-state scatter diagram into representative blocks

The fatigue damage from all 18 representative sea-states in each direction are weighted with the lumped probability of occurrence. Subsequently, the fatigue damage is then summed up with the directional probabilities for all 12 directions. The directional probabilities are applied to account for the probability of wave direction at the site as presented in Table 7-3.

Table 7-3 Directional Probabilities

Direction ( $^{\circ}$ )	Directional Probability (%)
0	12.61
30	19.98
60	14
90	4.61
120	2.64
150	1.41
180	1.16
210	2.72
240	10.5
270	11.89
300	8.68
330	9.8
<b>Total</b>	<b>100</b>

## 7.2.2 Assumptions

The following assumptions are used for the fatigue analysis:

1. The riser material is assumed to follow the S-N relationship
2. In this study, the fatigue damage is calculated using approach under the assumption of linear cumulative damage (Palmgren-Miner rule) as shown in following expression (DNV, 2010c).

$$D_{fat} = \sum_{i=1}^k \frac{n_i}{N_i}$$

Where:

$D_{fat}$  = accumulated fatigue damage

$k$  = number of stress blocks

$n_i$  = number of stress cycles in stress block  $i$

$N_i$  = number of cycles to failure at constant stress range ( $S$ )

3. The 18 representative blocks of the scatter diagram with 12 wave directions are assumed to cover sufficiently the range of possible sea-state condition of the site.
4. The Design Fatigue Factor (DFF) is 10 in this study (refer to section 3.4.7), considering a high safety class for the riser due to the difficulty to perform any inspection and repair activities in deep water and harsh environment area. The expected design life is 25 years. Consequently, the minimum acceptable fatigue life is 250 years.

## 7.2.3 Fatigue analysis Procedure

A general approach for calculation of wave frequency (WF) and low frequency (LF) fatigue damage is based on the following procedure (DNV, 2010a).

- The wave environment scatter diagram is divided into 18 representative blocks. Each representative sea-state block has the highest occurrence rate within that block.
- The non-linear time domain analysis is performed to calculate the stress time series for each representative blocks. A total time simulation of 1 hour and time step of 0.25 seconds is used for this analysis.
- The fatigue damage is estimated with all representative blocks using deterministic rain-flow-counting technique. This was completed in ORCAFLEX. The fatigue damage is assessed at 16 points around the circumference of the pipe distributed uniformly 360°.
- The fatigue damage from each representative sea-state block is weighted with the corresponding lumped probability of occurrence.
- The total fatigue damage in that direction is obtained from the summation of the weighted fatigue damage over 18 representative sea-state blocks.
- This procedure is repeated for all 12 directions and the total fatigue damage from all directions are obtained by applying directional probabilities as described in the following expression.

$$D_L = \sum_{i=1}^{N_s} D_i P_i$$

Where:

$D_L$  = long-term cumulative fatigue damage

$N_s$  = number of total wave direction

$D_i$  = short time cumulative fatigue damage

$P_i$  = directional probabilities of corresponding wave direction, given in Table 7-3.

- The fatigue life in years is obtained as the reciprocal of the total fatigue damage.

## 7.2.4 Fatigue Analysis Results

### Conventional SCR

The critical locations of the fatigue performance of the SCR are located at the TDP and below the flex joint. The fatigue life of the SCR is presented in Table 7-4 for the critical locations. The total fatigue damage over entire riser length is presented in Figure 7-4. It can be seen that the critical fatigue life occurred in a very short span at the TDP. It is observed that the minimum fatigue life is satisfactory for the location where the flex joint is occupied.

However, the minimum fatigue life at the TDP is less than the minimum acceptable fatigue life. The D-curve showed more fatigue damage compared to C2-curve. The minimum fatigue life considering D-curve is 80 years and the minimum fatigue life considering C2-curve is 159 years. These are less than 250 years. It can be concluded that the SCR is not feasible for satisfying the minimum criteria of the fatigue performance in this location.

Table 7-4 Fatigue Life Summary of SCR

SCR Critical Location	D-curve	C2-curve
Below flex joint	522 years	927 years
TDP	80 years	159 years

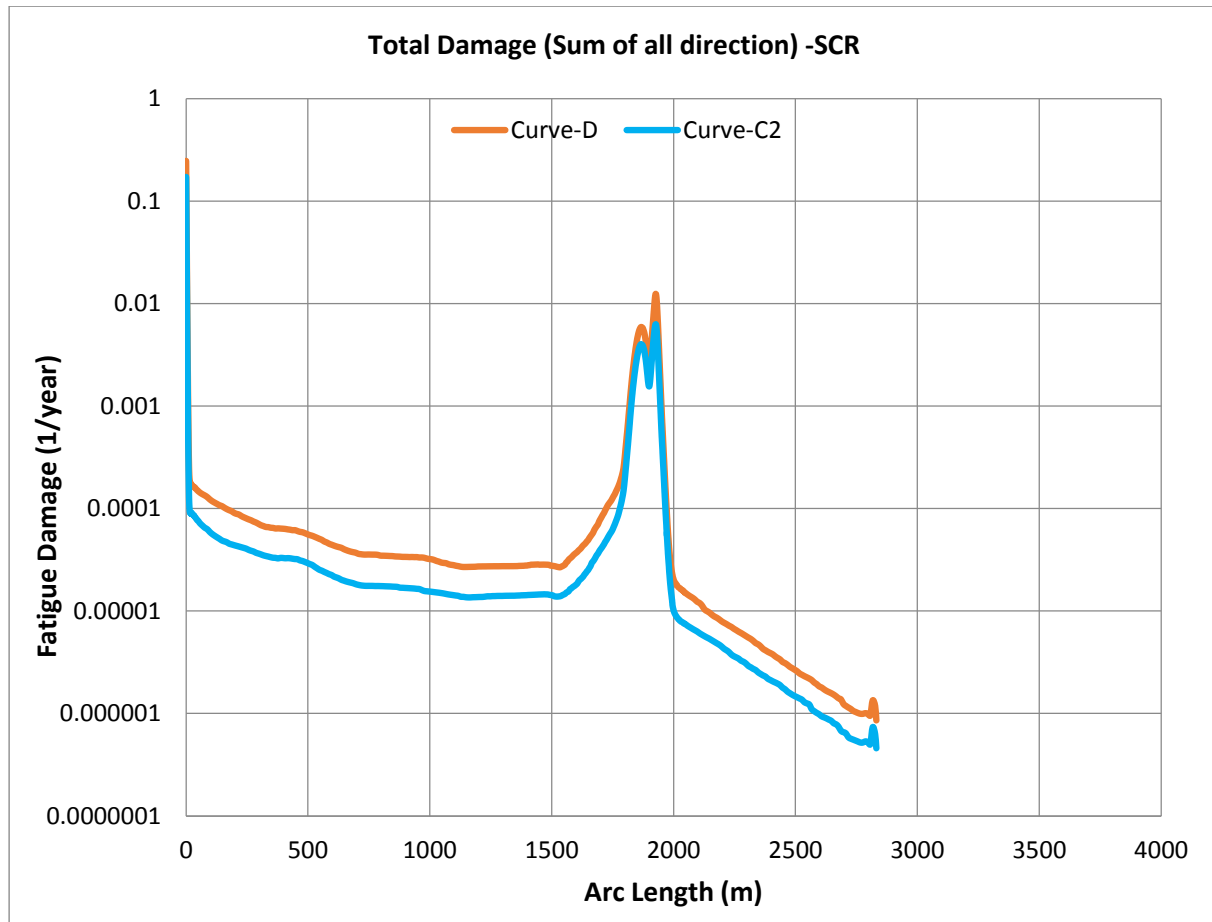


Figure 7-4 Total Fatigue Damage of SCR

**WDSCR**

The critical locations of the fatigue performance of the WDSCR are located at the TDP and below the flex joint. The total fatigue damage of the WDSCR over entire riser length is presented in Figure 7-5. It is seen that the critical fatigue damage of the WDSCR is lower than critical fatigue damage of the SCR. Table 7-5 presents fatigue life of the WDSCR for the critical riser sections. It is observed that the minimum fatigue life is satisfactory for the critical location where the flex joint is occupied.

It is seen that the fatigue performance is improved very well at the TDP for the WDSCR compared to the SCR. The minimum fatigue life considering D-curve is 247 years and the minimum fatigue life considering C2-curve is 533 years. This is an indication that the heavy cross section reduces the fatigue damage at the TDP very well. The cyclic stresses at the TDP is reduced, thereby, the more fatigue life is achieved with the heavy cross section at the bottom of straight section for the WDSCR.

Table 7-5 Fatigue Life Summary of WDSCR

WDSCR Critical Location	D-curve	C2-curve
Below flex joint	646 years	1179 years
TDP	247 years	533 years

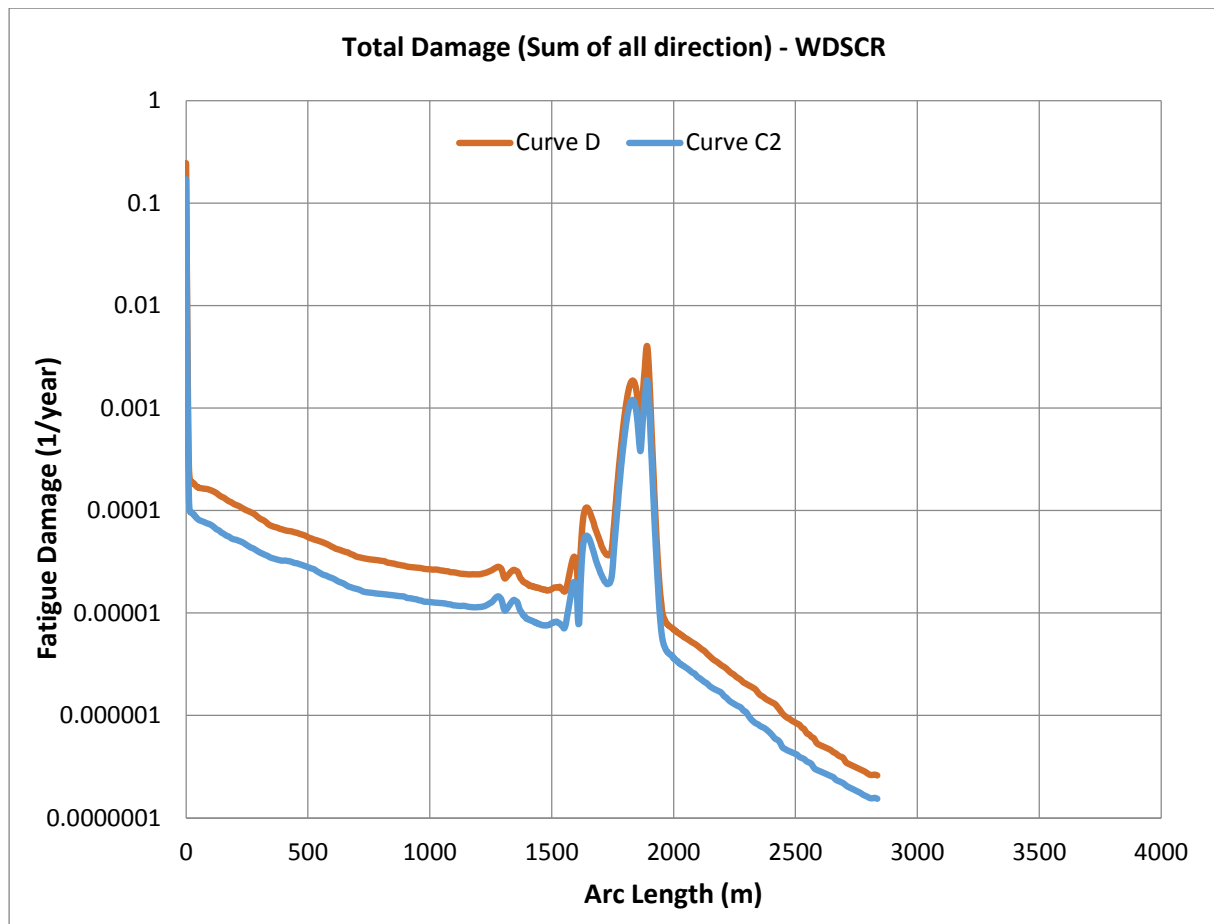


Figure 7-5 Total Fatigue Damage of WDSR

## SLWR

The critical locations of the fatigue performance of the SLWR are located at the TDP, hog-bend, sag-bend and below the flex joint. The fatigue life of the SLWR is presented in Table 7-6 for the critical locations. The total fatigue damage over entire riser length is presented in Figure 7-6. It is observed that all critical locations of the SLWR have satisfactory fatigue performance. The fatigue life at the critical location, where the flex joint is occupied, is 1164 years considering D-curve and is 2310 years considering C2-curve.

The fatigue life at the sag-bend and the hog-bend are more than 10000 years considering both D-curve and C2-curve. The minimum fatigue life at the TDP considering D-curve is 874 years and the minimum fatigue life at the TDP considering C2-curve is 1628 years. The results of minimum fatigue life are well above the minimum acceptable limit. It can be concluded that the SLWR has robust fatigue wave performance.

Table 7-6 Fatigue Life Summary of SLWR

SLWR Critical Location	D-curve	C2-curve
Below flex joint	1164 years	2310 years
Sag-bend	>10000 years	>10000 years
Hog-bend	>10000 years	>10000 years
TDP	874 years	1628 years

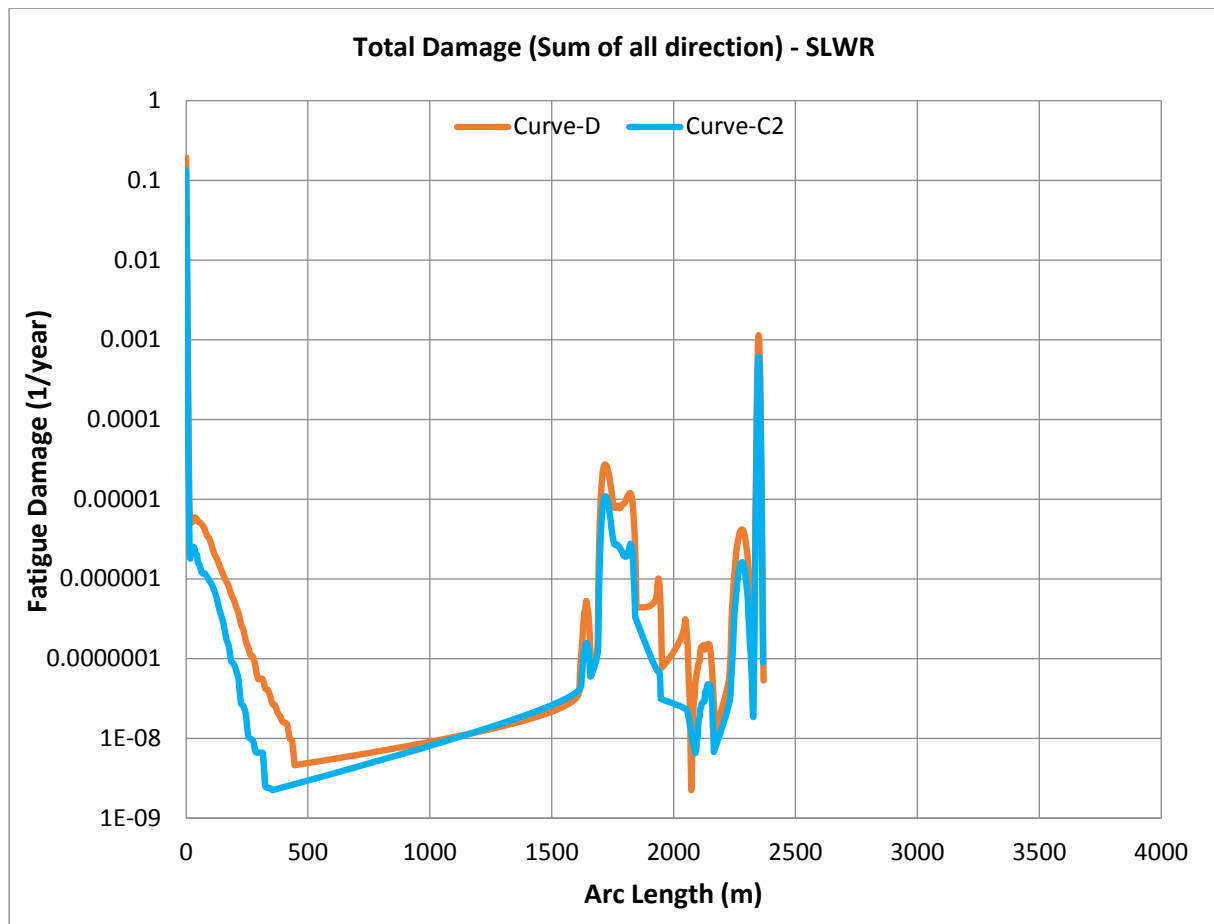


Figure 7-6 Total Fatigue Damage of SLWR

### 7.2.5 Discussion of Wave Induced Fatigue Performance

It can be seen that the most critical location of fatigue performance is located at the TDP. It is also noted that the hang-off area presented very low fatigue performance. In order to solve this, this section will, in practice, be occupied with flex joint and there are proven measures to manage it. Therefore, the hang-off area is not critical in the riser feasibility as it can be solved with proven measures. The critical fatigue performance at the TDP determines the riser feasibility since the method of controlling this section is limited. Thus, the major areas of concern for fatigue performance of the riser are the minimum fatigue life at the TDP.

The D - curve is identified to give more fatigue damage than C2-curve. The minimum fatigue life of the SCR is 80 years considering D-curve, which is less than the minimum acceptable fatigue life. The wave loads induce the vessel heave motion, which results in excessive cyclic stresses along the entire riser length, especially at TDP where the SCR is affected by soil-riser interaction.

This is an indication that the SCR is very sensitive to the vessel heave motion. Therefore, it is not feasible to develop the SCR for this harsh environmental condition. On the other hand, the WDSCR has better fatigue performance compared to the SCR. This is an indication that the heavy cross section at the bottom of straight section improves the fatigue performance very well. The heavy cross section reduces the dynamic motion and cyclic stresses at the TDP;



hence the fatigue performance is improved. However, the minimum fatigue life is 247 years considering D-curve which is slightly less than minimum acceptable fatigue life of 250 years.

The SLWR has most robust fatigue performance compared to the WDSCR and the SCR. It has the minimum fatigue life of 857 years at the TDP, considering D-curve. This indicates that the SLWR is feasible to satisfy the minimum acceptable fatigue life stipulated in acceptance criteria in this location. This study does not consider factors such as different floater offsets, floater drafts, and marine growth, which may contribute to fatigue damage at the TDP. Therefore, these fatigue results are conservative, as those factors are not considered. The total fatigue damage is calculated from the summation of long-term damages by considering each wave direction and directional probabilities. The summary of fatigue damage for each direction is given in Appendix D.

## 7.3 Vortex Induced Vibration (VIV)

### 7.3.1 Fatigue Analysis Procedure

The investigation of fatigue damage due to VIV is performed for only SLWR in this study, since only SLWR is feasible in this location. The consideration for VIV analysis is given to unidirectional current profiles, acting in parallel and perpendicular direction to the riser's plane. The parallel current direction is referred to as in-plane current and the perpendicular current direction is referred as out-of-plane current.

The VIV analysis is performed using VIVANA, a computer program designed to calculate the response of a slender structure excited by vortex shedding due to a current profile. VIVANA requires INPMOD and STAMOD as input data from RIFLEX. The input is the description of current profiles, structure and its static equilibrium which is established in INPMOD and STAMOD.

Therefore, the SLWR is remodeled in RIFLEX to establish the INPMOD and STAMOD as the input data for VIVANA. More detail information of this software program is provided in Appendix C. The resulting static configuration obtained in RIFLEX is checked and compared to the resulting static configuration obtained in ORCAFLEX. It was confirmed that both configurations are the same in respect to the response of the configurations such as effective tension and bending moment.

The VIV analysis procedure is based on VIVANA – theory manual (Vivana, 2005). The S-N curve is specified in this analysis. The D-curve and C2-curve with SCF of 1.2 are considered as used in the wave induced fatigue analysis. The VIV analysis was performed considering 14 current profiles. The surface current velocities range from 0.1 to 0.8 m/s. The 14 current profiles are provided in VIVANA script in Appendix C. The fatigue damage from each current profile was weighted with corresponding lumped probability of occurrence as presented in Table 7-7. The weighted fatigue damage accumulation from all current profiles can be expressed in the following formula.

$$D_L = \sum_{i=1}^{N_s} D_i P_i$$

Where:

- $D_L$  = total fatigue damage
- $N_s$  = number of considered current profiles
- $D_i$  = fatigue damage for current  $i$
- $P_i$  = lumped probability of occurrence

This procedure is performed for in-plane and out-of-plane unidirectional current. The directional probability used in this analysis is 50% for both in-plane and out-of-plane unidirectional currents. Taking into account the 14 current profiles and the 2 unidirectional currents, the total fatigue damage is calculated. The fatigue life in years was then calculated as the reciprocal of total fatigue damage. The minimum acceptable fatigue life due to VIV is at least 20 times the SLWR design life. The design life of SLWR is 25 years; therefore, the minimum acceptable fatigue life is 500 years.

Table 7-7 Lumped Probability of Occurrence

Current Profile No.	Lumped Probability of Occurrence
1	2 %
2	2 %
3	2 %
4	2 %
5	2 %
6	10 %
7	10 %
8	10 %
9	10 %
10	10 %
11	10 %
12	10 %
13	10 %
14	10 %
<b>Total</b>	<b>100 %</b>

### 7.3.2 Fatigue Analysis Results

The summation of total fatigue damage is presented in Figure 7-7. The minimum fatigue life is then calculated from the reciprocal of the maximum fatigue damage as presented in Table 7-8.

Table 7-8 Minimum VIV Fatigue Life

S-N Curve	Minimum Fatigue Life
D-curve	113 years
C2-curve	156 years

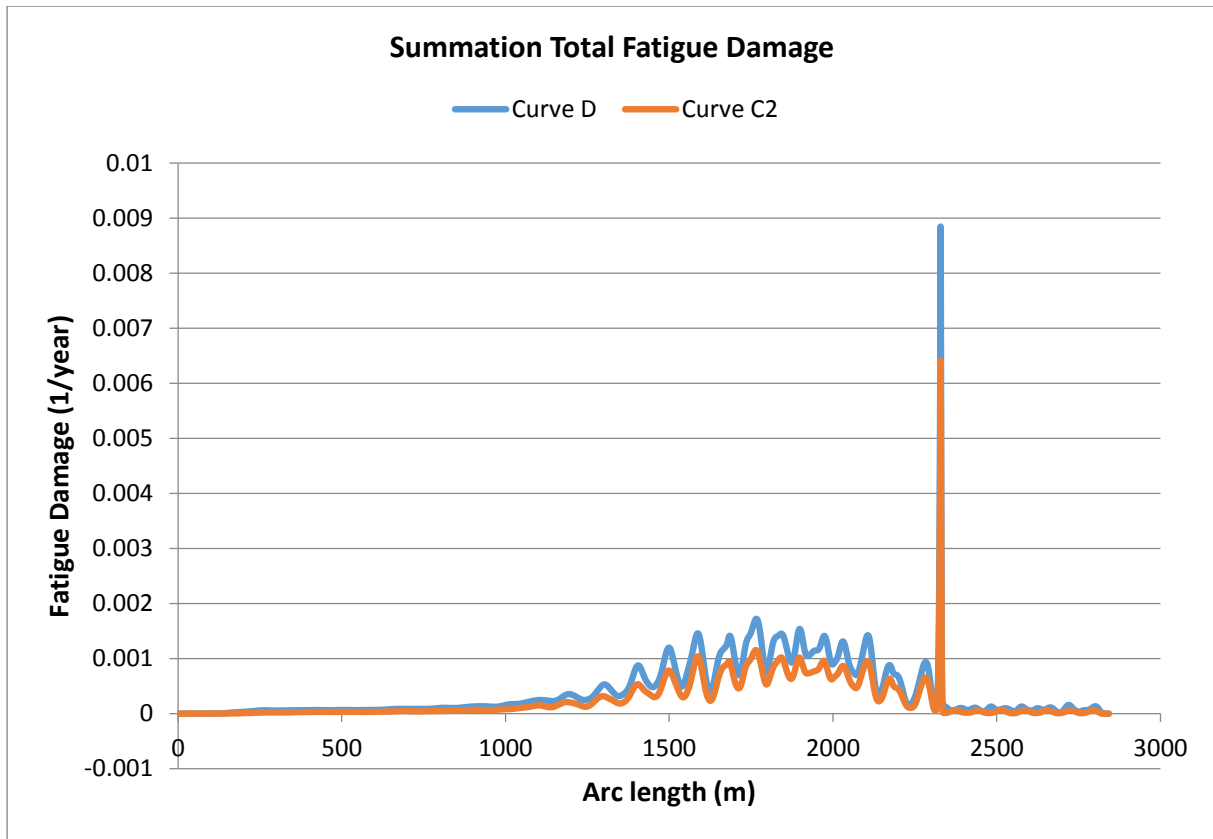


Figure 7-7 Total Fatigue Damage due to VIV over Entire Riser Length

### 7.3.3 Discussion of Fatigue Analysis due to VIV

The VIV fatigue damage is induced by cyclic stresses due to ocean currents. As the water flows towards the leading edge of the riser, vortices are shed from both sides of the riser, resulting in vibration on to the riser. These vortices are referred to as vortex shedding. The shedding frequency is defined as a full periodic cycle between two vortices occurred on alternate sides of the riser. The vortices change the velocity and pressure distribution, resulting in development of forces around the riser as seen in Figure 7-8. Vortex induced vibration (VIV) consists of two modes according to flow direction; in-line and cross-flow.

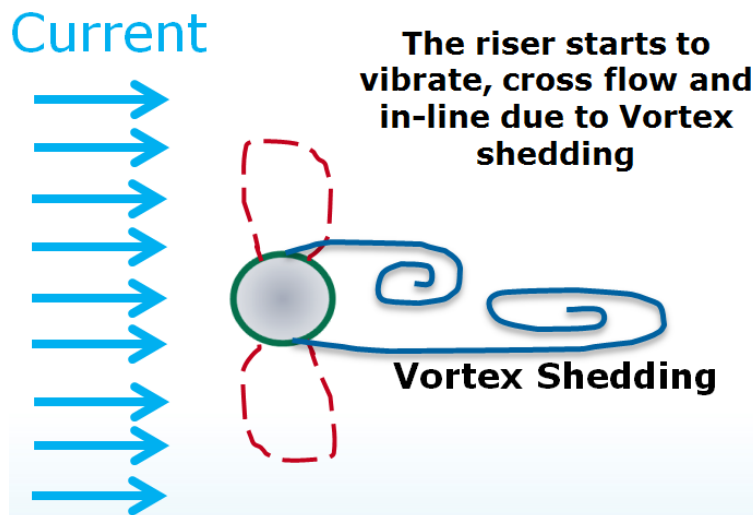


Figure 7-8 Vortex Shedding

The minimum fatigue life is 113 years considering D-curve and 156 years considering C2-curve, which are less than the minimum acceptable fatigue life due to VIV. The minimum fatigue life is found at the lower catenary of the SLWR between arc lengths 2300 m to 2400 m. It is also observed that the sag-bend and hog-bend sections are subjected to fatigue damage due to VIV.

It is observed that the out-of-plane current impacts more fatigue damage on to riser compared to the in-plane current. This is an indication that out-of-plane current, or also called as transverse current, is more critical to give worst fatigue damage on the riser. The detail fatigue results from each current profile for both in-plane and out-plane current are provided in Appendix D.

Although the fatigue life of the SLWR is less than the minimum acceptable fatigue life, the fatigue performance of the SLWR can still be improved by installing the VIV suppression along a specific length of the riser, such as helical strakes and fairings as shown in Figure 2-9. The geometry of the VIV suppression can disrupt the generated vortex on the downstream side of the flow, such that the fatigue damage can be reduced and fatigue performance of SLWR can be improved. The VIV suppression coverage length is expected to be around 50% in the middle section of the upper catenary, where the straight section of the SLWR is exposed to the current.

Fairing design allows to rotate freely such that they always align with the current's direction, hence vortex shedding is suppressed. The geometry of fairings can reduce the vibration from the vortex shedding without incurring an increase in riser's drag coefficient. The helical strakes design consists of 3 helical lines along the suspended riser. The helical strakes are widely used for suppressing vortex shedding, since helical strakes design is simple, effective, and easy to be installed. Due to their helical body, they can provide quick distraction of incoming flow pattern, reducing the vibrations from vortex shedding.

However, this helical design causes an increase in riser's drag coefficient. Careful consideration should be taken to avoid excessive fatigue damage due to VIV, while also optimize the length of helical strakes segment to avoid both excessive cost and excessive drag loading as this may have both design and cost implications. However, the helical strakes have been preferred option of the offshore industry compared to the fairings. The reasons are as follows:

- The helical strakes are fixed; meanwhile the fairings should be installed such that it may weather-vane with incidental current direction which may have a problem if it gets stuck during its design life.
- Installation of the helical strakes is simpler than the fairings
- The helical strakes have a longer track record than the fairings

## Chapter 8. Riser Fabrication and Installation

### 8.1 Introduction

This chapter presents the general description of the fabrication and the installation of the steel catenary riser (SCR), including the WDSCR and the SLWR. The content of this chapter is according to practical works and industrial knowledge on the fabrication and the installation. The technical feasibility of fabrication and installation of the steel catenary riser in deep water and harsh environments are discussed. The method of fabrication and installation need to be carefully selected during the initial design phases as major issues in total development cost.

In order to develop offshore oil and gas field, the operator faces the challenge in an effort to reduce development cost and also to ensure the satisfactory quality of the offshore facilities, especially for deep water riser systems. As developments move into deep water, the total development costs increase, as does the effort to reduce them. One of the challenges of the installation is the limit in the availability of installation vessels that have a good stability and the ability to accommodate the riser top tension and a large number of riser sections on board. The consideration of the fabrication includes welding processes to ensure that the high quality welding is performed.

### 8.2 Fabrication

A steel catenary riser is made up of a series of welded pipe joints. The weld material properties, joint dimensional tolerances, girth welds, welding procedure and inspection criteria are the main factors of riser's fatigue performance (Burgess and Lim, 2006). Therefore, an excellent quality welds are required so that the sufficient fatigue lives for SCR is achieved. Fabrication of the SCRs can be accomplished onshore and/or offshore.

The fabrication in offshore is conducted on the installation vessel by S-lay or J-lay. The pipe joints are welded together in the welding station. On the other hand, the fabrication in onshore has an added benefit. The benefit is that the girth welds can be fabricated and inspected in controlled surroundings in order to make sure that the required integrity of the welding of riser is achieved (Karunakaran et al., 2013).

The fabrication material in this study is carbon steel of grade X65. The internal surface of the pipe is exposed to the well fluids, which can be corrosive mainly due to CO<sub>2</sub> and H<sub>2</sub>S. Therefore, the fabrication of riser requires high quality of internal corrosion performance and internal weld root by utilizing corrosion resistant alloys (CRA) and internal gas purge. The selection of CRA material is based on the well fluids and mechanical properties (Karunakaran et al., 2005).

The operators should also provide appropriate measures to ensure high quality coatings as cathodic protection to reduce the risk of exposing welds to seawater and to ensure stringent fabrication requirements. The challenge of welding of riser is significant due to the strict weld acceptance criterion. The quality of girth weld is one of the key factors for the SCR fatigue

performance. According to Karunakaran et al. (2013), the following are the prerequisites for welding processes of SCR:

Table 8-1 Prerequisite for Fabrication of SCR Weld (Karunakaran et al., 2013)

Prerequisite	Description
Close control of pipe end tolerances and joint misalignment	Typical SCR may require joint hi/lo to be controlled to a maximum tolerance of $\pm 0.5$ mm. In order to maintain this limit, it typically requires counter boring of the pipe ends together with pipe end sorting and ID grouping of pipe section.
High integrity welding procedures	Close control of the welding parameters is required to ascertain freedom from lack of fusion defects and to provide satisfactory internal weld root and external weld cap profiles. This is because there are stringent requirements on allowable welding flaws for typical SCR.
High Fatigue Performance	For ensuring high fatigue performance of riser, it is necessary to flush grind the weld caps. This can give a significant improvement in fatigue life in riser where fatigue resistance is limited by crack initiation at the weld cap toe.

The following are some welding methods adopted for welding processes.

- Pulsed Gas Metal Arc Welding (PGMAW)
- Pulsed Gas Tungsten Arc Welding (PGTAW)
- Flux Core Arc Welding (FCAW)
- Gas Metal Arc Welding (GMAW)
- Gas Tungsten Arc Welding (GTAW)

The welding process of PGTAW is capable to produce high integrity girth welds. A mechanized PGTAW equipment and typical weld cap macro section are presented in Figure 8-1. The mechanized hot wire PGTAW process has been successfully performed for the BC-10 project by Subsea 7. Even though, the mechanized PGTAW process is proficient to manufacture high integrity girth welds, the welding production rates are limited.

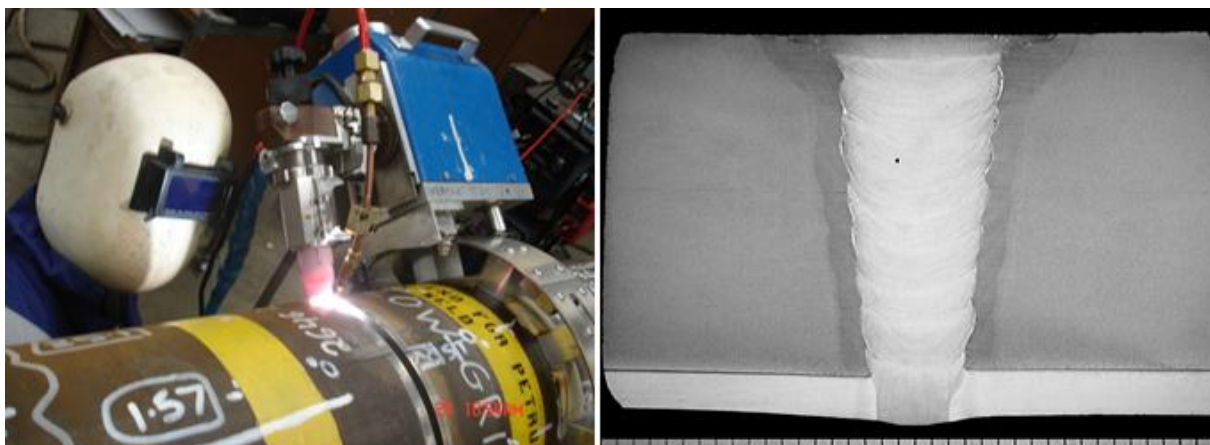


Figure 8-1 Mechanized PGTAW Equipment in Operation and Weld Cap Macro Section (Karunakaran et al., 2013)

Therefore, the mechanized PGMAW (Pulsed Gas Metal Arc Welding) process was introduced to attain higher production rates than the mechanized PGTAW. The mechanized PGMAW is capable to provide acceptable integrity girth weld for riser's fabrication. This method utilizes a feature of the Cold Metal Transfer (CMT) process for root welding. Such a feature allows the root welding to be achieved with the minimum temperature input, giving a good control of the weld root quality and profile (Karunakaran et al., 2013)

A pictorial representation showing typical mechanized PGMAW and CMT weld roots is shown in Figure 8-2. In 2012, the Vigra Spool Base implements the PGMAW/CMT weld solution for the fabrication of several clad and lined pipe projects, including Stjerne, Skuld, Visund Sor and Tordis (Karunakaran et al., 2013).



Figure 8-2 Mechanized PGMAW in operation and typical girth weld showing CMT weld roots (Karunakaran et al., 2013)

For post weld inspection, the Automated Ultrasonic (AUT) inspection should be performed to girth weld to prove the accuracy of the welding processes. The Non Destructive Test (NDT) is also carried out to verify the welding and coating quality. From those inspections, a reliable detection of very small defects is expected to ensure high fatigue performance of the SCR.

### 8.3 Installation

The driving factors of SCR installation include weather windows, vessel capability, installation method, water depth, environmental conditions, size and weight of the riser pipe. The harsh environment can limit the weather window and induce large motion of the installation vessel, which may harm the installation activities. Thus, the installation schedule will be established and agreed as weather restricted operation in harsh environment. In addition, the appropriate vessel installation is important to give a good stability and accommodation of riser top tension during the installation activity.

There are a limited number of companies in the world, providing pipe laying services in deep water and ultra-deep water. Some leading international installation companies that provide pipe-laying service are Allseas, McDermott, Saipem, Subsea 7, and Technip. The seven Oceans and Seven Borealis are the installation vessels which have been used for SCRs installation, owned by Subsea 7. The design of Seven Oceans and Seven Borealis makes the

pipe-laying activities able to withstand installation conditions in harsh environments as shown in Figure 8-3.



Figure 8-3 The Seven Oceans and Seven Borealis Pipe-lay Vessel, Figure from Subsea 7

This section contains the following of SCR installation aspects:

- Pipe-lay methods,
- Riser hook-up and
- Installation of modules.

### 8.3.1 Pipe-lay Methods

There are many methods for laying SCR into deep water. This study focuses on three installation methods, which are S-Lay, J-lay and reel-lay method.

#### S-lay Method

The S-lay method is widely used due to the abilities of quick installation for large diameter pipe. Commonly, the S-Lay method is suitable for shallow and intermediate water depths. The stinger is a frame structure located at stern with roller track to support the pipe during sliding down the pipe. The stinger controls the curvature of the pipe in order to avoid excessive deflection in an over-bend region.

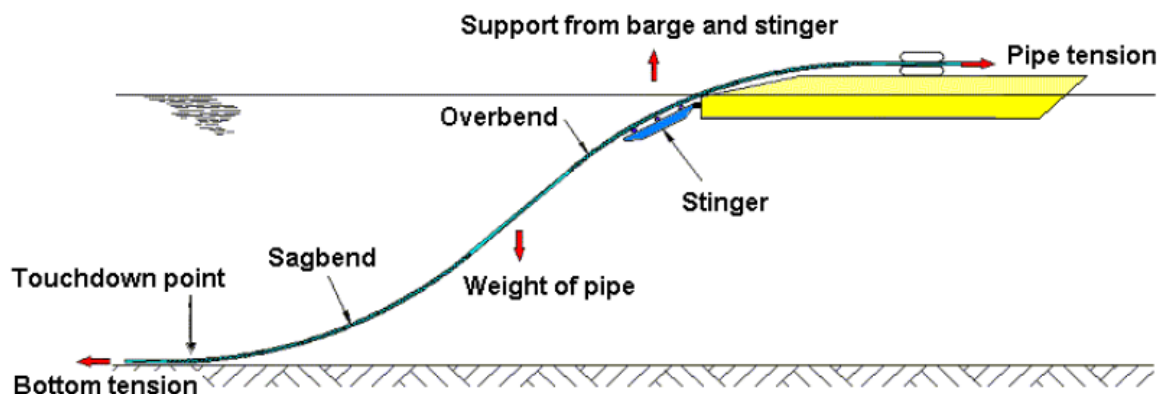


Figure 8-4 Sketch of S-Lay Method

As the installation vessel moves forward, the tensioners will be utilized to hold the entire pipe so it won't slide down to the seabed due to its self-weight during the installation process. Pipe leaves the stern of the ramp at the end of the vessel almost horizontally, going over the stinger



in an over bend region and going further down through the sea as a suspended span and then reaches the seabed at the touchdown point in the sag-bend region (Palmer and King, 2008). The sag-bend and over-bend area will form like the letter "S" as shown in Figure 8-4.

It is necessary to ascertain that the pipe can withstand the combined load of bending, external and internal pressure at the sag-bend and over-bend region. Normally, the pipe is installed empty to minimize the tension requirements. The benefits of using this method are the high production rate as it has several welding stations. In addition, it has the ability to install large diameter pipe with coating layer.

The S-Lay method can be utilized for pipe-lay operation in deep water, but it will require a long stinger and adequate tensioner capacity in order to hold the entire pipeline during the installation process. A very long stinger is avoided since it might incur excessive force from wave and current. It can be summarized that the S-lay is not preferred for the SCR installation in this study since it encounters difficulties in very deep water.

### **J-lay Method**

The SCR installation by J-lay has been well proven technology for pipe-lay operation. In this method, the pipe shape resembles the "J" letter during installation, see Figure 8-5. Unlike the S-lay, the J-lay does not introduce over-bend region since the pipe leaves the vessel nearly in a vertical position. No stinger is required for J-lay method. The ramp angle can be prescribed in line with the pipe catenary to the seabed. The J-Lay method is not appropriate for shallow waters as shallow water requires a steeper departure angle for pipe-lay activity.

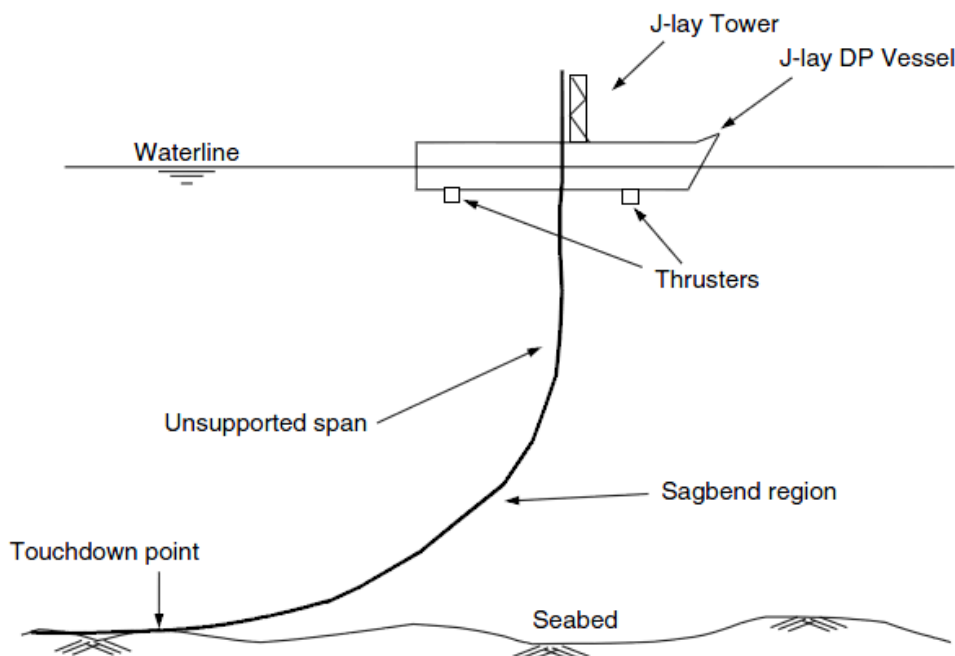


Figure 8-5 Sketch of J-lay Method (Chacko et al., 2005)

The installation vessel is equipped with J-lay collars to hold the pipe and also to act as buckle arrestors during installation operation. This method requires lower tensioner capacity compared to the S-lay method. However, compared to the S-lay methods, the J-Lay has a fairly low production rate due to only one or two welding stations. The J-lay and the S-lay can

both be employed aboard the Subsea 7 installation vessel of Seven Borealis as shown in Figure 8-3.

### **Reel-lay Method**

The reel-lay method is preferred choice for installation of the SCR in deep water and harsh environment in this study. The reel-lay method is chosen as a proposal in this study. This is because it is cost effective and offers a reliable production rate of installation. This method is suitable for installing a small diameter ranging from 4 inches to 18 inches. The coating thickness is limited to 100 mm for reeled installation (Karunakaran et al., 2005). This method is conducive with a small weather window which is associated with harsh environments. This method allows the whole riser length to be fabricated onshore and installed by a reeling lay vessel.

This is advantageous since the welding process can be performed onshore in a controlled environment to make sure that the required integrity of the welding of the riser is achieved (Karunakaran et al., 2013). Spool base is used to weld the pipeline stocks; Figure 8-6 shows a picture of spool bases of Vigra in Norway. After the pipe is fabricated and welded onshore, the pipe is reeled from the dock onto the reels on the vessel. However, the riser and its joint welds may undergo significant plastic deformation which may generate wrinkles during the reeling, unreeling and straightening processes (Hatton and Willis, 1998).

Therefore, a system of internal pressurization is employed to avoid wrinkles on the riser and an inspection is performed to verify if wrinkles have occurred during the reeling process (Maneschy, 2015). The reel-lay method can be employed using the Seven Oceans vessel of Subsea 7 as shown in Figure 8-3. The Roncador in Brazil, Guara & Lula in Brazil, and Blind Faith in Gulf of Mexico (GoM) have applied reel lay method to install many SCRs.

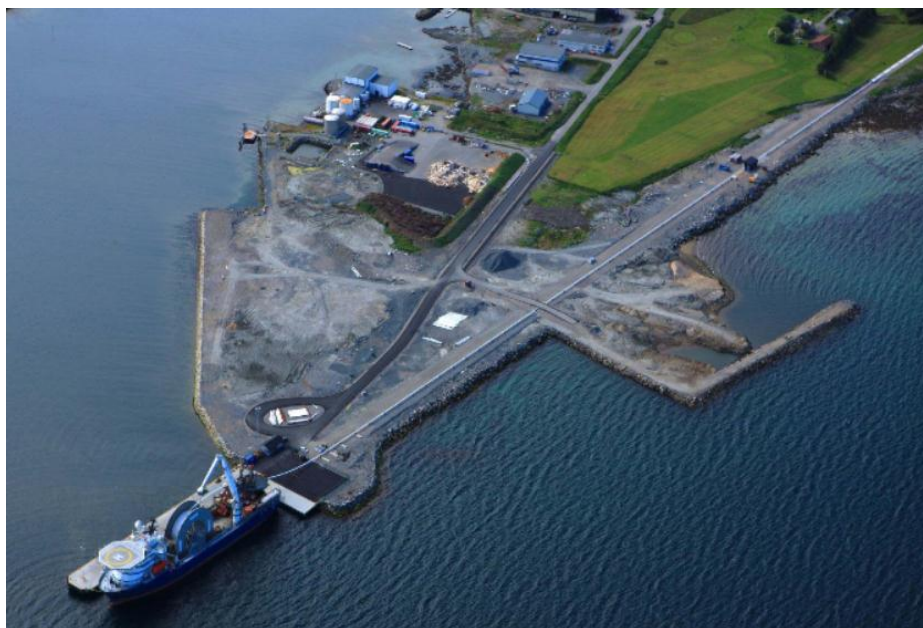


Figure 8-6 Spool Base Vigra of Subsea 7, Figure from Subsea 7

### 8.3.2 Riser Hook-up

After the pipe-lay operation has been performed, the next step is to connect the riser to the host platform. The harsh environment can limit the weather window of this operation. One way to deal with the harsh environment is to pre-install the riser in summer period before the host platform is in-place. Normally, support vessel is required to transfer the riser to the host platform. The RIT is hydraulic connector at the top end of the riser for lifting purposes. A pictorial representation showing typical Flex Joint and RIT is shown in Figure 8-2.

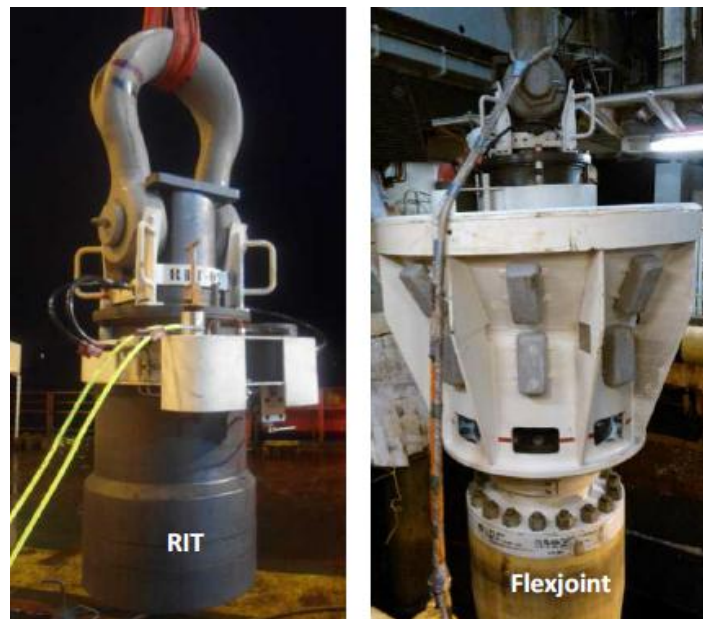


Figure 8-7 Typical RIT and Flexjoint (Maneschy, 2014)

After the host platform is in-place, the riser installation tool (RIT) is pulled into the flex joint of host platform by using the hydraulic winch. During this stage, the installation vessel should also be oriented such that it attracts smallest environmental loads. The mean hang-off angle at the flex joint is then verified using an inclinometer. The flexible joint was set to have minimum rotational stiffness for accommodating different hang-off angle during service life. During the installation phase, the bottom part of the riser is anchored to the seafloor by using suction piles to hold the configuration of the riser close to the touchdown point (TDP).

### 8.3.3 Installation of Modules

The WDSCR and the SLWR require added modules in order to shape the intended configuration. The SLWR configuration is achieved with buoyancy modules added along the relevant length of the riser. A picture showing buoyancy modules are shown in Figure 2-10. The installation of the buoyancy modules is conducted before it is lowered down into the water.

It is important to prevent the buoyancy modules from migrating from the desired position during the service life. Thereby the buoyancy modules are equipped with internal clamp, bolted onto the riser to firmly lock it axially. Figure 8-8 shows a picture of the installation team mounting a buoyancy module onto the riser string in the Caesar Tonga development in the Gulf of Mexico (GoM).



Figure 8-8 the Installation of buoyancy Module onto the Riser (Beattie et al., 2013)

The WDSCR configurations can be achieved with ballast modules at the bottom of the riser straight section. A pictorial view showing the ballast module is shown in Figure 2-11. The installation of ballast modules is similar to the installation of buoyancy modules. They are installed using an effective, firm and safe offshore installation procedure. The internal clamp is bolted directly onto the riser to securely lock the ballast module axially onto the riser (Karunakaran et al., 2013). The clamp is stiffened around the riser, and the both sides of the ballast module are strapped onto the internal clamp adjoining together with kevlar strap. Balmoral Offshore Engineering and Trelleborg are two qualified vendor of buoyancy modules and ballast modules.

## Chapter 9. Conclusion and Recommendation

### 9.1 Conclusion

This study outlines the feasibility of selected riser concepts in terms of capability to cope with the large motion from the Semi-submersible in deep water and harsh environment. The selected riser concepts are the conventional SCR, the Weight Distributed SCR (WDSCR) and the Steel Lazy Wave Riser (SLWR). The considered risers have an internal diameter of 10 inches and are made of low carbon steel of grade X65.

The riser concepts have been modeled using ORCAFLEX. The appropriate static configurations of riser concepts are achieved by performing several optimizations and evaluations. The static responses have been found satisfactory, which is within the allowable design criteria. After establishing the appropriate static configurations with satisfactory static responses, the riser concepts were subjected to extreme response analysis.

#### **Extreme Response Analysis**

The main challenge of riser system is the large motion from the host platforms due to the harsh environment for application in deep water. The large motion of the host platforms may induce excessive buckling and fatigue at the touchdown point. The key component of the large motion of the host platform is the downward velocity at the hang-off point where the top-end of the riser is attached to the host platform. The concern is also on the downward velocity in the touchdown area since a feasible configuration can be addressed by controlling the dynamic stresses at the TDP. It has been investigated that the downward velocity in the touchdown area is mainly caused by the downward velocity at the hang-off point.

By screening the downward velocities at the hang-off point in the time history graph, the time at which the critical responses (i.e. buckling utilization, bending moment and compression) peak is identified. The downward velocity at the hang-off point induces the bending moment and negative effective tension (compression) at the TDP. A combination of excessive bending moment and compression at the TDP may result in an incapability of the riser to satisfy the strength design requirement.

To assess the feasibility of the risers, an integrated system approach was adopted where the different downward velocities at the hang-off point was investigated to capture the limitations of riser integrity. The extreme response analysis was performed using load cases based on the different downward velocities at the hang-off point in the screening process.

The Conventional SCR has difficulty in meeting the strength design requirement in the harsh environment. The concept of weight distributed SCR showed a significant improvement to the SCR by establishing “near-bottom support” of heavy cross section at the bottom of straight section. Although the WDSCR and the conventional SCR has the same downward velocity at the hang-off point, the WDSCR has less downward velocity at the TDP compared to the conventional SCR. The heavy cross section of WDSCR reduces the critical responses (i.e. bending moment, compression and utilization) at the TDP and extend the feasibility of the

SCR. The study concludes that there is a significant improvement of strength design for the WDSCR compared to the conventional SCR.

The concept of “steel lazy” wave riser (SLWR) showed superior performance over the conventional SCR and the WDSCR. The lazy wave configuration can distribute the bending stress along the riser efficiently. The buoyancy modules are effective to isolate the dynamic motion of the floater from the TDP which results in lower bending stress at the TDP compared to both WDSCR and conventional SCR.

Overall, from the extreme response analysis study, the results showed that a feasible conventional SCR configuration can be obtained if the downward velocity at the hang-off point is restricted below 2.6 m/s. It is also found that the downward velocity at the sag-bend of the SCR is restricted below 3.03 m/s. On the other hand, a feasible WDSCR configuration can be obtained, if the downward velocity at the hang-off point is restricted below 3.2 m/s. It is also found that the downward velocity at the sag-bend of the WDSCR is restricted below 3.43 m/s.

The results showed that the SLWR configuration can cope with even downward velocity of 6 m/s at the hang-off point. Thereby the SLWR configuration is proven to be the most robust configuration to cope with large motion of the host platform in respect to strength and fatigue performance.

From a separate study, the SCR/WDSCR with uniform external coating showed less riser integrity compared to the SCR/WDSCR without uniform external coating. The density of uniform external coating is less than the density of sea water, resulting in a net buoyancy force on the riser structure. Thus, it can be concluded that the heavier the SCR/WDSCR, the better riser integrity is achieved to cope with the large motion of the host platform. The effect of uniform external coating is significant for free hanging configuration of SCR and WDSCR. On the other hand, the effect of uniform external coating is not significant for the SLWR.

### **Fatigue Performance**

The wave induced fatigue analysis of three riser concepts were performed using a comprehensive time domain analysis. A total of 216 load cases from 12 wave directions and 18 non-linear dynamic analyses, applying irregular sea states of JONSWAP, were considered. The results of the conventional SCR showed unsatisfactory wave induced fatigue performance. A minimum fatigue life of 80 years was observed at the TDP, considering D-curve.

The investigation of the WDSCR resulted in a better wave induced fatigue performance than the conventional SCR. The minimum fatigue life of 247 years was observed at the TDP, considering D-curve. However, this result is still under the acceptable limit of 250 years. On the other hand, the results of the SLWR showed satisfactory wave induced fatigue performance with the minimum fatigue life of 874 years, considering D-curve. This result is well above the acceptable limit of 250 years.

It is noted that the hang-off area presented very low fatigue performance. In order to solve this, this section will, in practice, be occupied with flex joint and there are proven measures to

manage it. Therefore, this result is useful for planning an appropriate design of the flex joint and other measures in order to reduce the fatigue damage in the hang-off area.

The VIV fatigue analysis of the SLWR was performed using a total of 28 load cases from 14 current profiles in in-plane and out-of-plane current directions. The results showed the minimum fatigue life of 113 years at the TDP, considering D-curve. This result is much below the acceptable limit of 500 years. However, this problem can be solved by introducing some proven measures to suppress the vortex shedding around the riser. The helical strakes have been proposed as a solution to mitigate the fatigue damage due to VIV. The helical strake coverage length is estimated to be approximately 50% in the middle section of the upper catenary, where the straight section of the SLWR is exposed to the current.

### **Summary**

In summary, several types of the SCR configurations have been developed by installing either buoyancy or ballast modules at the lower part of the riser. Each configuration has characteristics which make it better suited for particular applications. An optimization of riser configuration by combining ballast modules, which is known as the WDSCR, results in more applicable concept than the conventional SCR, while an optimization riser configuration by combining buoyancy modules, which is known as the SLWR, results in more applicable riser concept than both conventional SCR and WDSCR.

## **9.2 Recommendation**

In this study, the feasibility of the conventional SCR, weight distributed SCR and steel lazy wave configuration in terms of capability to cope with the large motion of the host platform has been investigated. The study was extensive with different load cases to see how riser concepts can cope with the different downward velocity at the hang-off point. However, there is abundant room for further work of this study. The following are recommendations for further works that need to be carried out in this study.

- The investigation of other riser concepts is recommended for further work of this study in order to understand the feasibility of other riser concepts in terms of capability to cope with the vessel heave motion.
- The riser is flooded with oil in this study, sensitivity study can be carried out in order to consider the empty riser condition.
- A uniform hydrodynamic coefficient was considered in this study, sensitivity study can be carried out in order to consider different hydrodynamic coefficient due to marine growth and Reynolds number along the suspended riser.
- Wave induced fatigue analysis may be performed with different vessel offsets and different vessel drafts to see how these factors contribute to the fatigue performance of the riser.
- VIV fatigue analysis may be performed with the introduction of helical strakes in the middle section of the upper SLWR catenary to have sufficient fatigue life within the FLS design criteria.

## References

---

1. Alderton, N. and Thethi, R. (1998). Choosing the Most Appropriate Rigid Catenary Riser Design for Various Deepwater and Harsh Environments. Advances in Riser Systems & Subsea Technologies for Deepwater. Aberdeen, UK.
2. Alliot, V., Legras, J.L., Perinet, D. (2005). Ultra-deepwater riser choice requires careful analysis. Available at: <<http://www.offshore-mag.com/articles/print/volume-65/issue-6.html>> [accessed on 11th March 2015]
3. API. (2006). Design of Risers for Floating Production Systems (FPSs) and Tension-Leg Platforms (TLPs). Recommended Practice, API-RP-2RD. American Petroleum Institute.
4. BALMORAL. 2014. Distributed Buoyancy Modules (Online). Balmoral Offshore Engineering. Available:<<http://www.balmoral-offshore-engineering/2-surf-distributed-buoyancy.php>> (Accessed 06 June 2014).
5. Baltrop, N. D. P. (1998). Floating Structure: A Guide for Design and Analysis (Vol. 2). London: The Center for Marine and Petroleum Technology.
6. Bai, Y. and Bai, Q. (2010a). Subsea Pipelines and Risers. Houston, USA: Elsevier Inc.
7. Bai, Y. and Bai, Q. (2010b). Subsea Engineering Handbook, USA: Elsevier Inc.
8. Beattie, M., Lahey, E., Burke R. W. and Balch, E. R. (2013). Caesar-Tonga Project Steel Lazy-Wave Riser Design. OTC 24232. Proceeding Offshore Technology Conference. Houston, Texas, USA.
9. Bell, J.M. and Chin, Y.D., Hanrahan, S. (2005). State of The Art of Ultra Deepwater Production Technologies. OTC 17615. Prepared for presentation at the OTC. Houston, Texas, U.S.A.
10. Burgess, M. and Lim, F. (2006). Installation of Deepwater Risers, 2H Offshore, UK.
11. Calqlata. 2010. Vessel Motion Calculator (displacements velocities accelerations). (image online) Available at: <<http://www.calqlata.com/productpages/00059-help.html>> (Accessed 10 March 2015).
12. Chacko, J., Ghalambor, A., Guo, B., and Song, S. (2005). Offshore Pipelines. Burlington, USA: Gulf Professional Publishing.
13. Chen, J., Cao, P., Zhu, H., and Jukes, P. (2009). Time Trace Window Based Approach for SCR Strength Analysis in Ultra Deepwater of Gulf of Mexico, OMAE Paper79529, Honolulu, Hawaii, USA.
14. Chen, J. and Cao, P. (2013). Design of Steel Lazy Wave Riser for Disconnectable FPSO. SBM Offshore.OTC24166. Prepared for presentation at the OTC. Houston, USA.
15. DNV. (2010a). DNV-OS-F201: Dynamic Riser. Norway: Det Norske Veritas.
16. DNV. (2010b). DNV-RP-C205: Environmental Conditions and Environmental Loads. Norway: Det Norske Veritas.
17. DNV. (2010c). DNV-RP-C203: Fatigue Design of Offshore Steel Structures. Norway: Det Norske Veritas.



18. DNV. (2010d). DNV-RP-F205: Global Performance Analysis of Deepwater Floating Structures. Norway: Det Norske Veritas.
19. DNV. (2011). DNV-OS-H101: Marine Operations, General. Norway: Det Norske Veritas.
20. DNV. (2013). DNV-OS-E301: Position Mooring. Norway: Det Norske Veritas
21. Foyt, E., Griffin, C. and Campbell, M. (2007). Weight Optimized SCR – Enabling Technology for Turret Moored FPSO Developments. Proceedings of the 26th International Conference on Offshore Mechanics and Arctic Engineering, 10-15 June 2007. San Diego, California, USA.
22. Hatton, S. A. and Howells, H. (1996). Catenary and Hybrid Risers for Deepwater Locations worldwide. 2H Offshore Engineering Limited Woking, Surrey, UK.
23. Hatton, S. A. and Willis N. (1998). Steel Catenary Risers for Deepwater Environments. OTC 8607. Proceeding Offshore Technology Conference. Houston, Texas, USA.
24. Haver, S. K. (2010). Prediction of Characteristic Response for Design Purpose. Norway: Statoil.
25. Howells, H. and Hatton, S. A. (1997). Challenges for Ultra-deep Water Riser Systems. Floating Production Systems IIR, London.
26. Journée, J.M.J. and Massie, W. W. (2001). Introduction in Offshore Hydromechanics (OT3600). Delft, Netherland: Delft University of Technology.
27. Karunakaran, D. and Baarholm, R. (2013). COBRA: An Uncoupled Riser System for Ultra-deep Water in Harsh Environment, OTC-23986-MS. Paper presented at the OTC, Houston, Texas, USA.
28. Karunakaran, D., Legras, J. and Jones, R. (2013). Fatigue Enhancement of SCRs: Design Applying Weight Distribution and Optimized Fabrication. OTC-23945-MS. Prepared for presentation at the OTC. Houston, Texas, USA: Subsea 7.
29. Karunakaran, D., Nordsve, N. T. and Olufsen, A. (1996). An Efficient Metal Riser Configuration for Ship and Semi Based Production Systems. International Offshore and Polar Engineering Conference 1996 Los Angeles.
30. Karunakaran, D., Meling T. S., Kristoffersen S. and Lund, K. M. (2005): Weight Optimized SCRs for Deepwater Harsh Environments. Proceedings Offshore Technology Conference, 2-5 May. Houston, Texas, USA.
31. Karunakaran, D. and Meling, T. S. (2006). Robust SCR Design against Fatigue in Deep water Harsh Environments, Proceedings Offshore Technology Conference, Houston, Texas, USA.
32. Kavanagh, W. K., Lou, J. & Hays, P. (2003). Design of Steel Risers in Ultra Deep Water – The Influence of Recent Code Requirements on Wall Thickness Design for 10,000ft Water Depth. Offshore Technology Conference. Houston, Texas.
33. Lien, T. (2010). Riser System. Retrieved from <http://subsea1.com> website: [http://subsea1.com/index/page?page\\_id=11018](http://subsea1.com/index/page?page_id=11018)
34. Maneschy, M., Romanelli, B., Butterworth, C., Pedrosa, J., Escudero, C. and Vargas T. (2015). Steel Catenary Risers (SCRs): from design to installation of the first reel CRA lined pipes. Part II: Fabrication and Installation. OTC-25857-MS. Proceedings Offshore Technology Conference, 5-8 May. Houston, Texas, USA.

35. Masturi, L. M. (2012). Comparison Study of Selected Uncoupled Riser Concepts in Deep Water and Harsh Environment. (MSc), University of Stavanger, Norway.
36. Nurwanto, T. (2012). COBRA Riser Concept for Ultra Deepwater Condition. (MSc), University of Stavanger, Norway.
37. NOROK. (2007). N-003: Action and Action Effects. Norway: Standards Norway.
38. Odland, J. 2013. Offshore Field Development: Platform concepts and design issues. OFF500 - Lecture Notes. Stavanger, Norway: University of Stavanger.
39. Olufsen, A., Loland, G., Gorf, P. and Webb, S. 2003. Evaluation Ranks Deepwater, Harsh Environments Floater, Riser Concepts. Oil and Gas Journal, 101, 39-46.
40. OGJ. (2010). Strategic Development on the Outer Edge. (Internet) Available at: <<http://www.ogj.com/articles/shell/perdido/2010/04/strategic-development-on-the-outer-edge.html>> (Accessed 12 February 2015).
41. Olufsen, A., Loland, G., Gorf, P. & Webb, S. 2003. Evaluation Ranks Deepwater, Harsh Environments Floater, Riser Concepts. Oil and Gas Journal, 101, 39-46.
42. Orcina. (2010). ORCAFLEX Manual (Version 9.4a). Cumbria, UK: Orcina Ltd.
43. Orimolade, A. P. (2014). Steel Lazy Wave Risers from Turret Moored FPSO. (MSc), University of Stavanger, Norway.
44. Palmer, A.C., and King, R.A. (2008). Subsea Pipeline Engineering. Tulsa, Oklahoma, USA: Penwell Corporation.
45. Perinet, D., and Frazer, I. (2007). J-Lay and Steep S-Lay: Complementary Tools for Ultra deep Water, Proceedings Offshore Technology Conference. Houston, Texas, USA.
46. Petruzka, D. J., Zimmermann, C. A., Krafft, K. M., Thurmond, B. F., Duggal, A. (2002) Riser System Selection and Design for a Deepwater FSO in the Gulf of Mexico. Offshore Technology Conference - OTC 14154. Houston, Texas.
47. Phifer, E. H., Kopp, F., Swanson, R. C., Allen, D. W. & Langner, C. G. (1994). Design and Installation of Auger Steel Catenary Risers. Offshore Technology Conference - OTC 7620. Houston, Texas.
48. Riflex. (2011). Riflex User Manual, V3.4. Høvik, Norway: Marintek.
49. Rodrigues, M. V., Hansen, V. L., Bahiense, R.A., and Raposo, C.V. (2008). Steel Catenary Riser Design Based on Prescribed Motions from Coupled Analysis Methodology. Proceedings Offshore Technology Conference, 5-8 May. Houston, Texas, USA.
50. Senra, S. F., Andrade, E. Q., Mourelle, M. M. and Torres, A. L. F. L. (2011). Challenges Faced in the Design of References SLWR Configuration for the Pre-Salt Area. Ocean, Offshore and Arctic Engineering, OMAE2011, 2011 Rotterdam, Netherlands.
51. St. Denis, M. and Pierson, W. J. (1953). On the Motion of Ships in Confused Seas. Transactions SNAME, 61:1-53.
52. Tawekal, R. L. (2010). Bangunan Lepas Pantai 2. Bandung, Indonesia: Institut Teknologi Bandung.
53. Vivsolutions. 2015 (Internet) Available at: <<http://www.vivsolutions.com/about-us/who-we-are/management/>> (Accessed 14 February 2015).

54. Vivana. (2005). VIVANA Theory Manual Version 3.4. Trondheim, Norway: Marintek.
55. Yue, B., Walters, D., Yu, W., Raghavan, K. and Thompson, H. (2011). Lazy wave SCRon Turret Moored FPSO. 2H offshore. Houston., USA.

# Appendix A - Wall Thickness Calculation

**DNV-OS-F101 version**  
 DNV-OS-F101 2007 Code check are done according to the 2007 version of DNV-OS-F101.

**Kilometer Post**  
 Start  End

**Material Input**  
 SMYS [MPa]   
 SMTS [MPa] X65   
 f<sub>y</sub> temp [MPa]   
 f<sub>u</sub> temp [MPa]   
 Young's modulus [GPa]   
 Poisson's ratio [-]   
 Anisotropy factor [-]   
 Hardening factor [-]   
 Fabrication factor [-]   
 Suppl. req. U fulfilled

**Load Input**

	Pressure [barg]	@ level [m]	Content mass density [kg/m3]
Design	<input type="text" value="500"/>	<input type="text" value="-1500"/>	<input type="text" value="800"/>
System test	<input type="text" value="575"/>	<input type="text" value="-1500"/>	<input type="text" value="1025"/>

Incidental to design pressure ratio [-]   
 Water depth [m]  and mass density [kg/m3]

	Functional	Environmental
Moment [kNm]	<input type="text" value="0"/>	<input type="text" value="0"/>
Axial force [kN]	<input type="text" value="0"/>	<input type="text" value="0"/>
Strain [%]	<input type="text" value="3"/>	<input type="text" value="3"/>

Load condition factor [-]

**Design Input**

Failure mode	Condition	Safety class	Corr.	Der.
Burst	Operation	High	<input checked="" type="checkbox"/>	<input type="checkbox"/>
Burst	System test	System test	<input checked="" type="checkbox"/>	<input type="checkbox"/>
Collapse	Empty	High	<input checked="" type="checkbox"/>	<input type="checkbox"/>
Propagating buckling	Empty	High	<input checked="" type="checkbox"/>	<input type="checkbox"/>

Load comb., LCC, lc = a  
 Load comb., LCC, lc = b  
 Load comb., DCC, lc = a      
 Load comb., DCC, lc = b

**Results**

Calc.	t <sub>req</sub> [mm]	Utilisation [-]	Utilisation [-]
<input checked="" type="checkbox"/>	21,42	0,846	<div style="width: 84.6%;"></div>
<input checked="" type="checkbox"/>	18,53	0,719	<div style="width: 71.9%;"></div>
<input checked="" type="checkbox"/>	17,07	0,486	<div style="width: 48.6%;"></div>
<input checked="" type="checkbox"/>	24,88	0,989	<div style="width: 98.9%;"></div>
<input checked="" type="checkbox"/>	-	-1,000	<div style="width: 100%;"></div>
<input checked="" type="checkbox"/>	-	-1,000	<div style="width: 100%;"></div>
<input checked="" type="checkbox"/>	-	0,843	<div style="width: 84.3%;"></div>
<input checked="" type="checkbox"/>	-	1,095	<div style="width: 109.5%;"></div>

Reports  Buckle Arrestors DNV-OS-F101

## Appendix B - Sensitivity Analysis Results

This section gives the summary results of the SLWR with coating and the SLWR without coating for load case 9, 10, 11, 12, 13, 14 and 15.

Load Case 9	Semi Position			
	Intact		Damage	
Coating	Far	Near	Far	Near
Effective Top Tension (kN)	2657	2396	2729	2395
<b>Sag-bend</b>				
Max. Effective Tension (kN)	854	335	948	316
Max. Bending Moment (kN.m)	167	333	165	354
DNV Utilization (LRFD)	0.40	0.67	0.36	0.62
<b>Hog-bend</b>				
Max. Effective Tension (kN)	849	305	946	291
Max. Bending Moment (kN.m)	141	231	144	247
DNV Utilization (LRFD)	0.36	0.51	0.34	0.47
<b>TDP</b>				
Max. Effective Tension (kN)	848	258	946	246
Max. Bending Moment (kN.m)	166	331	167	347
DNV Utilization (LRFD)	0.42	0.67	0.37	0.60

Load Case 9	Semi Position			
	Intact		Damage	
No Coating	Far	Near	Far	Near
Max. Effective Tension (kN)	2829	2622	2899	2620
<b>Sag-bend</b>				
Max. Effective Tension (kN)	877	372	974	352
Max. Bending Moment (kN.m)	161	331	156	354
DNV Utilization (LRFD)	0.40	0.66	0.35	0.61
<b>Hog-bend</b>				
Max. Effective Tension (kN)	875	322	972	306
Max. Bending Moment (kN.m)	121	203	121	217
DNV Utilization (LRFD)	0.33	0.47	0.31	0.43
<b>TDP</b>				
Max. Effective Tension (kN)	874	277	971	262
Max. Bending Moment (kN.m)	168	329	164	344
DNV Utilization (LRFD)	0.41	0.66	0.36	0.60

Load Case 10	Semi Position			
	Intact		Damage	
Coating	Far	Near	Far	Near
Effective Top Tension (kN)	2784	2483	2787	2505
<b>Sag-bend</b>				
Max. Effective Tension (kN)	915	353	989	331
Max. Bending Moment (kN.m)	172	335	176	356
DNV Utilization (LRFD)	0.40	0.67	0.38	0.62
<b>Hog-bend</b>				
Max. Effective Tension (kN)	895	318	980	302
Max. Bending Moment (kN.m)	149	233	161	250
DNV Utilization (LRFD)	0.38	0.52	0.36	0.48
<b>TDP</b>				
Max. Effective Tension (kN)	895	259	980	247
Max. Bending Moment (kN.m)	169	337	177	353
DNV Utilization (LRFD)	0.42	0.68	0.38	0.61

Load Case 10	Semi Position			
	Intact		Damage	
No Coating	Far	Near	Far	Near
Max. Effective Tension (kN)	2935	2698	2951	2710
<b>Sag-bend</b>				
Max. Effective Tension (kN)	928	389	1006	366
Max. Bending Moment (kN.m)	164	333	163	356
DNV Utilization (LRFD)	0.40	0.67	0.36	0.62
<b>Hog-bend</b>				
Max. Effective Tension (kN)	917	335	998	316
Max. Bending Moment (kN.m)	125	207	131	220
DNV Utilization (LRFD)	0.34	0.48	0.32	0.44
<b>TDP</b>				
Max. Effective Tension (kN)	916	278	998	262
Max. Bending Moment (kN.m)	169	332	169	351
DNV Utilization (LRFD)	0.41	0.67	0.37	0.61

Load Case 11	Semi Position			
	Intact		Damage	
Coating	Far	Near	Far	Near
Effective Top Tension (kN)	2815	2466	2833	2414
<b>Sag-bend</b>				
Max. Effective Tension (kN)	993	349	1081	329
Max. Bending Moment (kN.m)	202	338	202	358
DNV Utilization (LRFD)	0.45	0.68	0.41	0.62
<b>Hog-bend</b>				
Max. Effective Tension (kN)	990	316	1087	300
Max. Bending Moment (kN.m)	190	238	193	254
DNV Utilization (LRFD)	0.45	0.53	0.40	0.48
<b>TDP</b>				
Max. Effective Tension (kN)	989	259	1087	247
Max. Bending Moment (kN.m)	201	342	202	361
DNV Utilization (LRFD)	0.47	0.68	0.41	0.62

Load Case 11	Semi Position			
	Intact		Damage	
No Coating	Far	Near	Far	Near
Max. Effective Tension (kN)	2961	2681	2990	2640
<b>Sag-bend</b>				
Max. Effective Tension (kN)	999	386	1089	364
Max. Bending Moment (kN.m)	185	338	181	359
DNV Utilization (LRFD)	0.42	0.67	0.39	0.62
<b>Hog-bend</b>				
Max. Effective Tension (kN)	1000	333	1094	315
Max. Bending Moment (kN.m)	155	211	154	225
DNV Utilization (LRFD)	0.39	0.48	0.35	0.44
<b>TDP</b>				
Max. Effective Tension (kN)	999	279	1093	262
Max. Bending Moment (kN.m)	192	340	190	358
DNV Utilization (LRFD)	0.45	0.68	0.40	0.62

Load Case 12	Semi Position			
	Intact		Damage	
Coating	Far	Near	Far	Near
Effective Top Tension (kN)	2861	2521	2877	2520
<b>Sag-bend</b>				
Max. Effective Tension (kN)	1034	364	1127	338
Max. Bending Moment (kN.m)	193	341	200	361
DNV Utilization (LRFD)	0.43	0.68	0.41	0.62
<b>Hog-bend</b>				
Max. Effective Tension (kN)	1031	325	1138	307
Max. Bending Moment (kN.m)	179	239	192	256
DNV Utilization (LRFD)	0.43	0.53	0.40	0.49
<b>TDP</b>				
Max. Effective Tension (kN)	1030	259	1137	247
Max. Bending Moment (kN.m)	192	343	200	363
DNV Utilization (LRFD)	0.46	0.69	0.41	0.63

Load Case 12	Semi Position			
	Intact		Damage	
No Coating	Far	Near	Far	Near
Max. Effective Tension (kN)	3004	2725	3023	2726
<b>Sag-bend</b>				
Max. Effective Tension (kN)	1033	400	1121	371
Max. Bending Moment (kN.m)	179	340	179	362
DNV Utilization (LRFD)	0.41	0.68	0.38	0.63
<b>Hog-bend</b>				
Max. Effective Tension (kN)	1030	343	1127	321
Max. Bending Moment (kN.m)	146	211	153	227
DNV Utilization (LRFD)	0.37	0.48	0.35	0.45
<b>TDP</b>				
Max. Effective Tension (kN)	1029	278	1126	262
Max. Bending Moment (kN.m)	187	344	187	363
DNV Utilization (LRFD)	0.44	0.69	0.39	0.63



Load Case 13	Semi Position			
	Intact		Damage	
Coating	Far	Near	Far	Near
Effective Top Tension (kN)	3042	2609	3161	2593
<b>Sag-bend</b>				
Max. Effective Tension (kN)	1215	393	1379	363
Max. Bending Moment (kN.m)	233	344	247	364
DNV Utilization (LRFD)	0.50	0.69	0.47	0.63
<b>Hog-bend</b>				
Max. Effective Tension (kN)	1232	349	1402	327
Max. Bending Moment (kN.m)	232	243	252	259
DNV Utilization (LRFD)	0.52	0.53	0.48	0.49
<b>TDP</b>				
Max. Effective Tension (kN)	1232	258	1401	246
Max. Bending Moment (kN.m)	226	361	235	377
DNV Utilization (LRFD)	0.51	0.72	0.45	0.64

Load Case 13	Semi Position			
	Intact		Damage	
No Coating	Far	Near	Far	Near
Max. Effective Tension (kN)	3139	2807	3252	2796
<b>Sag-bend</b>				
Max. Effective Tension (kN)	1189	426	1343	396
Max. Bending Moment (kN.m)	206	345	209	367
DNV Utilization (LRFD)	0.45	0.69	0.42	0.63
<b>Hog-bend</b>				
Max. Effective Tension (kN)	1210	365	1363	342
Max. Bending Moment (kN.m)	182	214	192	229
DNV Utilization (LRFD)	0.44	0.49	0.40	0.45
<b>TDP</b>				
Max. Effective Tension (kN)	1209	280	1363	263
Max. Bending Moment (kN.m)	212	360	215	375
DNV Utilization (LRFD)	0.47	0.72	0.43	0.64

Load Case 14	Semi Position			
	Intact		Damage	
Coating	Far	Near	Far	Near
Effective Top Tension (kN)	3208	2655	3325	2708
<b>Sag-bend</b>				
Max. Effective Tension (kN)	1339	415	1516	384
Max. Bending Moment (kN.m)	284	347	311	367
DNV Utilization (LRFD)	0.59	0.69	0.56	0.63
<b>Hog-bend</b>				
Max. Effective Tension (kN)	1362	365	1548	342
Max. Bending Moment (kN.m)	299	246	334	262
DNV Utilization (LRFD)	0.64	0.54	0.59	0.49
<b>TDP</b>				
Max. Effective Tension (kN)	1361	259	1547	247
Max. Bending Moment (kN.m)	256	368	270	386
DNV Utilization (LRFD)	0.57	0.73	0.50	0.66

Load Case 14	Semi Position			
	Intact		Damage	
No Coating	Far	Near	Far	Near
Max. Effective Tension (kN)	3269	2846	3377	2885
<b>Sag-bend</b>				
Max. Effective Tension (kN)	1292	446	1455	416
Max. Bending Moment (kN.m)	237	350	249	371
DNV Utilization (LRFD)	0.51	0.70	0.48	0.64
<b>Hog-bend</b>				
Max. Effective Tension (kN)	1325	380	1489	356
Max. Bending Moment (kN.m)	225	215	245	231
DNV Utilization (LRFD)	0.51	0.49	0.47	0.45
<b>TDP</b>				
Max. Effective Tension (kN)	1324	279	1489	262
Max. Bending Moment (kN.m)	234	366	243	383
DNV Utilization (LRFD)	0.52	0.73	0.47	0.65

Load Case 15	Semi Position			
	Intact		Damage	
Coating	Far	Near	Far	Near
Effective Top Tension (kN)	3420	2812	3483	2779
<b>Sag-bend</b>				
Max. Effective Tension (kN)	1510	448	1684	429
Max. Bending Moment (kN.m)	340	352	397	371
DNV Utilization (LRFD)	0.69	0.70	0.67	0.64
<b>Hog-bend</b>				
Max. Effective Tension (kN)	1536	392	1725	376
Max. Bending Moment (kN.m)	369	245	439	262
DNV Utilization (LRFD)	0.76	0.54	0.73	0.49
<b>TDP</b>				
Max. Effective Tension (kN)	1536	267	1725	254
Max. Bending Moment (kN.m)	279	381	303	398
DNV Utilization (LRFD)	0.61	0.75	0.55	0.67

Load Case 15	Semi Position			
	Intact		Damage	
No Coating	Far	Near	Far	Near
Max. Effective Tension (kN)	3449	2971	3526	2946
<b>Sag-bend</b>				
Max. Effective Tension (kN)	1452	475	1617	455
Max. Bending Moment (kN.m)	275	359	309	376
DNV Utilization (LRFD)	0.57	0.71	0.56	0.64
<b>Hog-bend</b>				
Max. Effective Tension (kN)	1489	406	1657	388
Max. Bending Moment (kN.m)	275	228	323	236
DNV Utilization (LRFD)	0.60	0.52	0.58	0.46
<b>TDP</b>				
Max. Effective Tension (kN)	1488	291	1656	273
Max. Bending Moment (kN.m)	257	382	275	399
DNV Utilization (LRFD)	0.56	0.75	0.51	0.67

## Appendix C - Description of Software Used

### C.1 ORCAFLEX Software Program

#### Introduction

This section will give the general description of the ORCAFLEX software that is used in this thesis. The content of this section is mainly based on the ORCAFLEX Manual. ORCAFLEX is a fully 3D non-linear time domain finite element program, which is capable to deal with random large deflections of the flexible line from the initial configuration. ORCAFLEX is a program developed by Orcina for static and dynamic analysis of a wide range of marine facilities. This software comprises the main analyses of global analysis, moorings, installation, and towed system analysis. The software model several objects (i.e. Lines, Vessels, and Buoys) that can be built up and interlocked with special objects such as Link, Winch, and Shape to create a proper model of the system (Orcina, 2010).

This software is user-friendly and using a user interface system in order to input data easily. At initial startup, ORCAFLEX presents a 3D view window showing a blue line representing the sea surface and a brown line representing the seafloor. At the top of the screen are menus, a toolbar and a status bar arranged in the manner common to most Windows software. The menu bar has a number of commands such as commands for opening, saving, printing and exporting. The menu bar provides ease to edit input data, run the simulation and present results. It provides commands to perform modeling, starting, stopping, and replaying analyses. It also provides access to change views of the model. The toolbar is used as a shortcut to the menu bar; it provides a shortcut to access of the most commonly used commands. The status bar is used to see the current work state of ORCAFLEX such as the time of the simulation, completion of the simulation, etc. Figure C.1 below shows the sample of 3D model in ORCAFLEX. Table C.1 also shows the list of toolbar features, which is holding a selection of button that offer quick access to the most commonly used in menu bars.

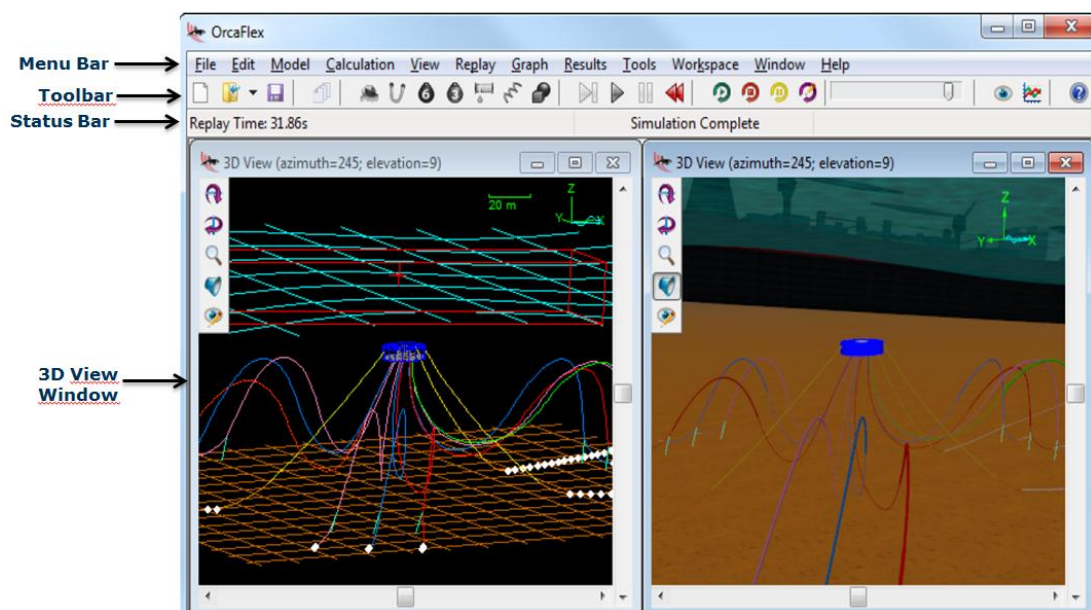

















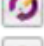





Figure C.1 3D View ORCAFLEX Computer Model (Orcina, 2010)

Table C.1 ORCAFLEX Tools (Orcina, 2010)

Button	Action	Equivalent Menu Item
	Open	File   Open
	Save	File   Save
	Model Browser	Model   Model Browser
	New Vessel	Model   New Vessel
	New Line	Model   New Line
	New 6D Buoy	Model   New 6D Buoy
	New 3D Buoy	Model   New 3D Buoy
	New Winch	Model   New Winch
	New Link	Model   New Link
	New Shape	Model   New Shape
	Calculate Statics	Calculation   Single Statics
	Run Simulation	Calculation   Run Dynamic Simulation
	Pause Simulation	Calculation   Pause Dynamic Simulation
	Reset	Calculation   Reset
	Start Replay	Replay   Start Replay
	Stop Replay	Replay   Stop Replay
	Step Replay Forwards	Replay   Step Replay Forwards
	Edit Replay Parameters	Replay   Edit Replay Parameters
	Add New 3D View	Window   Add 3D View
	Examine Results	Results   Select Results
	Help Contents and Index	Help   OrcaFlex Help

## Model States

ORCAFLEX builds and analyzes a mathematical model of the system for static and dynamic analysis. The model can be built up from a series of interconnected objects, (i.e. Lines, Vessels and Buoys). ORCAFLEX perform static and dynamic analysis through a sequence of states, the status bar shows the current state of the simulation. The figure C.2 presents a flowchart diagram of states and actions. Based on ORCAFLEX manual, the description of how model states work is presented as follows:

1. In Reset state, new model from a data file can be modeled or current model can be used as the starting point for analysis.
2. In Reset state, modification of the model can be performed by adding or removing objects to make it as required for the new model. It is normally better to use a very simple model in the early stages of design.

3. Run a static analysis to get the equilibrium of static state and prescribe the static position results. Make any corrections to the model, if needed. Any modification will automatically reset the model. Steps (2) and (3) are then repeated to get a proper model as required.
4. Run a simulation and monitor the results during the simulation (in Simulating state).
5. If the simulation is unstable, then reset the model and edit the model accordingly. Steps (2) to (5) are then repeated to get a proper model as required.
6. Complete the simulation of the model, and obtain the results. If more detail results are needed, then improve the discretization by reducing the time step sizes or increasing the number of segments used for Lines.

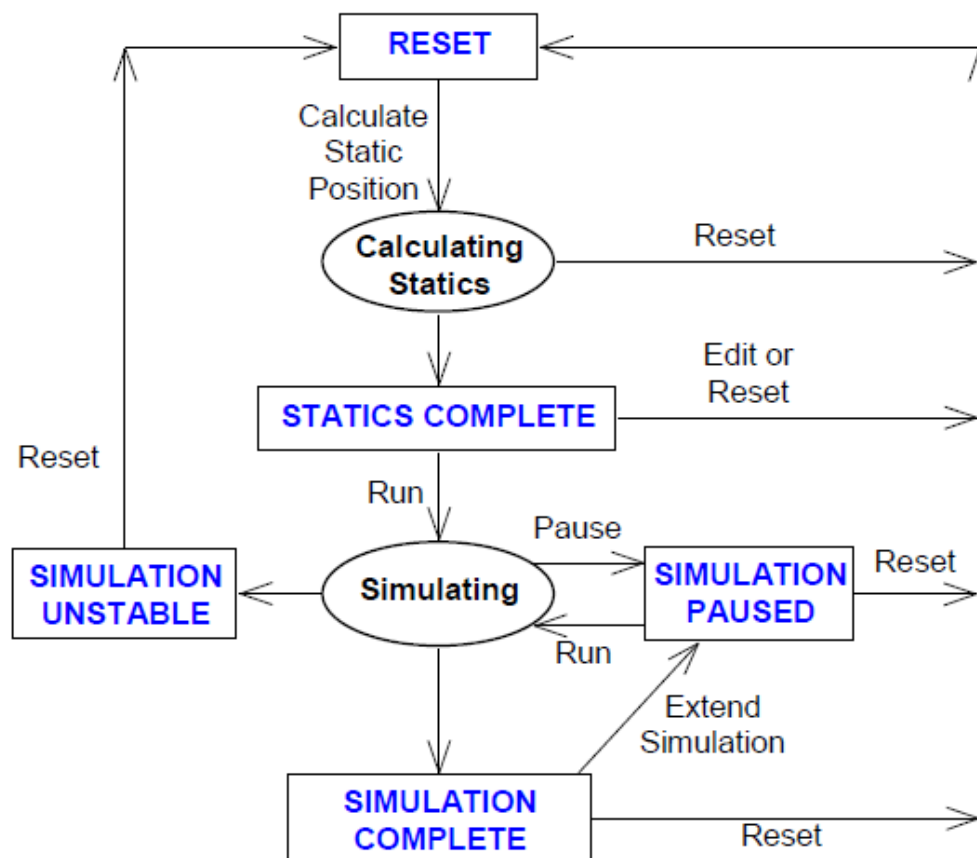


Figure C.2 Sequential Flowchart of ORCAFLEX (Orcina, 2010)

## Coordinate System

There are two coordinate systems that used by ORCAFLEX. They are global coordinate system (GX, GY, and GZ) and local coordinate system (x, y, and z). These coordinate systems are a right-handed system and normally its Z-axis are heading to the positive upwards. The Figure C.3 shows the description of the global coordinate systems and local coordinate system in ORCAFLEX.

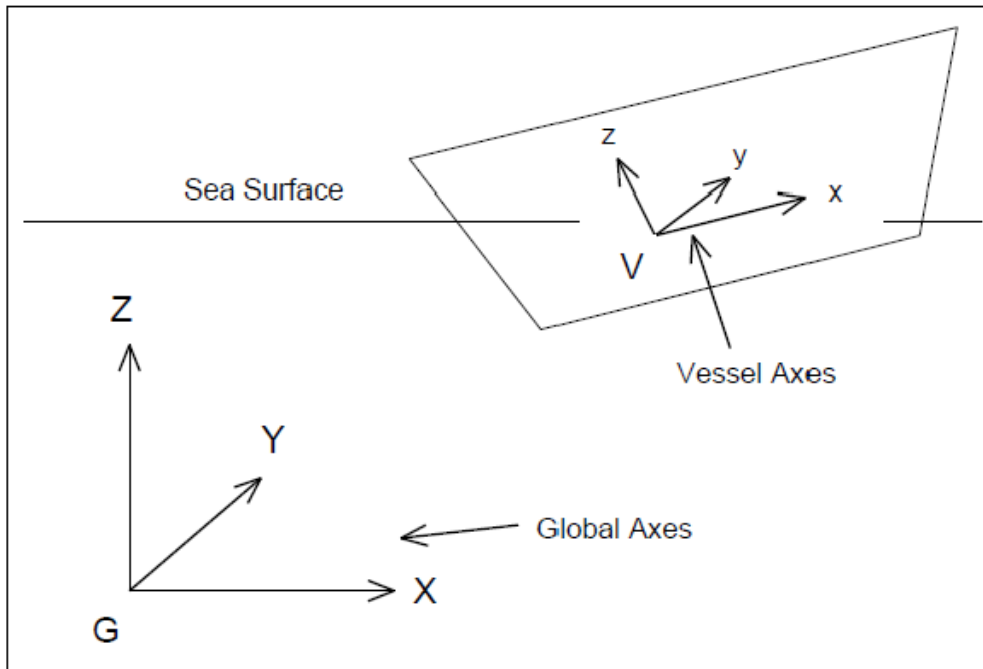


Figure C.3 Coordinate system (Orcina, 2010)

Directions and headings are specified in ORCAFLEX by giving the azimuth angle of the direction, in degrees, measured positive from the positive x-axis towards the positive y-axis, as shown in the following figure.

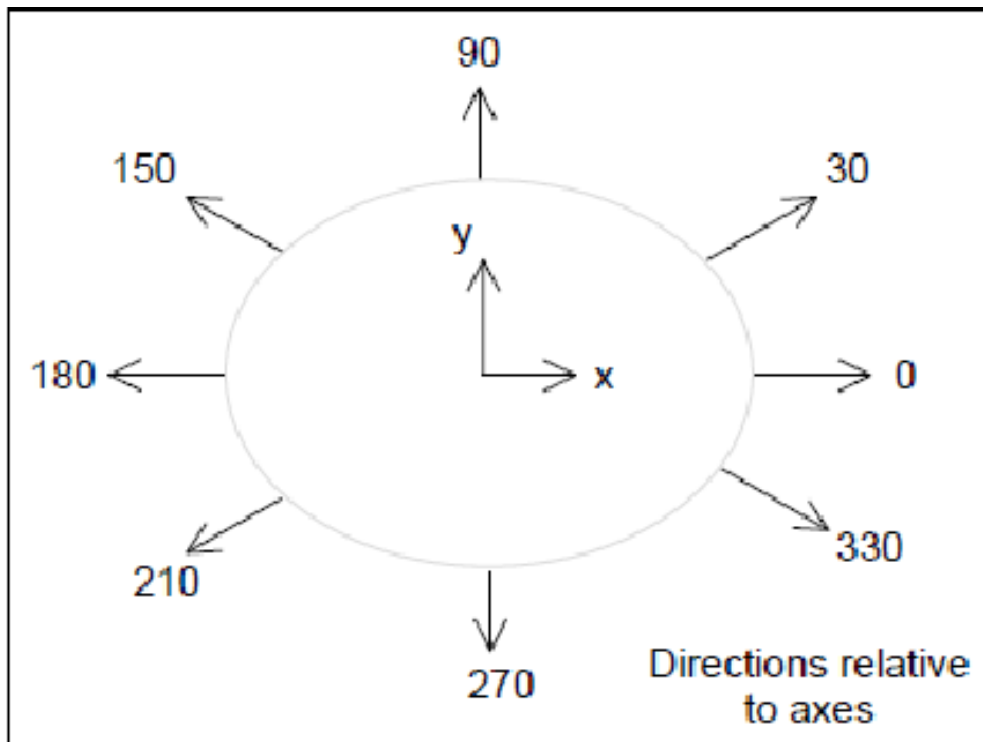


Figure C.4 Direction and Headings (Orcina, 2010)

Directions for waves, current and wind are specified by giving the azimuth direction, relative to global axes.

## Static and Dynamic Stage

The static analysis provides the initial static equilibrium condition of the computer model, and it becomes a startup point for dynamic simulation. The static analysis determines the equilibrium configuration of the system under self-weight, buoyancy, hydrodynamic drag, etc. Afterwards, the static analysis's result provide a starting configuration for dynamic simulation

The dynamic analysis run motions of the model over specified periods, starting from the position derived from the static analysis. The period of simulation is defined as a number of consecutive stages. Before the main simulation stage, there is a build-up stage, during which the wave and vessel motions are smoothly ramped up from zero to their full size. This provides a gentle start and reduces the transients that are generated from a static position to full dynamic motion. This build-up stage is numbered 0 and its length should normally be set to at least one wave period. The build-up stage is followed by stage 1 and stage 2 until the end of simulation time.

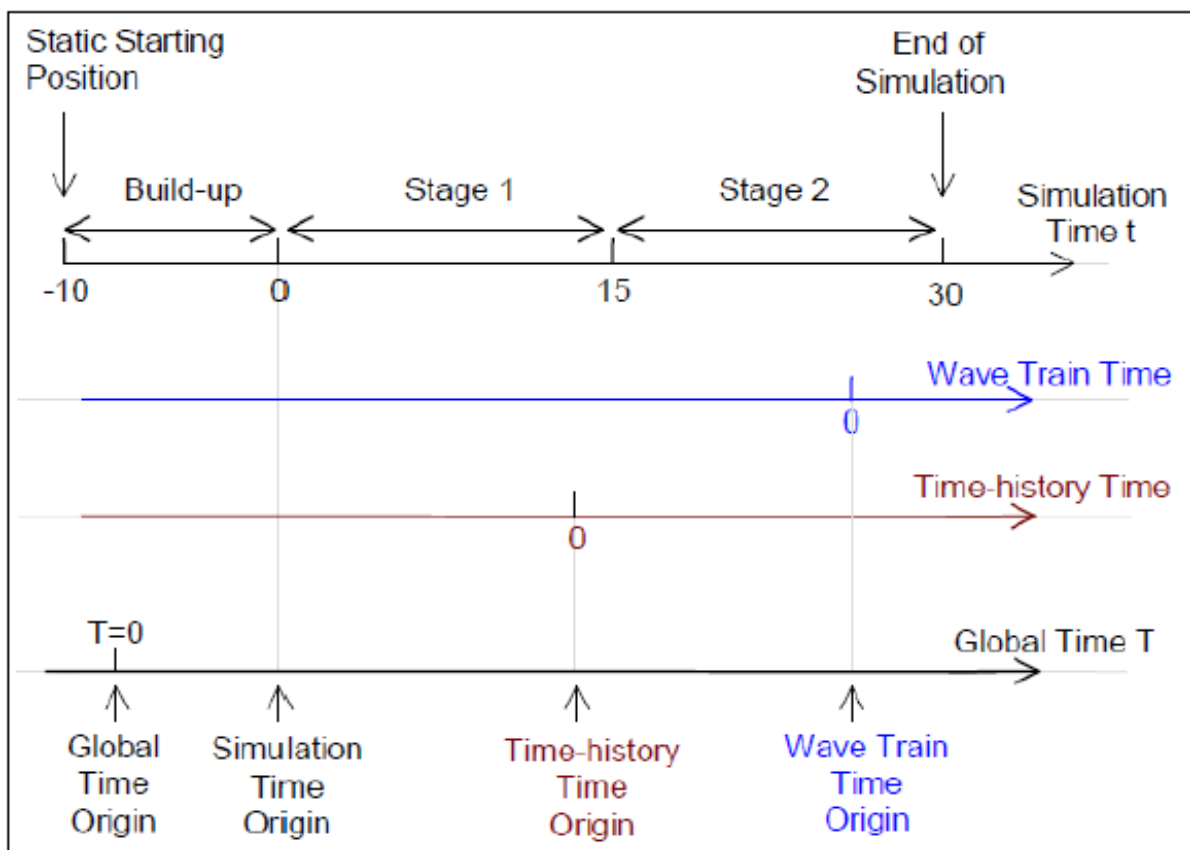


Figure C.5 Time and Simulation Stages of Dynamic Simulation (Orcina, 2010)

## Modeling of riser

ORCAFLEX uses a finite element model, comprising segments and nodes as the basic concept of modeling. For instance, a single length of pipe comprises several nodes and segments model as shown in Figure C.6. Each node is connected with a short straight line, so called segment, which represents the pipe section. Each line segment has therefore the properties of pipe (i.e. mass, weight, buoyancy, drag, diameter, thickness etc.). Nodes and



segments are ordered with a number from 1 to n, in which n is the total number of the nodes or segments sequentially from End A of the line to End B.

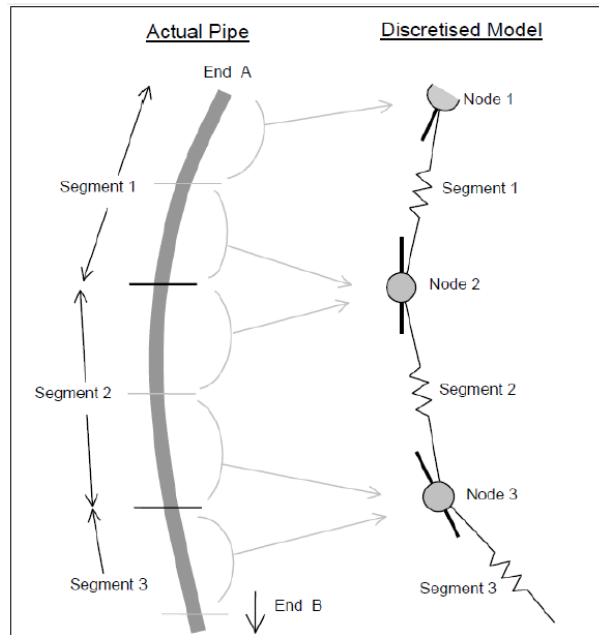


Figure C.6 Line Model in ORCAFLEX (Orcina, 2010)

Forces and moments are applied at the nodes. Each segment is represented as two co-axial telescoping rods that are connected by axial and torsional spring with dampers. The bending properties of the line are represented by rotational spring with dampers at each end of the segment. The model segments only model the axial and torsional properties of the line. Figure C.7 shows the structural detail of the line model.

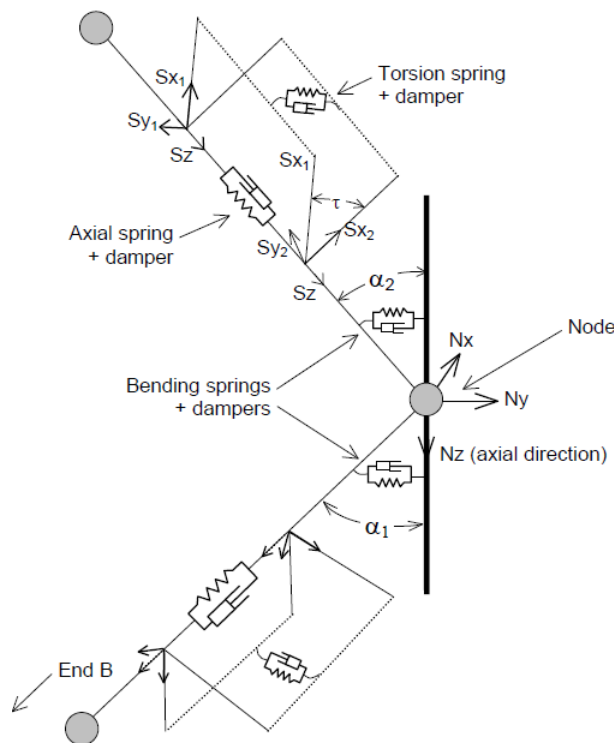


Figure C.7 Structural Detail of Line Model in ORCAFLEX (Orcina, 2010)

## C.2 RIFLEX Software Program

In this thesis, The SLWR is remodeled in RIFLEX in order to find fatigue damage due to VIV with VIVANA. RIFLEX is used to establish INPMOD and STAMOD of the SLWR to be applied as input to VIVANA. This section describes the general description of applied feature of RIFLEX, according to RIFLEX manual. RIFLEX is a computer program for analysis of slender structures, such as mooring lines, fish cage systems, pipelines and risers. It is a product of MARINTEK. RIFLEX comprises five modules communicating by a file system as shown in Figure C.8.

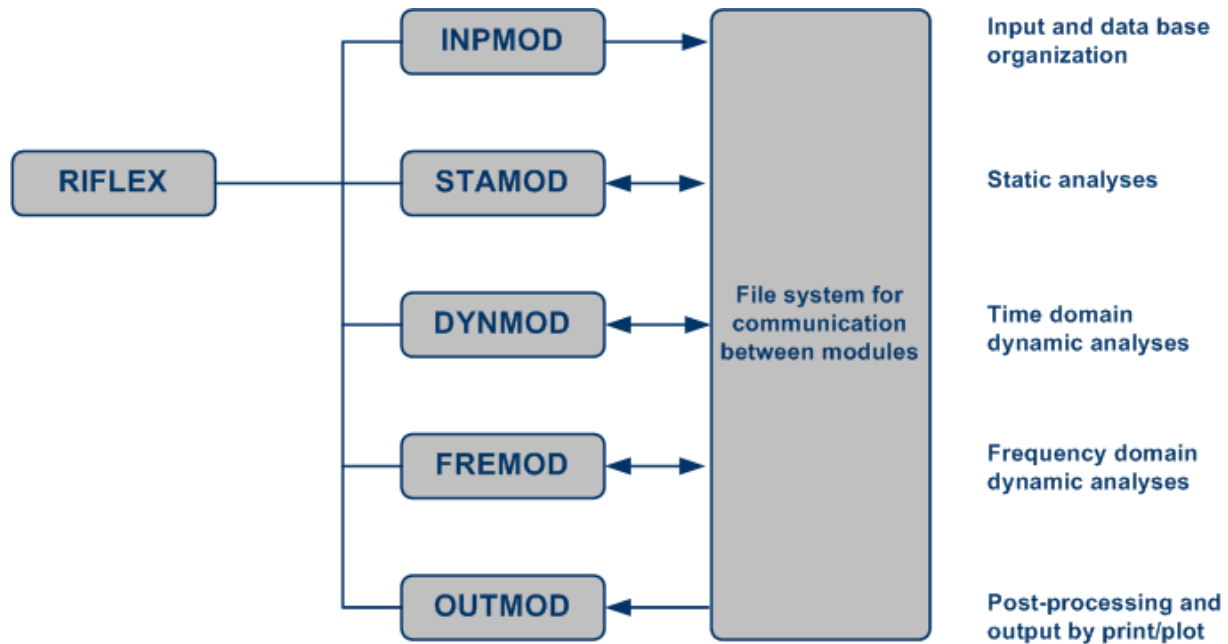


Figure C.8 RIFLEX Program Structure (Riflex, 2011)

Each module is described in the following table.

Table C.2 Description of Modules (Riflex, 2011)

Module	Description
<b>INPMOD</b>	The INPMOD module reads most input data and organizes a data base for use during subsequent analyses. Once the INPMOD module has been run, several analyses can be performed by the other modules without rerun of INPMOD.
<b>STAMOD</b>	The STAMOD module performs several types of static analyses. The results may be used directly in parameter studies etc., and are also used to define the initial configuration for a succeeding dynamic analysis. Element mesh, stressfree configuration and key data for finite element analysis are also generated by STAMOD based on system data given as input to INPMOD.
<b>DYNMOD</b>	The DYNMOD module carries out time domain dynamic analyses based on the final static configuration, environment data and data to define motions applied as forced displacements in the analysis. It is possible to perform several dynamic analyses without rerun of INPMOD and STAMOD. Response time series are stored on file for further postprocessing by OUTMOD and PLOMOD. In addition to dynamic response, natural frequencies and modeshapes can be calculated.

<b>OUTMOD</b>	OUTMOD performs postprocessing of selected results generated by STAMOD and DYNMOD. It is possible to store plots on a separate file for graphic output in the PLOMOD module. It is also possible to export time series via a standardized file format for further postprocessing by general purpose statistical analysis program (STARTIMES).
<b>PLOMOD</b>	Interactive plotting module for graphic presentation of plots generated by OUTMOD. An animation tool is available for visualization of the dynamic behaviour of the complete system (mooring lines, risers, vessel, waves).

In this study, only the INPMOD and STAMOD were used as the input for VIVANA. Since VIVANA requires an establishment of the static shape of the structure, INPMOD and STAMOD file is established to determine the model of SLWR in a static state. This appendix provides INPMOD and STAMOD scripts of the RIFLEX used in the VIV analysis for the SLWR without coating.

## **INPMOD Script**

```

*** INPMOD INPUT FILE ***
'
-----
INPMod IDENTification TEXT 3.6
SLWR from Semi-Submersible
10" API X65 Steel Grade Riser Pipe, 1500 m WD
Gilang Muhammad Gemilang - May 2015
'
UNIT NAME SPECification
' UTime  ULength  UMass   UForce   GRAV   GCONS
  s      m      kg      N      9.81  1.0
' seconds meter kilograms Newtons          m/s^2
'
----- RISER SYSTEM SPECIFICATION -----
'
' Super nodes
' Lines
' Segments
' Elements
'
-----
NEW SINGLE RISER
'
'iatyp idris
AR LONG
ARBITRARY SYSTEM AR
' nsnod  nlin  nsnfix  nves  no-of rigid-snodes
  4      3    2      0      0
' ibtang  zbot  ibot3D
  1     -1500  0
' Seafloor support conditions

```

```
' stfbot stfaxi stflat friaxi frilat
  1.0E6  1.0E5  1.0E0  0.3  0.5
' ilinty isnod1 isnod2
  1  1  2
  2  2  3
  3  3  4
'
' Boundary Conditions - upper end
' isnod ipos ix iy iz irx iry irz
  1  0  1  1  1  0  0  0 GLOBAL
' x0 y0 z0 x1 y1 z1 rot dir
  0  0 -500  48  0 -21  82
'
' Boundary Conditions - lower end
' isnod ipos ix iy iz irx iry irz
  4  0  1  1  1  1  1  1 GLOBAL
' x0 y0 z0 x1 y1 z1 rot dir
  2842  0 -500  1850  0.0 -1500
'
' Free nodes
' isnod X Y Z
  2  1680  0 -500
  3  2180  0 -500
'-----
'----- LINE DATA -----
'-----
NEW LINE DATA
'-----
' ilinty nseg icnlty ifluty
  1  5  0  98
' icmpty icnlty iexwty nelseg slgth
  1  0  0  4  2
  1  0  0  16  8
  1  0  0  254  1270
  1  0  0  125  250
  1  0  0  150  150
'-----
NEW LINE DATA
'-----
' ilinty nseg icnlty ifluty
  2  3  0  98
' icmpty icnlty iexwty nelseg slgth
  1  0  3  100  100
  1  0  3  300  300
```

1 0 3 100 100

-----  
NEW LINE DATA

-----  
' ilinty nseg icnlty ifluty

3 3 0 98

'icmpty icnlty iexwty nelseg slgth

1 0 0 100 100

1 0 0 200 200

1 0 0 181 362

-----  
'Total 2842

'10" Pipe with coating and Cd=1.1

-----  
NEW COMPONENT CRS1

' icmpty temp

1 10

'ams ae ai rgyr ast wst dst thst

172.014 0.072583 0.050671 0.0990 0.021913 0.001414 0.3040 0.0250

'iea iej igt ipress imf

1 1 1 0

'ea

4.536E9

'ej

4.449E7

'gt

3.422E7

'Hydrodynamic force coefficients

'cqx cqy cax cay clx cly icode d

0.0 1.0 0. 1.0 0. 0. 2 0.304

'tb ycurmx

1 1

'Distributed Buoyancy Module

-----  
NEW COMPONENT EXT1

' icmpty

3

'AMS AE RGYR FRAC

876.359 2.21863 0.433711 0.142333

'Hydrodynamic force coefficients

```
' CDX CDY AMX AMY CDLX CDLY
  1.0 1.0 0.5 1.0 0 0
'
'-----INTERNAL FLUID OIL-----
NEW COMPONENT FLUID
' icmpty
  98
' rhoi vveli pressi dpres idir
  800.0 0.0 50.0e3 0.0 2
'
'-----INTERNAL FLUID SEA WATER-----
NEW COMPONENT FLUID
' icmpty
  99
' rhoi vveli pressi dpres idir
  1025.0 0.0 0.0 0.0 2
'----- ENVIRONMENTAL DESCRIPTION -----
'-----
ENVIronment IDENTification
  Current conditions
'idenv
ENVIRONMENT
'
WATERdepth AND WAVEtype
'wdepth noirw norw ncusta
  1500 0 0 14
'
ENVIronment CONSTants
'airden watden wakivi
  1.3 1025 1.35E-6
'-----
' ----- Case1
NEW CURRENT STATE
' icusta ncuelv
  1 6
' curelv curdir curvel
  -10.0 180 0.067
  -50.0 180 0.058
  -200.0 180 0.044
  -500.0 180 0.039
  -1000.0 180 0.034
  -1500.0 180 0.022
'
' ----- Case2
```

NEW CURRENT STATE

```
' icusta ncuelv  
 2    6  
' curelv  curdir curvel  
 -10.0  180  0.105  
 -50.0  180  0.092  
 -200.0 180  0.081  
 -500.0 180  0.069  
 -1000.0 180 0.060  
 -1500.0 180 0.042
```

'----- Case3

NEW CURRENT STATE

```
' icusta ncuelv  
 3    6  
' curelv  curdir curvel  
 -10.0  180  0.139  
 -50.0  180  0.122  
 -200.0 180  0.112  
 -500.0 180  0.093  
 -1000.0 180 0.081  
 -1500.0 180 0.057
```

'----- Case4

NEW CURRENT STATE

```
' icusta ncuelv  
 4    6  
' curelv  curdir curvel  
 -10.0  180  0.174  
 -50.0  180  0.152  
 -200.0 180  0.141  
 -500.0 180  0.115  
 -1000.0 180 0.099  
 -1500.0 180 0.071
```

'----- Case5

NEW CURRENT STATE

```
' icusta ncuelv  
 5    6  
' curelv  curdir curvel  
 -10.0  180  0.210  
 -50.0  180  0.182  
 -200.0 180  0.171  
 -500.0 180  0.137
```

```
-1000.0 180 0.116
-1500.0 180 0.085
,
'----- Case6
NEW CURRENT STATE
' icusta ncuelv
  6   6
' curelv  curdir curvel
  -10.0  180 0.251
  -50.0  180 0.215
 -200.0  180 0.202
 -500.0  180 0.160
-1000.0  180 0.135
-1500.0  180 0.100
,
'----- Case7
NEW CURRENT STATE
' icusta ncuelv
  7   6
' curelv  curdir curvel
  -10.0  180 0.297
  -50.0  180 0.253
 -200.0  180 0.238
 -500.0  180 0.185
-1000.0  180 0.155
-1500.0  180 0.116
,
'----- Case8
NEW CURRENT STATE
' icusta ncuelv
  8   6
' curelv  curdir curvel
  -10.0  180 0.355
  -50.0  180 0.300
 -200.0  180 0.281
 -500.0  180 0.215
-1000.0  180 0.178
-1500.0  180 0.135
,
'----- Case9
NEW CURRENT STATE
' icusta ncuelv
  9   6
' curelv  curdir curvel
```



```
-10.0  180  0.435
-50.0  180  0.363
-200.0 180  0.339
-500.0 180  0.254
-1000.0 180 0.208
-1500.0 180 0.160
,
'----- Case10
NEW CURRENT STATE
' icusta ncuelv
  10   6
' curelv  curdir curvel
  -10.0  180  0.510
  -50.0  180  0.422
  -200.0 180  0.391
  -500.0 180  0.290
  -1000.0 180 0.235
  -1500.0 180 0.182
,
'----- Case11
NEW CURRENT STATE
' icusta ncuelv
   1   6
' curelv  curdir curvel
  -10.0  180  0.545
  -50.0  180  0.449
  -200.0 180  0.415
  -500.0 180  0.306
  -1000.0 180 0.247
  -1500.0 180 0.192
,
'----- Case12
NEW CURRENT STATE
' icusta ncuelv
   2   6
' curelv  curdir curvel
  -10.0  180  0.591
  -50.0  180  0.484
  -200.0 180  0.445
  -500.0 180  0.326
  -1000.0 180 0.262
  -1500.0 1800 0.205
,
'----- Case13
```

NEW CURRENT STATE

```
' icusta ncuelv
 3    6
' curelv curdir curvel
-10.0 180 0.658
-50.0 180 0.535
-200.0 180 0.490
-500.0 180 0.355
-1000.0 180 0.283
-1500.0 180 0.223
```

'----- Case14

NEW CURRENT STATE

```
' icusta ncuelv
 4    6
' curelv curdir curvel
-10.0 180 0.793
-50.0 180 0.636
-200.0 180 0.577
-500.0 180 0.412
-1000.0 180 0.325
-1500.0 180 0.259
```

END

## **STAMOD Script**

```
'*** STAMOD INPUT FILE ***
STAMod CONTROL INFORMATION 3.6
SLWR from Semi-Submersible
10" API X65 Steel Grade Riser Pipe, 1500 m WD
Gilang Muhammad Gemilang - May 2015
'-----
'irunco idris ianal iprdat iprcat iprfem iprform iprpor
 1 LONG 1 5 1 1 0 0
'-----
RUN IDENTification
'idres
SHAPE
'-----
ENVIRONMENT REFERENCE IDENTIFIER
'idenv
ENVIRONMENT
'-----
STATIC CONDITION INPUT
```

```
'nlcomp icurin curfac Icons
0 1 1.0 1
'-----
COMPUtational PROCedure
FEM
FEM ANALYsis PARAMeters
'-----
LOAD GROUP DATA
'nstep maxit racu
10 500 1.E-6
'lotype
VOLU
'-----
LOAD GROUP DATA
'nstep maxit racu
100 500 1.E-6
'lotype
DISP
'-----
LOAD GROUP DATA
'nstep maxit racu
10 500 1.E-6
'lotype
FRIC
'-----
LOAD GROUP DATA
'nstep maxit racu
10 500 1.E-6
'lotype
CURR
'-----
END
```

### C.3 VIVANA Software Program

The computer program VIVANA is used to calculate the fatigue damage due to the response of a slender structure excited by vortex shedding due to current. This response type is often referred to as vortex induced vibrations (VIV). The description in this section is based on VIVANA user manual. VIVANA is linked to RIFLEX to obtain the static state of slender structure. The two RIFLEX modules INPMOD and STAMOD are required by VIVANA program system. The general structure of the application between RIFLEX and VIVANA is shown in Figure C.9.

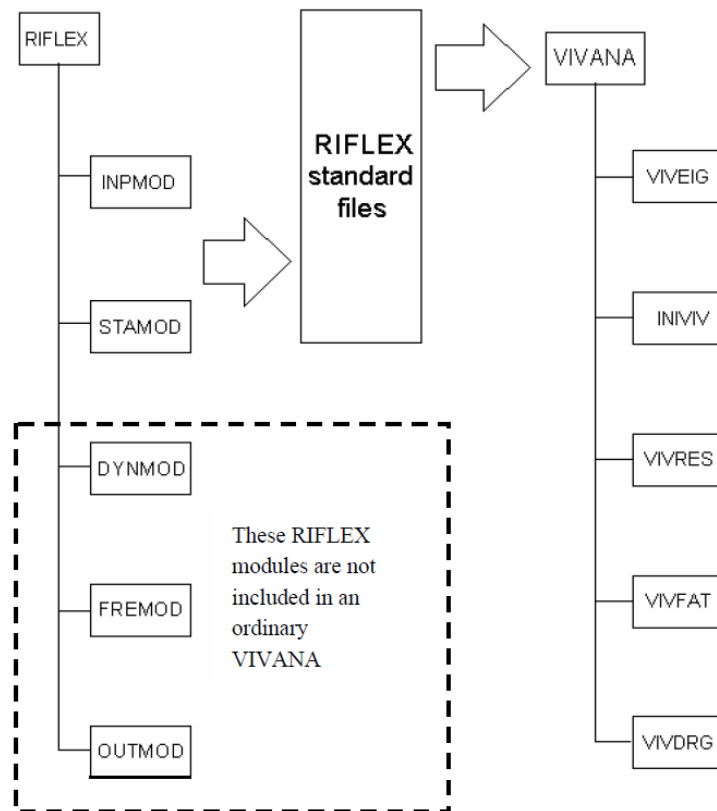


Figure C.9 VIVANA and RIFLEX overall structure (Vivana, 2005)

To obtain fatigue damage over the entire riser length due to VIV, the following are considered:

- An initial model is established in RIFLEX using the INPMOD and STAMOD modules.
- The VIVEIG module computes normal modes and eigen-frequencies.
- Calculation of some initial important parameters in INIVIV module.
- The dynamic analysis is carried out in VIVRES module.
- The results from VIVRES are then used to calculate fatigue damage in VIVFAT module.
- Final fatigue damage is calculated in VIVDRG module.

This appendix provides VIVANA script of the RIFLEX used in VIV analysis for SLWR without coating as follows.

## **VIVANA Script**

VIVANA CONTROL INFORMATION

SLWR from Semi-Submersible  
10" API X65 Steel Grade Riser Pipe, 1500 m WD  
Gilang Muhammad Gemilang - May 2015

```
' idris idstat idenv temp
  LONG SHAPE ENVIRONMENT 10
'-----
WORK ARRAY DIMENSION
' nwiwa
  9000000
'-----
EIGENVALUE ANALYSIS PARAMETERS
' neig nvec
  125 125
' eps1 eps2 eps3 ksr maxit kex shift maxniv
  0.0 0.0 0.0 1 7 0 0.0 0
'-----
EIGENVALUE PRINT OPTIONS
' npeig npvec
  125 125
'-----
SECTION PROPERTY SPECIFICATION
' nsegp
  11
' isegp iexczo iaddma iliftc idampg istrou
  1 0 0 0 0 1
  2 0 0 0 0 1
  3 0 0 0 0 1
  4 0 0 0 0 1
  5 0 0 0 0 1
  6 0 0 0 0 1
  7 0 0 0 0 1
  8 0 0 0 0 1
  9 0 0 0 0 1
  10 0 0 0 0 1
  11 0 0 0 0 1
'
'-----
PROPERTY EXCITATION ZONE
' nexzon
  2
' iprono cprpid fhmin fhmax
  2 Exc_norm 0.125 0.2
  1 Excit_02 0.125 0.2
'-----
PROPERTY DAMPING FACTORS
' ndpfac
```

4

```
' iprono cprpid fstill flowv fhighv
  1 Dmp_norm 1.0 1.0 1.1
  2 Damp_01 1.0 0.8 1.14
  3 Damp_02 1.0 0.9 1.13
  4 Damp_03 1.2 0.3 1.12
```

-----  
PROPERTY STROUHAL SPECIFICATION

```
' nstrsp
```

2

```
' iprono cprpdi npudsc strou
  1 Strou_01 18 0.18
```

```
' reynum strnum
```

```
  40. 0.1
  100. 0.18
  200. 0.19
  400. 0.195
  1000. 0.20
  4000. 0.205
  10000. 0.21
  40000. 0.215
  100000. 0.22
  200000. 0.4
  300000. 0.45
  500000. 0.45
  800000. 0.25
  1000000. 0.23
  4000000. 0.25
  10000000. 0.27
  20000000. 0.30
  38000000. 0.34
```

```
' iprono cprpid npudsc strou
  2 Strou_02 0 0.17
```

-----  
PROPERTY ADDED MASS

```
' nadcur
```

2

```
' iprono cprpid nampt
  1 Admas_01 12
```

```
' fhat addmco
```

```
  0.0 -0.6
  0.15 -0.6
  0.16 -0.3
```

```
0.17 1.7
0.18 2.0
0.2 2.2
0.21 2.0
0.24 1.7
0.27 1.5
0.33 1.2
0.40 1.0
0.5 1.0
,
' iprono cprpid nampt
  2 Admas_02 10
' fhat addmco
  0.0 -0.4
  0.16 -0.2
  0.17 1.5
  0.18 2.0
  0.2 2.2
  0.21 2.0
  0.24 1.7
  0.27 1.5
  0.33 1.2
  0.5 1.2
'
-----
PROPERTY LIFT COEFFICIENT
' nlccur
  1
' iprono cprpid nlcpt
  1 Test_211 26
' fhat acl0 aclmax clmax cla0
  0.120 0.149 0.100 0.10 0.000
  0.125 0.266 0.200 0.10 0.000
  0.127 0.400 0.214 0.10 0.016
  0.130 0.451 0.235 0.10 0.040
  0.135 0.505 0.270 0.10 0.080
  0.140 0.530 0.350 0.14 0.110
  0.150 0.588 0.450 0.20 0.180
  0.160 0.658 0.500 0.35 0.240
  0.165 0.746 0.500 0.50 0.300
  0.168 0.890 0.460 0.78 0.350
  0.172 0.900 0.430 0.80 0.400
  0.175 0.837 0.400 0.70 0.200
  0.180 0.761 0.400 0.40 0.100
  0.185 0.706 0.400 0.30 0.000
```

```
0.190 0.666 0.400 0.20 0.000
0.200 0.615 0.380 0.10 0.000
0.210 0.592 0.350 0.10 0.000
0.220 0.575 0.313 0.10 0.000
0.230 0.539 0.275 0.10 0.000
0.240 0.504 0.238 0.10 0.000
0.250 0.420 0.200 0.10 0.000
0.270 0.312 0.160 0.10 0.000
0.280 0.247 0.140 0.10 0.000
0.290 0.186 0.120 0.10 0.000
0.300 0.160 0.100 0.10 0.000
0.310 0.136 0.090 0.10 0.000
```

-----  
RESPONSE ANALYSIS PARAMETERS

```
' reldam gives damping as fraction of critical damping
' reldam conlim max_iter iprint ilim iuddf
0.01 0.010 30 1 2
'
' idomfrq
' 2
' 1
```

-----  
VIVRESPONSE FATIGUE DAMAGE

```
' nsect npc ioppr
0 4 0
' dscfa dscfy dscfz asi wsti
1.2 1.2 1.2 0.0305 0.00355
'
' nosl limind fatlim rfact
1 0 0.0 .000001
' rmi1 rcil
3.0 11.764
```

-----  
VIVANA RESULT PRINT

```
' iprelf iprstf iprdrg iprrsp iprcng
0 0 0 0 0
```

-----  
END



## Appendix D - Fatigue Results

### D.1 Wave Induced Fatigue

This section gives details of the fatigue results from wave induced fatigue analysis. The fatigue life of critical location where worst fatigue damage occurred is summarized in table for 12 wave direction. The detail fatigue result is presented for D-curve and C2-curve.

Wave Heading 0			Wave Heading 30		
SCR Critical Location	Curve-D	Curve-C2	SCR Critical Location	Curve-D	Curve-C2
Below flex joint	405 years	692 years	Below flex joint	1353 years	2968 years
TDP	61 years	120 years	TDP	174 years	367 years
WDSR Critical Location	Curve-D	Curve-C2	WDSR Critical Location	Curve-D	Curve-C2
Below flex joint	551 years	998 years	Below flex joint	1595 years	3686 years
TDP	180 years	376 years	TDP	632 years	1621 years
SLWR Critical Location	Curve-D	Curve-C2	SLWR Critical Location	Curve-D	Curve-C2
Below flex joint	1676 years	3645 years	Below flex joint	2074 years	4790 years
Sag Bend	>10000 years	>10000 years	Sag Bend	>10000 years	>10000 years
Hog Bend	>10000 years	>10000 years	Hog Bend	>10000 years	>10000 years
TDP	554 years	1022 years	TDP	4390 years	10531 years
Wave Heading 60			Wave Heading 90		
SCR Critical Location	Curve-D	Curve-C2	SCR Critical Location	Curve-D	Curve-C2
Below flex joint	859 years	1654 years	Below flex joint	371 years	668 years
TDP	130 years	267 years	TDP	64 years	126 years
WDSR Critical Location	Curve-D	Curve-C2	WDSR Critical Location	Curve-D	Curve-C2
Below flex joint	990 years	1931 years	Below flex joint	442 years	789 years
TDP	442 years	997 years	TDP	194 years	407 years
SLWR Critical Location	Curve-D	Curve-C2	SLWR Critical Location	Curve-D	Curve-C2
Below flex joint	1279 years	2622 years	Below flex joint	657 years	1235 years
Sag Bend	>10000 years	>10000 years	Sag Bend	>10000 years	>10000 years
Hog Bend	>10000 years	>10000 years	Hog Bend	>10000 years	>10000 years
TDP	2914 years	5905 years	TDP	728 years	1337 years
Wave Heading 120			Wave Heading 150		
SCR Critical Location	Curve-D	Curve-C2	SCR Critical Location	Curve-D	Curve-C2
Below flex joint	186 years	305 years	Below flex joint	158 years	263 years
TDP	28 years	39 years	TDP	21 years	30 years
WDSR Critical Location	Curve-D	Curve-C2	WDSR Critical Location	Curve-D	Curve-C2
Below flex joint	199 years	334 years	Below flex joint	158 years	269 years
TDP	82 years	122 years	TDP	65 years	93 years
SLWR Critical Location	Curve-D	Curve-C2	SLWR Critical Location	Curve-D	Curve-C2
Below flex joint	445 years	806 years	Below flex joint	309 years	557 years
Sag Bend	>10000 years	>10000 years	Sag Bend	>10000 years	>10000 years
Hog Bend	4168 years	8728 years	Hog Bend	2800 years	6002 years
TDP	249 years	436 years	TDP	218 years	380 years

Wave Heading 180			Wave Heading 210		
SCR Critical Location	Curve-D	Curve-C2	SCR Critical Location	Curve-D	Curve-C2
Below flex joint	180 years	301 years	Below flex joint	299 years	517 years
TDP	40 years	76 years	TDP	59 years	115 years
WDSCR Critical Location	Curve-D	Curve-C2	WDSCR Critical Location	Curve-D	Curve-C2
Below flex joint	198 years	341 years	Below flex joint	350 years	622 years
TDP	113 years	230 years	TDP	178 years	375 years
SLWR Critical Location	Curve-D	Curve-C2	SLWR Critical Location	Curve-D	Curve-C2
Below flex joint	306 years	543 years	Below flex joint	508 years	948 years
Sag Bend	>10000 years	>10000 years	Sag Bend	>10000 years	>10000 years
Hog Bend	7355 years	>10000 years	Hog Bend	>10000 years	>10000 years
TDP	408 years	733 years	TDP	636 years	1183 years
Wave Heading 240			Wave Heading 270		
SCR Critical Location	Curve-D	Curve-C2	SCR Critical Location	Curve-D	Curve-C2
Below flex joint	450 years	796 years	Below flex joint	515 years	917 years
TDP	77 years	154 years	TDP	88 years	173 years
WDSCR Critical Location	Curve-D	Curve-C2	WDSCR Critical Location	Curve-D	Curve-C2
Below flex joint	568 years	1001 years	Below flex joint	672 years	1236 years
TDP	242 years	523 years	TDP	284 years	614 years
SLWR Critical Location	Curve-D	Curve-C2	SLWR Critical Location	Curve-D	Curve-C2
Below flex joint	836 years	1606 years	Below flex joint	1081 years	2104 years
Sag Bend	>10000 years	>10000 years	Sag Bend	>10000 years	>10000 years
Hog Bend	>10000 years	>10000 years	Hog Bend	>10000 years	>10000 years
TDP	895 years	1707 years	TDP	994 years	1885 years
Wave Heading 300			Wave Heading 330		
SCR Critical Location	Curve-D	Curve-C2	SCR Critical Location	Curve-D	Curve-C2
Below flex joint	593 years	1056 years	Below flex joint	561 years	984 years
TDP	77 years	151 years	TDP	67 years	135 years
WDSCR Critical Location	Curve-D	Curve-C2	WDSCR Critical Location	Curve-D	Curve-C2
Below flex joint	828 years	1526 years	Below flex joint	790 years	1415 years
TDP	236 years	517 years	TDP	206 years	441 years
SLWR Critical Location	Curve-D	Curve-C2	SLWR Critical Location	Curve-D	Curve-C2
Below flex joint	2316 years	4921 years	Below flex joint	2521 years	5406 years
Sag Bend	>10000 years	>10000 years	Sag Bend	>10000 years	>10000 years
Hog Bend	>10000 years	>10000 years	Hog Bend	>10000 years	>10000 years
TDP	734 years	1363 years	TDP	601 years	1103 years

## D.2 Fatigue due to VIV

This section gives details of the raw fatigue results from VIV analysis; in-plane current and out-of-plane current.

